

The Telluric-Magnetotelluric Method in the Regional Assessment of Geothermal Potential

JOHN F. HERMANCE

RICHARD E. THAYER

Department of Geological Sciences, Brown University, Providence, Rhode Island 02912, USA

AXEL BJÖRNSSON

Department of Natural Heat, National Energy Authority, Reykjavik, Iceland

UNIVERSITY OF UTAH
RESEARCH INSTITUTE
EARTH SCIENCE LAB.

ABSTRACT

Before geothermal energy can be promoted as a major resource on a national scale, the scientific and engineering community should have a clear understanding of the fundamental constraints that nature itself places on the regional availability of the resource: in other words, what roles do global tectonic processes, such as sea-floor spreading, play in determining the distribution of heat in the crust and mantle on a regional scale? Is geothermal energy focused in certain broad areas and depleted in others? If so, what is the scale-size of zones of enhanced geothermal potential, and how do we detect them?

Using Iceland as an example of a region currently exhibiting crustal spreading, we have carried out a series of telluric-magnetotelluric experiments aimed at addressing these questions. At the present stage of our program, we feel that three important features of the distribution of geothermal energy have been identified: first, a uniform enhancement of temperatures in the upper mantle on a regional scale; second, broad zones where the base of the crust is being actively intruded by molten magma; third, sharp anomalies a few kilometers wide revealing highly conducting structures which clearly are the result of subsurface hydrothermal activity. The results of our experiments are promising and suggest that the telluric-magnetotelluric method may play a central part in the regional reconnaissance of geothermal energy, not only in Iceland where the method has been successful, but in other areas of the world, such as east Africa or western North America, where crustal spreading appears to be the dominant regional tectonic process.

INTRODUCTION

With the increased awareness, both among scientists and the public at large, that geothermal energy may be a significant resource for the future, geophysicists can expect to play a strategic role not only in detecting and evaluating local geothermal reserves but also in assessing the possibilities for developing geothermal energy on a regional scale. To accomplish this mandate, geophysicists have at their disposal a number of tools such as seismological, gravity,

magnetic, heat-flow, and electrical methods.

In this paper we shall focus on electrical methods, and more specifically on the telluric-magnetotelluric method (Hermance and Thayer, 1975). The electrical resistivity, after all, is the geophysical parameter which is proving to be the most useful indicator of enhanced subsurface geothermal activity.

During the summers of 1972 and 1973, a series of telluric-magnetotelluric measurements were made in a number of areas in Iceland (Fig. 1) in a cooperative project of the National Energy Authority of Iceland and Brown University. The objective of the research was to focus on fundamental questions regarding hydrothermal processes along the crest of the mid-ocean ridge system. Using Iceland as an example of a region currently exhibiting crustal spreading (Palmason and Saemundsson, 1974), we posed the following questions: How is heat distributed in the crust and upper mantle on a regional scale? Is geothermal energy focused in some areas and depleted in others? If so, what is the scale-size

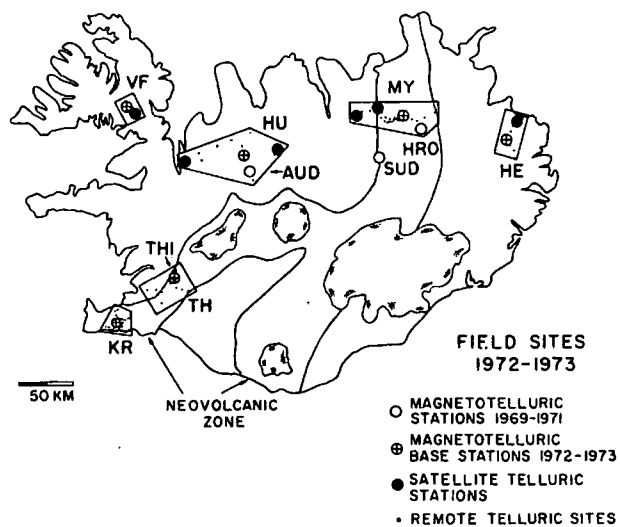


Figure 1. Location of survey areas in Iceland. Code letters refer to Krisuvik (KR), Thingvellir (TH), Westfjords (VF), Huna-vatnssysla (HU), Myvatn (MY), and Herad (HE).

of zones of enhanced geothermal potential, and how do we best detect them?

Our measurements are potentially important to an understanding not only of geothermal processes beneath mid-ocean ridges, but also those in other areas exhibiting crustal spreading, such as eastern Africa or western North America. Similarly, our results may contribute to understanding a number of geothermal-related processes such as hydrothermal energy, metallic ore migration and deposition, as well as deep-seated crustal vulcanism.

In the following discussion we present evidence supporting the following tentative conclusions. First, there is a uniform enhancement of temperatures in the upper mantle on a regional scale. Second, broad zones exist where the base of the crust is being actively intruded by molten magna. Third, there are sharp anomalies a few kilometers wide revealing highly conducting structures which clearly are the result of subsurface geothermal activity, although in some cases there may be no surface geologic manifestations of this activity.

THE TELLURIC-MAGNETOTELLURIC METHOD

Basic Concepts

Natural fluctuations in the earth's magnetic field occurring over a wide range of characteristic periods are caused by time-varying ionospheric and magnetospheric current systems as well as by tropospheric lightning storms. These magnetic field fluctuations induce electric currents in the conducting earth which in turn generate a secondary magnetic field. It is the measurement, analysis, and interpretation of the components of these naturally occurring electric and magnetic fields as seen at the earth's surface that comprise the telluric and magnetotelluric methods.

Usually two horizontal orthogonal components of the telluric (electric) field are measured at a particular site on the earth's surface. This is accomplished by measuring the difference of potential between two grounded stakes and dividing by the distance between them. The negative of this linear approximation to a directional derivative is simply the electric field component in the direction along which the stakes are aligned. Galvanized iron stakes seem to be appropriate for short-term measurements, but for longer-term measurements (of events having a period longer than a few minutes) electrode polarization effects may become important and must be minimized by using porous pot electrodes containing solutions of copper sulfate or cadmium chlorate. Components of the magnetic field can be detected using a number of devices such as induction-coil sensors and flux-gate magnetometers (Serson, 1973) or the highly sensitive superconducting "SQUID" devices recently developed for geophysical applications (Zimmerman and Campbell, 1975).

In a number of cases the earth can be represented by a series of plane layers which, although lossy, are nevertheless linear, homogeneous, and isotropic. Simple theory predicts that the electric field and magnetic field of an electromagnetic wave propagating through such a medium are orthogonal to one another. One would therefore expect that for a randomly polarized series of events the electric north component, say, should correlate with the magnetic south component. This type of correlation is demonstrated in Figure 2 (from Hermance, 1973b), in which magnetic

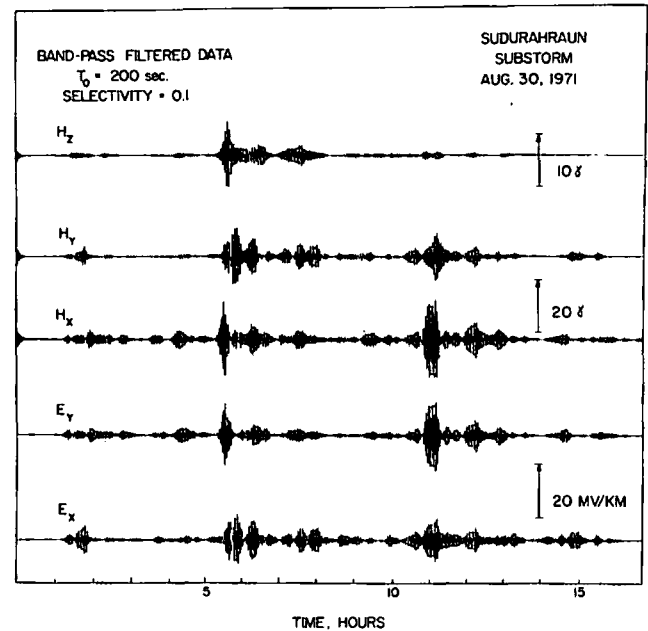


Figure 2. A comparison of magnetotelluric components recorded during a magnetic substorm and subsequently band-pass filtered using a digital filter having a center period of 200 sec and a selectivity of 0.1 (after Hermance, 1973b).

substorm data recorded on strip-chart records were subsequently digitized and numerically band-pass filtered at a period of 200 sec with a filter selectivity of 0.1. A visual scan of the fine structure of bursts of activity in the traces reveals an impressive correlation between the H_y and E_x components and between the H_x and E_y components. However, E_x and E_y , and H_x and H_y , do not look at all alike. In other words, the so-called "magnetotelluric orthogonal pairs" (E_x, H_y and E_y, H_x) exhibit in many cases a higher degree of correlation than do the "component pairs" (E_x, E_y and H_x, H_y) themselves.

Another result of the simple plane-layered model we are considering is that upon decomposing both the electric and magnetic field fluctuations into their respective Fourier spectral components one may determine a characteristic impedance, Z , for the earth given by

$$Z = E_x/H_y = -E_y/H_x, \quad (1)$$

where, following the usual convention, the electric field is given in mV/km and the magnetic field is given in γ .

A resistivity for the earth may be determined from

$$\rho = 0.2 T|Z|^2, \quad (2)$$

where ρ is the resistivity in ohm·m, T is the period in seconds of the spectral components in Equation (1), and Z is the characteristic impedance given by Equation (1). In reality, ρ should be called an "apparent" resistivity, since the essence of the magnetotelluric method lies in the contribution of Cagniard (1953) who noted that for a plane-layered earth, ρ as determined from Equation (2) should not be constant with period. He demonstrated that because of the so-called "skin-depth effect" of electromagnetic theory, short-period signals should not penetrate very deeply into the earth. Hence, at short periods Equation (2) should

give resistivities, or more properly apparent resistivities, characteristic of the layer or layers closest to the surface. On the other hand, long-period signals should penetrate to greater depth and lead to values for the apparent resistivity which are characteristic of deeper layers. Therefore calculating apparent resistivities from Equation (2) over a broad range of periods presents one with a measure of the true resistivity with depth. Perhaps it should be stressed that the magnetotelluric method is not a potential-field method, as is sometimes thought by workers unfamiliar with the technique, unless of course one makes a measurement or a profile of measurements at only a single point. By measuring the apparent resistivity over a sufficiently wide range of periods, one does not encounter the unique class of ambiguities associated with potential-field methods.

Field Relations Near Lateral Inhomogeneities

Although Cagniard's theory has led to a great deal of progress in studying areas where the plane-layered approximation is valid, one is not always assured that such a simple situation will be encountered. For example, the earth in the vicinity of a measuring site may not be plane-layered but may instead exhibit sharp lateral resistivity contrasts. Since these latter cases are by far the most interesting from the viewpoint of detecting geothermal reservoirs, one is forced to use theory more sophisticated than Cagniard's to interpret data from such situations.

One should not be surprised, for example, that in the close vicinity of a conductivity anomaly the electric current is significantly skewed from the direction it would have at some distance from the anomaly. A current flowing east-west might be distorted to flow, say, to the northwest. Although for a plane-layered earth an eastward current or electric field should correlate with a southward magnetic field, it should be apparent that, if the current is skewed in the vicinity of a lateral discontinuity, an eastward magnetic field may well induce a regional electric field which will be locally skewed to have a component to the east as well. In other words, it is quite possible that near lateral discontinuities each electric field component will correlate with both magnetic field components; thus one might expect the following linear relation to hold:

$$E_x = aH_x + bH_y \quad (3a)$$

$$E_y = cH_x + dH_y \quad (3b)$$

where a , b , c , and d are linear coupling coefficients, more commonly called magnetotelluric impedance tensor elements. Using the summation convention of repeated indices, Equations (3) may be abbreviated

$$E_i = Z_{ij} H_j, \quad (4)$$

$i = 1, 2 \quad \text{and} \quad j = 1, 2,$

where the set of coefficients Z_{ij} simply replaces the original a , b , c , and d .

A relation similar to Equation (4) is useful when only telluric fields are measured (the so-called telluric method; Berdichevskiy, 1965). In using this method an orthogonal set of electrodes is located at a base site and another orthogonal set of electrodes is located in sequence at a

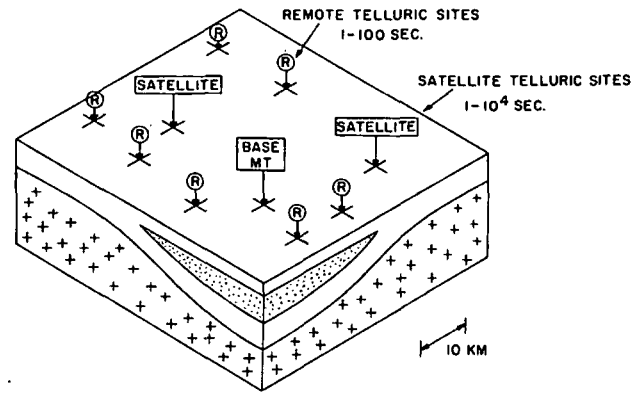


Figure 3. Schematic illustrating the relation between a base telluric or magnetotelluric site and the remote telluric sites. For convenience in describing a site, we distinguish between a remote site at which short-period (1 to 100 sec) measurements are made, and a satellite site at which long-period (1 to 10^4 sec) measurements are made, although the field systems are identical at either site.

number of remote sites, as shown in Figure 3. The objective of this method is to compare measurements at the various remote sites with simultaneous observations at the base site. An example of a telluric data set in its raw digitized form and after band-pass filtering is presented in Figure 4. Clearly there is a high degree of correlation between parallel telluric pairs. One cannot, however, always expect to find such a simple one-to-one correspondence, especially in the presence of lateral inhomogeneities. In such a case, one anticipates that either of the electric field components at the base site might be skewed into another direction at the remote site, so that one should expect a relation of the form

$$E'_i = T_{ij} E_j^b \quad (5)$$

where the set of coefficients (T_{ij}) is known as the telluric transfer tensor (Hermance and Thayer, 1975). Estimating the tensor elements in either the impedance tensor (Z) or the telluric transfer tensor (T) is a problem commonly encountered in data processing; various methods for accomplishing this are reviewed by Hermance (1973b) and Thayer and Hermance (in press).

A distinction is made between the telluric method, the magnetotelluric method, and what we have come to call the telluric-magnetotelluric method (Hermance and Thayer, 1975). Although the field procedure is still represented by Figure 3, the telluric-magnetotelluric method uses measurements of the electric and magnetic fields at the base site (E^b and H^b) to determine a base impedance tensor (Z^b) which is then transferred to the remote site using the telluric transfer tensor given by Equation (5). Therefore the electric field at the remote site is related to the magnetic field at the base site through the relation

$$E'_i = T_{ik} Z_{kj} H_j^b. \quad (6)$$

The new tensor which is formed is called the transfer impedance tensor and is given by

$$Z'_{ij} = T_{ik} Z_{kj}. \quad (7)$$

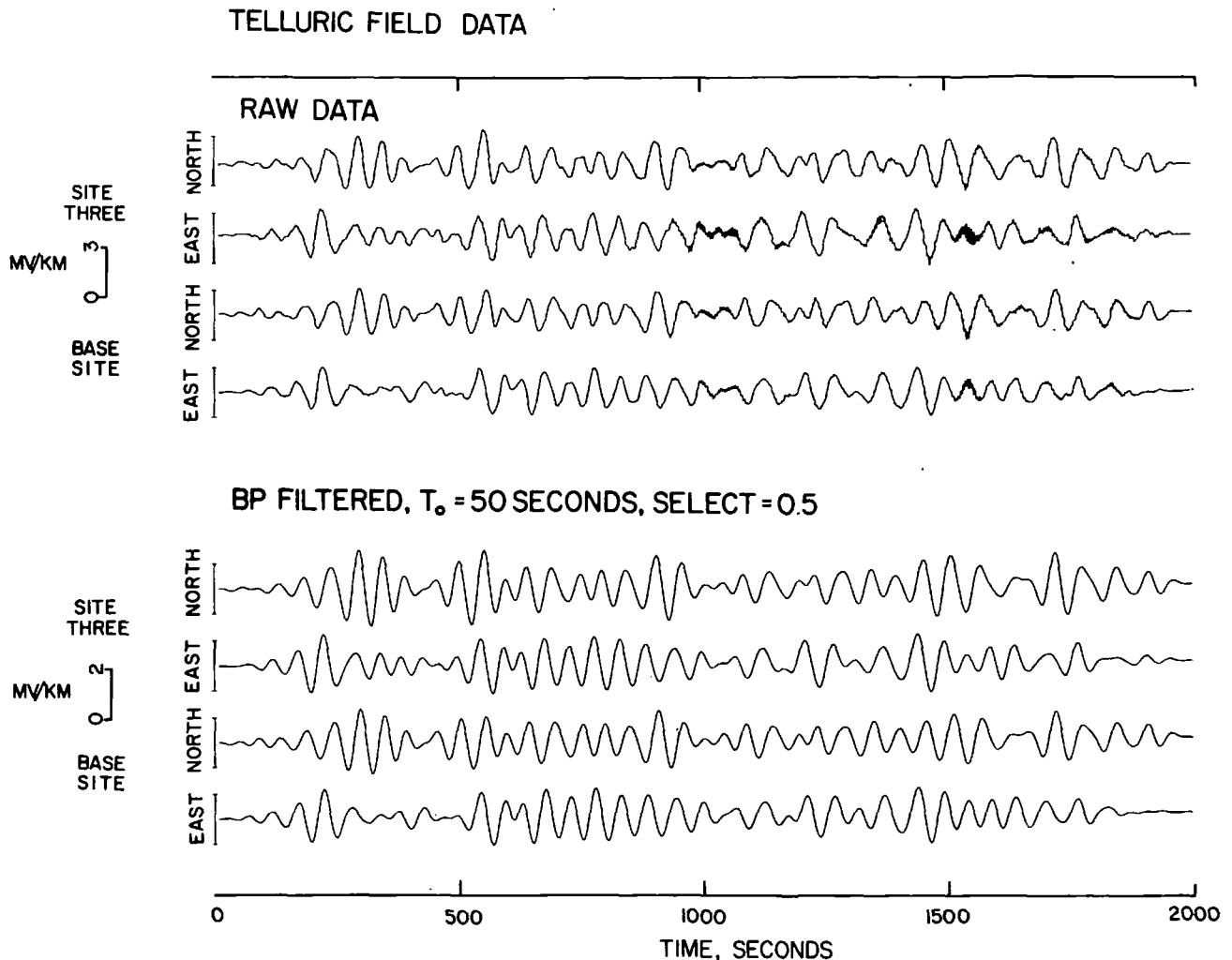


Figure 4. Telluric field data recorded simultaneously at the base site and site 3 during the Thingvellir survey. The raw data is simply a machine plot of unfiltered digitized chart records. The lower traces represent band-pass filtered data. Note the close correlation between the filtered north components at each site and between the filtered east components at each site (after Grillot, 1973).

Under the assumption that the magnetic field at the base site is approximately the same as that at the remote site, the transfer impedance tensor (Z') becomes a good approximation to the remote impedance tensor (Z'') which one would have obtained if *both* the electric and magnetic field measurements had been made at the remote site. One must keep in mind, in interpreting data, that (Z') is only an approximation to (Z'').

Field Procedure

At present we employ the following strategy for procuring telluric-magnetotelluric data during a regional reconnaissance survey. First, we select base sites spaced approximately 75 to 100 km apart, at which three magnetic and two electric field components are recorded. In the vicinity of each base site, within a radius of 20 km, five to ten or more short-period (1 to 100 sec) remote telluric sites (Figure 3) are occupied to investigate the nature of any possible local lateral inhomogeneities in the crust. At a distance from the base site of approximately 10 km, several long-period (1 to 10^4 sec)

satellite telluric sites are occupied to investigate the lateral homogeneity of mantle resistivities in the close vicinity of the deep-sounding experiment.

Preliminary hand calculations are done with the data while still in the field (see next section); these serve as a check on the quality of the data and provide information that would allow one to modify the experiment to improve coverage of an area.

Telluric-Magnetotelluric Parameters: Scalar

Raw energy ratios. Magnetic pulsation activity frequently occurs in a relatively restricted band (from periods of 30 to 80 sec). A primitive means of reducing telluric data for detecting crustal anomalies is to hand-digitize five or six cycles of an event from strip-chart records made simultaneously at a base site and a remote site. For example, for an event having a characteristic period of 50 sec, this might entail digitizing each component every 10 sec for a total of 31 points per component. After subtracting the mean, one then forms the Raw Energy Ratio (RER):

$$RER = \frac{\sum_{j=1}^N [(e_{xj}^r)^2 + (e_{yj}^r)^2]}{\sum_{j=1}^N [(e_{xj}^b)^2 + (e_{yj}^b)^2]} \quad (8)$$

where, for example, e_{xj}^r refers to the j th data point of the electric (x) component recorded at the remote (r) site, and N is the total number of points sampled.

Ellipse area ratios. A technique adapted from Berdichevskiy (1965) makes use of the fact that the telluric vector generally rotates in time, constantly changing amplitude and direction. Provided that data are sampled at close enough intervals, the telluric vector, in rotating from the j th to the $j+1$ st point, subtends approximately a triangular segment having an area $0.5(e_{xj}^r e_{yj+1}^r - e_{yj}^r e_{xj+1}^r)$. By summing over the entire sequence of areas subtended by the telluric vector, recorded at the remote site, for six cycles, say, and dividing by the total area subtended by the telluric vector recorded at the base site, one determines the Ellipse Area Ratio (EAR):

$$EAR = \frac{\sum_{j=1}^{N-1} |(e_{xj}^r e_{yj+1}^r) - (e_{yj}^r e_{xj+1}^r)|}{\sum_{j=1}^{N-1} |(e_{xj}^b e_{yj+1}^b) - (e_{yj}^b e_{xj+1}^b)|} \quad (9)$$

Spectral energy ratios. If one has narrow-band-filtered data (selectivity <0.3) before recording, one can form the Spectral Energy Ratio (SER):

$$SER = \frac{\int_0^T \{[\tilde{e}_x^r(t)]^2 + [\tilde{e}_y^r(t)]^2\} dt}{\int_0^T \{[\tilde{e}_x^b(t)]^2 + [\tilde{e}_y^b(t)]^2\} dt} \quad (10)$$

where the tilde denotes a field component that has been either analog or digitally narrow-band filtered. Equivalently, if Fourier spectral coefficients have been calculated, then one can form the SER from

$$SER = \frac{\int_{(\omega-\Delta\omega)/2}^{(\omega+\Delta\omega)/2} (|E_x^r|^2 + |E_y^r|^2) d\omega}{\int_{(\omega-\Delta\omega)/2}^{(\omega+\Delta\omega)/2} (|E_x^b|^2 + |E_y^b|^2) d\omega} \quad (11)$$

One can use Parseval's theorem to show that Equations (10) and (11) are equivalent and lead to the same values for SER.

Telluric-Magnetotelluric Parameters: Tensor

The parameters above are useful for rough reconnaissance investigations or for simple on-site reductions so that one can obtain a "feeling" for the experiment in order to modify the field program if need be. Quantitatively, however, these parameters have limited use. One can obtain far more precise information if one uses parameters derived from telluric transfer tensors or, better yet, impedance tensors.

Principal impedance or resistivity values. Having determined an impedance tensor in an arbitrary coordinate system (say geographic coordinates), one can determine a principal coordinate system in which the coupling effects between parallel magnetotelluric pairs are minimized. In a strictly two-dimensional situation one can show that the principal coordinates are parallel and perpendicular to the strike of the structure and that \mathbf{E} and \mathbf{H} measured in the principal coordinates are related by

$$E'_x = Z'_{xy} H'_y, \quad E'_y = Z'_{yx} H'_x \quad (12)$$

rather than by Equation (4), which is for a general orientation. The prime denotes that the terms in Equation (12) are determined for the principal coordinates. The tensor elements Z'_{xy} and Z'_{yx} are called the principal tensor elements; it is often useful in presenting the results of a telluric survey to plot these values as vectors on a map so that the length represents the magnitude of the principal element and the direction represents the principal direction. Alternatively, one can calculate principal apparent resistivity values given by

$$\rho'_{xy} = 0.2T |Z'_{xy}|^2 \quad (13a)$$

$$\rho'_{yx} = 0.2T |Z'_{yx}|^2 \quad (13b)$$

where T is the period in seconds and ρ'_{xy} and ρ'_{yx} are the principal apparent resistivities in ohm-meters.

Either of the above sets of parameters when plotted as vectors on maps of the survey area have proven very useful in obtaining a broad perspective of the region and in visualizing dominant structural patterns.

Normalized telluric ellipses. Equation (4) may be expressed in the alternative form

$$\begin{bmatrix} E_x \\ E_y \end{bmatrix} = \begin{pmatrix} Z_{xx} & Z_{xy} \\ Z_{yx} & Z_{yy} \end{pmatrix} \cdot \begin{pmatrix} H_x \\ H_y \end{pmatrix} \quad (14)$$

Once the impedance tensor, \mathbf{Z} , is calculated, then an arbitrary magnetic field, \mathbf{H} , can be used as a "driving function" to generate the resulting electric field \mathbf{E} . We now assume a particular form for the magnetic field, namely a unit amplitude (1 γ) field vector which is circularly polarized in the clockwise sense looking down.

If we express each complex tensor element in terms of its real and imaginary components as

$$Z_{jk} = A_{jk} + iB_{jk} \quad (15)$$

and the magnetic field vector in Equation (14) as

$$\begin{bmatrix} H_x \\ H_y \end{bmatrix} = \begin{bmatrix} \exp(i\omega t) \\ \exp(i\omega t - i\pi/2) \end{bmatrix} \quad (16)$$

then Equation (14) can be used to solve for

$$\text{Re}(E_x) = a \cos\omega t + b \sin\omega t \quad (17a)$$

$$\text{Re}(E_y) = c \cos\omega t + d \sin\omega t \quad (17b)$$

where

forms an extensive part of the thesis by Thayer (1975). Although a detailed interpretation of this area will appear elsewhere, it is instructive to discuss some preliminary results to illustrate the application of the telluric-magnetotelluric method to a gross reconnaissance problem.

So far we have concentrated our discussion on results obtained from calculating a tensor impedance. In this section we return to the more primitive parameters described earlier.

Although it is not indicated in Figure 10, sites 18 and 20 lie in the Namafjall high-temperature thermal area, as indicated by surface geological evidence (Ragnar et al., 1970). For comparison, we have plotted in Figure 10 the three scalar parameters described earlier: the Raw Energy Ratio (RER), Ellipse Area Ratio (EAR), and the Spectral Energy Ratio (SER). As we stated before, the RER and EAR are relatively easy to calculate by hand and serve as rough

indicators of telluric field behavior for the early interpretation of a reconnaissance survey. The hand-calculated ratios were determined using pulsation data in the 30- to 80-sec period band. The SER was calculated using smoothed Fourier coefficients determined by the analysis of time series consisting of 2000 points per component.

We see from Figure 10 that the three parameters track each other surprisingly well. In some cases the difference between the parameters can be explained as the result of using unfiltered data for the hand calculations versus calculating spectral energy ratios precisely at 50 sec. However, this effect does not seem in general to lead to significant differences between the values at each site.

Thayer (1975) has noted two features which stand out in the profile of Figure 10. First, a very sharp minimum is observed over the known high-temperature area. This

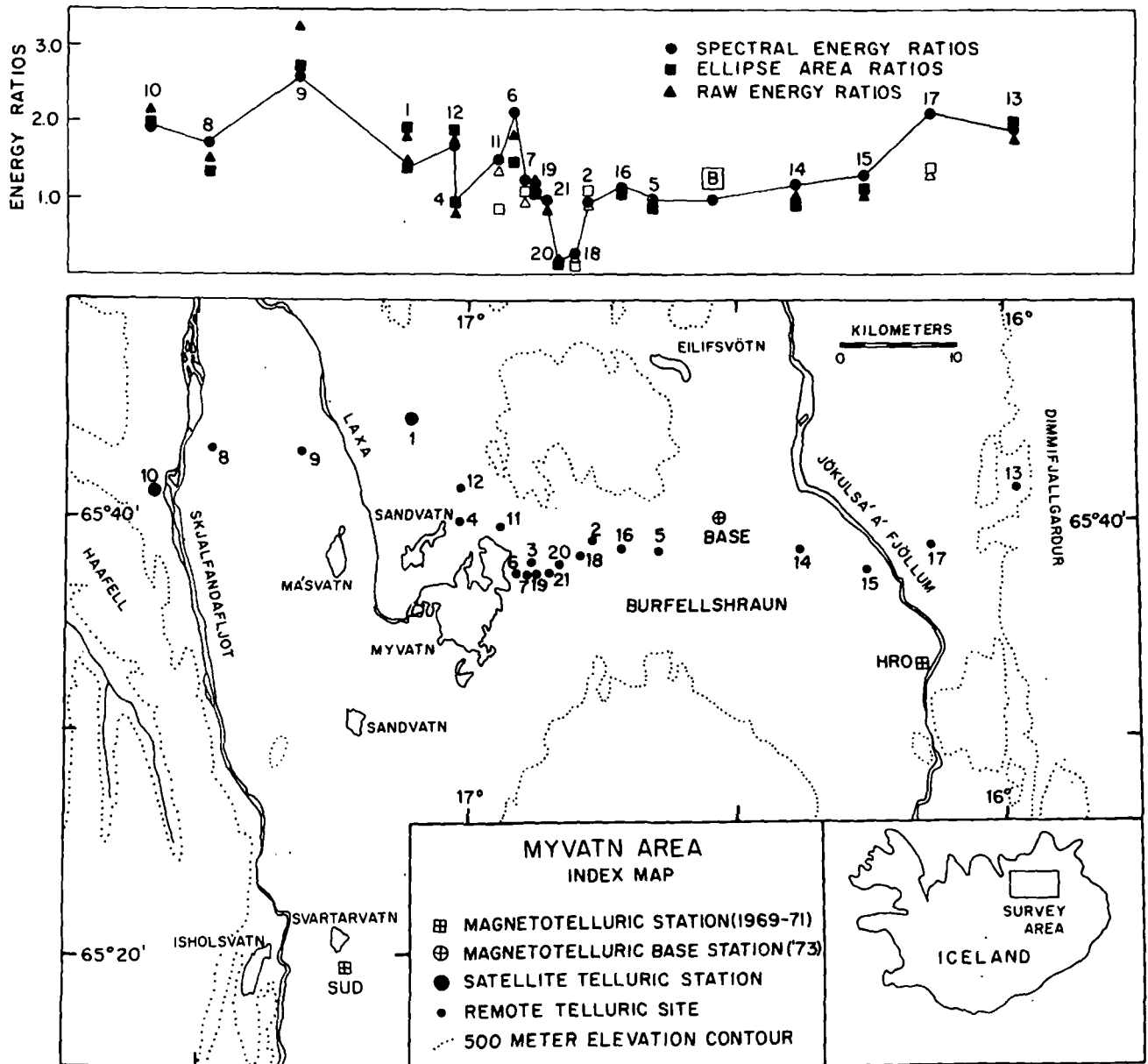


Figure 10. Map of Myvatn area and a profile comparing the ratio of telluric field energy at each remote site to that at the base site. Note the sharp telluric anomaly in the Namafjall area (sites 18 and 20). Also apparent is that telluric field energies are systematically higher on either end of the profile in comparison to the values in the vicinity of the base site (B) east of the Namafjall anomaly.

anomaly is very localized in lateral extent and sites less than 1 km outside the area have field values which have recovered to normal levels. Second, values for the telluric field energies at the easternmost sites (13 and 17) look very similar to the values at the sites west of the Namafjall area. On the other hand, telluric field energies in the median zone, at sites 2, 16, 5, 14, and 15, as well as the base site, are systematically lower. Since the energy ratios are proportional to apparent resistivity ratios, it seems that the depth-averaged resistivity is 25 to 50% lower for this median belt, which is approximately 25-km wide, than for the more resistive crustal blocks on either side. Clearly this broad resistivity low is associated in some way with the recent intense volcanism which is concentrated along this same zone. However, a more detailed discussion of the measurements in this area must be postponed for the present time.

The point we wish to make here is the useful role telluric measurements can play even in a gross reconnaissance survey of an area. One does not always have to rely on precise data analysis techniques to reveal first-order structural trends in an area. On the other hand, to extract the most information from one's data and to obtain the most stable electromagnetic parameters, there are indisputable advantages to calculating the tensor impedance at each site, either directly or indirectly by multiplying the base impedance tensor by the telluric transfer tensor as described above.

SUMMARY AND CONCLUSIONS

In this section we summarize the major points made in the previous discussion and draw upon our experience in Iceland to speculate on the applicability of these results to other regions where crustal spreading may be occurring.

The land-mass of Iceland occupies an area approximately 300 by 400 km. As best as we can ascertain at present, the temperature and composition of the mantle, which lies at a depth of 10 or 15 km, is essentially uniform—at least considerably more uniform than the crust appears to be. The situation is likely to be similar beneath a continental area, such as western North America, which is overriding an ocean rise. Even though a complicated geologic past is imprinted in the crustal rocks, the mantle beneath may have uniformly high temperatures over distances of hundreds of kilometers.

On a somewhat smaller scale-size, the crust of the neovolcanic zone in Iceland seems to have a systematically lower resistivity than does the crust of the older (10⁷ years B.P.) Tertiary basalt regions. This lower resistivity can be explained by the effects of enhanced hydrothermal activity at shallow depths ($d < 5$ km) and a small melt fraction (several percent) of basalt in the deep crust (5 to 10 km). This melt fraction could very easily be the result of a dynamic balance between the segregation of melt from the upper mantle and the creation of new crust along a zone of spreading. If this is the case, the zone of spreading in northern Iceland has a width on the order of 25 km (somewhat wider than the value of 12 km found by Harrison, 1968, for the submarine portion of the mid-ocean ridges). On the other hand, the width of a spreading center may be somewhat larger for continental areas. Clearly these zones have dimensions which make them attractive targets for regional reconnaissance studies.

On a still smaller scale, but of more immediate economic value, are high-temperature hydrothermal areas which, al-

though having a target size of only a few kilometers width, are nevertheless readily detected using the telluric-magnetotelluric method. In the Thingvellir area several anomalous zones were indicated that had little or no surface evidence of hydrothermal activity. In the Myvatn area a very dramatic telluric anomaly occurred in the vicinity of a known hydrothermal reservoir.

In conclusion, we feel that the telluric-magnetotelluric method has been successfully employed in Iceland for investigating problems having a variety of scale-sizes, from targets hundreds of kilometers wide to targets only a few kilometers wide. Moreover, these results demonstrate the central importance of the telluric-magnetotelluric method in the regional reconnaissance of geothermal energy.

REFERENCES CITED

- Annells, R. N., 1968, A geological investigation of a Tertiary intrusive centre in the Víðidalur-Vatnsdalur area, northern Iceland, [Ph.D. thesis]: St. Andrew's University.
- Arnorsson, S., 1970, Geochemical studies of thermal waters in the southern lowlands of Iceland: UN Symposium on the Development and Utilization of Geothermal Resources, Pisa, Proceedings (Geothermics, Spec. Iss. 2), v. 2, pt. 1, p. 547-552.
- Berdichevskiy, M. N., 1965, Electrical prospecting with the telluric current method: Colorado School Mines Quart., v. 60, no. 1, 216 p.
- Bodvarsson, G., 1954, Terrestrial heat balance in Iceland: Timarit Verkfræðingafélags Ísl., v. 39, p. 69-76.
- Cagniard, L., 1953, Basic theory of the magnetotelluric method of geophysical prospecting: Geophysics, v. 18, p. 605-635.
- Einarsson, T., 1954, A survey of gravity in Iceland: Rit 30, Reykjavik, Soc. Sci. Ísland., 22 p.
- Fridleifsson, I. B., and Kristjánsson, L., 1972, The Stardalur magnetic anomaly, SW Iceland: Jökull (Reykjavik), v. 22, p. 69-78.
- Grillot, L. R., 1973, Regional electrical structure beneath Iceland as determined from magnetotelluric data [Ph.D. thesis]: Dept. Geological Sciences, Providence, R. I., Brown University.
- Harrison, C. G. A., 1968, Formation of magnetic anomaly patterns by dyke injection: Jour. Geophys. Research, v. 73, p. 2137-2142.
- Hermance, J. F., 1973a, An electrical model for the sub-Icelandic crust: Geophysics, v. 38, p. 3-13.
- , 1973b, Processing of magnetotelluric data: Physics of Earth and Planetary Interiors, v. 7, p. 349-364.
- Hermance, J. F., and Grillot, L. R., 1974, Constraints on temperatures beneath Iceland from magnetotelluric data: Physics Earth and Planetary Interiors, v. 8, p. 1-12.
- Hermance, J. F., and Thayer, R. E., 1975, The telluric-magnetotelluric method: Geophysics.
- Palmason, G., 1971, Crustal structure of Iceland from explosion seismology: Rit 40, Reykjavik, Soc. Sci. Ísland., 187 p.
- , 1973, Kinematics and heat flow in a volcanic rift zone, with application to Iceland: Royal Astron. Soc. Geophys. Jour., v. 33, p. 451-481.
- Palmason, G., and Saemundsson, K., 1974, Iceland in relation to the mid-Atlantic Ridge: Annual Reviews of Earth and Planetary Sciences, v. 2, p. 25-50, Palo Alto, California, Annual Reviews, Inc.
- Ragnar, K., Saemundsson, K., Benediktsson, S., and Einarsson, S. S., 1970, Development of the Namafjall area—Northern Iceland: UN Symposium on the Development and Utilization of Geothermal Resources, Pisa, Pro-

- ceedings (Geothermics; Spec. Iss. 2), v. 2, pt. 1, p. 925-935.
- Serson, P. H.**, 1973, Instrumentation for induction studies on land: *Physics Earth and Planetary Interiors*, v. 7, p. 313-322.
- Sigurðeirsson, T.**, 1970, Aeromagnetic survey of SW Iceland: *Sci. Iceland*, v. 2, p. 13-20.
- Thayer, R. E.**, 1975, Telluric-magnetotelluric investigations of regional geothermal processes in Iceland [Ph.D. thesis]: Dept. Geological Sciences, Providence, R. I., Brown University, Dept. Geological Sciences.
- Waff, H. S.**, 1974, Theoretical considerations of electrical conductivity in a partially molten mantle and implications for geothermometry: *Jour. Geophys. Research*, v. 79, p. 4003-4010.
- Zimmerman, J. E., and Campbell, W. H.**, 1975, Tests of cryogenic SQUID for geomagnetic field measurements: *Geophysics*, v. 40, p. 269-284.

UNIVERSITY OF UTAH
RESEARCH INSTITUTE
EARTH SCIENCE LAB.

SUBJ
GPHYS
EM
Bore
SubVoid

Society of Exploration Geophysicists
Box 3098
Tulsa, Oklahoma 74101

Preprint subject to later revision, for information of delegates to
SEG Annual Meeting only.

SUBSURFACE VOID DETECTION USING SURFACE RESISTIVITY
AND BOREHOLE ELECTROMAGNETIC TECHNIQUES

by

T.E. Owen
S.A. Suhler

Department of Geosciences
Southwest Research Institute
San Antonio, Texas

Publication rights are reserved. This paper is to be presented at the 50th Annual International Meeting of the Society of Exploration Geophysicists in Houston, Texas. GEOPHYSICS has first claim on this paper for publication. Publication elsewhere is hereby restricted to the author's abstract or to an abstract of not more than 300 words, without illustration, unless the paper is specifically released by the Editor of GEOPHYSICS or the Executive Director on his behalf. Such abstract should contain appropriate, conspicuous acknowledgement. (If the paper is not available to GEOPHYSICS and the Program Chairman was so advised, the preceding paragraph may be omitted).

Discussion of this paper is invited immediately after its presentation. Written discussions will be considered for publication in GEOPHYSICS should the paper be accepted for publication.

SUBSURFACE VOID DETECTION USING SURFACE RESISTIVITY
AND BOREHOLE ELECTROMAGNETIC TECHNIQUES

by

T.E. Owen
S.A. Suhler

Department of Geosciences
Southwest Research Institute
San Antonio, Texas

ABSTRACT

Recent advances have been made in new geophysical earth resistivity survey methods and in borehole electromagnetic probing techniques for detecting shallow subsurface voids and cavities. Successful results have been obtained using an automatic recording pole-dipole resistivity method to detect soil sinkholes and solution caves in karst terrain and man-made tunnels in rock. Cavity size sensitivity and resolution achieved in these surveys ^{have} been exceptionally good as a result of precision digital data collected in the field and advanced data processing by digital computer.

Spatial redundancy in the resistivity field data permits enhancement of target anomaly signal-to-noise ratios in terrain where surface geologic noise presents a problem. This redundancy is used in a correlative model analysis technique to derived the approximate size and location of cavity targets.

Hole-to-hole ground-penetrating electromagnetic techniques have been applied to similar cavity detection surveys whereby the presence of cavities located between two boreholes is detected and accurately interpreted in size, depth, and location relative to the drill holes. Projections of received electromagnetic pulse signals along several source-to-receiver propagation paths permit a simple means of locating cavity targets between the drill holes.

When used in combination with a drilling program, the resistivity technique is a highly efficient surface survey method which can provide good guidance for the test boring operation. Complementary to this capability, the borehole electromagnetic method can provide significant additional coverage of the regions between boreholes.

INTRODUCTION

Detection and location of subsurface voids is an increasingly important requirement in geotechnical and engineering geophysics applications. The fact that such voids are often localized resistive anomalies in otherwise homogeneous ground has fostered the development of surface electrical and borehole electromagnetic geophysical techniques for detecting and mapping such targets. In application concept, the surface resistivity technique provides a search mode of operation whereby test borings in the vicinity of suspected anomalies serve as a practical means of void target verification. The borehole electromagnetic technique operates as a hole-to-hole probe to further verify the presence of cavities not intercepted by the drill holes and, hence, improve the efficiency of the drilling program.

is this a fact? doubt

The need for good threshold detection of small cavity targets located relatively deep below the surface and the need for direct data interpretation and display ^{has} led to the development of an automatic high-resolution earth resistivity survey system with computer-aided data processing and display. This system provides precision digital recording of field data from a spatially distributed array of pole-dipole electrodes which are automatically switched into operation along a predetermined survey traverse. Computer analysis of these data compensates for the effects of irregular surface terrain and compares the recorded field data with theoretical cavity target responses to selectively interpret and locate subsurface voids.

Use of the surface resistivity survey technique has resulted in more effective drilling program control where only anomalous subsurface conditions need be investigated. However, the fact that several drill holes are needed to delineate and map a subsurface cavity has led to the development of a hole-to-hole electromagnetic probe system capable of expanding the information obtainable from the minimum number of test borings. This system operates in a hole-to-hole pulse transmission mode to probe the ground between the holes. In particular, the presence of a void reduces the pulse travel time between two parallel drill holes and introduces distinctive spatial patterns in the forward scattered signals.

A VHF pulse signal having a time duration of about ten nanoseconds and a peak power of about 6KW is radiated by the transmitter module. By receiving transmitted pulses while the source and receiver probes are hoisted simultaneously, the region between the drill holes is scanned in detail. Digital records of the received signals are displayed in nested wiggle-trace form to indicate the presence of localized dielectric contrasts between the drill holes. More elaborate two-dimensional imaging techniques based upon travel time and absorption between holes are also practical.

These specialized geophysical methods were originated for use in military applications concerned with detecting and mapping man-made tunnels.* More

*Work performed under contract support of the U.S. Army Mobility Equipment Research and Development Command, Fort Belvoir, Virginia.

recently, both techniques have been successfully demonstrated to detect and map limestone cavities in karst terrain.** The resistivity technique has also been used successfully in detecting shallow abandoned coal mine workings.*** A variety of other potential applications in mining, high-resolution exploration, and geotechnical measurements also appear practical.

SURFACE RESISTIVITY SYSTEM

Surface resistivity measurements operate by injecting low-frequency current into the ground and measuring the resulting surface potentials. In homogeneous ground the injected current diverges radially away from a point source electrode and the measured surface potential gradient diminishes inversely with distance away from the source.

In the presence of a subsurface void, the current is forced to flow around the high resistance void and, therefore, the surface potential distribution is distorted from its uniform ground characteristic to reveal the anomaly. For air cavities the local surface potential is increased, indicative of a higher than normal apparent resistivity.

A water- or mud-filled cavity is more conductive than the surrounding medium and the injected current tends to concentrate in the conductive zone. The surface potential in the vicinity of the anomaly is reduced corresponding to lower than normal apparent resistivity.

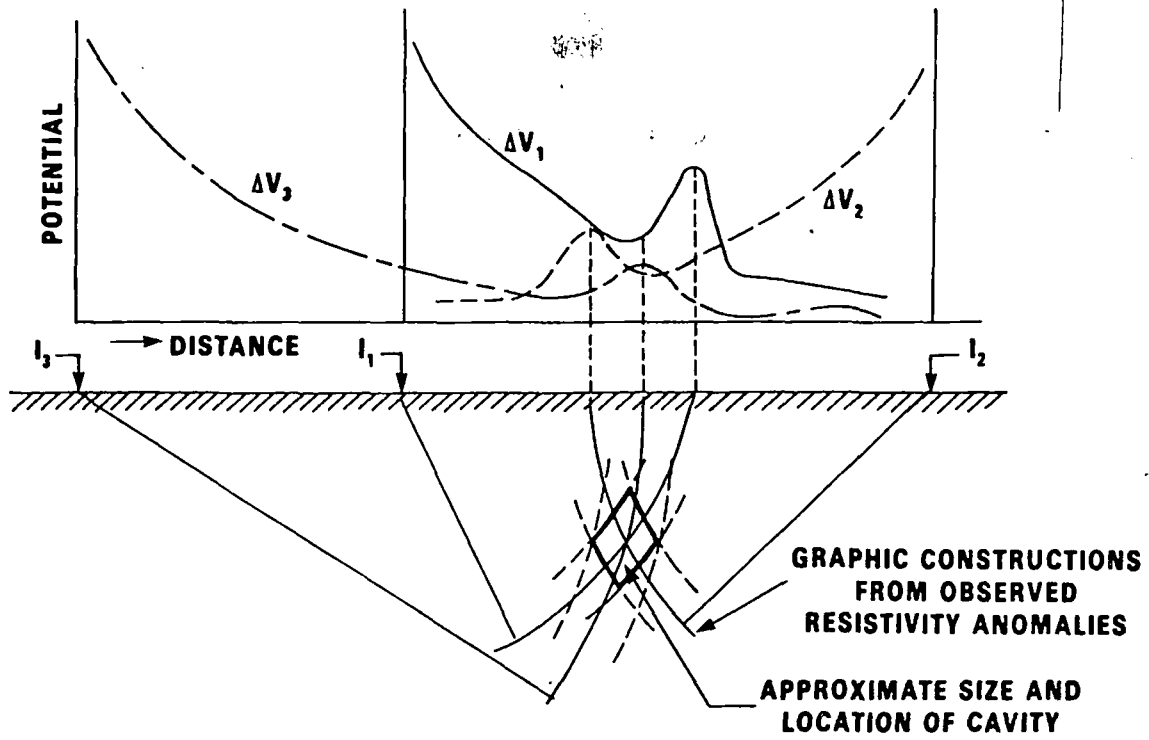
Apparent resistivity anomalies observed from several pole-dipole measurement positions can be analyzed in a simple way to locate an underground cavity in homogeneous ground. By drawing circular arcs from the location of each high resistivity perturbation, the location of the subsurface target can be inferred.

An automatic pole-dipole earth resistivity survey system was recently developed to provide automatic current injection into the ground via a commutated sequence of current electrodes. The current sink electrode is remotely located at a distance five to ten times greater than the maximum target depth of interest. The system is equipped to operate with up to 64 current source electrodes spaced at ten meters apart along the survey traverse. Earth potentials are measured by a portable two-meter dipole electrode pair which is moved along the survey line each time the current electrodes are sequenced.

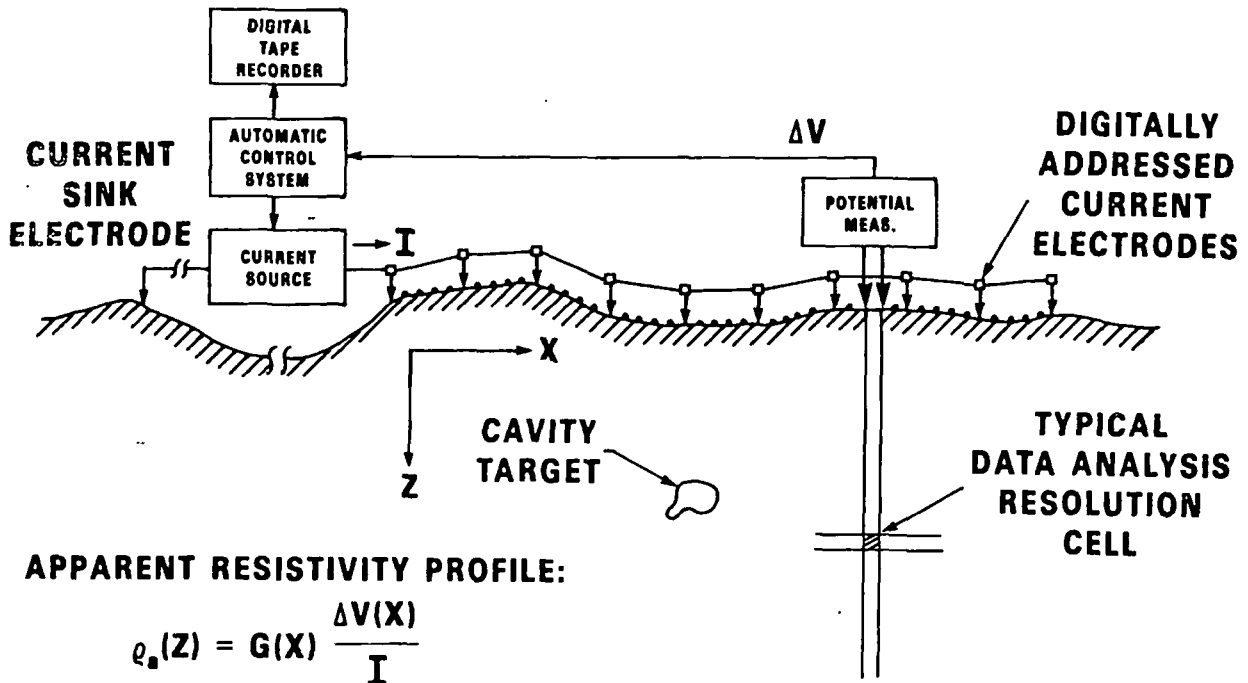
The automatic earth resistivity system consists of a central control unit by which automatic operation of the system is programmed and monitored, a precision constant current source having a square wave output waveform at selectable frequencies of 10, 17, or 25 Hz, and a digital magnetic tape data recorder. The source current is conveyed to the various electrodes along the survey line via a multi-conductor cable and individual remote current control modules. The

**Supported by the U.S. Army Corps of Engineers Waterways Experiment Station, Vicksburg, Mississippi.

***Supported by the Bureau of Mines, Denver Research Center, Denver, Colorado.



SIMPLIFIED EARTH RESISTIVITY DATA ANALYSIS



AUTOMATIC EARTH RESISTIVITY DATA ACQUISITION

current control modules are digitally addressable from the central control unit as part of the automatic system operation. The earth potentials are measured by a gain-ranging high-impedance preamplifier and are transmitted via a separate cable to the central control unit for digital recording on magnetic tape.

During a current commutation timing interval of two seconds, the desired current electrode is digitally addressed and connected for operation via a remote current control module located at each electrode, a precision constant current (up to two amperes) is turned on by the system control unit, after current stabilization the earth potential is sensed at the remote dipole preamplifier and coupled by wire line to the control unit where it is converted to 12-bit digital form, and finally digital information designating the particular current electrode address, potential pair location, source current, preamplifier gain, and the earth potential reading are recorded on magnetic tape. The current is then turned off and the next current source electrode is addressed.

After all preprogrammed current source electrodes are addressed and the associated potentials recorded, the potential electrode pair is moved one two-meter distance interval along the tranverse and the current commutation process repeated. An entire 630-meter traverse can generally be surveyed in a period of a day.

The magnetic tapes recorded in the field are processed to yield a cross-sectional image of resistivity anomalies underlying the survey line. In particular, the cavity target is modeled numerically in the computer analysis to predict the apparent resistivity anomaly for various possible target positions under the traverse. In this process, the cavity model is systematically assumed to occupy each possible resolution cell and the associated theoretical apparent resistivity profile derived for each current source electrode position. The theoretically predicted resistivity profiles for each assumed target location are then cross correlated with the experimentally measured resistivity profiles to compare their perturbations in apparent resistivity.

What sort of modeling program? 2-D?
What about anomaly interference

The result of this matched filter process is a correlation coefficient for each assumed target location whose values are plotted in the respective resolution cells analyzed. This model analysis and correlation with actual data is performed for each subsurface resolution cell of interest underlying the survey traverse. The results assigned to each cell form a two-dimensional image of apparent resistivity when displayed as shade-of-gray or contour line plots corresponding to the correlation coefficient values.

The computer analysis also incorporates a generalized conformal mapping algorithm* which corrects the measured surface potentials for terrain elevation irregularities so that the model analysis performed in a flat-surface halfspace can be compared with the field data. The cross correlation results obtained in the analysis are then mapped back to the actual terrain contour for display.

*Spiegel, R.J., Sturdivant, V.R., and Owen, T.E., "Modeling Resistivity Anomalies from Localized Voids under Irregular Terrain," Geophysics, Vol. 45, No. 7, pp. 1164-1183, July 1980.

HOLE-TO-HOLE ELECTROMAGNETIC SYSTEM

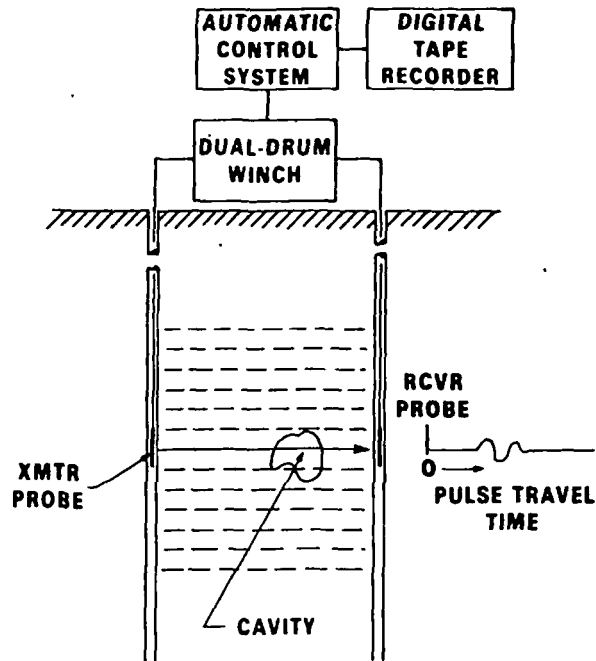
The hole-to-hole electromagnetic system provides through-transmission probing of geologic materials via a transmitter probe operating in one drill hole and a matching receiver probe operating in another drill hole. The transmitter radiates a VHF spectrum pulse characterized approximately as one oscillatory cycle of a 100 MHz sine wave. The peak amplitude of this pulse waveform is approximately 550 volts, corresponding to a peak pulse power of 6,000 watts. The repetition rate of the transmitter pulse is 60,000 pulses per second.

By drilling test holes to find a subsurface cavity suspected from a resistivity survey, for example, if the target is not intercepted after the first two holes, then hole-to-hole electromagnetic tests can be applied. For this purpose the transmitter and receiver probes are first lowered to the deepest depth of interest and hoisted while operating as a through-transmission source-receiver pair. The radiated pulse travels through the geologic medium between the holes and is detected and recorded in amplitude and time by the receiver system.

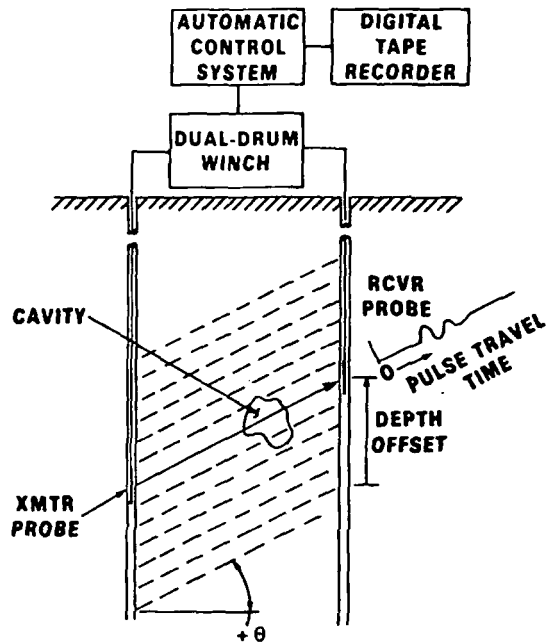
The propagation velocity and amplitude attenuation of the transmitted pulse is governed by the dielectric^{constant} and electrical conductivity of the geologic medium. For example, electromagnetic waves traveling along ray paths passing through an air-filled cavity travel slightly faster than those through the surrounding host ground. The finite boundaries and geometric shape of the cavity also diffract and scatter the transmitted pulse.

By offsetting the transmitter and receiver probes by known distances along their respective boreholes, the presence and approximate location of the cavity can be determined by simple graphic projections of the common cavity anomaly. More elaborate data acquisition procedures are also practical whereby small source-receiver offset distances are employed to gather many closely spaced transmission ray paths through the geologic medium being probed. Computer analyzed tomographic images can then be constructed to depict the dielectric and conductive contrasts and associated scattering structures located between the drill holes.

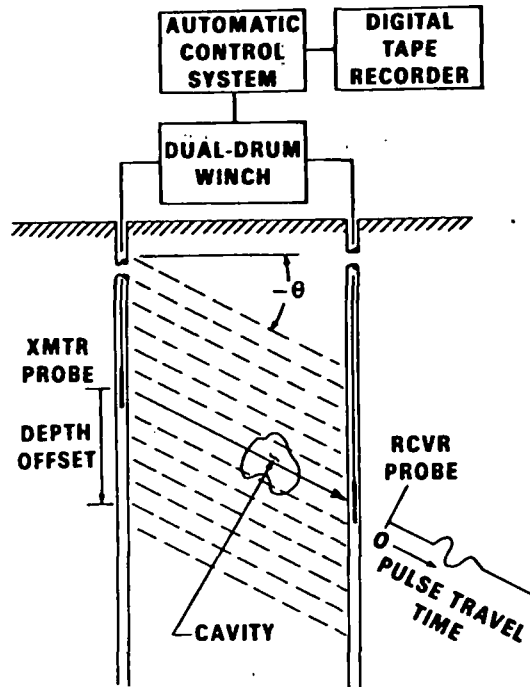
The hole-to-hole electromagnetic system consists of a 2-1/4 inch diameter probe eight feet long, a similar size receiver probe, a dual-drum wireline winch, a surface control unit, and a digital magnetic tape data recording system. The fiberglass borehole probes contain resistively-loaded dipole antennas and the respective pulse transmitter and receiver electronic modules are contained within the antenna probes. Time synchronization of the receiver with respect to the transmitter pulse is provided to allow time-domain sampling of the received signals. This sampling system translates the 30-300 MHz VHF downhole receiver range to the 600-6,000 Hz audio frequency range for transmission uphole via conventional armored logging cable.



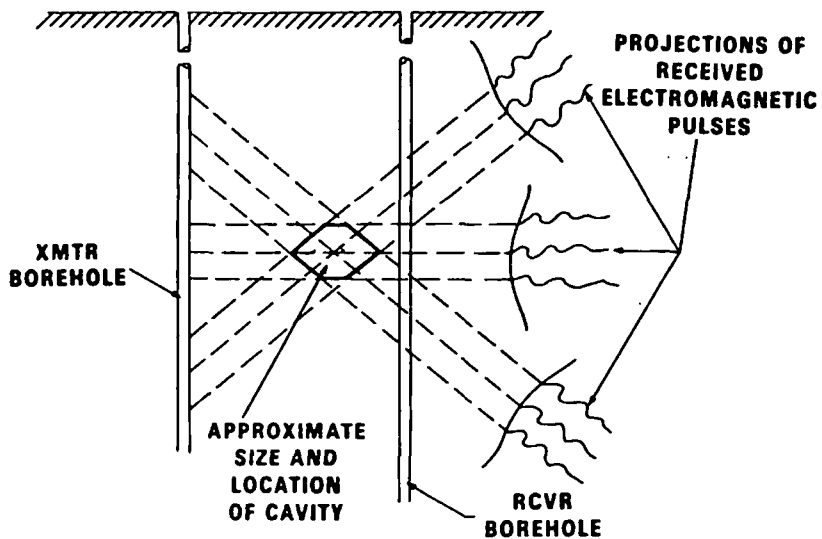
HOLE-TO-HOLE ELECTROMAGNETIC DATA ACQUISITION



OFFSET ELECTROMAGNETIC TRANSMISSION TESTS



OFFSET ELECTROMAGNETIC TRANSMISSION TESTS



HOLE-TO-HOLE ELECTROMAGNETIC TRANSMISSION ANALYSIS

The surface control unit powers and operates the downhole probes and accepts the time-domain-sampled pulse waveforms for conversion to digital format for recording on magnetic tape. A dual-drum wireline winch provides independent depth positioning of the transmitter and receiver probes. A single drive motor raises or lowers the probes either independently or simultaneously via a combination of brakes and clutches.

APPLICATIONS AND PERFORMANCE CAPABILITIES

The surface resistivity system and hole-to-hole electromagnetic system have been successfully demonstrated to detect soil sinks in karst terrain, natural limestone solution cavities, man-made tunnels, and abandoned mine workings. Both air-filled and water- or mud-filled cavities have been detected with good results.

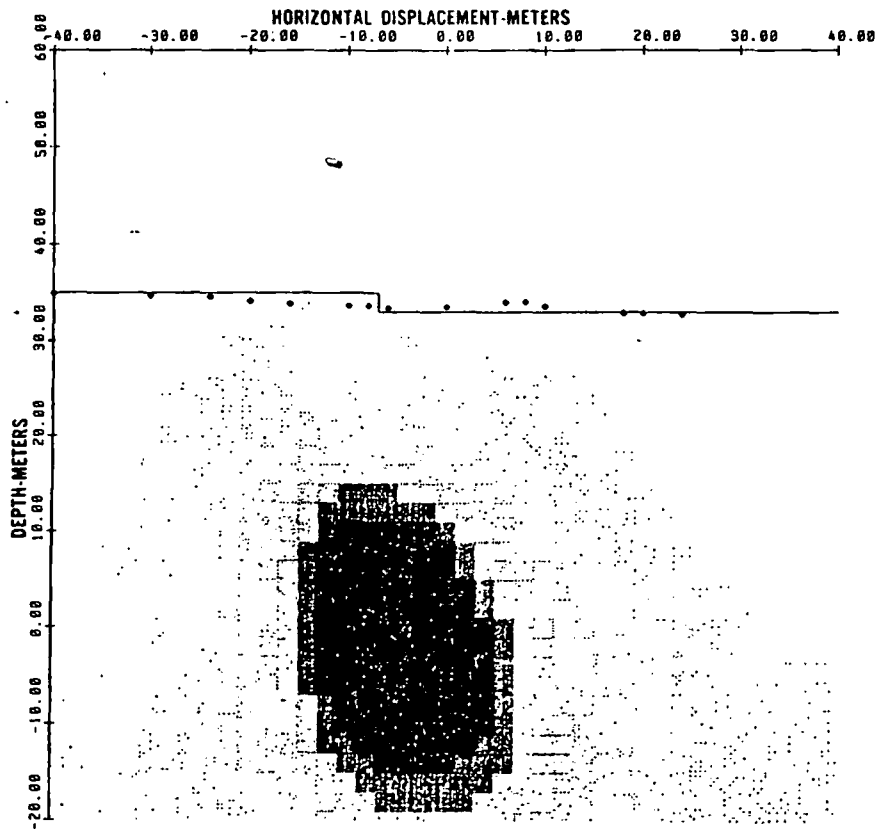
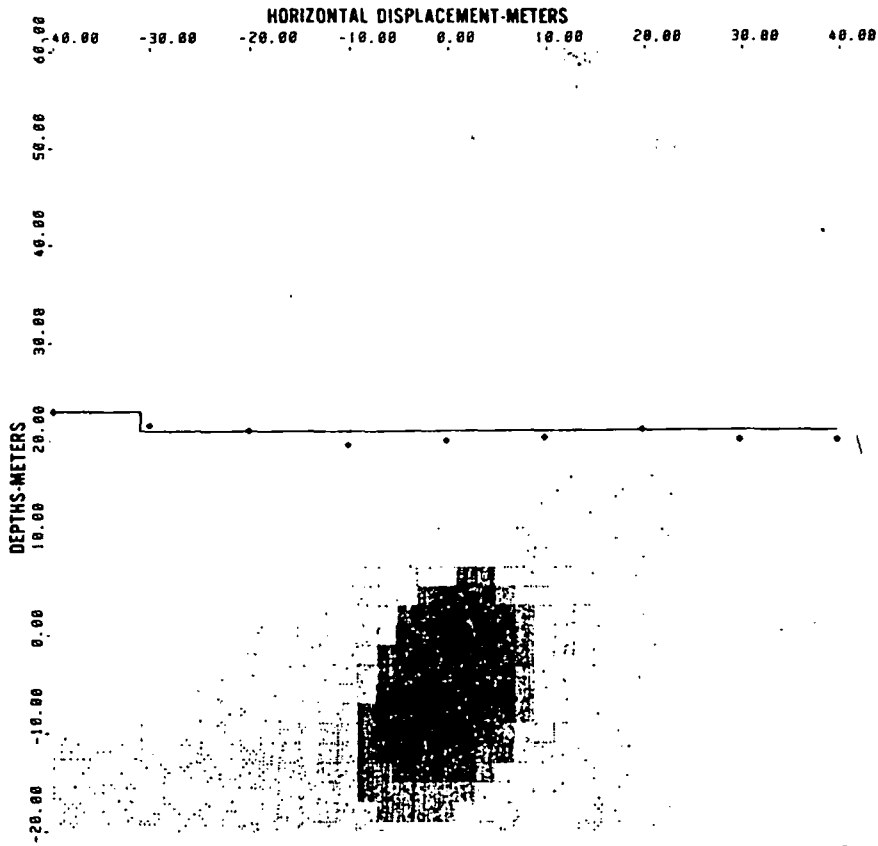
The performance capability of the resistivity technique is unusual in its threshold sensitivity to small localized targets. The system has successfully detected and located cavities having depth-to-diameter ratios in the range of about ten to one.

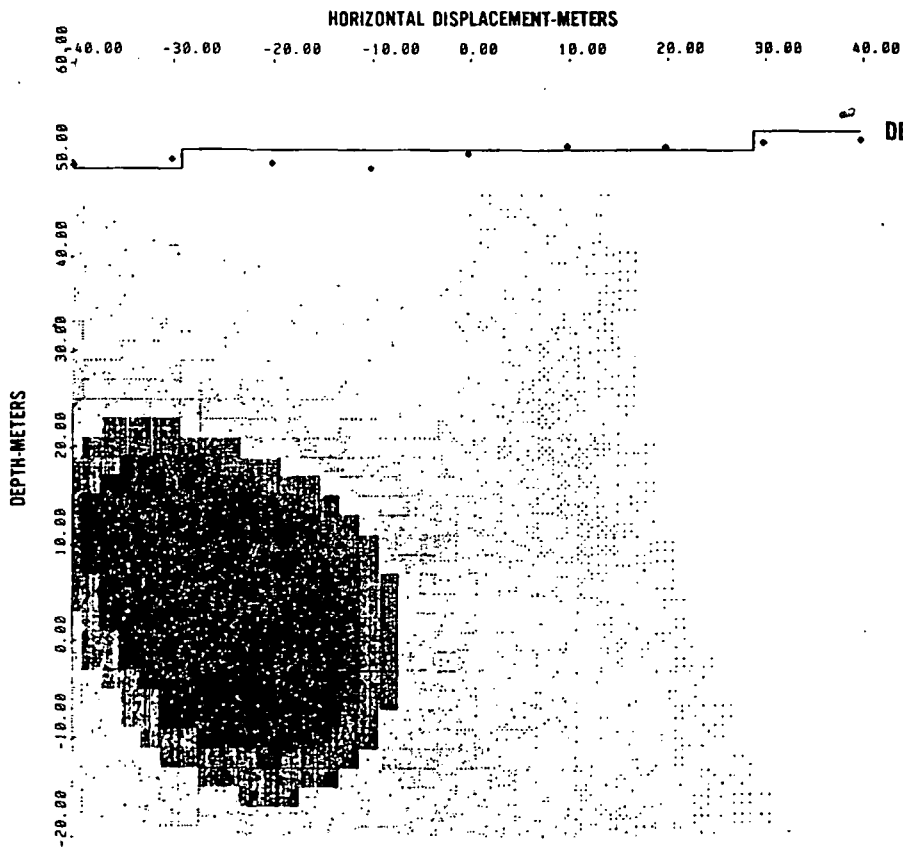
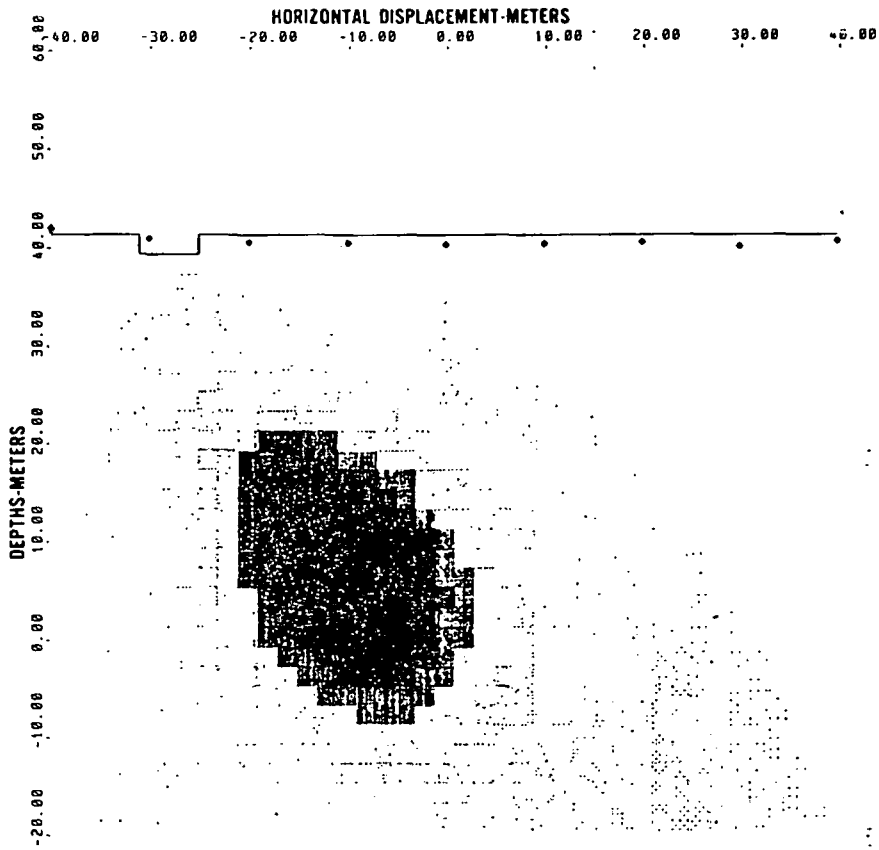
Performance of the hole-to-hole VHF electromagnetic system may be defined by the spatial resolution of the pulse waveform in the geologic medium and the typical limitations in hole-to-hole separation distance. The practical hole spacing used with the VHF electromagnetic system has ranged from a few meters to about 30 meters. In geologic materials having a relative dielectric constant of about nine, the nominal spatial dimension of the transmitter waveform is about one meter. This pulse length can provide a practical spatial resolution of about one-half meter in the processed results.

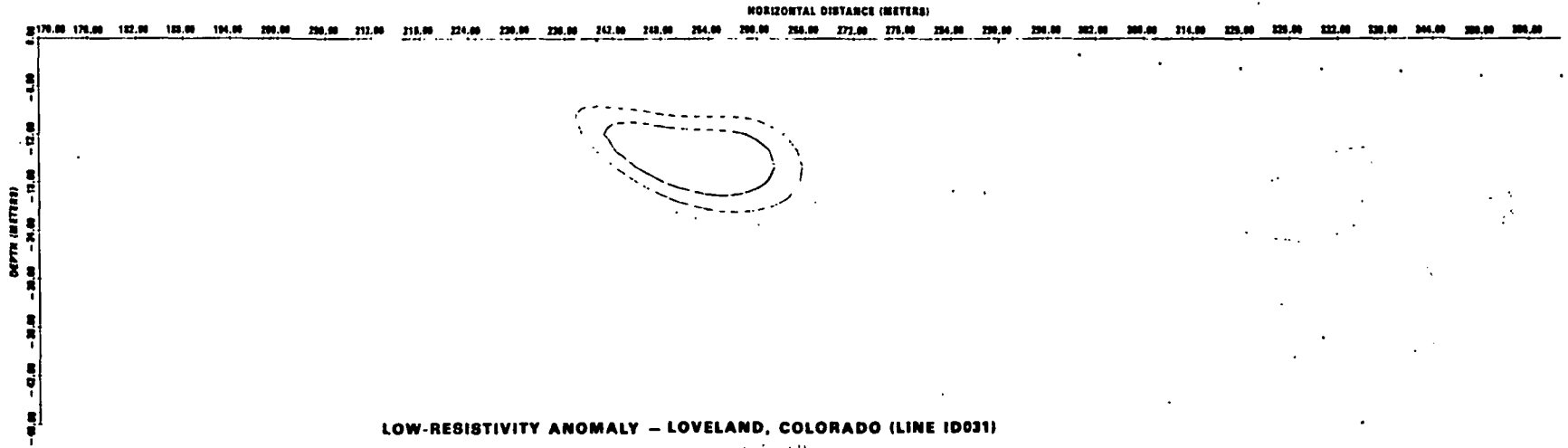
FIELD TEST RESULTS

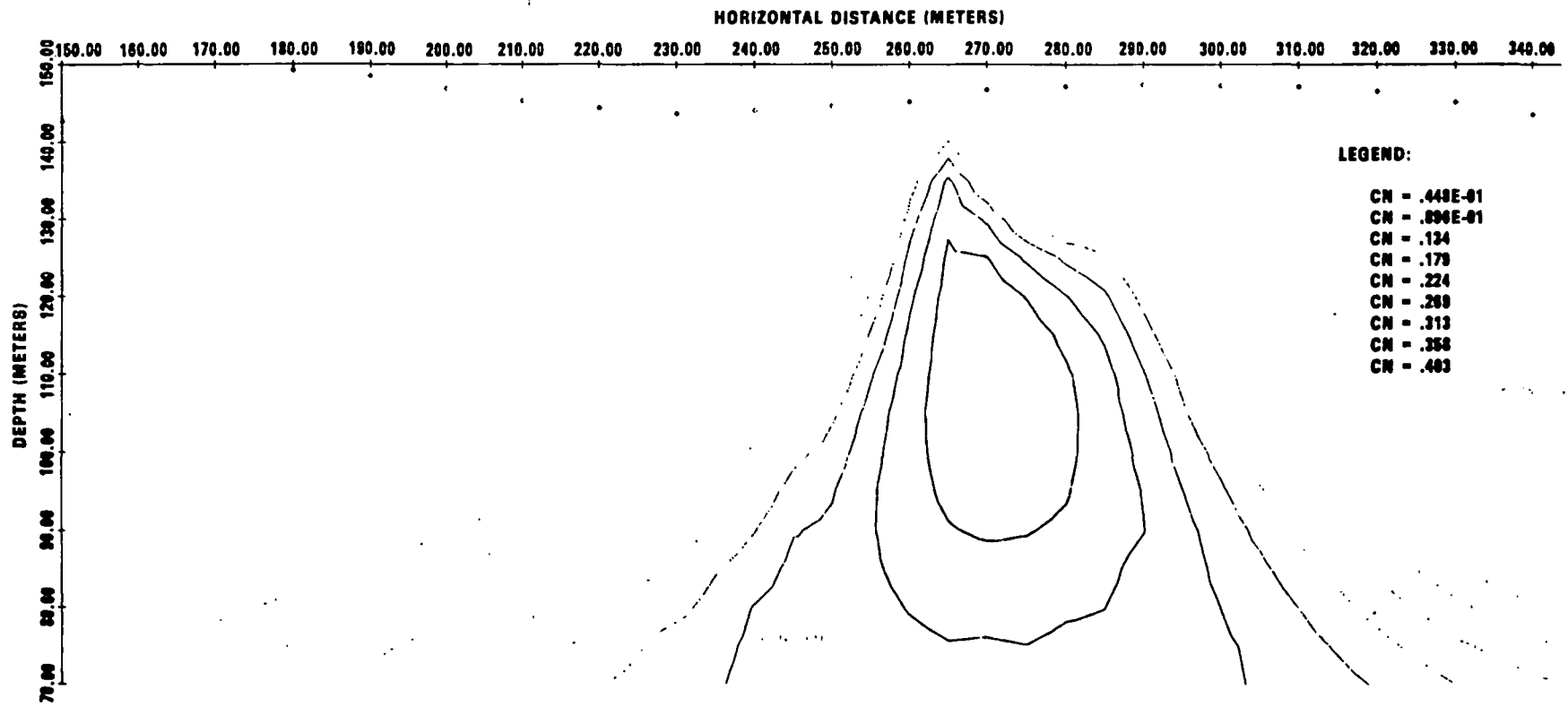
Field evaluation tests of the automatic earth resistivity system were first performed over two man-made aquaduct tunnels. The first of these sites was near Basalt, Colorado where the terrain was rocky and uneven granite covered by a thin layer of residual soil. This tunnel was approximately three meters in diameter and varied in depth below surface from about 20 meters to about 70 meters. The tunnel was dry during the tests. The tests at this site were successful in detecting the aquaduct at 20, 33, 40, and 50 meters, the deepest survey conducted at this site.

The second test site was a water-filled aquaduct near Loveland, Colorado. Surveys over this three-meter diameter tunnel were conducted at overburden thicknesses ranging from about 30 meters to about 50 meters. The water-filled tunnel and a deep surface soil deposit to the north of the tunnel offered low resistivity anomalies at this site. The low resistivity anomalies were detected at the correct horizontal locations, but in the case of the tunnel target, the derived anomaly was too shallow. This error in depth is believed to be caused by an increasing resistivity profile with depth. The computer analysis program is not designed to compensate for such resistivity gradients.

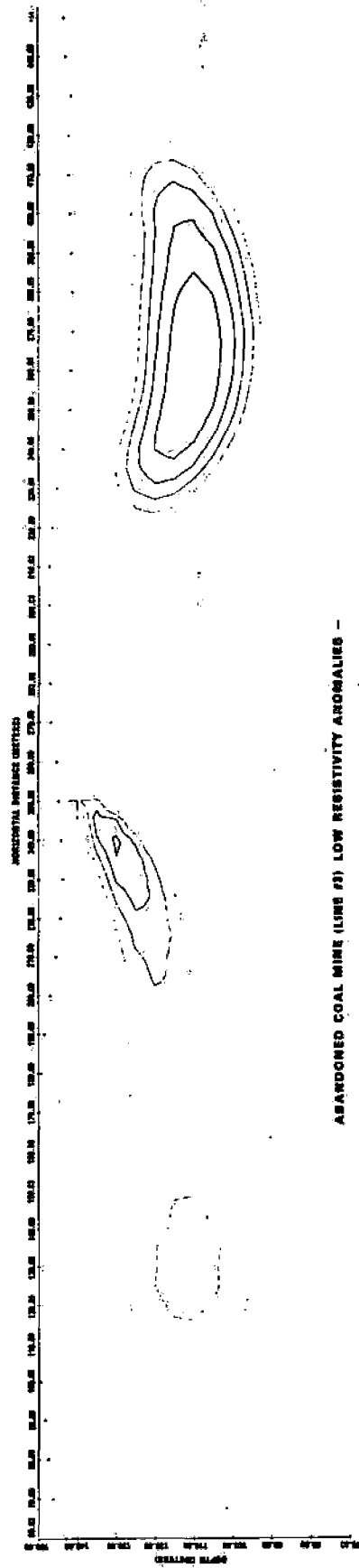


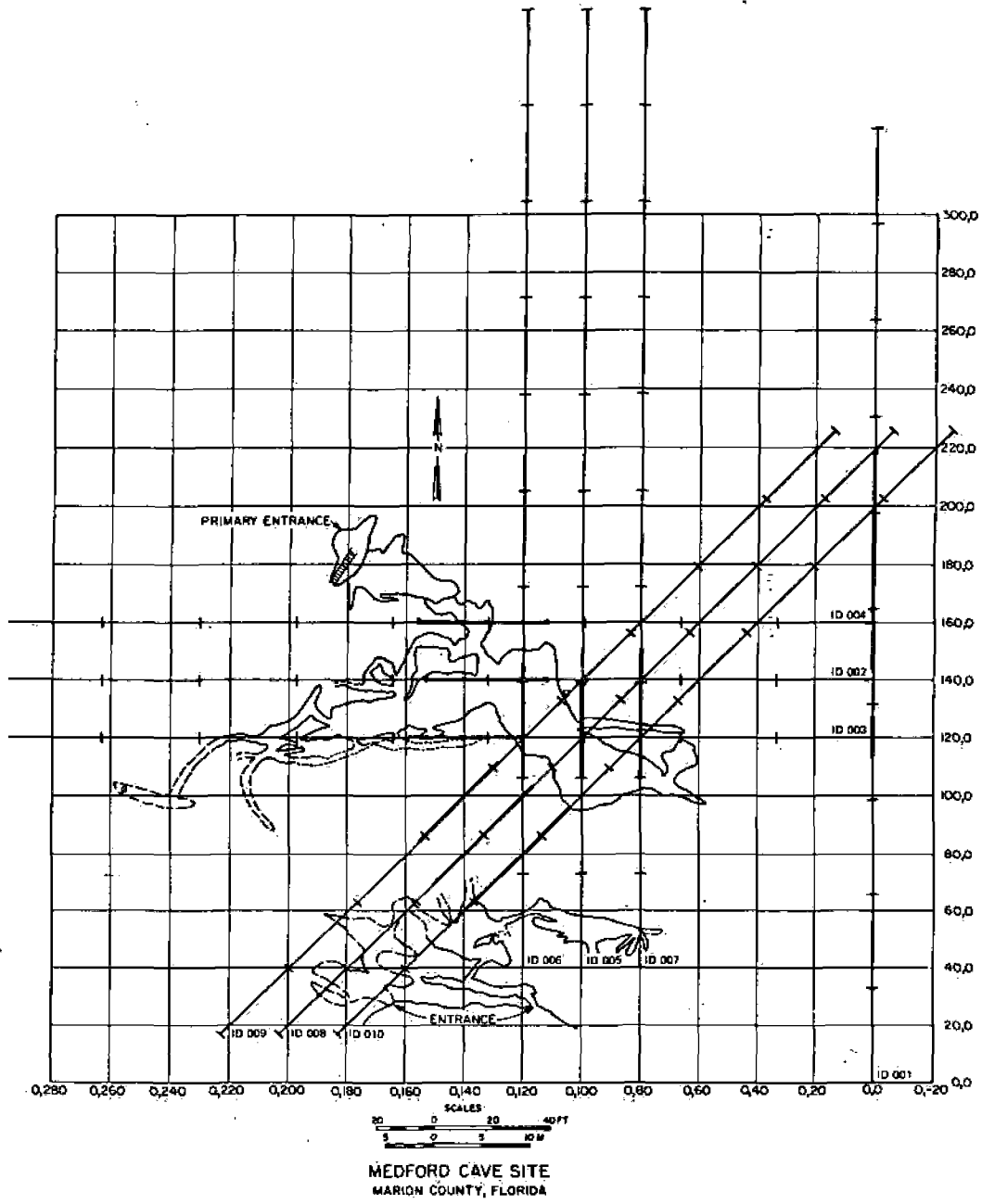




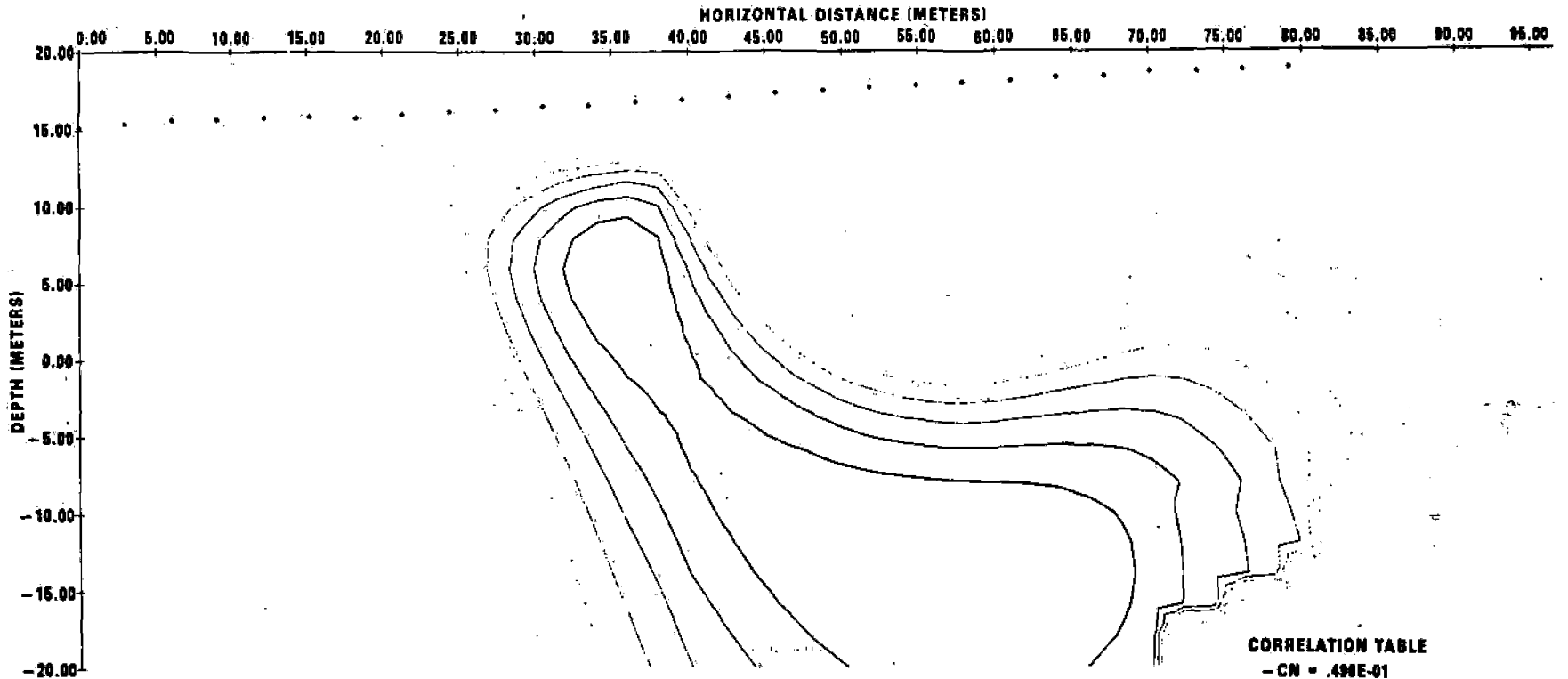


HIGH RESISTIVITY ANOMALY - COAL MINE ENTRY (LINE #3)





17

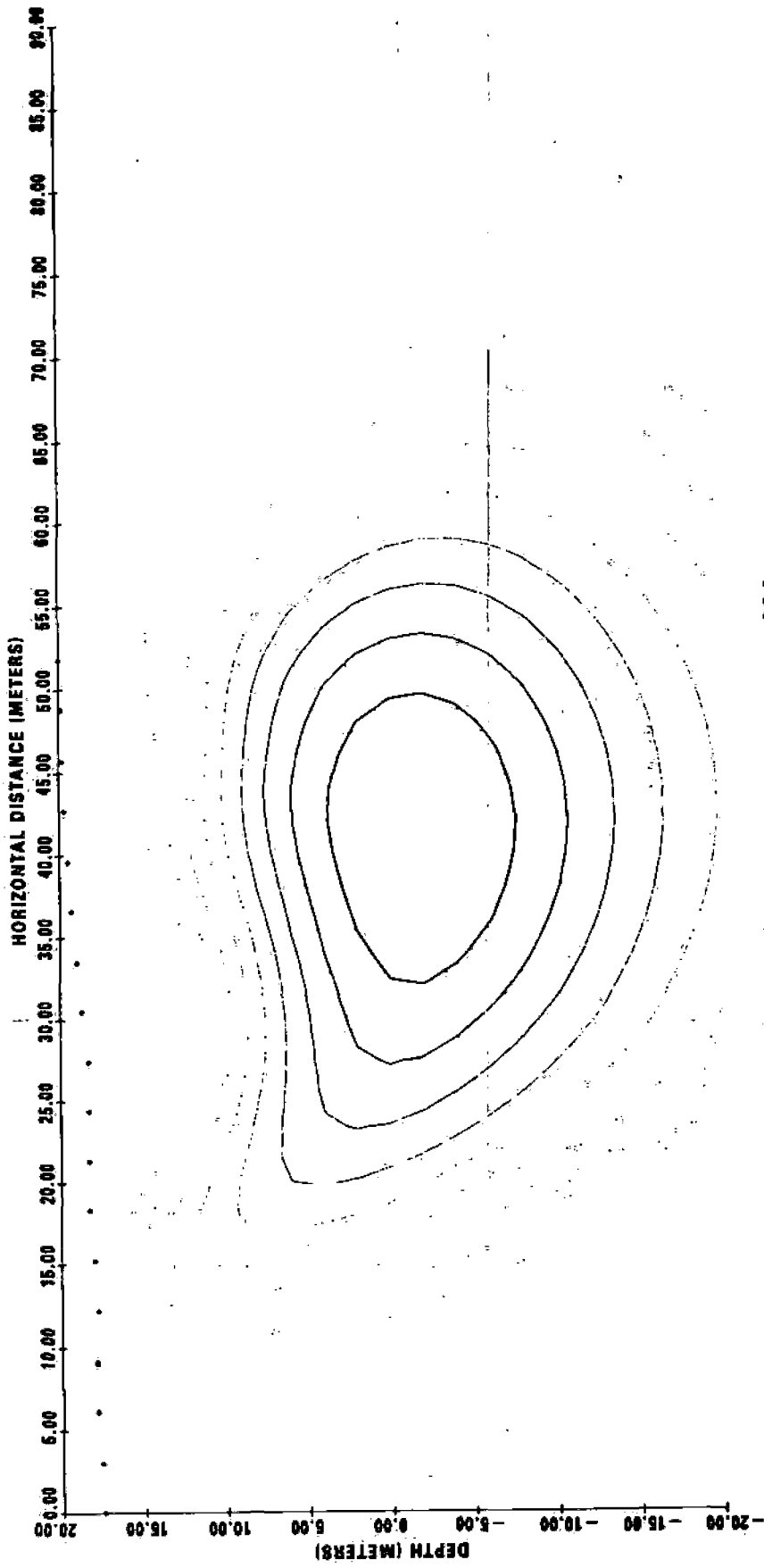


MEDFORD CAVE, FLORIDA — LINE ID-001

NOTE: DIMENSIONS ARE IN METERS. ZERO
ON VERTICAL SCALE IS CENTER OF ANOMALY.

CORRELATION TABLE

- CN = .498E-01
- CN = .991E-01
- CN = .149
- CN = .198
- CN = .248
- CN = .297
- CN = .347
- CN = .397
- CN = .448
- *CN IS CORRELATION NUMBER



MEDFORD CAVE, FLORIDA - LINE ID-004

18

A recent earth resistivity survey was conducted over an abandoned coal mine in Kentucky. The results of this survey accurately detected and located the air-filled main entry of the mine. The depth of this target was indicated to be only about half as deep as the real mine. The inaccurate target depth is a result of the irregular resistivity profile associated with the sedimentary geologic overburden structure at this site.

Low resistivity anomalies were also detected along the same survey traverse corresponding to a section of the mine known to be flooded.

Field surveys have recently been conducted at the Medford Cave near Gainesville, Florida where both the resistivity and hole-to-hole electromagnetic systems were evaluated.

Medford Cave is a limestone solution cavity underlying flat and clear terrain. The cave ranges in depth from about five meters to about 20 meters in the mapped areas. The rooms of the cave range in size from the largest at about three meters diameter by 20 meters long to narrow man-size passages and some passages too small to explore and map.

The high-resistivity anomaly detected along Line ID-001 indicates the presence of a cavity in the unmapped vicinity of the cave. Test borings carried out after the data analysis and target interpretation revealed a cavity at this anomaly.

The survey over a shallow section of the mapped cave along Line ID-004 is correct in horizontal location but is larger and deeper than the cave passage underlying the survey traverse. This error is attributed to the close lateral proximity of the large cave room located about ten meters south of the line.

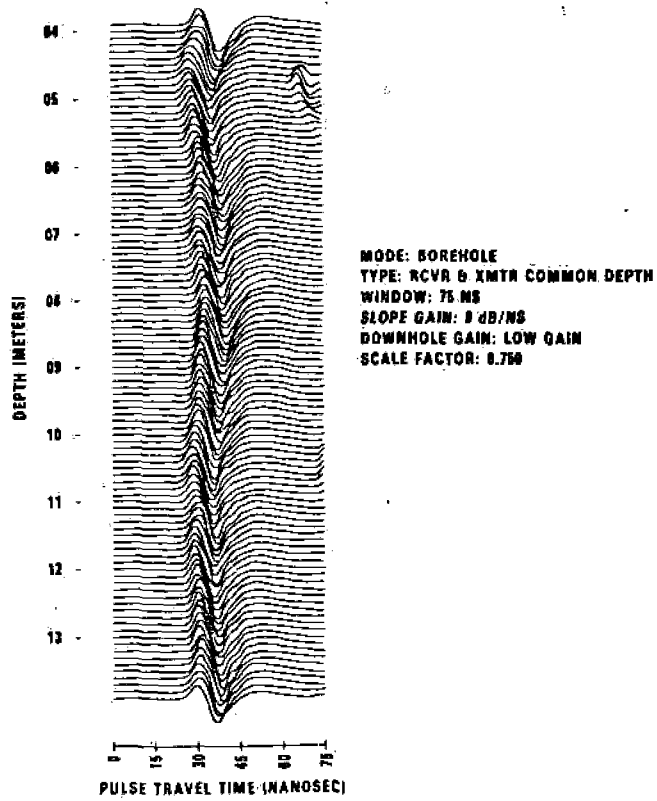
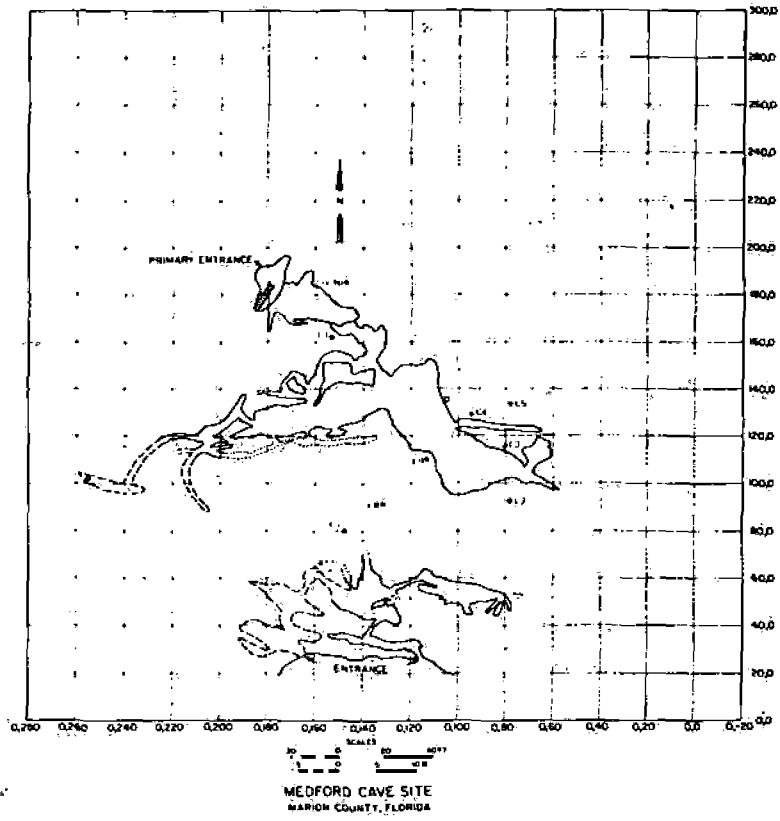
The hole-to-hole electromagnetic tests at Medford Cave gave strong verifications of the subsurface cavities. Tests between holes C4 and C5 show the general uniformity of the limestone rock structure where no cavities exist.

Tests between holes C5 and C3 indicate a small thin cavity at a depth of about seven meters below surface.

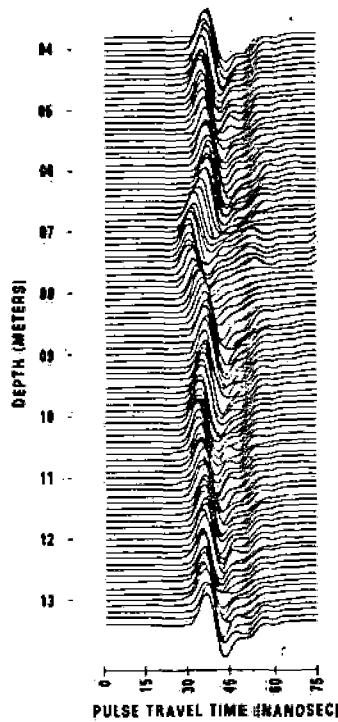
Tests between holes C2 and C3 show a larger room of the cave at a depth of about nine meters.

Tests between holes C2 and C5 show the combined effects of the two previous cavities as observed between two more widely spaced holes.

Tests between holes C4 and C8 show the hole-to-hole electromagnetic response to the main room of the cave as observed using holes spaced about 24 meters apart.

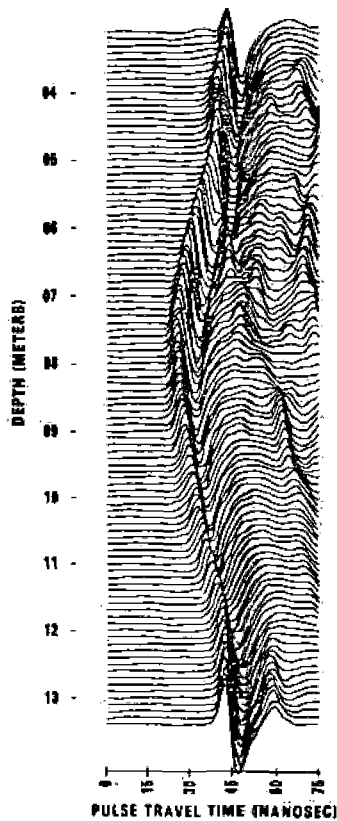


MEDFORD CAVE, FLORIDA
TEST HOLES C5 → C4



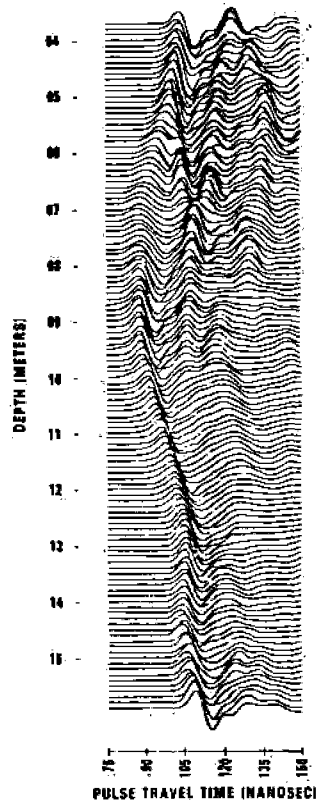
MODE: BOREHOLE
 TYPE: RCVR & XMTR COMMON DEPTH
 WINDOW: 75 NS
 SLOPE GAIN: 0.48/NS
 DOWNHOLE GAIN: LOW GAIN
 SCALE FACTOR: 1.000

**MEDFORD CAVE, FLORIDA — TEST
 HOLES C5→C3**



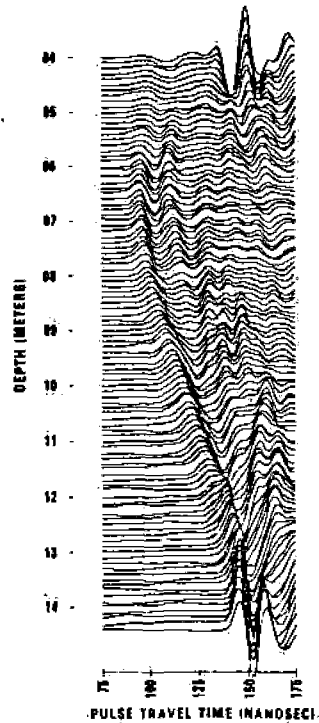
MODE: BOREHOLE
 TYPE: RCVR & XMTR COMMON DEPTH
 WINDOW: 75 NS
 SLOPE GAIN: 0.48/NS
 DOWNHOLE GAIN: LOW GAIN
 SCALE FACTOR: 0.750

**MEDFORD CAVE, FLORIDA
 TEST HOLES C2→C3**



MODE: BOREHOLE
 TYPE: RCVR @ XMTR COMMON DEPTH
 WINDOW: 75 NS
 SLOPE GAIN: 0 dB/MS
 DOWNHOLE GAIN: LOW GAIN
 SCALE FACTOR: 1.000

**MEDFORD CAVE, FLORIDA
 TEST HOLES C2→C5**



MODE: BOREHOLE
 TYPE: RCVR @ XMTR COMMON DEPTH
 WINDOW: 75 NS
 SLOPE GAIN: 0 dB/MS
 DOWNHOLE GAIN: LOW GAIN
 SCALE FACTOR: 1.000

**MEDFORD CAVE, FLORIDA
 TEST HOLES C4→C8**

CONCLUSIONS AND NEW POTENTIAL APPLICATIONS

The automatic pole-dipole earth resistivity technique has been demonstrated to perform well as a surface search method for detecting subsurface voids. As a companion system, the hole-to-hole electromagnetic technique has also proven to be effective in verifying the presence of voids suspected from such resistivity surveys. These methods have been successfully applied to problems of military interest, to highway subgrade stability problems caused by soil sink-holes, and to the location of natural cavities.

In addition to these applications, the resistivity and electromagnetic techniques are potentially useful in several other applications. Some of these new potential applications are: (1) monitoring of rubblization processes in block caving and in preparation of in situ oil shale retorts (EM method); (2) surface exploration for small localized mineral deposits (both methods); (3) detection of geologic anomalies other than voids (both methods); (4) mapping and/or monitoring of in situ coal gassification processes (both methods); (5) detection and mapping of salt dome flanks (EM method).

SUBJ
GPHYS
EM
Gnd
Void

WR1647

**SOCIETY OF
MINING ENGINEERS**

**UNIVERSITY OF UTAH
RESEARCH INSTITUTE
EARTH SCIENCE LAB.**

**OF
AIME**

CALLER NO. D, LITTLETON, COLORADO 80123

**PREPRINT
NUMBER**

81-89



USE OF AN AUTOMATIC EARTH RESISTIVITY SYSTEM FOR
DETECTION OF ABANDONED MINE WORKINGS

Wendell R. Peters
Senior Research Engineer

Department of Geosciences
Southwest Research Institute
San Antonio, Texas

Richard G. Burdick
PreMining Hazards Division

U.S. Bureau of Mines
Denver Research Center
Denver, Colorado

For presentation at the AIME Annual Meeting
Chicago, Illinois - February 22-26, 1981

Permission is hereby given to publish with appropriate acknowledgments, excerpts or summaries not to exceed one-fourth of the entire text of the paper. Permission to print in more extended form subsequent to publication by the Institute must be obtained from the Executive Secretary of the Society of Mining Engineers of AIME.

If and when this paper is published by the Society of Mining Engineers of AIME, it may embody certain changes made by agreement between the Technical Publications Committee and the author, so that the form in which it appears here is not necessarily that in which it may be published later.

These preprints are available for sale. Mail orders to PREPRINTS, Society of Mining Engineers, Caller No. D, Littleton, Colorado 80123.

PREPRINT AVAILABILITY LIST IS PUBLISHED PERIODICALLY IN
MINING ENGINEERING

Abstract. Shallow underground voids resulting from early coal mining and other resource recovery activities over the past several decades are now being recognized as a significant cause of ground subsidence problems. Uncertain knowledge of abandoned coal mines also imposes potential hazards in current mining operations since water inundation or the release of methane gas is a serious hazard when mine excavation operations break into an abandoned mine.

Requirements for detecting and mapping subversive man-made tunnels in previous work has led to the development of a surface-operated automatic earth resistivity survey system and associated computer data processing system for military applications. Field demonstration tests of this system have resulted in successful detection of tunnels at depth-to-diameter ratios greater than ten to one.

Under the sponsorship of the Bureau of Mines, a similar high-resolution earth resistivity system was designed and constructed for use as a potential means of detecting coal mine workings. The hardware and software aspects of the new system are described together with applications of the method to the survey and mapping of abandoned coal mine workings. Field tests are presented showing the detection of both air-filled and water-filled mine workings.

Introduction

Shallow underground voids resulting from early coal mining and other resource recovery activities over the past several decades are now being recognized as a significant cause of ground subsidence problems in developing areas. Over this period of time towns, cities, and highways have developed on top of many of these shallow mines areas and are continuing to expand without accurate knowledge of the existence or the locations of the potential subsidence hazards. Uncertain knowledge of abandoned coal mines also imposes potential hazards in coal excavation operations since water inundation or the release of methane gas can cause serious dangers when mining operations break into old workings.

Drilling methods offer a positive means of detecting shallow mining voids. However, because of the high density of test borings required and the relatively high cost of drilling services, drilling no longer offers an economically viable approach to void detection and mapping. Instead a more cost-effective alternate method is needed to detect shallow mined areas in order to simplify and minimize the drilling investigations required to delineate the subsurface extent of abandoned mines.

An early project demonstrated the effectiveness of earth resistivity survey techniques for detecting and locating shallow soil sinkholes and solution cavities in karst terrain. Subsurface anomalies of this type are common in the U.S. and frequently lead to ground subsidence and surface collapse. To investigate such potential subsidence problems along highways, an innovative approach to the surface remote sensing of air- and mud-filled cavities was investigated using a high-resolution earth resistivity survey technique. This method,

based upon a pole-dipole electrode array configuration using very closely spaced dimensions, was found to detect localized cavities at depth-to-diameter ratios of about ten to one. Further, the method employed a simple graphical analysis and interpretation method for locating the detected cavities in both position and depth along the survey path. Evaluation tests were conducted in Alabama and in Florida to demonstrate the ability to detect small cavities in soil and in shallow limestone rock at depths ranging from about ten feet to about eighty feet. These cavities were verified later by test borings which accurately confirmed their interpreted depth and approximate size and the fact that they were either air-filled (high resistivity) or mud-filled (low resistivity) anomalies.

More recent military requirements for an effective method for detecting and mapping relatively deep air-filled tunnels have resulted in an automatic earth resistivity survey system with computer-aided data processing and display. This system provides precision digital recording of field data from an array of pole-dipole electrodes which are automatically switched into operation along a predetermined survey traverse. Computer analysis of this data compensates for the effects of irregular surface terrain and compares the recorded field data with theoretical cavity target responses to selectively interpret and locate subsurface voids. Field tests conducted to demonstrate this system performance resulted in successful detection of tunnels in hard rock at depth-to-diameter ratios exceeding ten to one. With this high-resolution target detection capability and automatic system operation, earth resistivity surveys can be made with unprecedented accuracy and speed.

The digitally-operated system reduces the number of field personnel required to perform a high resolution survey and eliminates human errors in manually reading and recording the measured data.

Under the sponsorship of the Bureau of Mines, a similar system was constructed and field tests were conducted to demonstrate the ability to detect air-filled and water-filled abandoned coal mine workings in sedimentary geology. The site chosen to test the system was the Brown-Badgett, Inc., Busick Coal Mine near Central City, Kentucky. This mine offered a complex combination of both air-filled and water-filled targets at several depths.

Resistivity Techniques Used

Many electrical resistivity survey methods have been devised over the past 70 years. However, the measurement and analysis concepts for these methods are essentially the same. If an electrical current distribution is established within the earth, this current will generate a pattern of electrical potentials at the earth's surface dependent on the composition and structure of the subsurface. If the earth at the measurement site consists of homogeneous resistivity materials, the surface potentials will show a direct relationship with the apparent resistivity of the earth. For sites with horizontally layered materials exhibiting contrasting resistivities, the analysis predicting the electrical potentials

becomes more complicated, but the observed apparent resistivity consists of a composite representation of the separate layer resistivities at the site. If there is a void or other major discontinuity within the volume of earth materials being measured, a perturbation or anomaly in the measured apparent resistivity will result. These anomalies may be interpreted in terms of possible subsurface structure or materials differences.

In the case of subsurface voids, such as tunnels or abandoned mine workings, two cases must be considered. First, for an air-filled void the resistivity contrast is quite pronounced. The rock and its associated moisture will exhibit a much lower apparent resistivity than the air or gas in the void, which has an almost infinitely high resistivity. Therefore, the anomaly from this void will be quite strong and well defined. In the second case, that of a water-filled void, the water in the void may be from nearby rocks or from surface sources. For either source the water may have a resistivity which is close to that of the surrounding media. Thus, the resistivity contrast between the rock and the void may be relatively small and difficult to detect.

With the older resistivity survey techniques, the maximum depth to which an air-filled void could be detected was assumed to be about four times the diameter of the void. This was due to the large amount of host earth material in the measurement volume as compared with the volume of the void. This limited capability is obviously not applicable for detecting old mine voids as the void would have to be extremely large to be detectable at normal mining depths. For this reason, a technique developed by the English speleologist, Bristow using a pole-dipole array was modified for the purpose of detecting these mine voids. Figure 1 shows in a very general way the current flow and equipotential lines for the Wenner (typical of the older techniques) and the pole-dipole methods. For the Wenner method to respond to deeper anomalies, it is necessary to extend the electrode spacings. This results in a greater penetration depth, but also expands the effective measurement volume as the cube of depth. For the pole-dipole array to respond to deeper anomalies, it is necessary to increase the distance between the potential pair and the current electrode. The effective measurement volume also increases with depth with this method, but only fractionally as compared with the Wenner array. The Wenner array may be viewed as measuring the apparent resistivity of the complete volume for a hemisphere whereas the pole-dipole array measures the apparent resistivity of a small volume along the surface of the same hemisphere. Obviously, the same anomaly will appear much more pronounced with the pole-dipole method than with the Wenner. This relative manner of volumetric resistivity response is one of the reasons that the detection limit for abandoned workings has been increased in the high-resolution survey technique.

As seen in the Figure 1b, a void or other anomaly will be detected anywhere within the volume of the hemispherical shell. However, its location within this volume is indeterminate without the benefit of other information.

Therefore, a survey technique was developed to avoid this ambiguity. In essence, the method consists of utilizing a number of observations along each line and cross-correlating any anomalies encountered with one another to define the position of the void. This process is performed by the automated system and its associated computer programs. Figure 2 shows a simplified illustration of how the analysis may be done graphically. The resistivity anomaly position is located on the ground surface and an arc constructed using the current source electrode as the center. The various arcs associated with anomalies intersect at the probable location of the anomaly-causing void. This graphic method is a very simplified illustration of how the field data is processed by a computer assisted analysis program. The computer program presently in use compares the measured resistivity anomaly patterns with those predicted by a computer modeled anomaly void located at many hypothetical trial positions along the survey traverse. The most probable location of the actual target is identified as that location where the correlation between the experimental field data and the model data correlate to a maximum degree.

Instrumentation

The automatic pole-dipole earth resistivity survey system provides automatic current injection into the ground via a commutated sequence of current electrodes. The current sink electrode is remotely located at a distance five to ten times greater than the maximum target depth of interest. Figure 3 shows a conceptual sketch of the automatic resistivity data acquisition system. The primary equipment components are a digital system control unit, a cassette magnetic tape digital data recorder, a precision constant current power source, and a potential measuring module. In combination, this system automatically switches through the various current electrode positions and logs the resulting potential readings on tape. Field operator functions involve only the movement of the potential electrodes along the survey path at the appropriate data acquisition intervals. The power unit and data logger shown in the left of Figure 3 are set up in a central location such as in a tent or trailer. As many as 64 current electrodes are then connected to the constant current source through individual remote current control modules connected to a multi-conductor cable up to 640 meters long.

The current control modules are digitally addressable from the control unit as part of the automatic system operation. The earth potentials are measured by a gain-ranging, high-impedance preamplifier and are transmitted via a separate cable to the central control unit for digital recording on magnetic tape.

Magnetic tapes recorded in the field are processed to yield a cross-sectional image of resistivity anomalies underlying the survey line. The computer analysis program corrects the measured surface potentials for terrain elevation irregularities. In the program, an anomaly is assumed at some point along the survey line and the field data are cross-correlated with the

predicted response. A number (correlation coefficient) is generated which gives a measure of the match between the model predictions and measured data. The predicted anomaly is then moved to another location and the cross-correlation is again computed. This procedure is repeated until the entire survey line has been profiled. The results are plotted as a two-dimensional grid in a plane underlying the survey line. Resistance anomalies detected along the survey lines can be plotted in two forms of image patterns using either shade-of-gray or contours. Figure 4 shows a contour plot in which the contour line show the location of equal correlation coefficients for detected anomalies. Figure 5 shows a shade-of-gray plot in which the darkest shades of gray depict the location and depth of the highest probability for resistivity anomalies corresponding to the analysis model.

Field Test Results

Field evaluation tests of the automatic earth resistivity system were first performed on a water-filled aquaduct near Loveland, Colorado. Surveys over this three-meter diameter tunnel were conducted at overburden thicknesses ranging from about 20 meters to about 50 meters. The low resistivity anomalies associated with the water-filled aquaduct were for the most part detected at the correct horizontal locations but too shallow. Figure 4 is an example of the results of one line on this survey. The tunnel is located at a horizontal distance of 250 meters at a depth of 20 meters. The contour plot places the depth at about 15 meters. This error in depth is believed to be caused by an increasing resistivity profile with depth. The computer analysis program is not equipped at this time to compensate for an overburden of varying resistivity.

Another test of the system was conducted over a dry man-made tunnel near Basalt, Colorado. At that site the terrain was rocky and uneven with large granite outcroppings along the survey line. The tunnel was approximately three meters in diameter. Survey lines were selected to cross over the tunnel at overburden thicknesses of 20, 33, 40, and 50 meters. Figure 5 is the computer generated shade-of-gray plot for the 33 meter overburden scan. The tests at this site were successful in detecting the aquaduct at all depths. The shallowest overburdens resulted in highest accuracy for the detected anomalies.

A third controlled field test of the system was conducted over Medford Cave near Gainesville, Florida. This cave is a limestone solution cavity underlying flat and open terrain. The cave ranges in depth from about five meters to about twenty meters in the mapped areas. The rooms of the cave range in size from the largest at about three meters diameter by twenty meters long to narrow man-size passages and some passages too small to explore and map.

In most cases, computed anomalies for the Medford Cave were in close agreement with mapped portions of the cave. Figure 6 is a contour plot of a high resistivity anomaly where zero on the vertical scale is the center of the anomaly. On one line, a high-resistance

anomaly was detected in an unmapped area near the cave. Test borings carried out after the data analysis revealed a cavity at this anomaly. On another line over a shallow section of the mapped cave, a high-resistance anomaly was detected which was larger and deeper than the cave passage underlying the survey traverse. This error is attributed to the close lateral proximity of a large cave room located about ten meters to one side of the survey line.

Resistivity surveys were made over the Busick Coal Mine near Central City, Kentucky. The four lines surveyed were selected to examine the ability of the system to delineate water-filled and dry sections of the mine. The depth of the mine below the surface was approximately fifty meters. The results of the survey accurately detected and located the air-filled main entry of the mine located between 238 and 340 meters on the horizontal axis as seen in the contour plot of Figure 7. The depth of this target, however, was indicated to be only about half as deep as the real mine. The inaccurate target depth was a result of the layered resistivity profile associated with the sedimentary geologic overburden at this site.

Other features of the mine were detected with varying degrees of success. In the worst case, an air-filled section of the mine was overlain by an area where strip mine spoil had been placed. This site did not show any indication of a resistivity high as expected. This result is probably due to a water-saturated, low resistance layer lying near the bottom of the spoil area. This conducting layer appeared as a series of low resistivity anomalies in the computer generated display.

Future Research

During the 1981-1982 field seasons the Bureau of Mines plans more investigations in a variety of mining areas. These surveys will involve locating abandoned mines in a variety of geologic provinces to expand the experimental field data base. Areas planned at present include iron mines in northern Minnesota, coal mines in southern Illinois, northern Wyoming, and central Colorado, and solution voids in central Nebraska and subsidence problems in central Colorado.

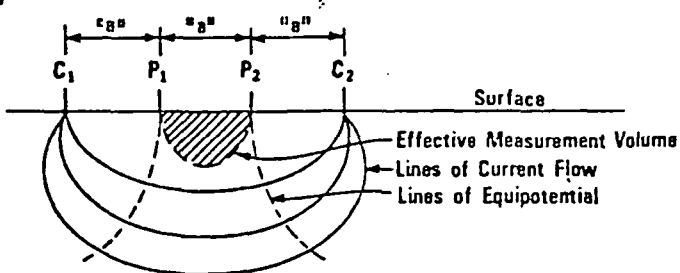
The idealized current flow lines shown in Figure 1 do not accurately portray the pattern when layered sedimentary rocks are encountered. When geologic layers of different resistivity are encountered as in coal mining areas, the current flow lines are warped and any interpretation assuming current distributions based upon homogeneous ground will be in error. The magnitude of the error depends on both the number of layers involved and the amount of resistivity variation between layers. Additional research is scheduled to develop a more accurate computer model for analyzing field data collected in sedimentary geology.

As mentioned previously this technique can work at depth to diameter ratios exceeding ten to one. This resolution means that at a 300 ft. depth (100M), a single void or cluster of voids such as a system of mine

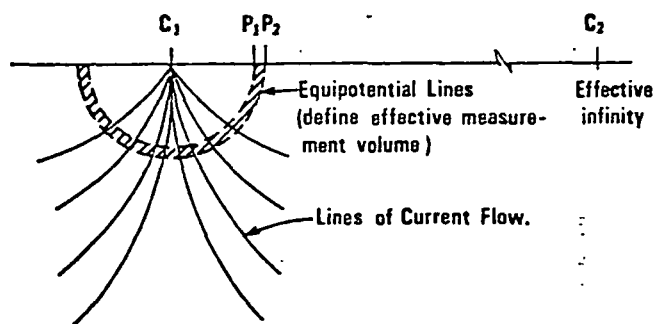
entries, must have an effective diameter of at least 20 ft. to be detected. At greater depths the diameter must be larger. Consideration is being given to developing a method of focusing the source current into the ground to increase the resolving power of the method. This will involve a considerable research effort, but if successful will render the technique more effective in locating voids to the greatest practical depth.

Conclusions

The automatic pole-dipole earth resistivity technique performs well as a surface method for detecting subsurface voids. The system has been applied to problems of military interest, to highway stability problems caused by soil sinkholes, to abandoned coal mines, and to the location of natural cavities. In most of the field test results obtained to date, resistivity highs and lows were interpreted in good correlation with known air-filled and water-filled voids. Horizontal position of the anomaly along the survey line is in general more accurate than the corresponding depth indications. Most of the errors encountered in the surveys are due to the electrical inhomogeneity of the ground. To improve the accuracy, further work is needed to modify and adapt the software data reduction method to account for the effects of layered rock above the targets, multiple entry targets, and targets of complex geometrical shapes, such as room and pillar sections.



a.) Wenner Array Method



b.) Pole-Dipole

FIGURE 1. EQUIPOTENTIAL LINES AND CURRENT LINES FOR THE WENNER AND POLE-DIPOLE ARRAYS

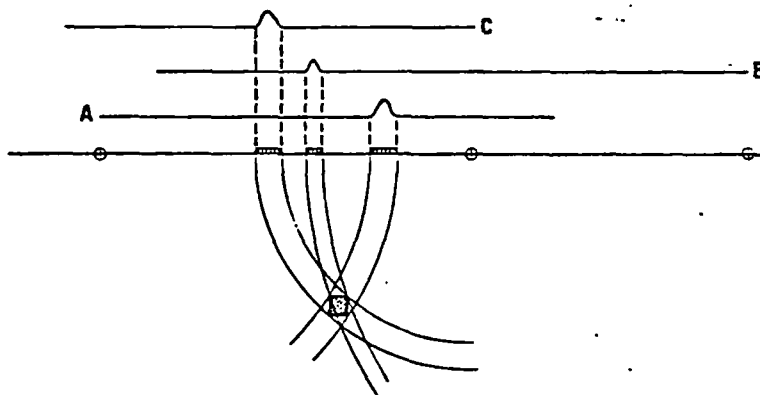


FIGURE 2. EXAMPLE SHOWING GRAPHICAL METHOD FOR LOCATING A RESISTIVITY ANOMALY

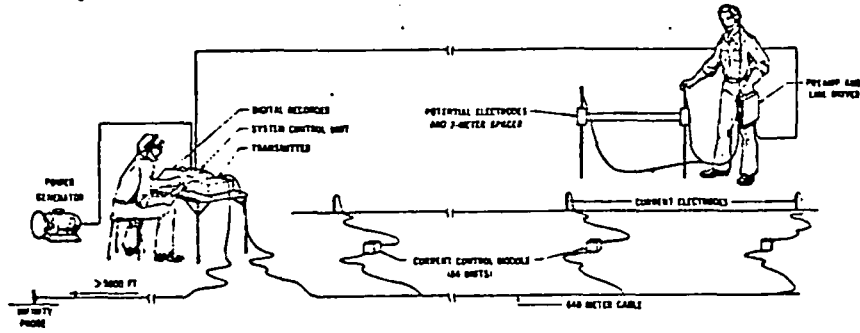


FIGURE 3. CONCEPTUAL DIAGRAM OF THE EARTH RESISTIVITY DATA ACQUISITION SYSTEM

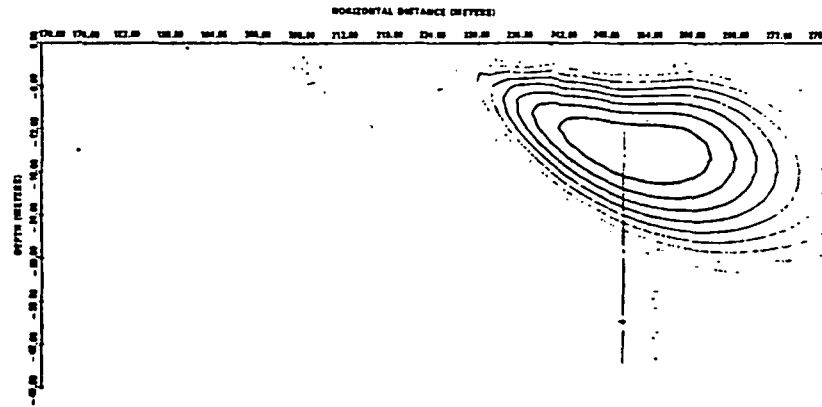


FIGURE 4. CONTOUR PLOT OF A LOW-RESISTIVITY ANOMALY DETECTED ABOVE A 20 METER DEEP AQUEDUCT NEAR LOVELAND, COLORADO

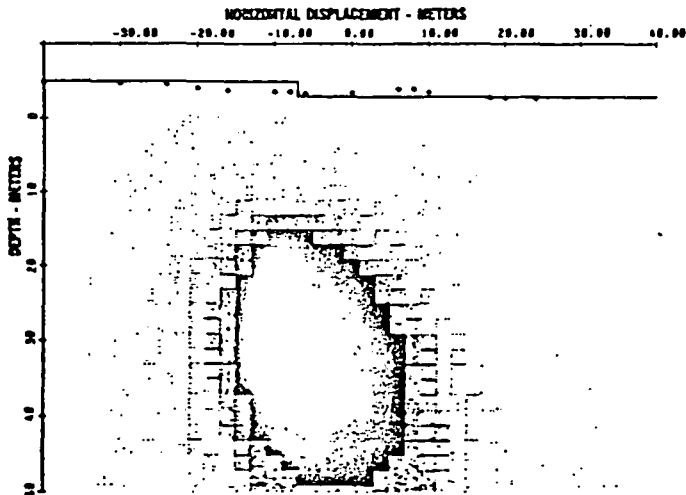


FIGURE 5. SHADES-OF-GRAY PLOT OF A HIGH-RESISTIVITY ANOMALY DETECTED ABOVE A 33 METER DEEP DRY TUNNEL NEAR BASALT, COLORADO

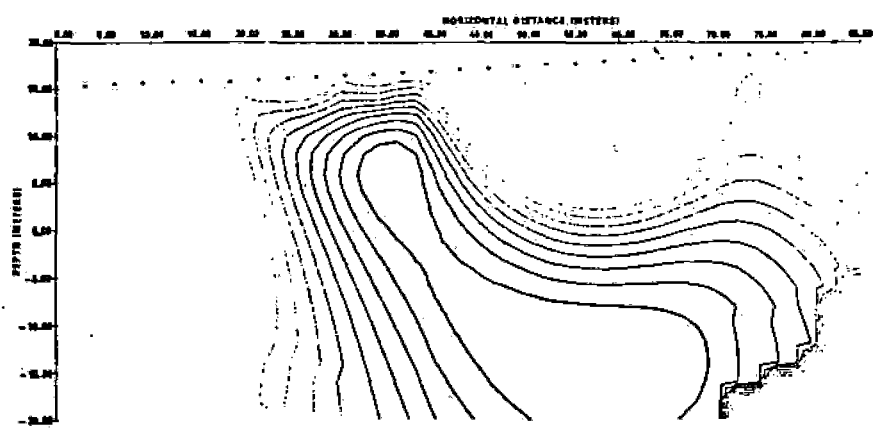


FIGURE 6. CONTOUR PLOT OF A HIGH-RESISTIVITY ANOMALY DETECTED ABOVE THE MEDFORD CAVE

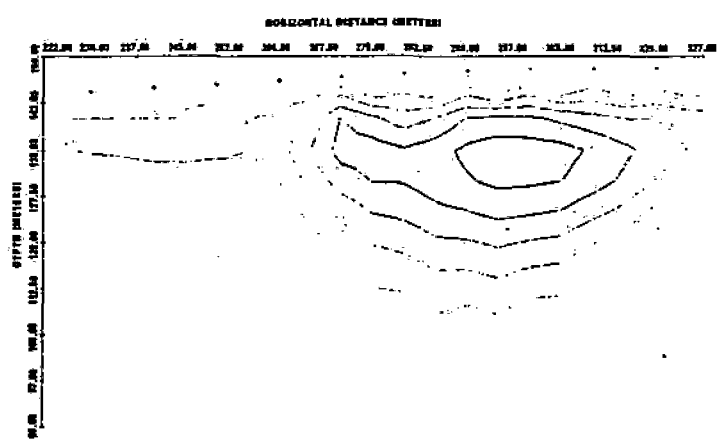


FIGURE 7. CONTOUR PLOT OF THE HIGH-RESISTIVITY ANOMALY DETECTED NEAR THE AIR-FILLED MAIN ENTRY OF A COAL MINE WITH A 50 METER OVERBURDEN

Electrical Parameters for Clay Samples in the Frequency and Temperature Dependence (First Results)

UNIVERSITY OF UTAH
RESEARCH INSTITUTE
EARTH SCIENCE LAB.

GIOVANNI FINZI-CONTINI * AND SERBAN VELICIU **

ABSTRACT

In this work some results are given referring to laboratory experiments carried out on clay samples in the ranges $1 \cdot 10^{-2}$ - $5 \cdot 10^3$ Hz and 20° - 100° C. The diagrams of conductivity, permittivity and loss-tangent have been obtained, and certain anomalies can be recognized in them.

Introduction

In the sphere of a series of researches on the temperature behaviour of rocks found in geothermal areas, it seemed useful to examine the behaviour of the clays; these rocks are of considerable interest to geothermal prospecting in different regions and in Italy in particular, as these clays generally form the cover rock in geothermal fields. Another determinant factor which has promoted this research on clays is their classic behaviour in a thermal regime.

This work was carried out within the sphere of the scientific activity sponsored by UNESCO: one of the authors (VELICIU) spent a training period at the Geophysical Observatory of Siena University during his International Post-Graduate Course in Geothermics at the International Institute for Geothermal Research, Pisa, Italy.

So far many studies have been carried out on the frequency dependence of conductivity, permittivity and loss-tangent of rock samples (FULLER, WARD 1970; COLLETT, KATSUBE 1973; KATSUBE, COLLETT 1973; KATSUBE ET AL. 1973; NENCINI 1973; CHELIDZE, CHELIDZE 1963; VAN KEYMEULEN, DEKEYSER 1957; DOSTOVALOV 1947; KEEVIL, WARD 1962). Among these studies, laboratory measurements which also involve the effect of other parameters (e.g. water content, temperature, electrolyte activity) are of great interest to surface geophysical techniques (CHELIDZE, CHELIDZE 1963; VAN KEYMEULEN, DEKEYSER 1957; DOSTOVALOV 1947; KEEVIL, WARD 1962). This paper tries to contribute to the knowledge of electrical properties of clay samples, in the induced polarization (IP) frequency dependence in particular (FULLER, WARD 1970; CHELIDZE, CHELIDZE 1963; VAN KEYMEULEN, DEKEYSER 1957; DOSTOVALOV 1947).

In our program of experiments a special electric measuring system was assembled for the collection of data on the electrical properties of samples in the frequency range from $1 \cdot 10^{-2}$ to $5 \cdot 10^3$ Hz, whereas a suitable device was set up to study temperature effects between 20° and 100° C. The accuracy of each apparatus was carefully checked and the results of the measurements obtained indicated some interesting aspects with regard to the trends of the electrical properties studied in our rock samples (Pliocenic clays of the Siena region).

Electrical parameters

The parameters that define the electrical characteristics of a rock are conductivity σ , permittivity ϵ and consequently loss-tangent $\tan \delta$ (COLLETT 1959; PARKHOMENKO 1967). If the potential difference ΔV is applied to a medium, that is, in our case to a rock specimen, in general both the loss current i_σ and the displacement current i_ϵ flow through it: for this reason, conductivity and permittivity are the two major electrical parameters of the rocks. They can easily be calculated for samples of regular geometrical form, when properly energized (PARKHOMENKO 1967, pp. 80-83). The ratio of the loss to the displacement current gives the loss-tangent (or dissipation factor)

$$\tan \delta = \frac{i_\sigma}{i_\epsilon} = \frac{\partial \Delta V}{\omega \epsilon \Delta V} \frac{k}{k} = \frac{\sigma}{\omega \epsilon}$$

where $\omega = 2\pi f$, f being the frequency, and k is a geometrical factor.

It is widely accepted (KELLER, FRISCHKNECHT 1966; PARASNIS 1966; MADDEN 1967), that in the low frequency range, particularly below 10^3 Hz, electrochemical polarization effects become important; they are closely related to the content of moisture in the rocks. This type of frequency dependent behaviour in certain rocks, as in clays, for instance, has been termed membrane IP (MARSHALL, MADDEN 1959): some information follows on this subject.

It is generally supposed that a diffuse cloud of cations is characteristic of clay-electrolyte systems (KELLER, FRISCHKNECHT 1966, Fig. 261; FRASER ET AL.

* Director, Osservatorio Geofisico, Università di Siena, Siena, Italy.

** Institutul de Geofizica Aplicata, Str. Izvor 78, Bucuresti, Romania.

1971, Fig. 4). On application of an electric potential, positive-charge carriers easily pass through the cationic cloud, but negative-charge carriers pile up. Therefore, something similar to an ion-selective membrane exists, which causes a decrease in the anion mobility, owing to the model summarized above. This reduction in mobility is most effective for electrical potential variations which are low (e.g., frequencies under 0.1 Hz), with respect to the diffusion times of the anions between adjacent membrane-zones. On the other hand, the mobility of the anions is not very greatly affected when the potential variations are fast (e.g., frequencies above 1000 Hz). With reference to this model, it must be added that the motion of the electric charge carriers is also influenced by the temperature. For instance, it is well-known that the higher the temperature, the lower the water viscosity. Consequently, the mobilities of the electric-charge carriers also increase. A schematic quantitative approach to this problem was attempted (FINZI-CONTINI 1971), introducing the concept of Theoretical Complex Mobility (TCM) and suggesting expressions for rock specific admittance for simulating membrane polarizing rocks (FINZI-CONTINI ET AL. 1972a; FINZI-CONTINI ET AL. 1972b).

Electric measuring system

The research aspect of our laboratory measurements was concerned with determining conductivity, permittivity and loss-tangent. The work performed during this laboratory activity referred in particular to three samples of clay found near Siena (Italy). In order to keep the humidity content in these samples appreciably equal to the actual content they had « in situ », our specimens were sealed up immediately after sampling until they were subjected to the experiments.

The main admittance measuring system (FINZI-CONTINI 1972; FINZI-CONTINI ET AL. in prep.) basically consisted of a sine function generator with frequency range from $5 \cdot 10^{-1}$ to $5 \cdot 10^3$ Hz, two amplifiers and an oscilloscope: a block diagram of this system is reproduced in Figure 1; the other apparatus used are also shown. The data for calculating admittance were determined by voltage and current measurements on the screen of the scope. It must be emphasized that for the lower frequencies (i.e., less than $1 \cdot 10^3$ Hz), as it was difficult to follow the spot on the screen, pictures were taken by means of a Polaroid Camera System; see for instance Figure 2, which shows a Lissajous' figure set.

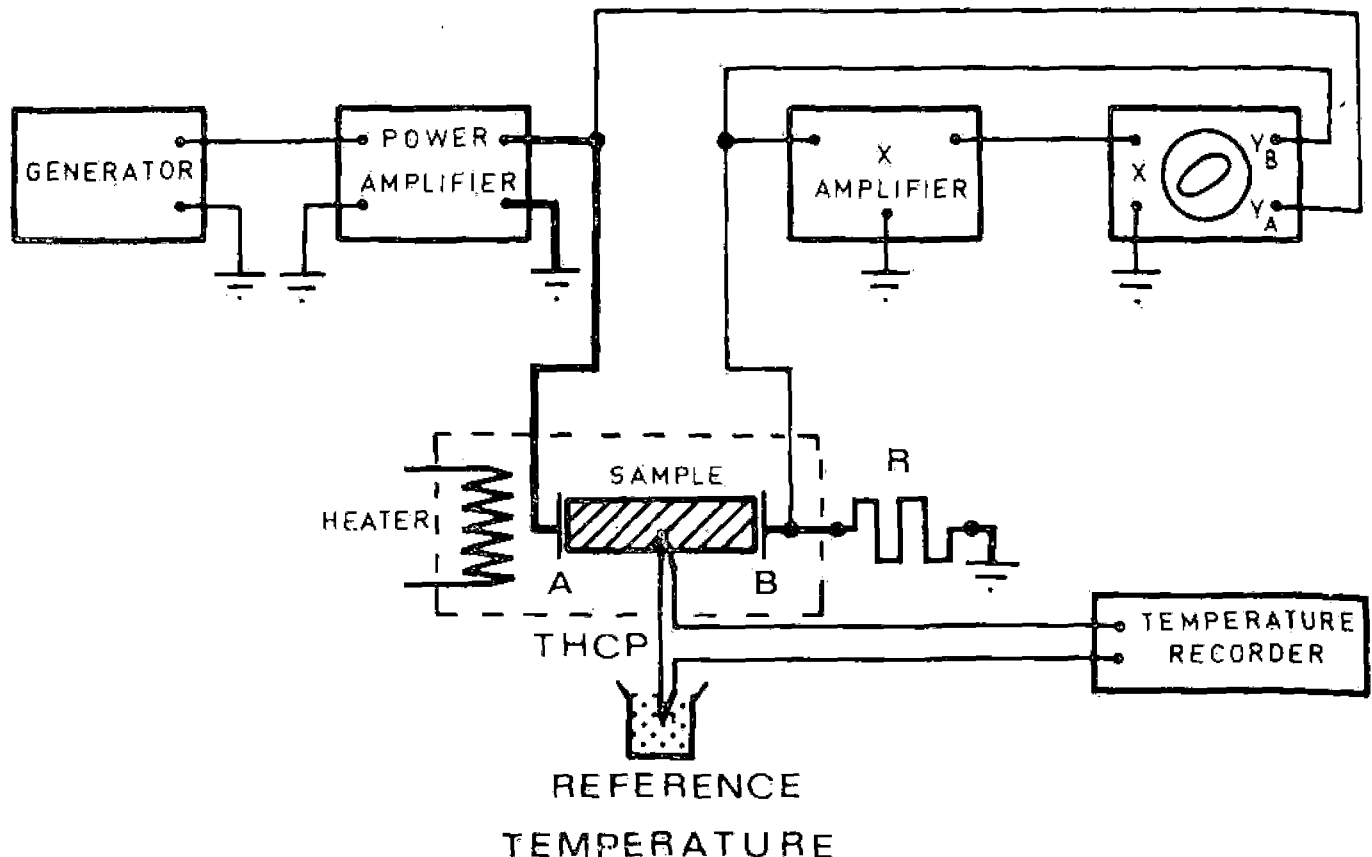


FIG. 1. — A simplified block diagram of the measuring system. One can see the sample, energized by the generator via a power amplifier, the ohmic resistance R being in series to the sample circuit (heavy lines). The R voltage difference, proportional to the sample current, is applied to the scope x-axis, after due amplification, whereas the scope y-axis receives the voltage difference signal between A and B, measured with respect to a suitable point. A and B electrodes work without copper sulphate solution in order to avoid clay poisoning. In this Figure the heater as well as the thermocouple THCP are schematized.

As an accessory equipment for heating our specimens from 20° to 100°C a thermostatic furnace was used, which is able to keep the temperature constant within $\pm 0.5^\circ\text{C}$. Moreover, in a very small hole drilled

in every specimen, a thermocouple was introduced, connected to a recording system. This ensured that steady thermal conditions were reached. During our measurements each sample was housed in a sample-holder, which was immersed in a bath containing a mineral oil with high insulating properties. This bath was placed inside our furnace, suitably housing all the described sample equipment.

By this technique we attempted 1) to limit the water content losses during heating, 2) to ensure the thermal stability of the sample and 3) to permit recognition of thermal equilibrium in the sample's interior, according to the thermocouple data. To give an idea of certain dimensions, we might add that our samples were of cylindrical shape (50 mm long and 23 mm diameter), the current densities being within the range $2.6 \cdot 10^{-1} \text{ A/cm}^2$

Typical results

A selection of our experimental data is shown in Figures 3, 4, and 5; it can be added that the Lissajous' figures pointed out the existence of anomalous non-linear phenomena for frequencies between 10^{-2} and about 1 Hz, as shown in Figure 2. It is to be noted that the conductivity diagrams, Figure 3, exhibit anomalies between 50°-60°C; a typical result can also be seen in the loss-tangent diagrams versus temperature and for different frequency values, Figure 5: it must be noted that the maxima obtained above 50 Hz are located near the above temperature interval. Other interesting data for $\tan \delta$ have been obtained for measurements at 100°C above about 10 Hz.

These experimental results suggest the existence of a connection between electric and thermodynamic phenomena, linked to the presence of water in clay rocks: one might also be induced to suppose that the movement of electric charge carriers in the adopted media are strongly affected by heating in the conditions under study.

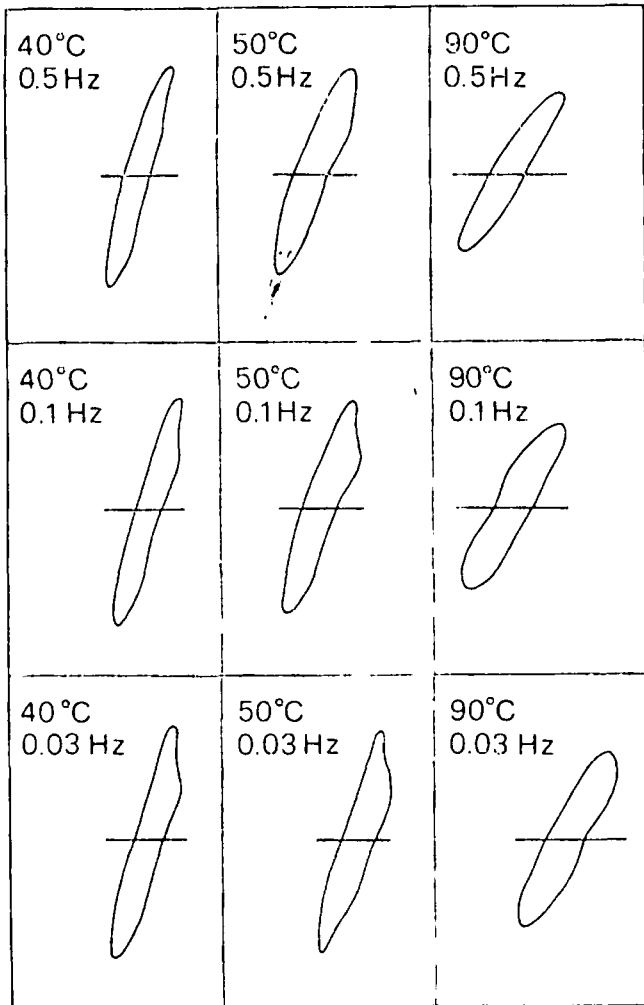


FIG. 2. — A selected set of Lissajous' curves obtained for sample No. 2 for a number of comparable energizing situations. Anomalous non-linear phenomena appear more evident when frequency and temperature decrease.

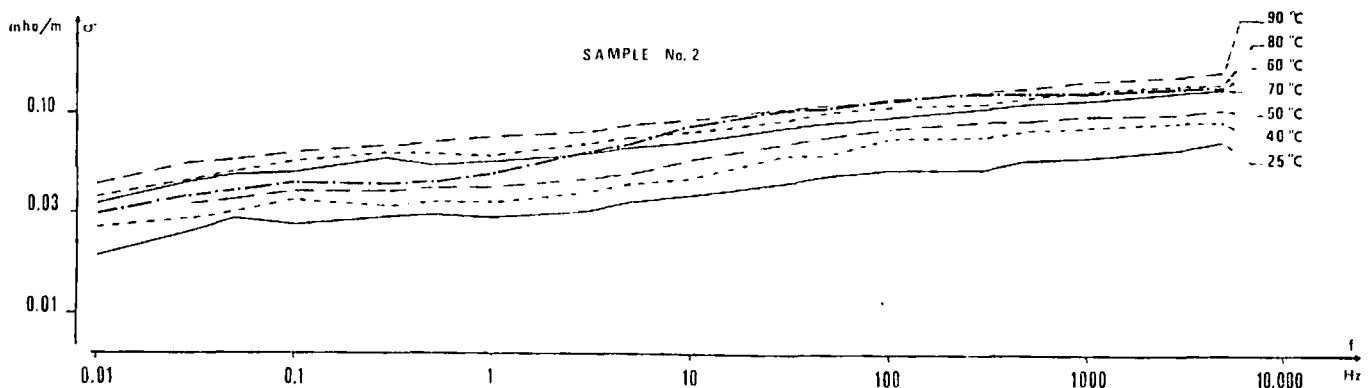


FIG. 3. — The conductivity diagrams for sample No. 2. One notes that these trends are individually in agreement with classical theories (PARKHOMENKO 1967, p. 193, and its consequences), while the 60°C diagram (heavy, dashed-and-dotted line) clearly exhibits an anomalous trend with regard to the others.

It seems opportune to mention that other physical properties of clays, such as interlayer absorption of water (VAN OLPHEN 1969) and results of thermodynamic experiments on ion-exchange equilibrium (VAN BLADER, MENZEL 1969), as well as differential thermal analysis on clay minerals (KODOMA, SCHNITZER 1969), appear able to give measurable responses right in our temperature interval.

It appears not so easy now to explain in which way all these measurements can be linked together and framed theoretically. In the next section possible future

trends of our work towards studying this argument will be sketched.

Conclusions and possible research trends

This first research of ours on the electric behaviour of clay samples carried out in temperature and frequency dependence has already brought to light some not so obvious aspects of this problem.

These first results obtained indicate, for our clay samples, such behaviour in the low-frequency domain and versus temperature, which can be considered par-

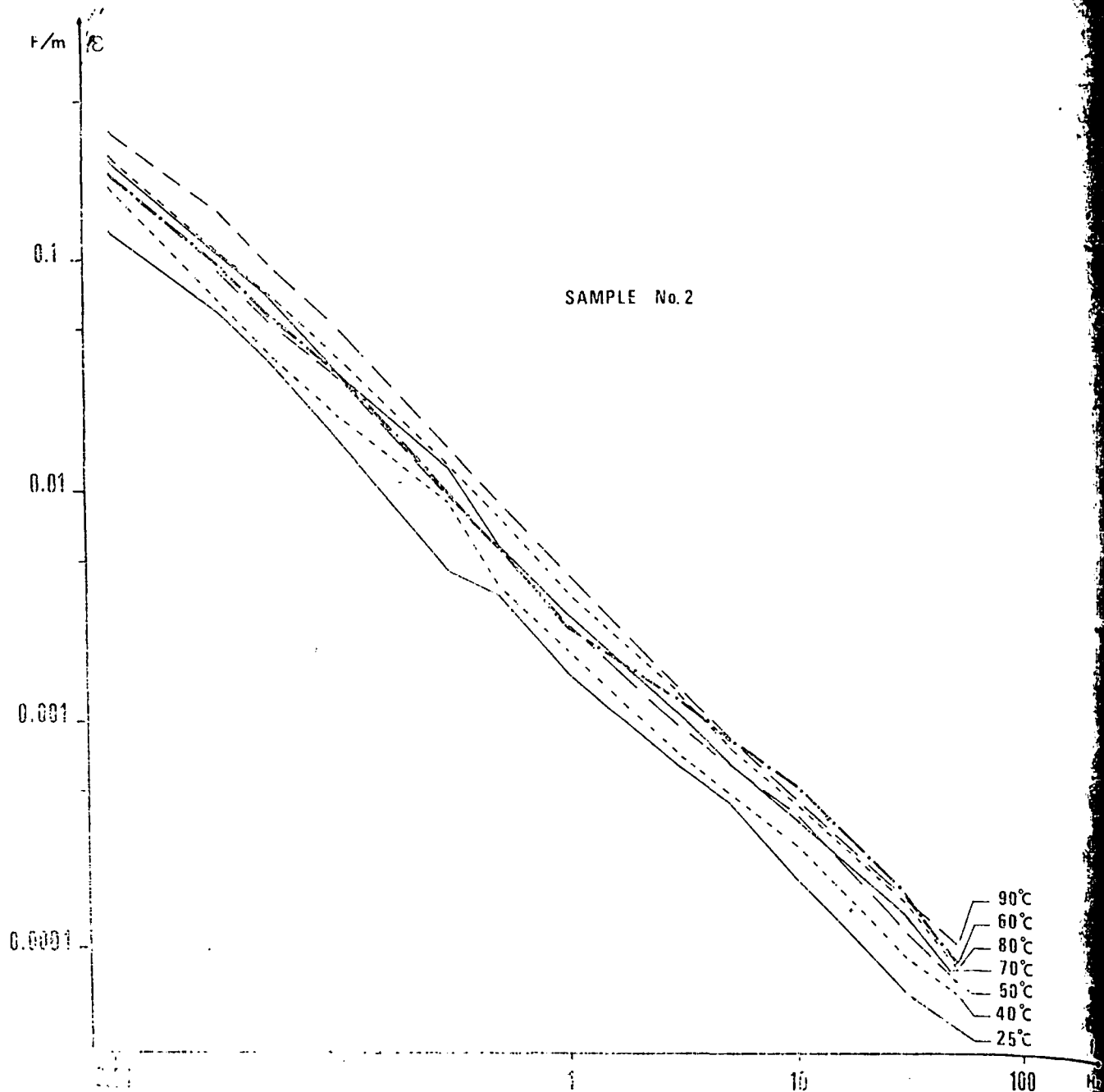


FIG. 4. — The permittivity diagrams for sample No. 2. One notes that these trends are individually in agreement with classical theories (PARKHOMENKO 1967, p. 193), whereas the 60°C diagram (heavy, dashed-and-dotted line) clearly exhibits an anomalous trend with regard to the others.

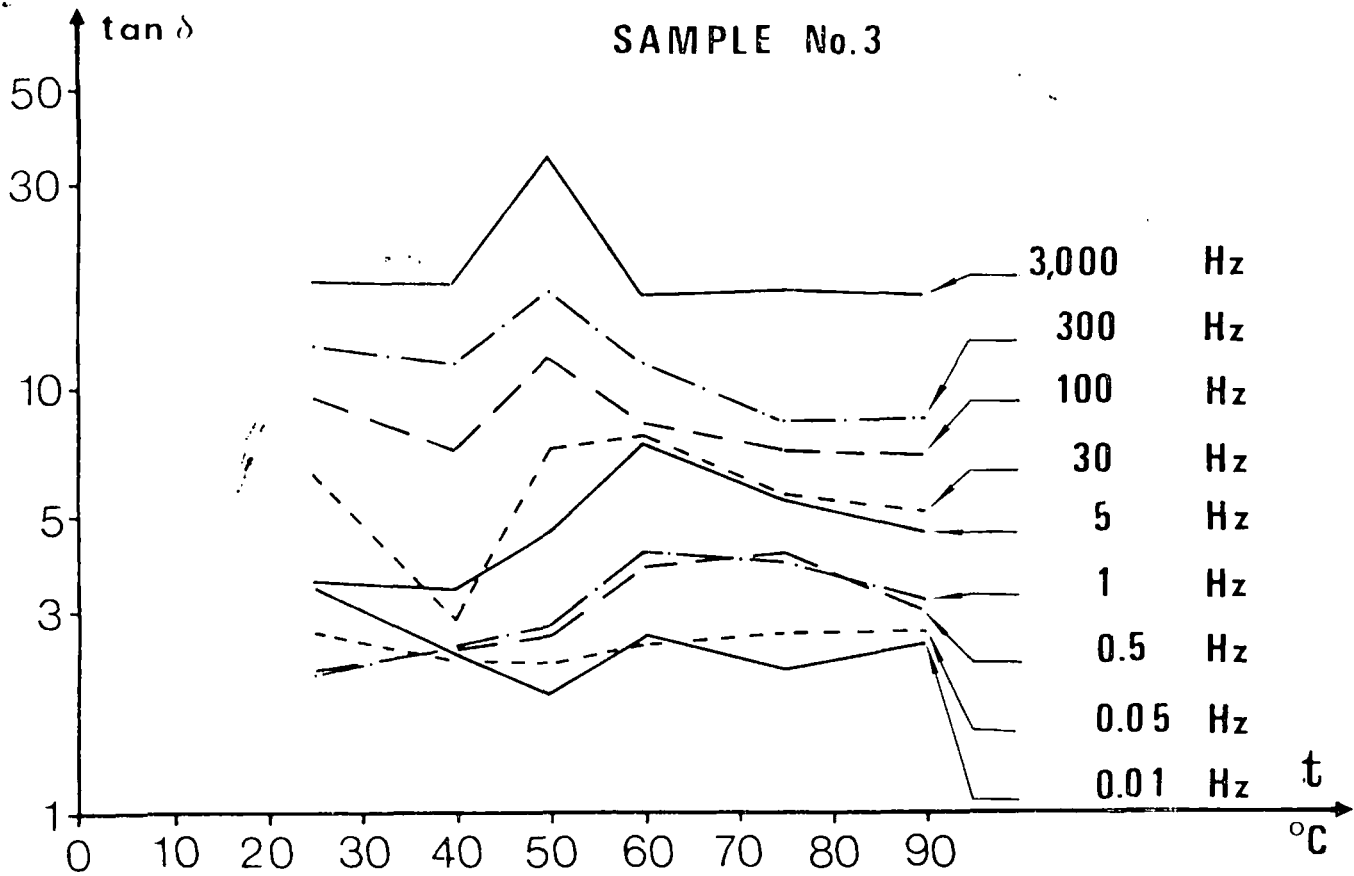


FIG. 5. — Some $\tan \delta$ trends vs. temperature for sample No. 3. One can see that, at least according to the amount of data in our hands at the moment, the trends of these diagrams suggest the existence of an interesting behaviour in the range 50°-60°C for frequencies higher than 1 Hz.

ticular; this also applies to other measurements on different types of rocks (e.g., pyrite-bearing samples) carried out: for more information and comments see Rocchi, in prep. Perhaps one of the most significant results is the anomaly in the trends of the electrical parameters around 60°C. In future it will be necessary to explore carefully the 50°-70° C temperature interval for the same type of clay, possibly in close connection with differential thermal analysis procedures for different, natural water contents.

Our intention is also to extend our researches to other sedimentary rocks, according to the above-mentioned concepts, in order to get information on the electrical responses of media of interest to both geothermal and geoelectrical prospectings.

Acknowledgements

The authors wish to express their gratitude to Professor Ezio Tongiorgi, Director of the International Institute for Geothermal Research, for his kind help and assistance.

Thanks are also given to Dr GABRIELLA LOSITO and Dr CARLO TURRIANI for their useful support.

This work was also carried out with the financial support of the National Research Council, Italy. The help given by Banca Toscana, Pisa, Italy, is gratefully acknowledged.

REFERENCES

- CHELIDZE L. A., CHELIDZE T. L. 1963 — Concerning the Question of the Electrical Properties of Bentonite Clay in AC Fields. *Tr. Kutai. Gos. Ped. Inst. im. «A. Tsulukidze»*, v. 25.
- COLLETT L. S. 1959 — Laboratory Investigation of Overvoltage. In Wait J. R., «Overvoltage Research and Geophysical Applications», Pergamon Press, London, 58-59.
- COLLETT L. S., KATSUBE T. J. 1973 — Electrical Parameters of Rocks in Developing Geophysical Techniques. *Geophys.*, v. 38, 1, 76-91.
- DOSLOVALOV B. N. 1947 — Electric Characteristics of Frozen Rocks. *Tr. Inst. Merzlotovedeniya (Permafrost) im. «V. A. Obrucheva»*, v. 5.
- FINZI-CONTINI G. 1971 — Theoretical Study on Membrane Polarization and Complex Mobility in Moist Rocks. *Geol. Surv. of Canada Paper*, 71-1, B, 23-24.
- FINZI-CONTINI G. 1972 — Una metodologia per ottenere su rocce «in situ» spettri frequenziali di conducibilità elettrica e permittività. *Riv. Ital. di Geof.*, Vol. XXI, 5-6, 170-176.
- FINZI-CONTINI G. ET AL. — A Frequency-Domain and Temperature Measuring System for Rock Samples, in preparation.
- FINZI-CONTINI G., MARCHISIO M., LOSITO G. 1972a — Su alcuni comportamenti elettrici simulati di campioni di roccia. *Paper presented at the 1st A.G.I. Congress-Assembly, Rome.*
- FINZI-CONTINI G., MARCHISIO M., LOSITO G. 1972b — Frequency Spectra of Rocks Electric Responses Studied through Distributed Geophysical Parameters. *Paper presented at the 34th E.A.E.G. Congress, Paris.*

- FRASER D. A., KEEVIL N. B. jr., WARD S. H. 1964 — Conductivity Spectra of Rocks from the Craigmont Ore Environment. *Geophys.*, v. 29, 5, 832-947.
- FULLER D. F., WARD S. H. 1970 — Linear Description of the Electrical Parameters of Rocks. *IEEE Transactions on Geosci. Electr.*, v. GE-8, 1, 7-18.
- KATSUBE T. J., AHRENS R. H., COLLETT L. S. 1973 — Electrical Non-Linear Phenomena in Rocks. *Geophys.*, v. 38, 106-124.
- KATSUBE T. J., COLLETT L. S. 1973 — Measuring Techniques for Rocks with High Permittivities and High Loss. *Geophys.*, v. 38, 1, 92-105.
- KEEVIL N. B. jr., WARD S. H. 1962 — Electrolyte Activity: Its Effect on Induced Polarization. *Geophys.*, v. 37, 5, 677-690.
- KELLER G. V., FRISCHKNECHT F. C. 1966 — Electrical Methods in Geophysical Prospecting. *Pergamon Press, Oxford*.
- KODOMA H., SCHNITZER M. 1969 — Thermal Analysis of a Fulvic Acid-Montmorillonite Complex. *Proceedings of The Intern. Clay Conf., Tokyo, 765-774*.
- MADDEN T. R. 1967 — Induced Polarization and its Application to Mineral Exploitation. *UN Sem. on New Methods for Mineral Exploration with Emphasis on Geophysical Techniques, Moscow, July*.
- MARSHALL D. J., MADDEN T. R. 1959 — Induced Polarization, a Study of its Causes. *Geophys.*, v. 24, 790-816.
- NENCINI C. 1973 — Studio elettrico in frequenza ($10^{-2} \div 5 \cdot 10^3$) di campioni di rocce umide mineralizzate a solfuri. *Thesis, Univ. of Siena (Italy). Facoltà di Scienze MM., FF. e NN.*
- PARASNIS D. S. 1966 — Mining Geophysics. *Elsevier Publ. Co., Amsterdam*.
- PARKHOMENKO E. I. 1967 — Electrical Properties of Rocks. *Plenum Press, New York*.
- ROCCHI M. — Effetti della temperatura sul comportamento elettrico in frequenza di campioni di rocce (intervalli 10^{-2} Hz - $5 \cdot 10^3$ Hz; 20°-90°C). In preparation.
- VAN BLADER R., MENZEL R. 1969 — A Thermodynamic Study of Sodium-Strontium Exchange on Wyoming Bentonite. *Proceedings of The Intern. Clay Conf., Tokyo, 619-634*.
- VAN KEYMEULEN J., DEKEYSER W. 1957 — Dielectric Loss on and Defects in Clay Minerals. *J. Chem. Phys.*, v. 27, 1.
- VAN OLPHEN H. 1969 — Thermodynamics of Interlayer Adsorption of Water in Clays II. Magnesium Vermiculite. *Proceedings of the Intern. Clay Conf.*, v. 1, Tokyo, 649-657.

SUBJ
GPHYS
FCI

FROM, 1977, ~~THE~~ HEACOCK, JOHN G., (ed.), THE EARTH'S CRUST - ITS
NATURE AND PHYSICAL PROPERTIES, AGU Monograph 20,
P. 693-704

FLUID CIRCULATION IN THE EARTH'S CRUST

Denis Norton

Department of Geosciences, University of Arizona
Tucson, Arizona 85721

Abstract. Numerical simulation of thermally driven fluid flow caused by igneous intrusives in the upper crust indicates that fluid circulation is an inevitable consequence of lateral density gradients in pore fluids characteristic of these environments. Thermal perturbations associated with igneous plutons are predicted to be sufficiently large to generate hydrothermal systems in which the magnitude of convective heat transport exceeds that of conductive heat transport for rock permeabilities greater than 10^{-18} m^2 [Norton and Knight, 1977]. Furthermore, the style of the heat transfer is significantly different from systems in which conduction is the dominant heat transfer mechanism, particularly when the transport and thermodynamic properties of the fluid phase are taken into account. As a consequence of the critical end point which exists in the H_2O and related systems, the region above plutons is predicted to contain extensive vertical zones of nearly constant temperature. These first-order approximations of fluid circulation reveal two points relevant to predicting the thermal regime of the crust: (1) thermal gradients above convection-dominated systems are very nonlinear and cannot uniquely predict subsurface temperatures within our present scope of knowledge and data and (2) since fluid circulation may extend through a considerable portion of the upper crust in tectonically active regions, the thermal regime of these crustal regions is poorly understood.

Introduction

Temperature conditions in the earth's crust are normally predicted on the basis of extrapolated temperature-gradient data, petrologic arguments, and numerical approximations of conductive heat transfer processes in which various thermal energy sources, as well as rock properties, are considered. Analyses of thermal convection have usually indicated fluid circulation to be an important heat transport process, at least in geothermal areas [Elder, 1965; Ribando et al., 1976; Lister, 1974; Lowell, 1975]. However, the consequences of fluid circulation on the thermal conditions in the crust have only recently been analyzed for situations in which (1) the transport and thermodynamic properties of the fluid phase are allowed to vary with temperature and pressure changes and (2) an igneous intrusive body is present in the upper crust.

The unique characteristics of fluid systems for which H_2O is a principal component suggest that the properties of these types of fluids should contribute significantly to the heat transport process in con-

UNIVERSITY OF UTAH
RESEARCH INSTITUTE
EARTH SCIENCE LAB.

vection-dominated systems [Norton and Knight, 1977]. Enthalpy, density, and viscosity of phases in the pure H₂O system and in salt-H₂O systems are very dependent on temperature and pressure in a temperature-pressure region which starts at the critical end point and extends to higher pressures. As a consequence of this dependence, natural systems are predicted to have thermal characteristics distinctly different from those predicted on the basis of constant fluid properties or even those predicted on the basis of properties approximated by simplistic equations of state. Most equations of state that have been previously used merely predict fluid properties along the two-phase surface in the H₂O or salt-H₂O systems.

Crustal environments which contain hot igneous bodies inevitably cause fluid circulation, and if the intrinsic host rock permeability is greater than 10⁻¹⁸ m², heat transfer by convection accounts for at least 10% of the total heat transfer, and at permeabilities greater than 10⁻¹⁸ m², convection greatly predominates over conduction [Norton and Knight, 1977]. Fluid-driving forces are generated as a natural consequence of the near-vertical side contact of intrusives, which cause lateral perturbations in the density of pore fluids. Instability of the fluids and the onset of convection is therefore instantaneous in these systems; the magnitude of the initial fluid flux depends principally on permeability of host intrusive rocks.

The purpose of this communication is to review the nature of fluid circulation related to transient thermal anomalies in the crust and to consider the consequences this fluid circulation might have on our concepts of the thermal environment in the crust.

Numerical Simulation of Fluid Circulation

Lateral density perturbations in fluids contained in the flow porosity of rocks cause fluid flow. The magnitude of this flow in natural systems can be determined by Darcy's law:

$$\bar{q} = \frac{k}{v} (\nabla P + \rho \bar{g}) \quad (1)$$

where the mass flux \bar{q} is a function of intrinsic rock permeability k , fluid viscosity v , density ρ , the gradient in pressure ∇P , and the gravitational vector \bar{g} . Density gradients, which may be the result of concentration as well as thermal gradients on the fluid, give rise to $\nabla_x P$ and $\nabla_y P$ terms in the horizontal plane. Although both types of density gradients are ubiquitous in the crust, only those resulting from thermal anomalies are included in the computations.

Thermal anomalies often cause and are coincident with extensive fracture zones and therefore probably represent the most significant contribution to fluid circulation in the crust, except in sedimentary basin environments where large concentration gradients are common. The inferred association of permeable fractured rocks with thermal anomalies in the upper 10-15 km of the crust suggests that fluid circulation is a characteristic feature in these environments.

Fluid flow caused by thermal anomalies related to igneous plutons are effectively scaled and represented in two dimensions by partial differential equations which describe the conservation of mass, momentum, and energy for the fluid-rock system [Norton and Knight, 1977]:

and

where
the t
id; k
volum
numbe
ordin
apply
The
that
resul
defin
flux,
trans
(2);
mal a
rise
decre
the t
heat
ferer
the d
and t
provi
fluid
and r
main.
aly a
solut
vals.
used
the c
syste
which
funct
on cc

The
natur
for a
Cor
ments
resul
diffe

UNIVERSITY OF UTAH

$$\gamma \frac{\partial T}{\partial t} + q \nabla H = \nabla \cdot \kappa \nabla T \quad (2)$$

and

$$\frac{v \nabla \cdot v}{k} \nabla \Psi = R \frac{\partial \rho}{\partial y} \quad (3)$$

where T is the temperature; Ψ the stream function; q the fluid flux; t the time; H , ρ , and v the enthalpy, density, and viscosity of the fluid; k the permeability of the rock; κ the thermal conductivity; γ the volumetric heat capacity of the fluid saturated media; R the Rayleigh number; t the time; ∇ the gradient operator; and y the horizontal coordinate in the two-dimensional section to which these equations apply.

The physical meaning of (2) and (3) is apparent if one considers that the fluid density gradients on the right-hand side of (3), which result from a thermal anomaly, cause fluid circulation. That is, they define gradient values of the stream function and therefore fluid flux, since $q_z = -\partial \Psi / \partial y$ and $q_y = \partial \Psi / \partial z$. The fluid flux q in turn transports heat away from the thermal anomaly, second term on left of (2); at the same time, thermal energy is conducted away from the thermal anomaly, right-hand side of (2). Both of these processes give rise to a decrease in temperature with respect to time and therefore decrease the horizontal fluid density gradients. And, consequently, the thermal anomaly is decreased by combined convective and conductive heat transfer. Equations (2) and (3) are approximated by finite difference numerical equations which permit computation of the values of the dependent variables at discrete points in the domain from initial and boundary values specified for the system. The numerical analysis provides the option to include variable transport properties of the fluid (H_2O system) and rock, general boundary and initial conditions, and radioactive and volumetric heat sources in a two-dimensional domain. The transport processes related to the transient thermal anomaly are approximated by a time sequence of steady state numerical solutions to (2) and (3), computed at explicitly stable time intervals. An alternating-direction-implicit finite difference method is used to approximate the spatial derivatives at discrete intervals of the order of 0.1 to 0.5 of the system height. Fluid pressure in the system is computed at each steady state step by integration of (2), in which the fluid properties, viscosity and density, are expressed as a function of temperature and pressure. The following discussion relies on computations and analyses using these methods.

The Nature of Fluid Circulation Related to Thermal Anomalies

The style of fluid circulation in the upper 10 km of crust and the nature of pluton cooling has been simulated [Norton and Knight, 1977] for a variety of host rock permeability values and geometries.

Convection dominates heat transfer in hot igneous pluton environments if rock permeabilities are of the order of 10^{-18} m^2 or greater, resulting in a spatial redistribution of thermal energy significantly different than that in similar environments in which conductive heat

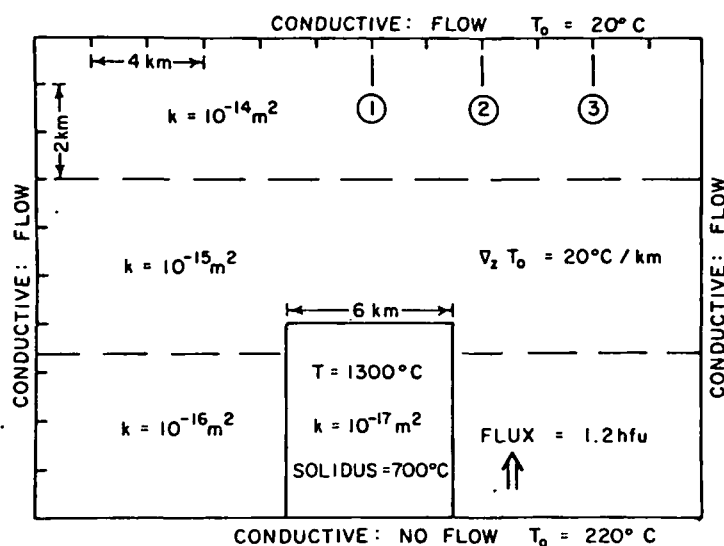


Fig. 1. Two-dimensional cross section of a crust 10 km deep and 24 km wide containing an igneous pluton 4 km high and 6 km wide. Initial value and boundary conditions are for a magma body emplaced instantaneously at 6 km below the surface. Pluton permeability is effectively zero until the temperature of discrete points in the body decreases to 700°C; then permeability at those points is set to 10^{-17} m^2 . Regional heat flux is set at 1.2 HFU for the duration of the system. The initial thermal gradient is 20 C/km, whereas the magma is homogeneous and is connected to a magma reservoir below the base of the pluton at $T = 1300^\circ\text{C}$ for the initial 50,000 years. Thermal conductivity is constant at 0.6 cal/m sec $^\circ\text{C}$; the circulating fluid is pure H_2O and does not react with the enclosing rocks.

transfer predominates. Although the time duration of convection-dominated thermal anomalies is similar to that of conduction-dominated systems when the pluton itself is impermeable, the cooling time is significantly shortened by increases in permeability such as might accompany extensive fracturing of the pluton. The direct application of these modeling results to actual systems must be made with caution since the in situ values of rock permeability are virtually unknown. However, analogies drawn between permeability values of rocks for which permeability data are available and estimates of permeability suggest that permeability values exceeding the 10^{-18} m^2 minimum may characterize a substantial portion of the upper crust [Norton and Knapp, 1977].

A numerical model of a system which illustrates the convective transfer of heat around igneous plutons is presented. A basaltic magma at $\sim 1300^\circ\text{C}$ is presumed to be emplaced relatively rapidly, with respect to the rate of heat transfer away from the magma body, into host rocks whose permeability increases upward from 10^{-16} m^2 to 10^{-14} m^2 (Figure 1). The relatively rapid intrusion rate only requires magma flow velocities on the order of a few centimeters per year, a value which seems to be reasonable. Since cooling of magmas is nor-

mally accompanied by fracture development resulting from reactions that increase or decrease the pluton volume, the pluton permeability is changed from effectively zero to 10^{-17} m^2 as the temperature of discrete grid points in the pluton decreases to $<700^\circ\text{C}$, thereby simulating fracture development and permitting fluid circulation through the pluton.

Boundary conditions selected for this system are analogous to natural systems where thermal energy is conducted through all the boundaries. The bottom and top boundary temperatures are set to 220°C and 20°C , respectively. Thermal conductivity of the domain is assumed to be constant, $0.6 \text{ cal/ms } ^\circ\text{C}$, and since the bottom boundary is conductive, the domain has a constant regional flux of $1.2 \text{ } \mu\text{cal/m}^2 \text{ sec (HFU)}$ and the host rocks have an initial background thermal gradient of 20°C/km . The relative permeability values within the domain are set to simulate the decrease in continuous fractures with depth, and the magnitude of the permeability is set to illustrate the effects of fluid circulation. The side and top boundaries are permeable, but the base is impermeable in order to further simulate the decrease in permeability with depth. The permeable top boundary condition does not, however, permit convection of thermal energy out of the system. This latter condition simulates natural systems which do not have hot springs emerging at the top boundary, e.g., the fluids flow through and thermally equilibrate with the rocks at the top boundary. This system was then simulated by using a spatial discretization of 160 points, which results in a 0.1 vertical increment and a 0.06 horizontal increment. The numerical approximations represent the partial differential equations to within a truncation error of the order of 0.05 times the value of the dependent variable. Discrete time increments are computed on the basis of stability criteria, which results in convergence errors of the order of 0.005 times the dependent variable.

The thermal anomaly, introduced by the pluton, causes pore fluids in the host rocks to circulate from the sides and top boundaries of the domain toward the pluton then upward along its side margins and out the top of the domain (Figures 2-4). This circulation pattern significantly increases the heat flux over the pluton top with respect to a purely conductive process. As a consequence of the convective heat transfer, thermal gradients in the domain directly over the pluton are relatively steep near the surface, i.e., 0-0.5 km, decrease sharply and remain constant over several kilometers, then gradually increase toward the pluton top (Figures 5a-5c). The convective heat flux at the surface directly above the pluton varies from 1.2 HFU at the initial time to 15 HFU at 8×10^4 years, whereas the vertical component of convective flux at 0.5 km depth ranges from 0.5 HFU at 2×10^4 years to 20 HFU at 8×10^4 years and then gradually decreases to 10 HFU at 1.5×10^5 years.

The caveat about these values at the surface is that they are arbitrary to the extent that they are a function of the numerical discretization. However, the relative comparison between the values in the same system at various times is a reasonable approximation of what can be expected in nature. Finer discretization merely results in a nonlinear thermal gradient and predicts it to better precision. Progressive fracturing of the pluton contributes to the persistence of

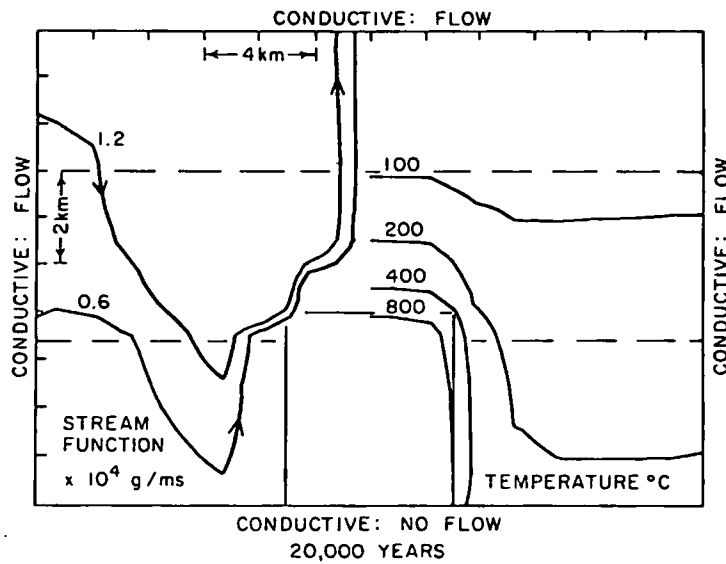


Fig. 2. Scalar stream function (g/m sec) and temperature (degrees Celsius) distributions after 2×10^4 years elapsed time, illustrating steady state fluid circulation and temperature, respectively. Vertical fluid fluxes of the order of $5 \times 10^{-5} \text{ g/m}^2 \text{ sec}$ are realized 3 km directly above the pluton, which, together with conductive heat transfer, cause the 100°C isotherm to migrate upward at about 0.05 m/yr .

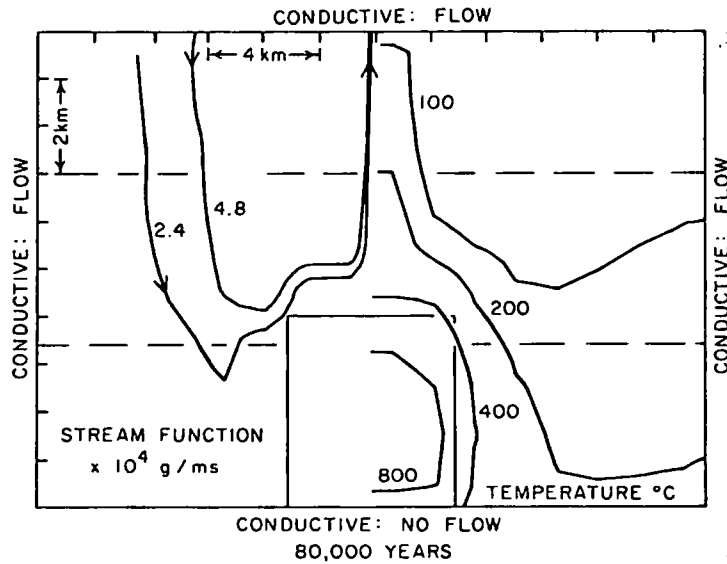


Fig. 3. Scalar stream function and isotherm distributions after 8×10^4 years elapsed time. Vertical fluid fluxes of the order of $10^{-3} \text{ g/m}^2 \text{ sec}$ are realized 3 km directly above the pluton, and 8 km laterally away from this upflow zone, downward fluid fluxes, $\sim 10^{-7} \text{ g/m}^2 \text{ sec}$, occur.

Fig
1.5
pos
at
ly
out
the
tem

large
time
regi
year
La
down
of t
time
resp
of t
over
Th
grad
temp
domi
Tran
 H_2O
cont
gion
for
resp
visc
cond

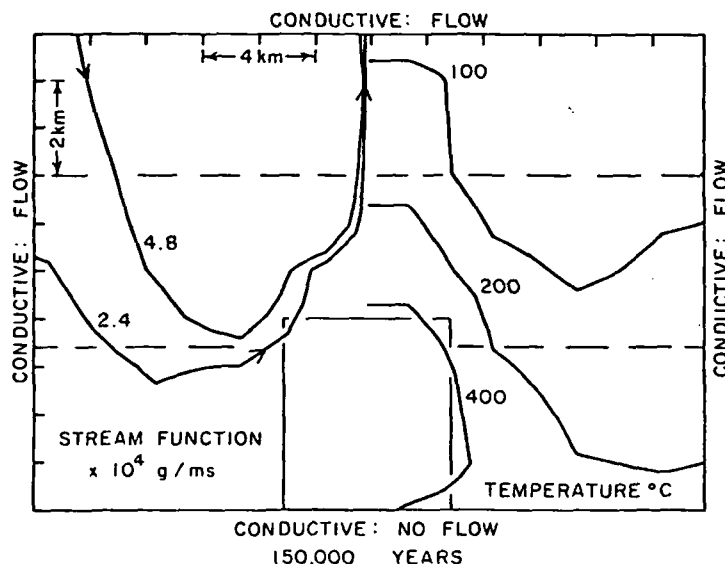


Fig. 4. Scalar stream function and isotherm distributions after 1.5×10^5 years elapsed time. Vertical fluid fluxes at comparable positions in previous times have decreased to about 50% of the fluxes at 8×10^4 years. The 100°C and 200°C isotherms have moved to slightly deeper portions in response to the decreasing convective flux. The outer 1.5 km of the upper 2 km of the pluton fractured at 10^5 years, thereby increasing the cooling rate of the body. The average pluton temperature is 800°C at this time.

large convective heat fluxes over a long time period. The estimated time duration for which convective fluxes will be greater than the regional heat flux in the upper 2 km of the system is about 5×10^5 years.

Laterally away from the pluton, thermal gradients in the fluid downflow zone are depressed below the regional gradients as a result of the convective heat flux of -3 HFU. In these regions, at cooling times $\sim 1.2 \times 10^5$ years, the isotherms are depressed downward with respect to their regional position, cf. 200°C isotherm. The portion of the anomaly, at temperatures $>100^\circ\text{C}$, in the upper 3 km is dispersed over an area equivalent to the pluton top.

The several-kilometer vertical extent of relatively constant thermal gradients in the host rocks overlying the pluton and the corresponding temperature values, 100 – 400°C , are characteristic of convection-dominated systems which we have analyzed [Norton and Knight, 1977]. Transport and thermodynamic properties of supercritical fluid in the H_2O system and salt- H_2O systems are characterized by extremes which contribute to these thermal gradient features (Figure 6). In the region which extends from the critical end point, $\sim 375^\circ\text{C}$ and 220 bars for the H_2O system, derivatives of fluid density and enthalpy with respect to temperature at constant pressure are maximums, and fluid viscosity is a minimum. Therefore thermal perturbations at these conditions result in the largest fluid density gradients which togeth-

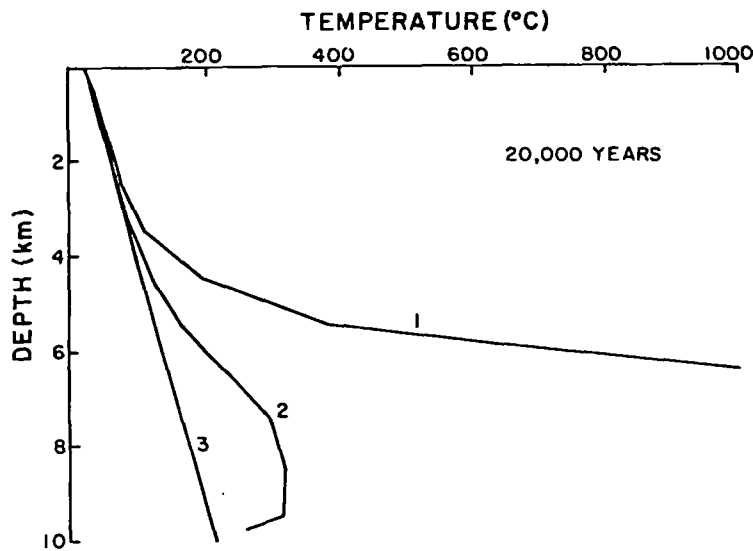


Fig. 5a. Vertical thermal gradients from the surface to the base of the system at elapsed time of 2×10^4 years. Vertical sections are located along the center line, line 1, of the pluton; 1 km away from the side wall of the pluton, line 2; and 5 km away from the side wall of the pluton, line 3 (cf. Figure 1 for positions).

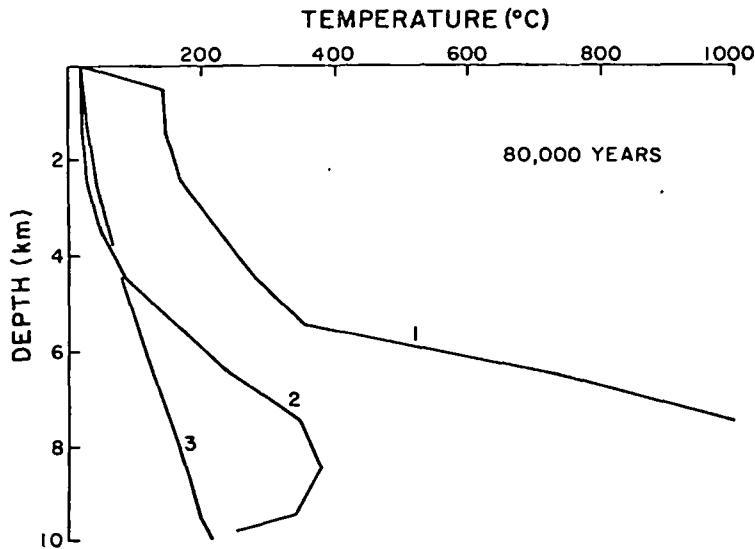


Fig. 5b. Vertical thermal gradients from the surface to the base of the system at elapsed time of 8×10^4 years. Vertical sections are located along the center line, line 1, of the pluton; 1 km away from the side wall of the pluton, line 2; and 5 km away from the side wall of the pluton, line 3 (cf. Figure 1 for positions).



Fig. 5c. Vertical thermal gradients from the surface to the base of the system at elapsed time of 2×10^4 years. Vertical sections are located along the side wall of the pluton, line 4 (cf. Figure 1 for positions).

er with the mi
fluxes. The h
conditions, an
this temperat
tremes tend to
end point to l
point and relat
temperatures a
which contain
have a critical
fluid propertie
pure H₂O system

The nature of
thermal anomal
values of fluid
ties, at least
reasonably ass
acteristic of e
anomaly tempera
than 220 bars,
components are
realized at pro
tures.

The example s
of rock permeab
conditions in t

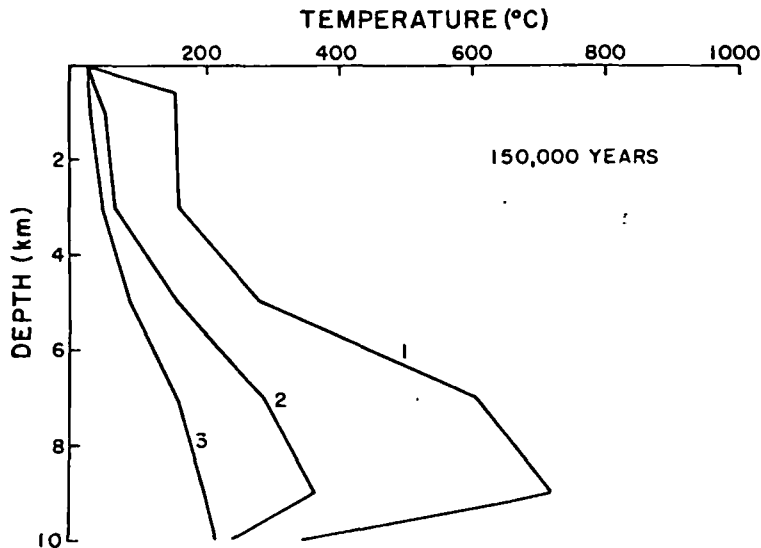


Fig. 5c. Vertical thermal gradients from the surface to the base of the system at elapsed time of 1.5×10^5 years. Vertical sections are located along the center line, line 1, of the pluton; 1 km away from the side wall of the pluton, line 2; and 5 km away from the side wall of the pluton, line 3 (cf. Figure 1 for positions).

er with the minimum in the fluid viscosity tend to maximize the fluid fluxes. The heat capacity of the fluid is also a maximum under these conditions, and hence the convective heat transport is maximized in this temperature-pressure region. As a point of interest these extremes tend to decrease in magnitude from the region near the critical end point to lesser extremes at higher pressures. The critical end point and related extremes in fluid properties are displaced to higher temperatures and pressures for salt-H₂O systems (Figure 6). Fluids which contain dissolved components equivalent to a 3 m NaCl solution have a critical end point at 590°C and 850 bars, and the extremes in fluid properties extend into a region analogous in position to the pure H₂O system (Figure 6).

The nature of the thermal gradients within permeable rocks overlying thermal anomalies in a natural system is clearly predicated on the values of fluid properties and permeability. Since the fluid properties, at least for the H₂O system, are relatively well known, one can reasonably assume that these thermal gradients will at least be characteristic of environments where rock permeabilities are $>10^{-18} \text{ m}^2$ and anomaly temperatures are $>375^\circ\text{C}$ at depths where pressures are greater than 220 bars, i.e., $\sim 2.2 \text{ km}$. In natural environments where dissolved components are relatively more concentrated, these effects will be realized at progressively greater depths and slightly higher temperatures.

The example system discussed above contains relatively high values of rock permeabilities with respect to our current best guesses of conditions in the crust. However, fluid circulation effects have been

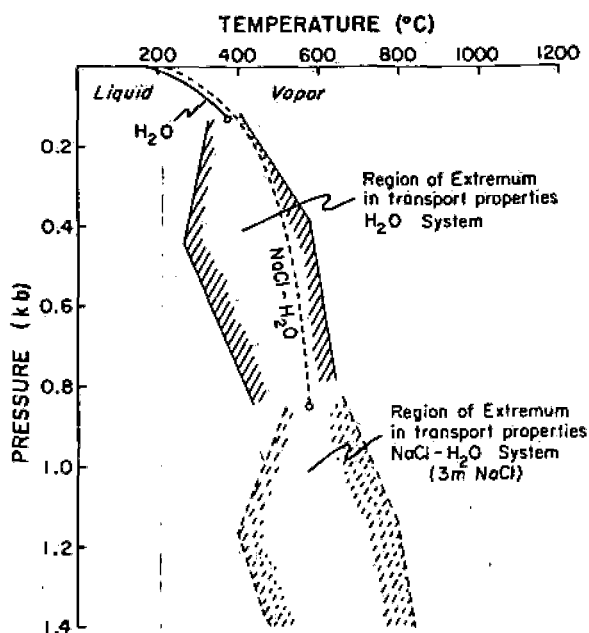


Fig. 6. Temperature-pressure sections through the NaCl-H₂O systems depicting the two-phase surface, liquid-vapor, and critical end point for 0 m and 3 m NaCl concentrations. The approximate region of anomalous extreme in transport properties of supercritical fluid is depicted for 0 m and 3 m solutions. Note the shift of the critical end point and associated anomalous regions to higher temperatures and pressures as a result of adding NaCl to the system.

observed in models where the pluton tops are 12-km deep, within low-permeability rocks (10^{-20} m^2), but are overlain by higher permeability (10^{-18} m^2) zones which simulate vertical fractures. Thermal gradients are more linear in these systems than in the system discussed above, but only a few percent contribution to the heat flux by convection may have a significant effect on our interpretations of the thermal environment in the crust. The most significant feature of the simulated system is that vertical thermal gradients in systems where convective heat transfer occurs do not provide a unique set of data with which subsurface temperatures can be predicted.

Fluid Circulation in the Crust

Fluid circulation in the upper crust is predicted to be more extensive than was previously thought; its magnitude may be large enough to contribute significantly to the redistribution of thermal energy in this environment. The magnitude of the contribution of fluid circulation to heat transport depends entirely on the magnitude of permeability in crustal rocks and the distribution, with respect to thermal anomalies, of fluid-saturated rocks with permeabilities $>10^{-18} \text{ m}^2$. The minimum permeability value is realized in rocks which have con-

tinuously open-planar fractures spaced 0.1 km apart with an effective aperture of ~ 20 μm [Norton and Knapp, 1977; Snow, 1970]. This abundance of continuous fractures is easily realized in tectonically active regions and in pluton environments [Villas, 1975; Villas and Norton, 1977], but apertures and continuity of fractures with respect to depth are unknown. In tectonically quiescent regions neither abundance nor aperture of fractures have been documented. However, indirect evidence suggests that permeabilities sufficient to permit significant heat transfer by convection may be realized in the upper crust. First, in tectonically active regions, continuous fractures develop to considerable depths, as is indicated by earthquake hypocenter data. Second, igneous intrusive processes contribute to development of fracture sets in the rocks they intrude. The extent and magnitude of the permeability resulting from combined tectonic and igneous intrusive events is clearly conducive to extensive fluid circulation, as is evidenced by eroded equivalents to these environments which show abundant mineral alteration, as well as by large gains and losses of chemical components in and adjacent to fractures. Transport of thermal energy into the crust by magma or simple conduction also produces fractures due to the differential thermal expansion of pore fluids and rocks [Knapp and Knight, 1977]. In tectonically less active regions, permeability values can be inferred from electrical and, perhaps, seismic properties, empirical relationships between pore continuity, and electrical resistivity [Brace, 1971] or variations in seismic wave velocity [Nur and Simmons, 1969]. These indirect lines of evidence suggest that crustal rocks contain a fluid phase, which may be relatively concentrated in dissolved components, and that they are sufficiently permeable to warrant further efforts toward quantitative determination of bulk rock permeability.

Analyses of transport phenomena in permeable media suggest that fluid circulation through fractured rocks may contribute significantly to heat transfer through the crust, at least to depths of 10-15 km. As a consequence of fluid circulation, several effects may be realized in nature: lower than normal thermal gradients over several-kilometer vertical distances in the upper crust, abnormally low conductive thermal values coincident with fluid downflow zones, and gross errors in predicting subsurface temperatures by downward extrapolation of thermal gradients. These effects are undoubtedly present in active geothermal systems and can be predicted, with reasonable confidence, to occur in the vicinity of virtually all igneous bodies emplaced into the upper crust. The more widespread realization of the effects in more normal crust is mere speculation at this time, and many questions remain that will require more precise numerical models and data acquisition. However, this first approximation suggests that the nature of the upper crustal environment may indeed be the result of dynamic fluid systems, the extent of which is unknown.

Acknowledgments. This work was supported by funds provided by ERDA, contract E-11-1-2763, and NSF grant EAR74-03515 A01 for which the author is grateful. Discussions with Professor H. C. Helgeson, R. Knapp, J. Knight, and R. N. Villas have contributed to the author's ideas. I am also grateful for discussions with W. F. Brace and for his published work, which provided the incentive to consider the

problem of permeability distribution in the crust, and to L. McLean for her editorial assistance in preparing the manuscript.

References

- Brace, W. F., Resistivity of saturated crustal rocks to 40 km based on laboratory measurements, in The Structure and Physical Properties of the Earth's Crust, Geophys. Monogr. Ser., vol. 14, edited by: J. G. Heacock, pp. 243-255, AGU, Washington, D. C., 1971.
- Elder, J. W., Physical processes in geothermal areas, in Terrestrial Heat Flow, Geophys. Monogr. Ser., vol. 8, edited by W. H. K. Lee, pp. 211-239, AGU, Washington, D. C., 1965.
- Knapp, R., and J. Knight, Differential thermal expansion of pore fluids, fracture propagation, and microearthquake production in hot pluton environments, J. Geophys. Res., 82, in press, 1977.
- Lister, C. R. B., On the penetration of water into hot rock, Geophys. J. Roy. Astron. Soc., 39, 465-509, 1974.
- Lowell, R. P., Circulation in fractures, hot springs, and convective heat transport on mid-ocean ridge crests, Geophys. J. Roy. Astron. Soc., 40, 351-365, 1975.
- Norton, D., and R. Knapp, Transport phenomena in hydrothermal systems: The nature of porosity, Amer. J. Sci., 277, in press, 1977.
- Norton, D., and J. Knight, Transport phenomena in hydrothermal systems: Cooling plutons, Amer. J. Sci., 277, in press, 1977.
- Nur, A., and G. Simmons, The effect of saturation on velocity in low porosity rocks, Earth Planet. Sci. Lett., 17, 183-193, 1969.
- Ribando, R. J., et al., Numerical models for hydrothermal circulation in the oceanic coast, J. Geophys. Res., 81(17), 3007-3012, 1976.
- Snow, D. T., The frequency and aperture of fractures in rocks, J. Rock Mech., 7, 23-40, 1970.
- Villas, R. N., Fracture analysis, hydrodynamic properties, and mineral abundances in altered igneous rocks at the Mayflower Mine, Park City District, Utah, Ph.D. dissertation, 254 pp., Univ. of Utah, Salt Lake City, 1975.
- Villas, R. N., and D. Norton, Irreversible mass transfer between circulating hydrothermal fluids and the Mayflower stock, Econ. Geol., 72, in press, 1977.

NU
LI
Pi
De
Ho

re
st
vc
an
Wi
an
di
D,
co
eq
me
Ni
re
st
su
a
ri
re
de

co
ge
La
im
th
Ra
ti
an
pa
ci
eq
gr
fo
by

The Flow of Heat from the Earth's Interior

A global heat-flow map can be drawn on the basis of thousands of individual field measurements on continents and ocean floors. The heat-flow pattern is interpreted in terms of plate tectonics

by Henry N. Pollack and David S. Chapman

"Straight through the dim and open portal we entered unopposed, and I, eager to learn what part of Hell's bowels those burning walls enclosed, began to look about." So did Dante write of his descent into the Inferno. Miners of later centuries might well have believed he was describing their daily working environment, since it has been widely observed that without proper ventilation and cooling a mine gets hotter with depth. There are of course many other indications that the earth's interior is hot, the most obvious being an erupting volcano. Only slightly less spectacular are the handful of areas around the world that display hydrothermal activity, such as the hot springs, steam vents and geysers of Yellowstone National Park. One of the fundamental axioms of physics, embodied in what is known as Fourier's law of heat conduction, is that heat flows from the warmer parts of a body to the cooler ones. It can therefore be inferred that since the temperature increases with depth in the earth's crust, there is a flow of heat outward from the earth's interior.

The transfer of heat within the earth and its eventual passage to the surface by conduction through the crust play a fundamental role in all modern theories of geodynamics. In the 19th century the earth's internal heat also figured significantly in the protracted debate over the age of the earth between William Thomson (Lord Kelvin) and several of his scientific contemporaries. Kelvin's dissertation at the University of Glasgow in 1846, titled "Age of the Earth and Its Limitations as Determined from the Distribution and Movement of Heat within It," was the first of a long series of papers in which he laid out the argument that the earth's thermal gradient (the rate at which the temperature increases with depth) would continue to diminish with time as the earth cools following its formation and solidification from mol-

ten rock. By determining the earth's thermal gradient from measurements in mines and boreholes, he maintained, one could tell how long the earth had been cooling and so could determine the age of the earth. Records of temperatures at various depths in mines could be found in mining journals, and Kelvin supplemented them with measurements of his own in Scotland. His conclusion was that the temperature, at least to modest depths below the surface, increased at a rate of between 20 and 40 degrees Celsius for every 1,000 meters of depth. To Kelvin this relation indicated that the earth had been cooling for only a few tens of millions of years, a period far shorter than many geologists and biologists of the time thought necessary for the development of the known stratigraphic and fossil record. The ensuing debate spanned half a century and pitted Kelvin against such prominent evolutionists as Charles Darwin and Thomas Huxley.

Kelvin's calculation was based on the assumption that the heat being lost by the earth was drawn from the reservoir of heat left over from the earth's originally molten condition. That assumption, which was essentially unchallenged for decades, was to be the undoing of all estimates of the earth's age based on the measurements of its heat. Three observations made Kelvin's estimate of the age of the earth based on its initial heat no longer tenable: the discovery of radioactivity by Henri Becquerel in 1896, the observation by

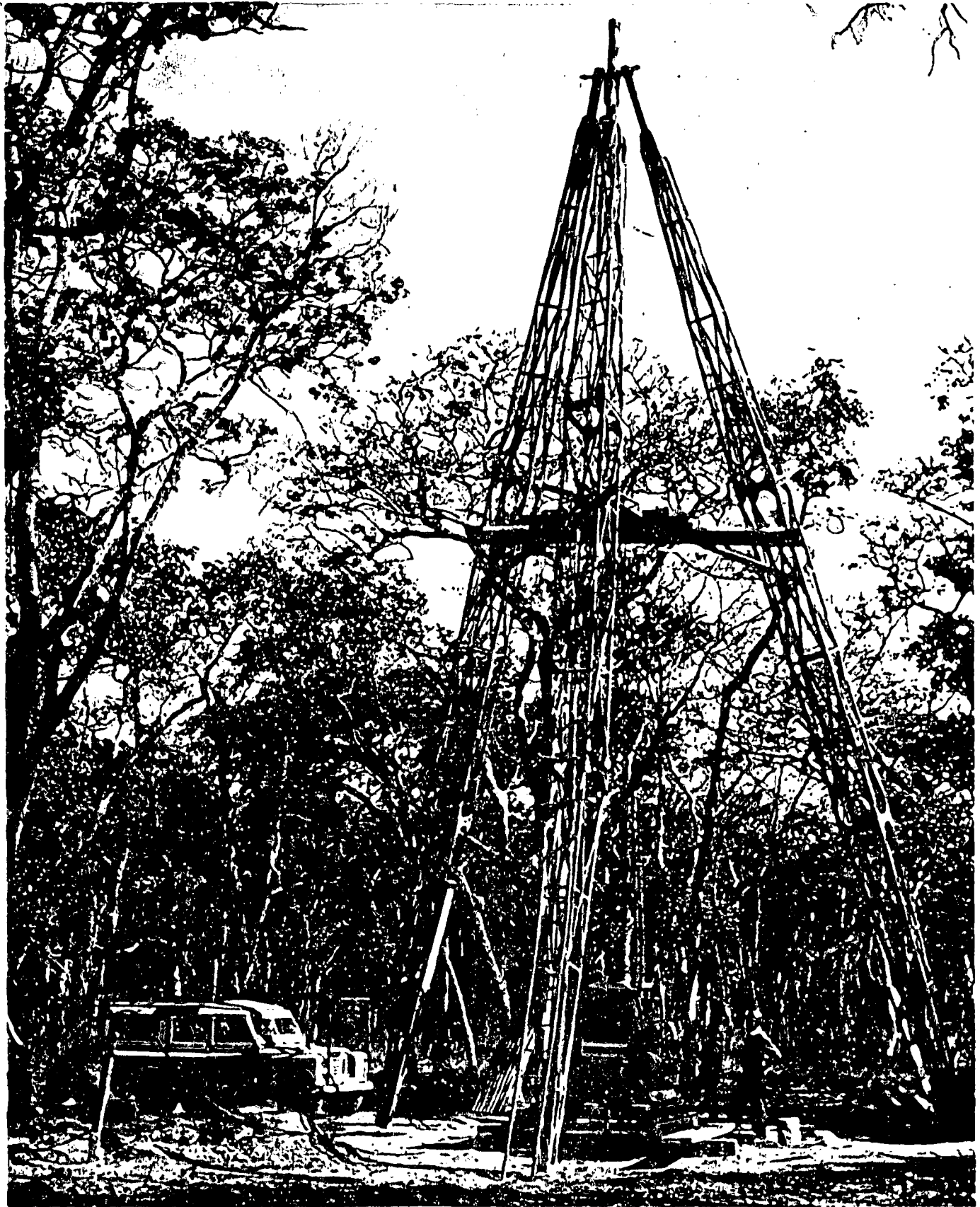
Pierre Curie in 1903 that the radioactive decay of certain isotopes liberates heat and the confirmation by Robert Strutt in 1906 that common rocks found in the earth's crust contain sufficient amounts of radioactive isotopes to yield a significant fraction, if not all, of the earth's observed heat flow.

Measuring Heat Flow

How much heat is the earth losing today as a result of conduction from its interior? The global average is close to .06 watt per square meter of surface, or about 30 trillion watts over the entire planet. The amount of energy arriving from the sun is almost 6,000 times greater, and it is completely dominant in establishing the temperature of the earth's surface. The flow of heat from the interior is scarcely a trickle; the heat conducted through an area the size of a football field is roughly equivalent to the energy given off by three 100-watt light bulbs. The evolution of the earth covers vast reaches of time, however, and a trickle of energy over aeons can do significant geological work, such as making continents drift, opening and closing ocean basins, building mountains and causing earthquakes. The geographic variation in the flow of heat from the earth's interior is not great: most measurements lie within a factor of three around the mean value. The patterns of heat flow in continental regions differ from those in oceanic ones, but the average heat flow through both

DRAMATIC EVIDENCE of the power of the earth's internal heat to mold the geology of the surface is provided by this photograph of the 1971 Mauna Ulu eruption on Kilauea volcano in Hawaii. The photograph was made by Wendell A. Duffield of the U.S. Geological Survey as he was standing on the rim of the Mauna Ulu crater and looking almost straight down. The bluish gray background is the comparatively cool crust of partly solidified basaltic lava that forms on the surface of the hot liquid-lava "lake" below. The jagged orange streaks are cracks through which molten lava is upwelling. The entire scene, Duffield points out, is analogous to the spreading of new sea floor from mid-ocean ridges visualized in the plate-tectonic model.





DRILL RIG IN ZAMBIA, originally set up to bore into the earth in search of copper, provided one of several "holes of opportunity" used by the authors and their co-workers as part of their program to obtain heat-flow measurements in areas of Africa and South America where the existing data are sparse. The earth's temperature is taken by lowering an electrical-resistance thermometer (called a thermistor) down the borehole, making measurements at several depths. The records are used to establish the rate at which the temperature of the

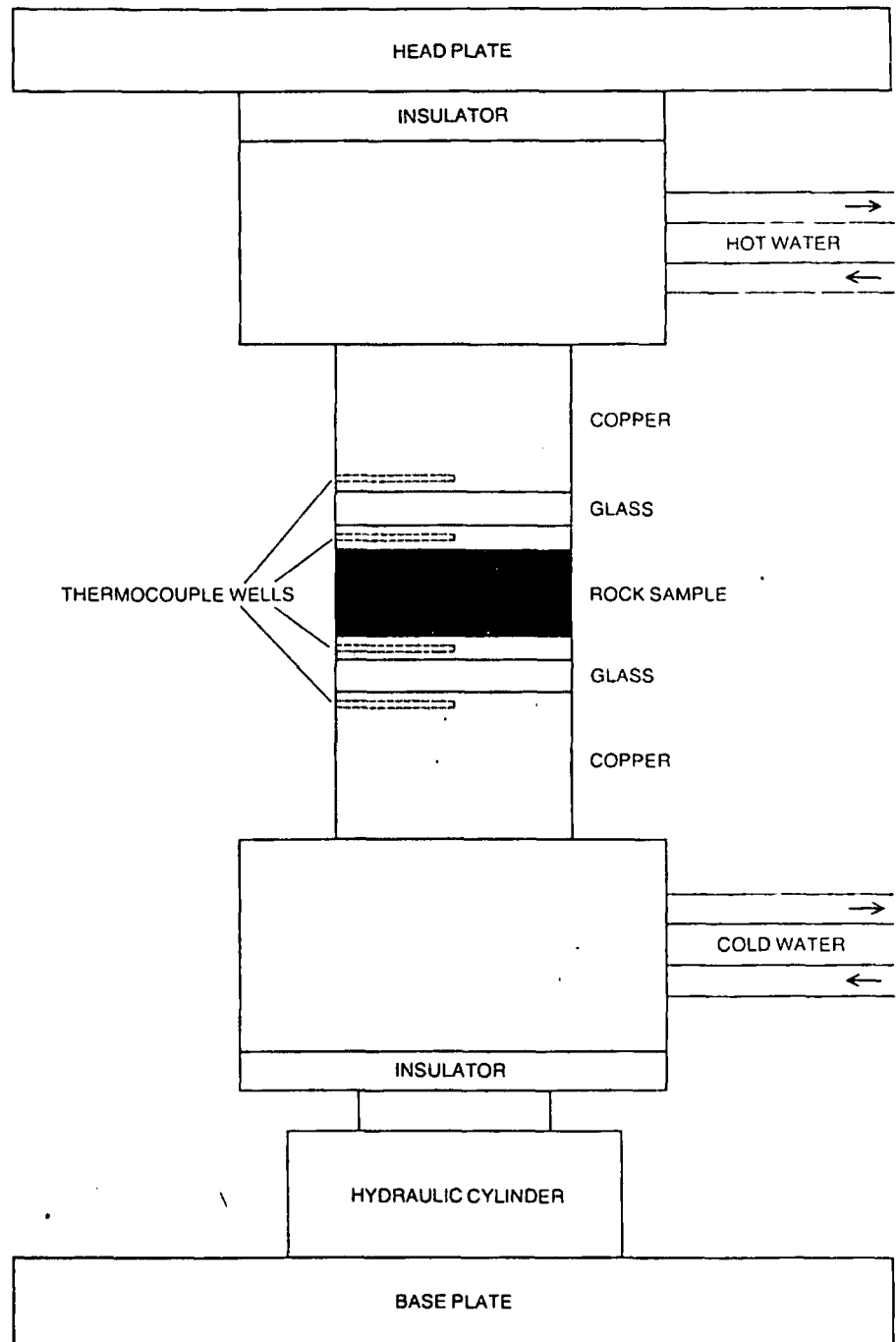
rock increases with depth, a local quantity known as the geothermal gradient. The Zambian heat-flow measurements were carried out four years ago while the authors were on leave from the University of Michigan and were based at the University of Zambia. More than 50 such drill holes were surveyed at eight different Precambrian geological sites in the country. The results of the survey were interpreted by the authors as indicating the presence of anomalously warm material only a few tens of kilometers below the surface of the earth.

is surprisingly similar. Some areas, such as Iceland, exhibit an extraordinary heat flow, and geothermal areas of this type can be tapped as an energy resource.

If heat is being transported through the earth's crust by thermal conduction, the amount of heat in transit is equal to the product of the temperature gradient times the thermal conductivity (a property of the rock that describes how easily it transmits heat). Any experimental study of the earth's heat flow is concerned with measuring these two quantities. On continents temperature gradients are measured by lowering sensitive electronic thermometers—thermistors—down drill holes or by measuring the temperature of the rock at different levels in mines. The process of drilling a hole disturbs the thermal equilibrium at the site; hence several weeks or months are allowed to lapse between the drilling and the measuring. Even after the disturbance has become negligible, subsurface temperatures are disturbed by such effects as the daily and annual fluctuation in the surface temperature, unevenness in vegetative cover, unevenness in topography, the movement of ground water, the uplift or erosion of the surface and variations in climate. Most of these disturbances diminish to an acceptable level beyond depths of a few tens of meters; some, however, can extend to several hundreds of meters. Although reliable heat-flow measurements can sometimes be made in holes as shallow as 50 meters, most workers who make such measurements prefer to do so in holes that are 300 meters or more in depth.

On the ocean floor, where sediments are comparatively soft and the blanket of seawater provides an environment of almost constant temperature, the drilling of a hole is unnecessary. There temperature gradients are determined by plunging a long cylindrical probe several meters into the soft sediment and measuring the temperature at one-meter intervals with fixed thermistors.

For measurements of thermal conductivity two methods are widely used. For hard continental rock a sample from the drill hole is cut and polished in the form of a disk and is inserted into a column between silica disks of known conductivity. A constant temperature difference maintained between the ends of the column causes a flow of heat through the sample and the silica standards, and the measurement of the relative drop in temperature across the components of the stack yields the thermal conductivity of the sample. For softer continental rocks and marine sediments a thin needle is inserted into the sample and is heated along its length. From a record of the rise of temperature with time the thermal conductivity can be calculated easily.



THERMAL CONDUCTIVITY of a hard rock sample obtained from a drill hole is measured in the apparatus depicted here. The sample, cut and polished in the form of a disk, is inserted in a column between silica disks of known conductivity. Constant temperature differences maintained between the ends of the column cause a flow of heat through the sample and the silica standards. The sample's thermal conductivity is determined by measuring the relative drop in temperature across the components of the stack. The heat flow at the drill site is equal to the product of observed local temperature gradient times thermal conductivity of the rock.

More than 5,000 such heat-flow measurements have been reported in a recent compilation by Alan M. Jessop of the Canadian Department of Energy, Mines and Resources and by John G. Sclater and Michael A. Hobart of the Massachusetts Institute of Technology. Although the number of measurements is sufficient for several types of regional analysis, the data set is still geographically uneven: more than twice as many

measurements have been made at sea as on land. The middle-latitude oceans, North America, Europe and Australia are quite well surveyed, whereas large areas of the high-latitude oceans and of South America, Africa, Asia and Antarctica have no measurements at all. In the past four years our group from the University of Michigan has helped to remedy some of this geographic imbalance on the continents by conduct-

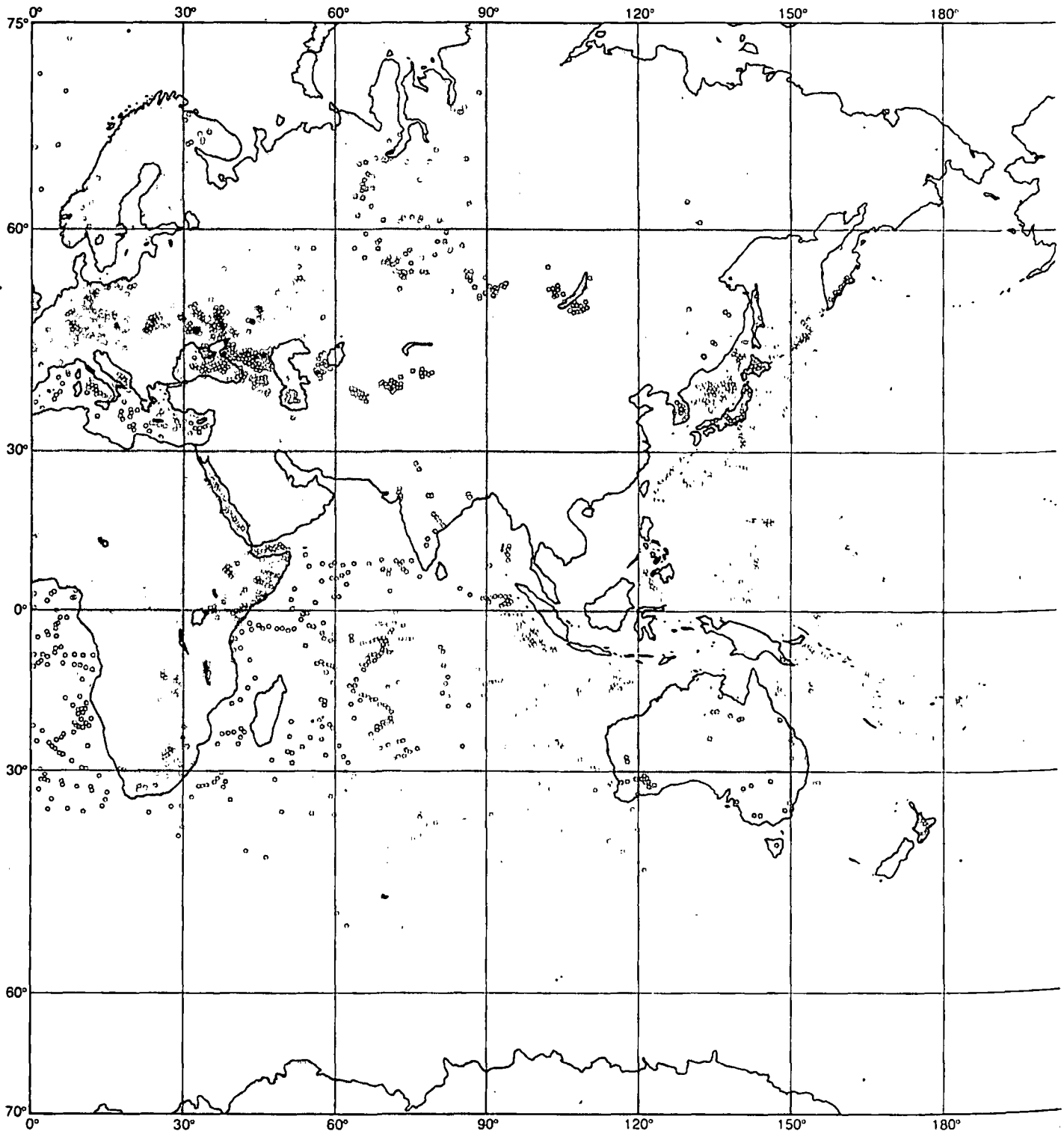
ing heat-flow measurement programs in Zambia, Niger and Brazil.

An analysis of the global data without regard for specific site location or geologic setting indicates a fairly wide distribution of results asymmetrically spread around a modal (or most commonly observed) value of 50 milliwatts per square meter [see top illustration on page 66]. Individual values range from

near zero to several hundred milliwatts per square meter, the latter being located mainly within geothermal areas associated with the worldwide system of mid-ocean rifts. Subdividing the data into continental and oceanic regions reveals similar modal values for both sets; the oceanic data, however, have a wider distribution than the continental data, and the high level of asymmetry forces

the means, or average values, for each of these regions well above the modes.

This gross grouping of heat-flow measurements has been useful in the past, and the similarity between continental and oceanic measurements has served to stimulate much discussion among geophysicists and geologists who had expected quite different results in the two settings. As with many other aspects of



UNEVEN GEOGRAPHIC DISTRIBUTION of oceanic and continental heat-flow measurements (colored circles) is evident on this

world map, which is based on one prepared by the National Geophysical and Solar-Terrestrial Data Center. The number of such measure-

earth science, however, heat-flow observations now find a compelling new interpretation in terms of the concepts of sea-floor spreading and plate tectonics.

Heat Flow and Plate Tectonics

According to plate tectonics, the lithosphere, the outer shell of the earth, is made up of a dozen or so rigid plates

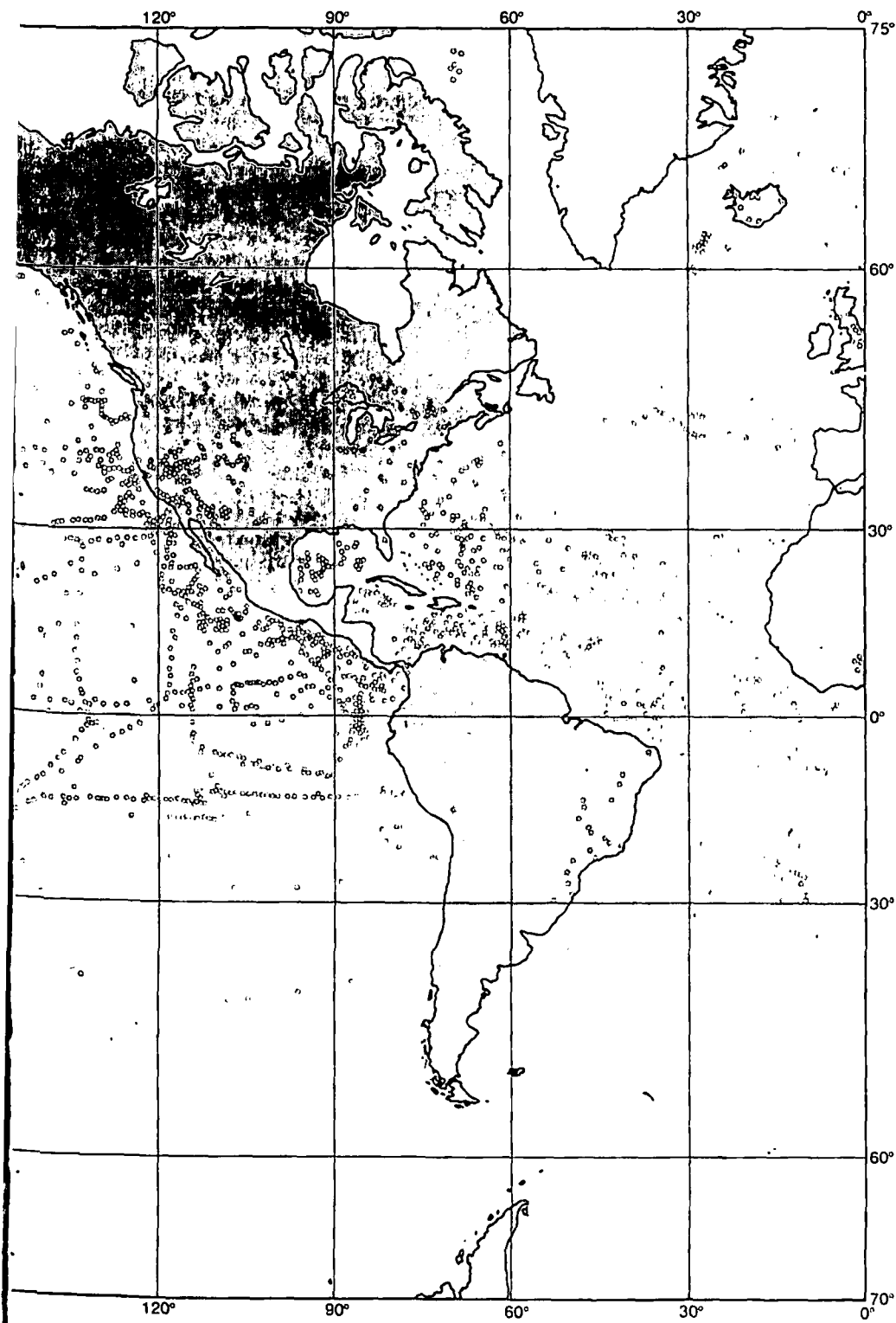
that are being moved about on the earth's surface. Wherever plates are moving apart the gap is filled by hot material flowing upward from the earth's underlying mantle. This material accretes to the edges of the separating plates; the accreting edges form the mid-ocean ridges. The new rock cools as it moves away from the ridge. Across the plate from a ridge one usually finds a

great oceanic trench, which marks a site where older and cooler plate is subducted, or recycled back into the interior. Frictional and conductive heating of the plate in the subduction zone melts part of it, and the melted fraction rises buoyantly to the surface to form the volcanoes and island arcs typically arrayed behind the trenches. Such subduction processes, together with other forms of plate interactions, give rise to thermal metamorphism, the generation of volcanic magma and mountain building on continents.

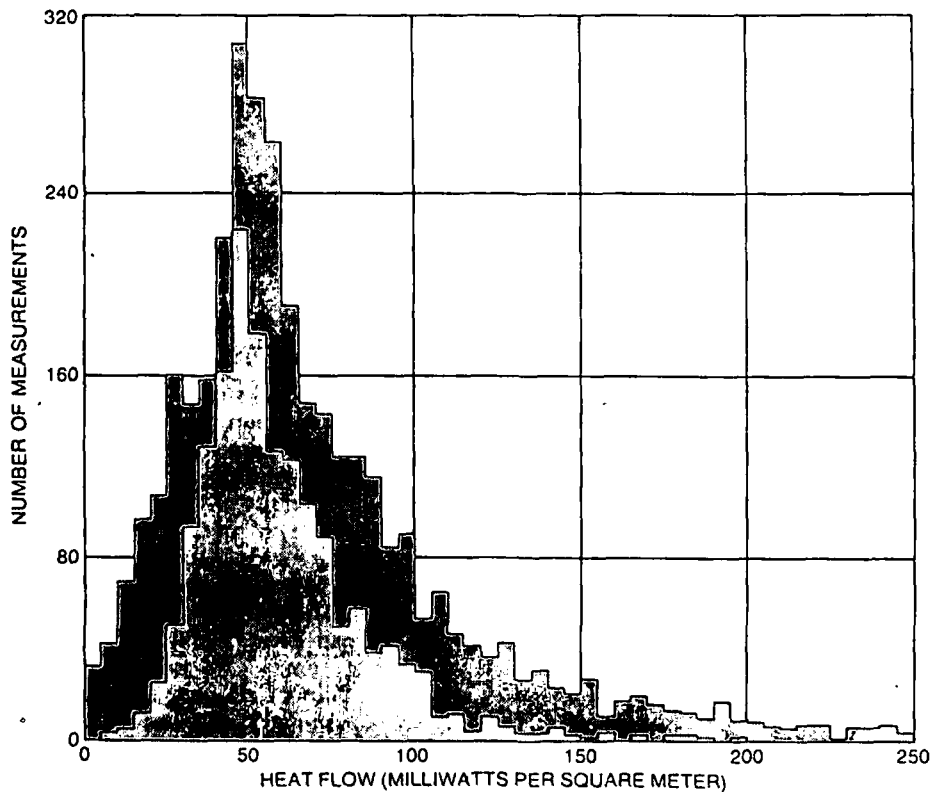
One first looks to the oceanic plates with their comparatively simple geology to obtain evidence for the thermal model of plate evolution. Edward C. Bullard of the University of Cambridge, who reported the first marine heat-flow measurements for the Atlantic in 1954, noted at that time the near-equality of the mean heat flow from the continents and the ocean floor. Today, with the addition of some 3,500 measurements in ocean floor of all ages, it is possible to see a systematic decrease of heat flow with increasing age and hence depth [see bottom illustration on next page]. For those sites where a thick, impermeable cover of sediments prevents the removal of heat by seawater circulating through the fractured oceanic crust, heat-flow measurements agree extremely well with predictions based on mathematical models of a cooling plate.

Such models of plate cooling also explain the broad topographic features of the ocean floor. The newly formed crests of mid-ocean ridges are typically 1,000 to 3,000 meters below sea level, whereas the oldest ocean basins are 5,500 meters below sea level. Thus in 200 million years the sea floor subsides by about 3,000 meters. The reason is that the recently accreted rock is hot and thermally expanded, whereas the older material has cooled and contracted. The match between the observed topography and the theoretically calculated topography is so good that it seems unlikely the subsidence will be explained in any way other than in terms of a simple cooling model.

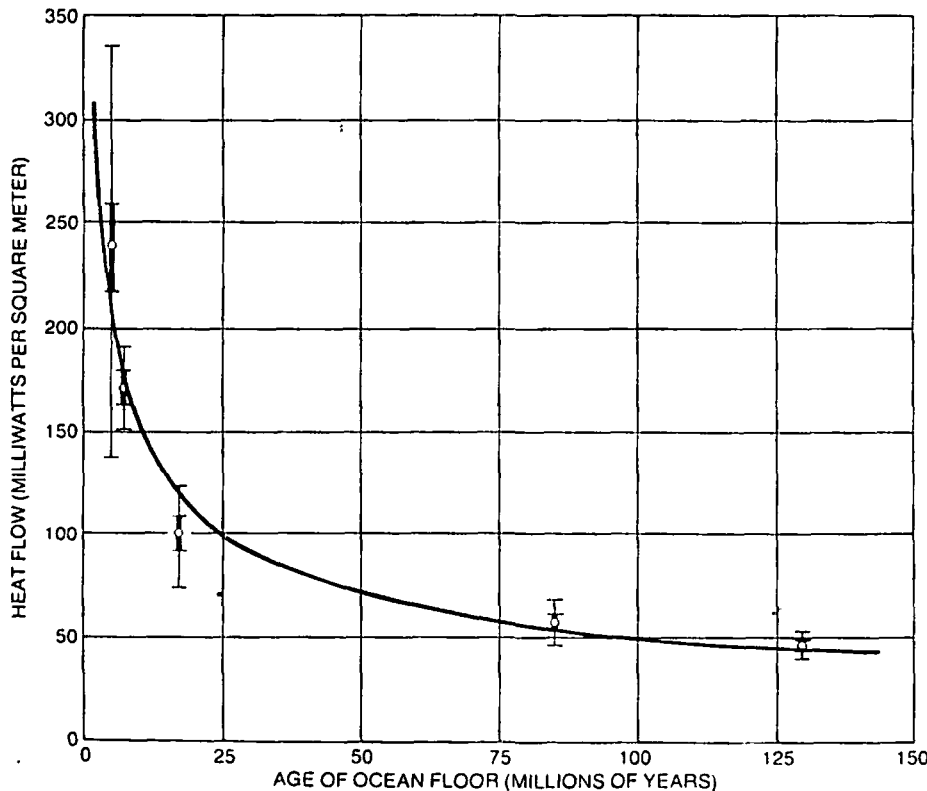
The concept of the thermal evolution of an oceanic plate may also provide an answer to a long-standing puzzle in geology: What gives rise to transgressions of the sea onto continents? The Upper Cretaceous period was one such time of great marine transgression. Starting about 100 million years ago the sea level rose; it crested between 90 and 70 million years ago and withdrew from the continents about 60 million years ago. From the spacing of magnetic lineations on the ocean floor it can be shown that the Upper Cretaceous was also a period of rapid sea-floor spreading. Since the cooling and subsidence of an oceanic plate is time-dependent, an increase in



ments has increased rapidly in recent years: from 47 in 1954 to 1,162 in 1962 to more than 5,000 at present. More than twice as many measurements have been made at sea as on land.



STRIKING SIMILARITY is seen in the asymmetrical distribution of heat-flow values for both continents (color) and oceans (gray). Most of the observed values are in the range between 20 and 120 milliwatts per square meter, with the global average being at about 60. The modal, or most commonly observed, values for continents and oceans (peaks of profiles) are both closer to 50. It is not known at present whether the near-equality of the continental and the oceanic heat-flow measurements is a fundamental characteristic of the movement of heat within the earth or is merely a coincidence arising from incomplete sampling. The data for this chart were compiled by Alan M. Jessop of the Canadian Department of Energy, Mines and Resources and by John G. Sclater and Michael A. Hobart of the Massachusetts Institute of Technology.



HEAT FLOW DECREASES with increasing age of ocean floor, as indicated here by the distribution of measured heat-flow values for five selected areas on the floor of the Pacific Ocean. Data points give the mean value for each age grouping. Heavy bars show the probable error; light bars show standard deviation about the mean. Measurements agree extremely well with a theoretical estimate of heat flow expected from a cooling plate of oceanic crust (colored curve).

the spreading rate would have broadened the oceanic ridge and increased its volume. This in turn would have reduced the water capacity of the ocean basins and displaced the sea onto the continents. The subsequent regression was apparently caused by a reduction in the rate of sea-floor spreading that began about 85 million years ago.

Above subduction zones the heat-flow patterns are more complex, but they nonetheless provide important clues to the subduction process. A pattern generally observed at subduction zones, and particularly well documented for the Japan arc system, is one of low heat flow near the oceanic trench and very high heat flow to the landward side of the island arc [see illustration on opposite page]. The pattern suggests that the top part of the cool subducting plate acts as a heat absorber, causing the band of low heat flow observed adjacent to the trench. Deeper in the subduction zone frictional and conductive heating are sufficient to melt part of the plate, yielding as a product the volcanic island arc itself and the augmented heat flow behind the arc.

The western U.S. provides another example of an elongated zone of low heat flow adjacent to a region of magmatic activity and high heat flow [see illustration on page 68]. Here, however, there is at present no active major subduction zone nearby. David D. Blackwell of Southern Methodist University and others have suggested that this zone represents a fossil heat-flow pattern, established some tens of millions of years ago when subduction was active along the boundary between the Pacific plate and the North American plate.

Continental heat flow in areas removed from plate boundaries also falls into recognizable patterns. Measurements on continents now number about 1,700, and from these data one can draw two major conclusions. First, there is a general decrease in heat flow with the increasing age of a geologic province [see top illustration on page 73]. This result is similar to that for oceans, but the time scale is apparently quite different. Whereas oceanic heat flow drops below 50 milliwatts per square meter after 100 million years of cooling, on continents one finds such heat flow in geologic settings four or five times older.

The second major result is that for large areas of continents there is a clear relation between surface heat flow and the radioactivity of the surface rocks. That continental rocks, granites in particular, generate significant quantities of heat by the spontaneous disintegration of radioactive elements has been known since early in this century. In 1968 A. Francis Birch, Robert F. Roy and Blackwell, all then working at Harvard University, demonstrated that when heat-flow measurements are plotted with respect to radioactive heat generation for

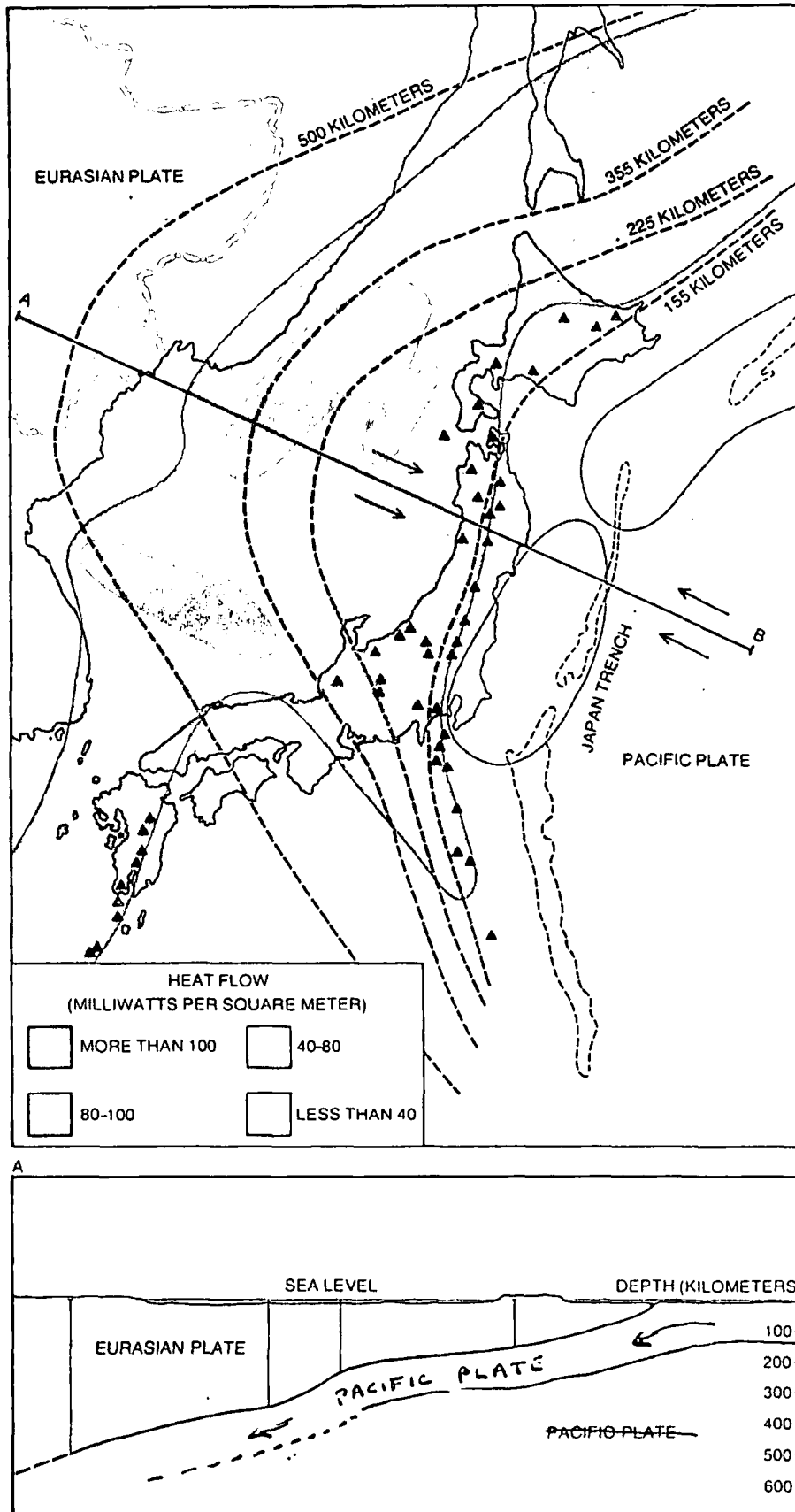
the rocks at various sites, the plotted values fall along a straight line [see bottom illustration on page 73]. Different lines were obtained for the eastern U.S., the "basin and range" geologic province of Nevada and Utah, and the Sierra Nevada region, but within each region a linear relation holds. This finding implies that for a given region the heat flow at the surface has two components: a crustal component that varies from site to site according to the local radioactivity and a deeper component that originates in the earth's mantle and is uniform for all sites in the region. Since 1968 this relation has received much attention. Arthur H. Lachenbruch of the U.S. Geological Survey has looked into its consequences for the distribution of heat-producing isotopes in the earth's crust, and he has explained why the concentration of such isotopes should be expected to diminish exponentially with depth.

The variation of the mantle-derived component of the observed heat flow between different provinces has been less well studied, but on the basis of the limited data available we have speculated that in most heat-flow provinces there is a regular partitioning of the heat flow, with about 40 percent of the mean surface flux coming from within the zone of crustal enrichment and 60 percent coming from below. This partitioning, if confirmed, suggests that the average heat production of the continental crust should vary inversely with its age, because in general the older provinces display less heat flow. Such a relation can be explained with a model in which radioactivity diminishes with depth, on the assumption that the older geologic provinces have been eroded to greater depths than the younger ones.

Another intriguing finding has been reported recently by Tom Crough of Stanford University and V. M. Hamza of the University of São Paulo. They show that when one subtracts the heat-flow contribution originating in the zone of crustal enrichment, the remaining heat flow continues to show an inverse dependence on the age of the province, but the time scale of this residual heat flow appears to be one of a simple cooling process, much like what is observed in the oceans. The cooling on the continents is apparently much further along, however, and it must have penetrated more deeply there. Could it be that we are seeing residual heat from a tectonic event 600 million years ago? If we are, the implication is that such events must involve at least the outer 500 kilometers of the earth in order for any residual heat to be making its way to the surface today.

Global Heat Flow

Let us now turn our attention to the broad features of the thermal field of the



DISTINCTIVE HEAT-FLOW PATTERN is produced by the subduction of the tectonic plate underlying the Pacific Ocean as it dives under the islands of Japan. The arrows in the map at the top indicate the relative convergence of the Pacific and the Eurasian plates, and the broken lines show the depth to the subducted slab. The corresponding depths are also indicated in the cross-sectional diagram at the bottom, which is drawn approximately to scale along the line AB. The low heat-flow zone (lightest color) observed between the Japan trench and the island arc suggests that from the surface to a depth of about 120 kilometers the cool subducting plate acts as an absorber of heat from the earth's mantle. The volcanoes of the island arc (black triangles) and the region of high heat flow (darkest color) between Japan and mainland Asia result from frictional heating and partial melting deeper in the subduction zone.

entire earth and in doing so combine results from both the continental and the oceanic regions. Before 1974 several attempts had been made to plot the observed variations in heat flow on a global scale. In spite of the growing number of heat-flow measurements, however, there were still large areas of the globe where no data had been gathered. A mathematical representation of the global distribution of heat-flow measurements was desirable in order to correlate regional heat flow with other geophysical phenomena, such as the earth's gravitational field. The analysis was beset with difficulties because of the need for extensive extrapolation into unsurveyed areas.

By 1974, however, the relation between heat flow and age for both continental and oceanic regions was well established. Could these known correlations not be utilized to make estimates

of the probable heat flow in unsurveyed areas and so guide the heat-flow contouring on a global map? They could if geological maps were available showing the ages of all continental and oceanic regions. Although such maps had existed for the continents for some time, it was not until 1974 that Walter C. Pitman, Roger L. Larson and Ellen M. Herron of the Lamont-Doherty Geological Observatory summarized on a single map the detailed ages of all the oceanic regions based on magnetic anomalies on the ocean floor and the recorded reversals of the polarity of the earth's magnetic field. Soon after obtaining the map we divided the entire earth into grid elements five degrees on a side and proceeded to assign to each element a heat-flow value based on the relation of heat flow to tectonic age and the fraction of different age groups present in the grid element. In effect we were creating a

synthetic estimate of heat flow in unsurveyed areas. The full data set, comprising observations supplemented by estimates, could then be fitted by appropriate mathematical functions and plotted with a minimum of distortion [see top illustration on pages 74 and 75].

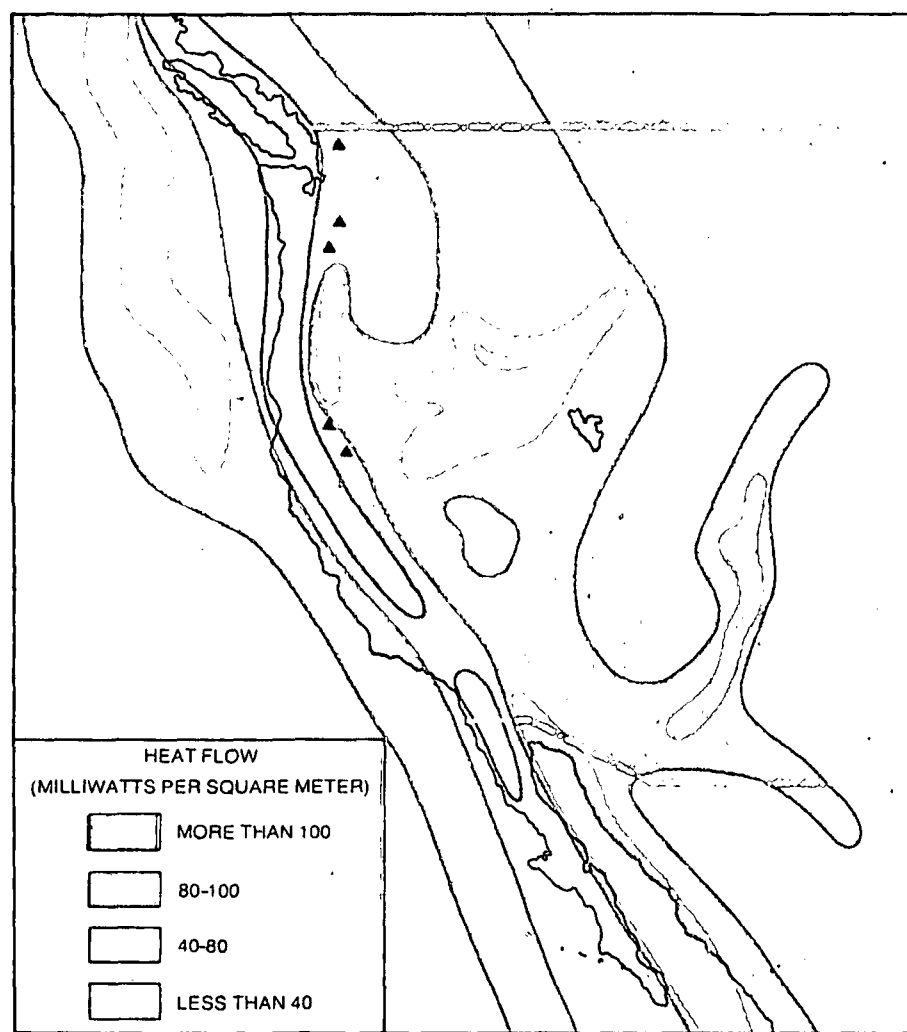
The new world heat-flow map constructed in this way showed for the first time on a global scale variations in heat flow that had been recognized in regional surveys. All the major oceanic-ridge systems can be seen as heat-flow highs, as are Alpine Europe, much of western North America and the marginal basins of the western Pacific. The Galápagos spreading center and the Chile Rise appear as bulges on the dominant East Pacific Rise. Regions of low heat flow include all the major continental shields and sedimentary platforms and the oldest oceanic regions.

The Thickness of the Lithosphere

The determination of the thickness of the lithosphere has until recently been a seismological endeavor. The seismologist's method is to observe the dispersive effects of a given region of the earth on earthquake surface waves that propagate across it. The analysis of dispersion patterns yields information about the elasticity of the crust and the upper mantle; in particular the pattern of dispersion can confirm the existence and locate the position of a zone where seismic waves travel at low velocity. Such a zone is probably a manifestation of a region of partial melting in the mantle, and many geophysicists identify this zone as the asthenosphere postulated in the plate-tectonic model. Since the lithosphere is what lies above the asthenosphere, the depth to this low-velocity zone is equal to the thickness of the lithosphere.

It has been known for some time that under the old Precambrian shields of the continents the seismic low-velocity zone either is absent or is deep and only weakly developed. In contrast, the young and active geologic provinces such as those in the western U.S. have a shallow and well-developed low-velocity zone. Recently a number of reports have appeared suggesting that the depth to the low-velocity zone under the oceans also increases with the age of the ocean floor, implying that the oceanic lithosphere progressively thickens with time.

The depth at which partial melting takes place in the mantle in a given region depends on the temperature at which the rock of the mantle begins to melt and on the variation of temperature with depth. The depth profile of the actual temperature, called the geotherm, in turn depends strongly on the heat flow. Thus with the aid of considerable extrapolation surface heat-flow



FOSSIL SUBDUCTION ZONE appears to account for the elongated region of low heat flow observed adjacent to a magmatic region of high heat flow in western North America. Sea-floor spreading under way at present in the Gulf of California and at the Gorda and the Juan de Fuca oceanic ridges results in high heat flow offshore. Inland the parallel belts of low and high heat flow mark the shallow and deep parts respectively of a subduction zone that was active during the early Cenozoic era. Although the subduction of the oceanic plates off central California ceased more than five million years ago, a heat-flow pattern similar to that seen in the currently active Japan arc system persists. Black triangles again denote recent volcanoes.

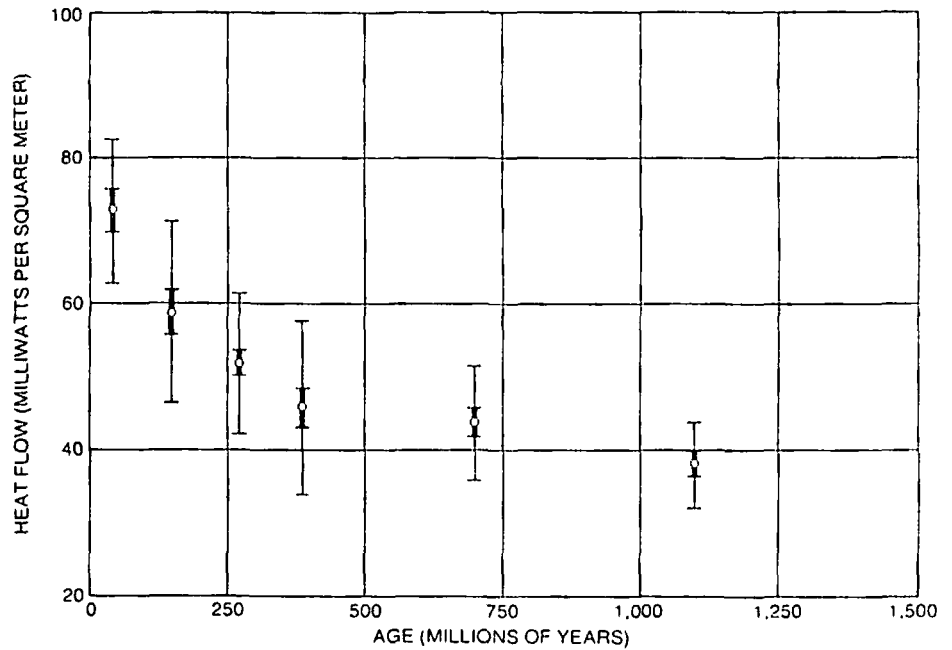
data can be used to predict the thickness of the tectonic plates.

Since direct measurement of temperatures in the earth is limited to the top 10 kilometers of the crust, the extrapolation of temperatures to depths of 100 kilometers or so involves several assumptions. One needs to know how the thermal properties of the rock vary with temperature, how radioactivity is related to depth and for oceanic regions how the oceanic plate cools after it is formed at the ridge. Recent laboratory measurements and field observations have provided enough data for the construction of detailed models, so that one can calculate characteristic geotherms for both continental and oceanic regions with some confidence [see illustration on page 76]. The depths to partial-melting conditions predicted from such calculations agree well with the seismologists' results from their surface-wave studies. Both the heat-flow measurements and the seismological data indicate that oceanic plates thicken as they age, from a few kilometers soon after their formation at a ridge to 100 kilometers or more in the oldest ocean basins, where the heat flow is low.

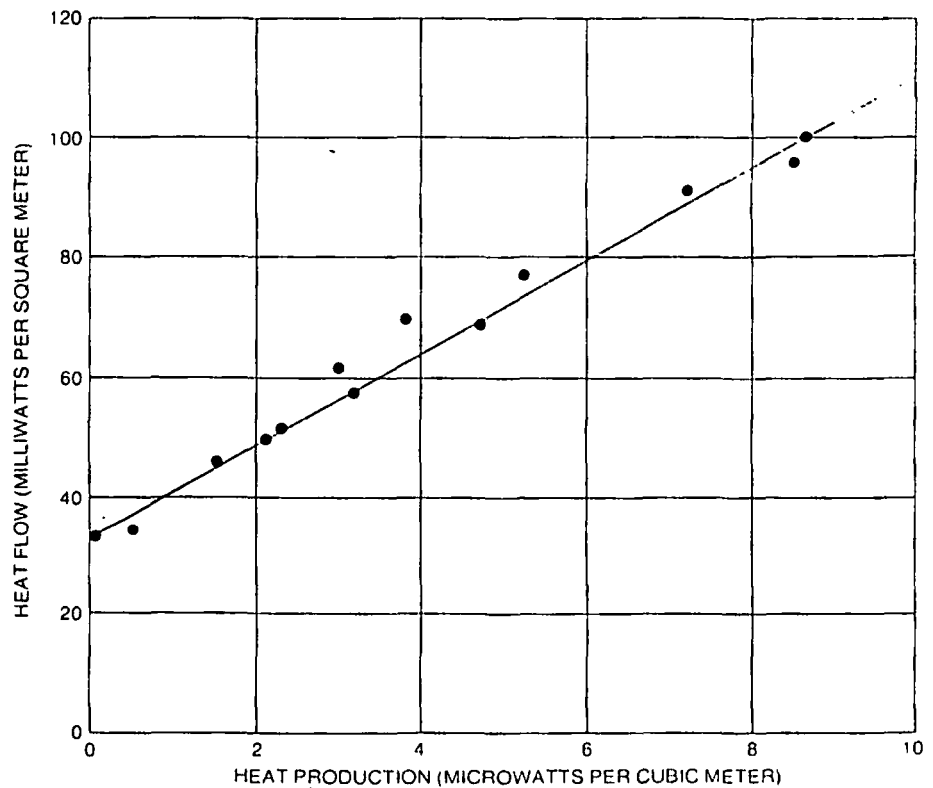
The continental portions of the tectonic plates also show a systematic variation in thickness, from 40 kilometers in young geologic provinces whose heat flow is high to several hundred kilometers under continental shields whose characteristic heat flow is much lower [see bottom illustration on next two pages]. For some shields the geotherm does not intersect the mantle's melting curve at any depth, and so in a strict sense the asthenosphere should not exist under the shields. In these areas thick lithosphere would be coupled directly to the deeper interior, acting as an "anchor" to retard the motion of the plate system. More realistically, we expect that the plate constituting a shield does decouple from the deeper interior, probably at a depth at which the geotherm makes its closest approach to the melting curve of the mantle. In a sense, then, the continental shields are at present probably dragging anchor.

Thermal History of the Earth

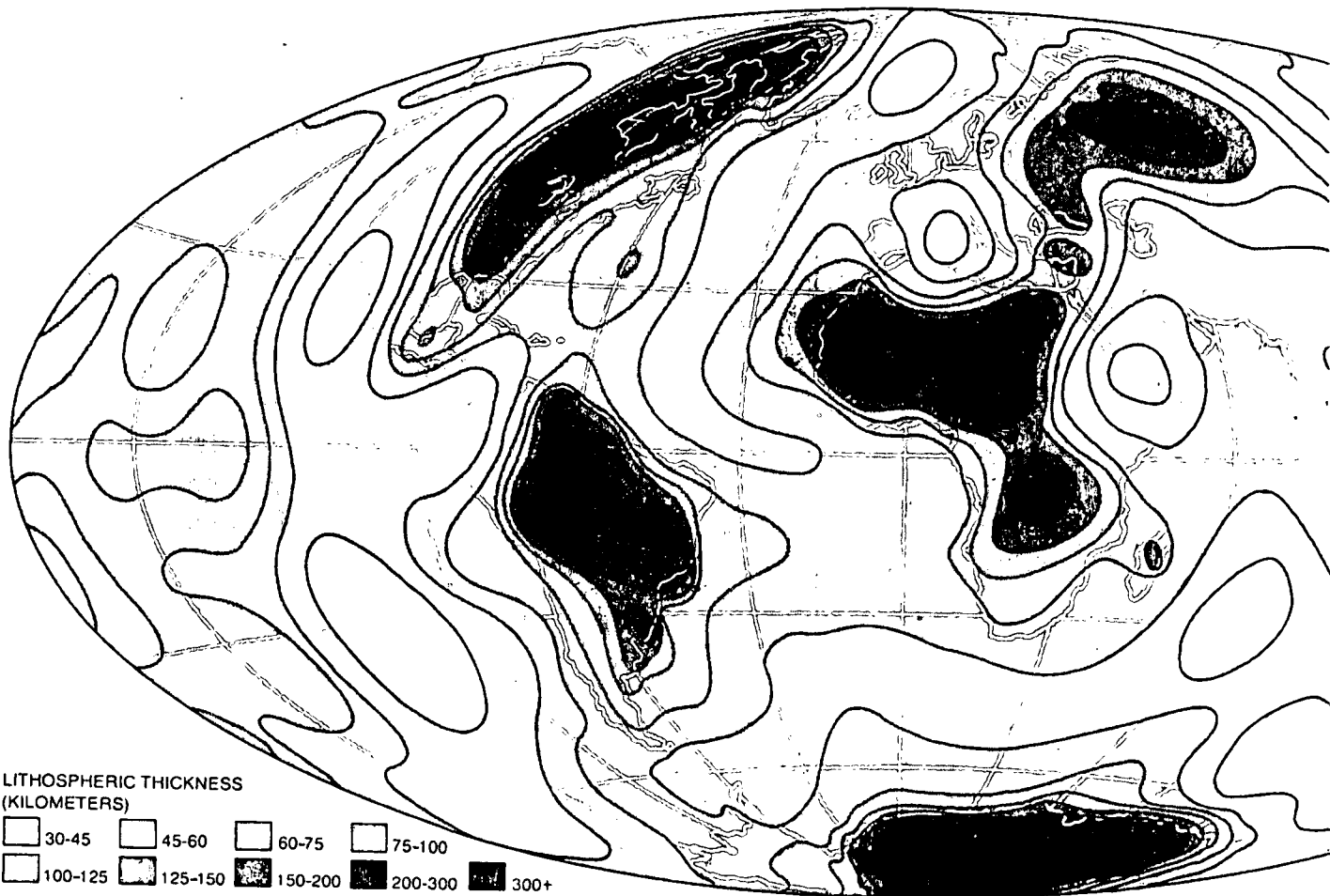
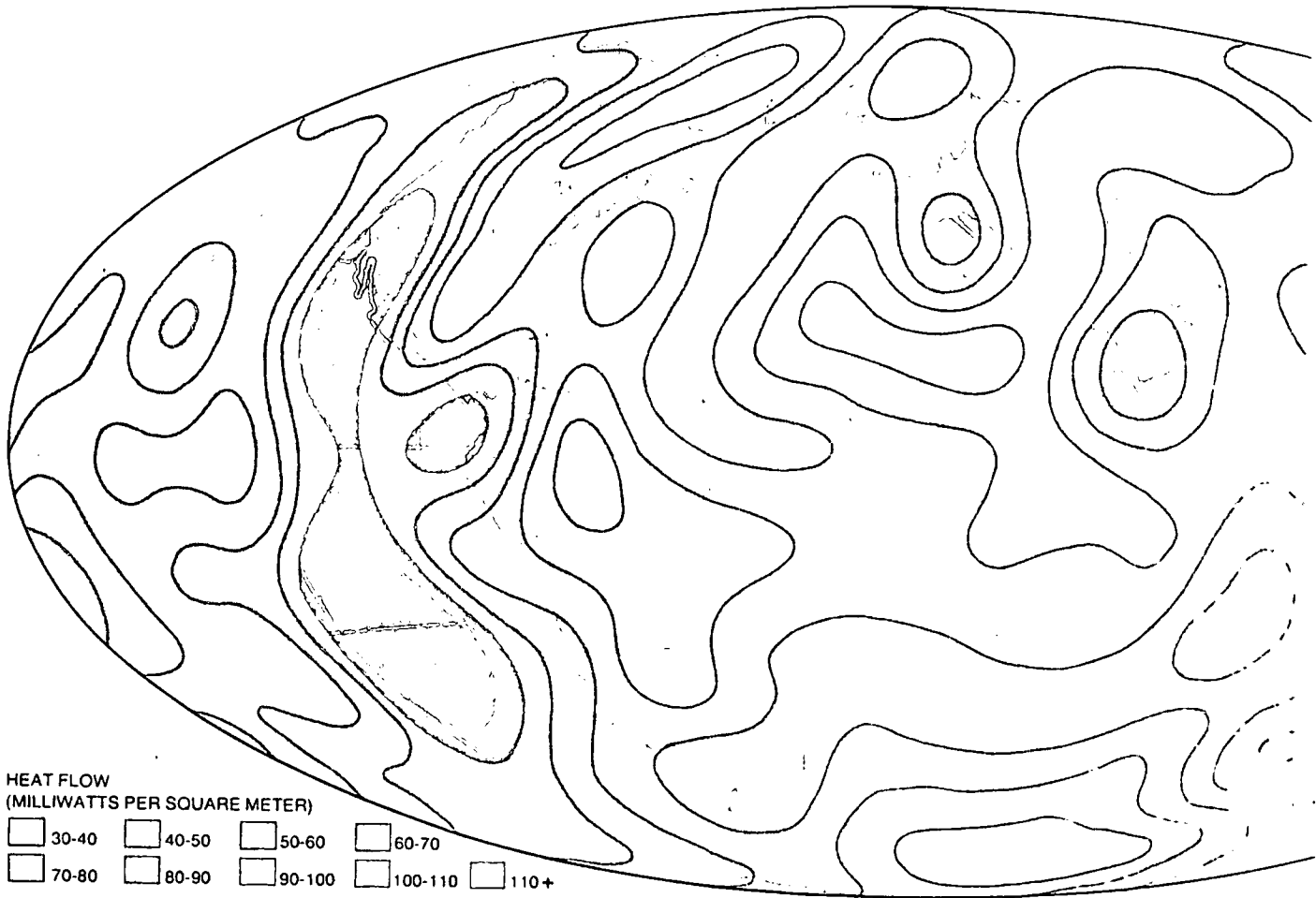
What can be said about the thermal state of the earth in times long past? Most treatises on this subject begin by telling why the problem is a difficult one and then offer a series of disclaimers in case one or another assumption should turn out to be invalid. (The lesson of Kelvin has not been lost on others!) Nevertheless, some observations can be ventured that make possible certain broad inferences, even though the details necessarily remain indistinct. One first must note the abundance within the earth's crust of the principal heat-pro-



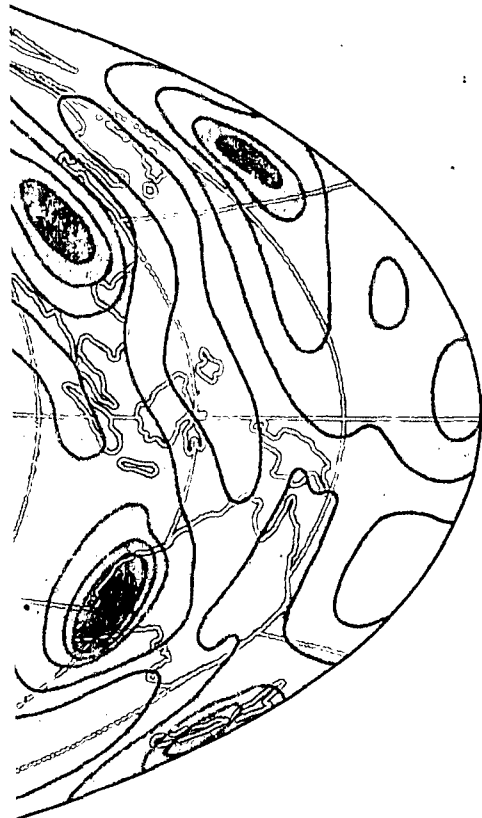
ON CONTINENTS the distribution of heat-flow values also shows an apparent relation to the age of the last major tectonic event that affected the region, just as the distribution of oceanic heat-flow values is associated with the time elapsed since volcanic rock began to cool following the extrusion of mantle material at an oceanic ridge. In the case of continents, however, the measurements indicate that the loss of heat after the tectonic event extends over an interval that is four or five times longer than the decay time for heat flow from the oceanic plate.



CHARACTERISTIC LINEAR RELATION is frequently discovered in plotting heat flow against heat production for a particular region, as can be seen in this graph for data obtained in the eastern U.S. (black dots). Such variations in heat-flow data for different continental regions can often be attributed to differing concentrations of heat-producing radioactive isotopes in the outer few kilometers of the earth's crust. The point where the colored line intercepts the vertical heat-flow axis indicates the amount of heat flow coming from below this zone of crustal radioactive-isotope enrichment. The slope of the line tells how deep within the crust the enrichment persists. The slope and intercept values together serve to characterize different heat-flow provinces. The variation of heat flow within a province is governed by the regional variability of the crustal isotopic enrichment. The differences in heat flow between provinces arise principally from variations in the amount of heat flow coming from below the crust.



WORLD HEAT-FLOW MAP, constructed by the authors on the basis of the available observations supplemented by estimates, shows variable patterns of heat flow on a global scale. The main zone of high heat flow (*darker shades of color*) is in the eastern Pacific Ocean off Central America and South America. This zone coincides with the East Pacific Rise, a major oceanic ridge where new sea floor is being extruded and carried away quite rapidly to yield a comparatively broad band of high heat loss. The oceanic ridges in the Atlantic Ocean and the Indian Ocean are spreading more slowly and hence result in a narrower zone of above-average heat flow. Other regions of fairly high heat flow include the marginal ocean basins of the western Pacific, which overlie active subduction zones, the western cordillera of North America, where subduction ceased between five and 10 million years ago, and Alpine Europe. The principal regions with below-average heat flow (*lighter shades of color*) include all the ancient Precambrian shield and platform areas of the continents and the oldest parts of the ocean floor.



ducing radioactive isotopes: thorium 232, uranium 238, potassium 40 and uranium 235. The continental crust averages 40 kilometers in thickness, less than 1 percent of the earth's radius, yet its endowment of these heat-producing isotopes is great enough for 40 percent of the heat flow at the earth's surface to arise within the crust itself. The concentration of isotopes in the oceanic crust is less, but it still represents a significant enrichment. The implication of this upward concentration is that there has been a major geochemical segregation within the earth. The fact that continental rocks more than 3.5 billion years old show this enrichment indicates that the segregation took place very early in the evolution of the earth, in all likelihood at the same time that the earth differentiated into a dense metallic core and a lighter silicate mantle.

Significant information about the thermal and tectonic processes in the earth's interior comes from a consideration of how certain physical properties of the earth, such as its strength and viscosity, change with temperature. Viscosity is a measure of the ability of materials, including solids, to flow; a highly viscous material approaches rigidity, whereas a low-viscosity material is much more like a fluid. Elevated temperatures generally promote a lower viscosity. At the surface of the earth and within the lithosphere the rocks are comparatively cold and stiff, but deeper in the earth the increase of temperature with depth almost certainly is accompanied by a decrease of viscosity, which eventually enables the interior to behave like a fluid. Accordingly the interior is likely to be dominated by fluidlike movements driven by density differences of both compositional and thermal origin, in contrast to the purely conductive thermal regime that exists with-

in the lithosphere. In the early evolution of the earth it was probably the gradual reduction of viscosity as the earth was warmed by the radioactive heat that began the process of density stratification giving rise to the core and the upward concentration of the heat-producing isotopes. The rearrangement of the earth's mass as the core settled liberated gravitational energy, which must have accelerated the process. The formation of the earth's core was a unique mechanical and thermal event in the history of the earth, unmatched in scope or drama by the events of later aeons, in spite of the current preoccupation of the earth sciences with contemporary geodynamics as embodied in plate tectonics.

The long-term thermal evolution of the earth is closely linked to the abundance and life span of its heat-producing isotopes. For an isotope to be important in the earth's thermal history, it must be abundant enough and its radioactive half-life must be long enough for it to contribute significant amounts of heat over times comparable to the age of the earth (4.6 billion years). Only the isotopes mentioned above (thorium 232, uranium 238, potassium 40 and uranium 235), with their respective half-lives of 14.1, 4.51, 1.26 and .71 billion years, satisfy these requirements. Taking their relative abundances into account, and calculating the rate of heat generation three billion years ago, one finds that 2.2 times as much heat was being generated by radioactive decay then as is being generated now. This enhanced heat production was probably reflected in a commensurate increase in the heat flow at the earth's surface, from which one can infer that the lithospheric plates then were probably thinner, more easily fractured and hence probably smaller in area but greater in number than the plates of today. The asthenosphere un-

THICKNESS OF THE EARTH'S LITHOSPHERE, or rigid outer shell, can be estimated by selecting for each five-degree-square region of the earth's surface the "geotherm" that corresponds to the mean surface heat flow (*see illustration on next page*). The depth at which the geothermal curve intersects the incipient melting curve determines the thickness of the lithosphere in that region. As the map shows, the lithosphere is thinnest along the oceanic ridges and other regions of high heat flow and thickest under continental shields. According to authors, "there seems to be little doubt that this great thickness of comparatively cold and stiff rock imparts the long-term stability that has come to be associated with the Precambrian shields."

Amateur Telescope Making

Edited by Albert G. Ingalls
Foreword by Harlow Shapley

This three-book set is the authoritative reference library of the enthralling hobby of amateur telescope making. Through these books thousands have discovered a fascinating mechanical art combined with a great science.

BOOK ONE begins at the beginning, teaches the basics of glass grinding and how to complete the first telescope. (497 pages, 300 illustrations.)

BOOK TWO leads on into advanced methods of amateur optical work and describes new projects for the telescope maker. (650 pages, 361 illustrations.)

BOOK THREE opens up further fields of enterprise: binoculars, camera lenses, spectrographs, Schmidt optics, ray tracing (made easy). (644 pages, 320 illustrations.)

SCIENTIFIC

AMERICAN ATM Dept.,
415 Madison Avenue, New York, N. Y. 10017

Please send me postpaid the following AMATEUR TELESCOPE MAKING books.
My remittance of \$ _____ is enclosed.

- BOOK ONE \$ 8.00
- BOOK TWO \$ 9.00
- BOOK THREE \$10.00

For shipment outside U.S. add 75¢ each

Name _____

Address _____

City _____

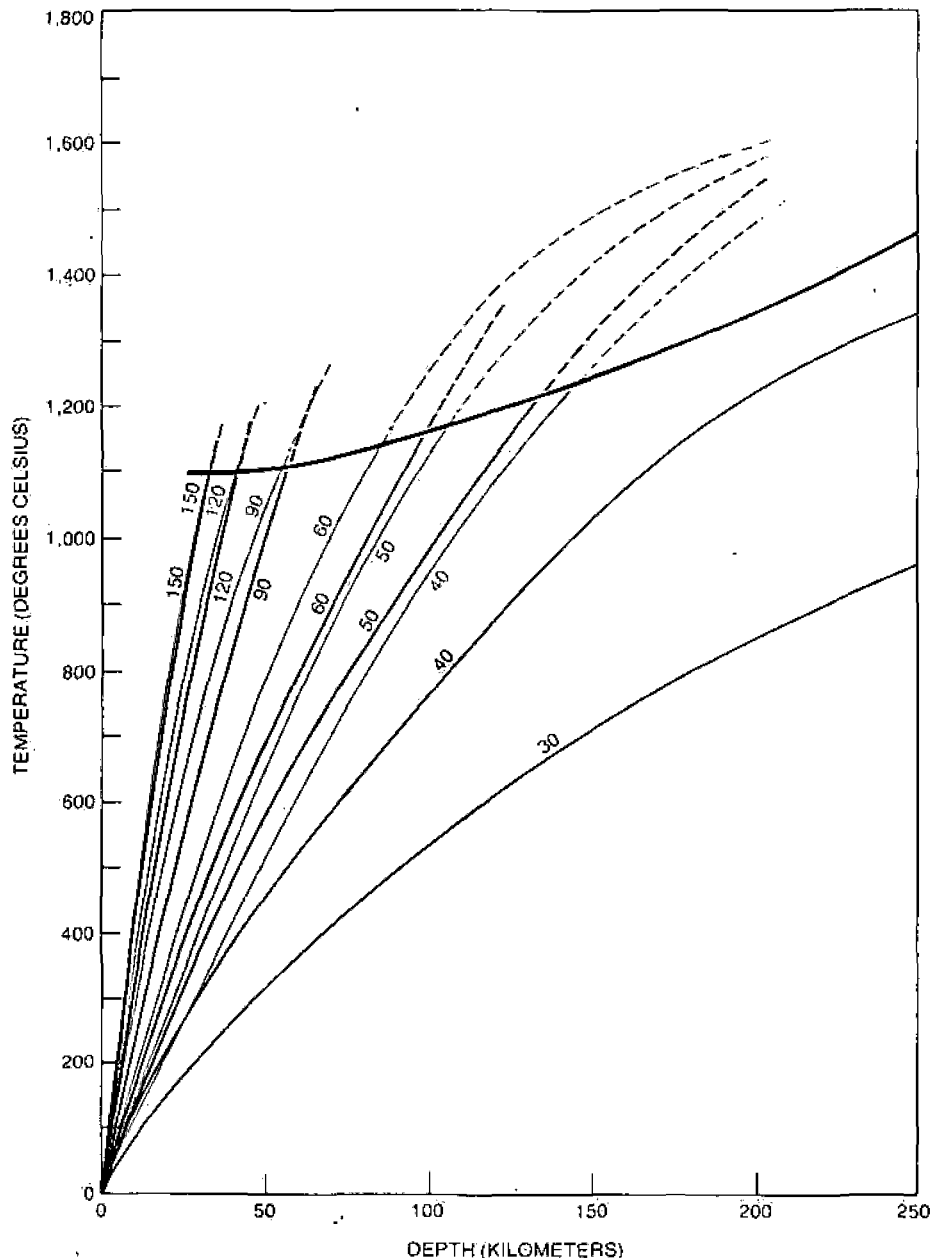
State _____ Zip _____

Residents of New York City please add city sales tax. Other NYS residents please add state sales tax plus local tax.

derlying the plates was probably in a more vigorous state of activity than it is at present.

In the future the lithosphere will continue to thicken and the asthenosphere will become more viscous, owing to the continued cooling of the earth and the slow decay of its radioactive heat sources. The motion of the thickening plates will become more sluggish and retarded, although interruptions in this long-term trend similar to the fragmentation and dispersal of the "supercontinent" of Pangaea over the past 180 mil-

lion years should be anticipated. As the continental shields continue to thicken and to develop substantial viscous anchors one can expect the motion of the plates eventually to cease, bringing to an end the plate-tectonic phase of the earth's evolution. Thus for the diminishing band of earth scientists who still adhere to a nonmobile view of the earth there may be some small solace in the fact that the earth will eventually conform to their concept of it. They must be patient, however, since that time is probably some two billion years hence.



TWO TYPICAL FAMILIES of geotherms (curves representing the variation of the earth's temperature with respect to depth) are shown here for a continental province (*black*) and an oceanic province (*color*). The members of each family of geotherms are labeled according to the heat flow (in milliwatts per square meter) produced at the earth's surface. As might be expected, the temperature found at a given depth in a region of high heat flow will be higher than the temperature at the same depth in a region of low heat flow. Heavy black curve most geothermal curves intersect represents the temperature at which rock will begin to melt in the earth's mantle. The depth at which such melting is observed is variable, depending on the heat flow and the geotherm for that region. Under some continental regions with low heat flow (in particular the stable Precambrian shields) there is probably no melting. Many geologists and geophysicists believe the base of the rigid lithosphere is defined by the onset of partial melting.

SUBJ
GPHYS
GET

UNIVERSITY OF UTAH
RESEARCH INSTITUTE
EARTH SCIENCE LAB.

GROUNDNOISE EXPLORATION TECHNIQUES

By

Lewis J. Katz

Utah Geophysical Inc.

P.O. Box 9344

Salt Lake City, Utah 84109

Publication rights are reserved. This paper was presented at the 48th Annual Meeting of the Society of Exploration Geophysicists in San Francisco, California. GEOPHYSICS has first claim on this paper for publication. Publication elsewhere is hereby restricted to the author's abstract, or to an abstract of not more than 300 words, without illustration, unless the paper is specifically released by the Editor of GEOPHYSICS or the Executive Director on his behalf. Such abstract should contain appropriate, conspicuous acknowledgment.

ABSTRACT

Groundnoise crustal inversion techniques have successfully been used to define overburden layer thicknesses. Power Spectral Density (PSD) estimates are generated from groundnoise data and observed spectral peaks are used for interpretation. Since the spectral peaks are related to the resonant frequency of the layer, travel time of the layer can be ascertained. Examples of determining thicknesses for one and two layer cases overlying basement are presented. Results are compared to drill hole depths and other geophysical surveys. The groundnoise depths appear to offer greater accuracy and resolution than gravity, magnetic, and refraction surveys in the area investigated.

INTRODUCTION

The use of seismic groundnoise (microtremors) in determining overburden layer thicknesses and normal faulting has proven successful in several geophysical exploration programs. Applications of this technique have ranged from determining depth to bedrock of several thousand feet for copper exploration in Arizona to mapping buried channels for uranium exploration in Wyoming. These surveys have proven successful in areas where refraction, gravity, and magnetic surveys have failed. In the following sections of this paper a brief discussion on theory and two case histories will be presented to demonstrate the technique and provide insight into its application. For the reader desiring a more in depth discussion on theory he is referred to Katz (1976). The two case studies presented were chosen because there was well control to confirm results, other geophysical surveys for comparison, and availability of non-proprietary data.

THEORY

The energy source used in these studies are naturally occurring microtremors (groundnoise) which are low amplitude oscillations of the ground surface that are everywhere present. When these are generated

from non-cultural sources (i.e. not from cars, trains, etc.) their source spectrum has been found to be white (flat) over the frequency range of interest (1-30 Hz) and they appear as a compressional (P-wave) form of seismic energy. Microtremors entering a low velocity layer or system of layers overlying a half-space are multiply reflected at the top and bottom acoustic impedance interfaces. These processes combine to cause the layer to enhance selected frequencies related to the periodicity of the layer. This effect is known as resonance and can be observed on microtremor Power Spectral Density (PSD) estimates. That is, groundnoise PSD plots recorded over a layered system exhibit resonant peaks. Since these resonant peaks are related to the frequency-amplification characteristics of the low velocity layer, travel time of the layer can be determined. An estimate of layer velocity can also be obtained from the spectrum.

Two additional points should be made. Normal incidence is assumed and several investigators have indicated that they believe that the source mechanism for microtremors are Rayleigh waves rather than P-waves. To the knowledge of the author, none of these investigators have established Rayleigh waves to exist at higher frequencies (above 2 Hz) using naturally occurring microtremors. Hudson and Douglas (1975) have

reported that they have found Rayleigh wave spectral peaks, group velocity minima, and P-wave resonance of a layer all to occur at about the same frequency. If this be the case, results would be independent of wave mode. However, the author could not substantiate this in practice (Katz and Bellon, 1978).

DATA ACQUISITION AND PROCESSING

Sprengnether MEQ-800 microearthquake systems, together with DataMagnetics (Oklahoma City) digital tape units, were used to record field data. Halls Sears HS-10(1Hz) vertical geophones were used as sensors with the above recording equipment. All recording equipment were standard types conventionally used in microearthquake surveys, with the exception of the tape recorders. The digital tape recorders were operated continuously for 24 hours sampling at 100 points per second. The advantage of digital compared to analog recording in acquiring microtremor data is in their high dynamic range (72 db) and reduction in system noise. Each site was occupied for 24 hours.

Field data were edited using smoked paper records recorded in the field to locate portions of data not containing transient noise sources (i.e., automobile traffic). The microtremor data were then broken into

blocks of 1024 samples. A Fast Fourier Transform was performed on each block and spectra from 175 data blocks (30 minutes) were stacked to produce each PSD estimate. The amount of data used is significant in obtaining high (90-95%) statistical confidence limits in the PSD estimates (Katz, 1976).

Computer models used for interpretation are based on the Thompson-Haskell matrix transformation. (Haskell, 1962). For a single layer overlying basement the model peaks at the theoretical resonance frequencies of the layer

$$f = \frac{(2n-1)\alpha}{4h}$$

where

$$n = 1, 2, 3 \dots$$

$$\alpha = \text{P-wave velocity of the layer}$$

$$h = \text{thickness of the layer}$$

The amplitude of these peaks are proportional to the impedance mismatch of the layer and basement.

RESULTS

Two cases are presented: Case 1 is a single layer overlying basement and Case 2 is two layers overlying basement.

Case 1 - Beatty, Nevada; Single layer

Beatty, Nevada, provided an area of study in which a drill hole, well log, and refraction data were available. Thus, the geology was well known and the validity of the groundnoise technique could be verified. Geology obtained from the above mentioned sources and instrument deployment is summarized in Fig. 1. Station 1 was located above the drill hole and its PSD estimate (solid curve) is shown in Fig. 2 along with that of Station 8 which was on hard rock. The dotted curve is the computer model used for interpretation. Note that the hardrock PSD does not exhibit any predominate amplitude lobes, whereas, the layered PSD plot does. This is to be expected since there is no layer at the hardrock site to cause resonance. It can be assumed that the hardrock spectrum is similar to the input (source) spectrum at the base of the layer. Therefore, it can be seen that the amplitude lobes are entirely a result of the layer response and not derived from source effects. The frequency at which the peak amplitude of the model occurs is inversely proportional

to the travel time of the layer being modeled. Thus, a one-way travel time of 30 msec is obtained for the layer at Station 1. The travel time (30 msec) times the velocity of the layer (1340 m/sec) results in a depth of 41 meters which is the same as that obtained from the drill hole. Stations 2 and 5, Figures 3 and 4 respectively, indicate a layer thickness of 39 meters which agrees with the refraction results. A secondary lobe seen at about 15 to 17 Hz is attributed to a nearby water pump. Thus, the validity of groundnoise crustal inversion techniques in determining over-burden layer thickness has been demonstrated.

Case 2 - Milford, Utah; Two layers. Data were obtained from several groundnoise stations used to delineate a geothermal heat source at Roosevelt Hot Springs, Utah (Fig. 5). The University of Utah has several gravity and magnetic profiles (Crebs and Cook, 1976), drill holes (Whelan, 1977), and resistivity lines (Ward and Sill, 1976) throughout the area. In addition, two Phillips Petroleum Co. wells (54-3 & 3-1) and one Thermal Power Corp. well (14-2) have been drilled along these geophysical profiles. Drill hole information is summarized in Table 1.

Groundnoise Station 5 is located at the intersection of University of Utah east-west profile 4000N and their north-south baseline (0) profile. Drill holes DDH1A and DDH1B are also located near this site. There may be

Table 1
Summary of Drill Hole Data

Well	Depth to Bedrock	Geology	Reference
DDH1A	35 m	0-35m - Altered Alluvium (Alunite) 35-66m (T.D.) Altered Precambrian gneiss	Parry <u>et al.</u> (1976)
DDH1B	47 m	0-47m - Altered Alluvium 47m-70m (T.D.) Altered Precambrian gneiss	Whelan (1977)
54-3	91 m		Ward & Sill (1976)
3-1	195 m		Phillips Petroleum Co.
14-2	49 m	0-49m - Alluvium 49-488m - Quartz Monzonite 488-625m - Biotite Granite (intensely altered) 625m - Hornblende Biotite Quartz Monzonite (weakly altered)	U of Utah Research Institute

a small discrepancy as to the exact locations of drill hole DDH1A and the other surveys because of the mislocation of a quarter section marker used as a reference. Parry, et al. (1976) describes the surface layer at DDH1A as an altered alluvium being 35 meters thick which overlies a clay altered Precambrian gneiss from 35 meters to the total depth of the drill hole (66 m) and probably to a depth of 500 or 600 meters (Ward and Sill, 1976). A sonic log from well 14-2 showed a velocity of 5640 m/sec (18,500 fps) for unfractured igneous basement rocks. Velocities of 2440 m/sec (8000 fps) for the altered alluvium layer and 4725 m/sec (15,000 fps) for the altered gneiss (or fractured igneous) layer were estimated from the PSD plots.

Interpretation of one-way travel time in each layer is determined by fitting computer models to observed groundnoise PSD plots. The interpretation model for Station 5W (Fig. 6) has been broken into separate components to illustrate the contributions from each layer. The dotted curve corresponds to the second layer. It has an amplitude peak at its fundamental frequency (1.5 Hz) and harmonics at multiples of $2n+1$ times this frequency. The first harmonic is seen at 4.5 Hz. One way travel time of this layer is 167 msec corresponding to a peak amplitude at 1.5 Hz. Because of the small impedance difference between this layer and

basement, amplitude lobes are small. The dashed curve is the contribution from the surface alluvial layer and the frequency (18 Hz) at which its peak amplitude occurs corresponds to a layer travel time of 14 msec. Observed groundnoise PSD plots (solid), computer models (dashed) and geological sections interpreted from the groundnoise data are shown for Stations 5E, 5S, and 5N in Figs. 7 through 9, respectively.

COMPARISON OF RESULTS

The east-west gravity profile (4000N) through Stations 5W and 5E is shown in Fig. 10. Interpreted thickness from groundnoise and gravity data for Station 5W agree at 34 meters for the alluvium layer. Both agree with drill hole DDH1A. However, at Station 5E there is a large discrepancy. The groundnoise indicates a thickness of 48 meters, whereas, the gravity indicates a thickness of 210 meters. The north-south gravity profile, Fig. 11, through Stations 5S and 5N indicates a depth to bedrock of about 125 meters which also disagree with the groundnoise depths of 53 meters for Station 5W and 76 meters for Station 5N.

Discrepancies are difficult to resolve without additional drill hole information. However, several points can be made in support of the groundnoise results.

Drill hole DDH1B to the southwest of Station 5S had a measured depth of alluvium of 47 meters which is comparable to the 53 meters found at Station 5S. Drill hole DDH1A is believed to lie along the north-south (baseline) gravity profile. At this location the depth of alluvium indicated by gravity modeling is 125 meters compared to 35 meters found by drilling. Since this gravity profile ties gravity profile 4000N, it too appears to be indicating a depth of alluvium that is too large. Projecting these findings eastward to Station 5E, the 48 meters determined by groundnoise appears to be reasonable. However, the gravity thickness determined at Phillips Petroleum's well (3-1) located about 400 meters east of Station 5E agrees with well results of 195 meters. Perhaps difficulty was encountered in gravity interpretation when rock alteration was present. Gravity results failed to differentiate the gneiss layer, although this second layer was used in modeling magnetic data (Crebs and Cook, 1976) around Station 5. It is also possible that groundnoise Station 5E was on the upthrown block of the Dome fault and the gravity results were obtained from the downthrown side since there is some question of exact locations.

Altered Precambrian gneiss has been reported in drill holes (Parry et al., 1976) west of the Dome fault and fractured igneous-metamorphic rocks east of the Dome

fault. The magnetic interpretation at Station 5 used a thickness of about 125 meters for the second layer (altered Precambrian gneiss). The groundnoise determined this layer to be about 788 meters thick. Resistivity interpretation (Ward and Sill, 1976) show this layer to be about 600 meters thick which would support the groundnoise interpretation. It is interesting to note that this second layer is thicker at Station 5E than at the other stations. This would indicate thickening of the layer to the east or possible fault displacement at depth. A more likely reason for this effect is that Station 5E lies over an area where the second layer is composed of fractured igneous-metamorphic rocks resulting in slower velocities and thus an apparent increase in travel time. Indications of this can be seen by examining the peak to trough amplitude difference of spectral lobes appearing at about 10 Hz. On spectra from Stations 5S and 5E which are close to the Dome fault, the amplitude of these lobes are about 6 db compared to 12 db at Stations 5N and 5W. These amplitudes are related to the impedance or velocity ratio at the alluvium/fractured igneous or gneiss interface. Therefore, if the velocity of the second layer decreases, the velocity ratio between layers becomes smaller and the amplitude of spectral peaks diminishes. Since amplitude peaks appearing on spectra at Stations 5S and 5E located near the Dome fault are smaller than those

at Stations 5N and 5W, it can be assumed that the alluvium layer at these stations are underlain by fractured igneous rocks having lower velocities than the gneiss under Stations 5N and 5W. A higher velocity for the gneiss layer would probably have resulted in a better model fit at Stations 5N and 5W. At well 14-2 the fractured igneous layer is about 600 meters thick.

A shallower fault is believed to exist between Stations 5W (34 m) and 5N (76 m). This interpretation is based on the 42 meters difference in alluvial thicknesses at these two closely spaced stations. Parry, et al. (1976) also inferred a fault in this location from surface mapping of opalized alluvium.

DISCUSSION AND CONCLUSIONS

In general, there appears to be more evidence supporting results obtained by groundnoise techniques than those results obtained from gravity and magnetics. Any error in the groundnoise interpretation would have been caused from an incorrect velocity being used. A 10% change in velocity would result in a 10% change in thickness. Results from this technique are similar to those of seismic reflection surveys in that both record travel time information to which velocities have to be applied.

There are several advantages of groundnoise surveys over other geophysical surveys. Compared to gravity and magnetics they offer greater resolution and accuracy. Gravity techniques depend on density contrasts between layers. The groundnoise uses the product of density and velocity at the interface. The velocity ratio being larger offers greater resolution, as was seen in its ability to detect a second layer at Milford, Utah. A refraction survey was also attempted at Roosevelt Hot Springs but ran into difficulty with weak arrivals. Similar problems with refraction surveys were encountered in other areas where the groundnoise proved successful. In addition, refraction surveys depend on tying several stations together to get apparent velocities and depths.

This can result in large errors. Groundnoise interpretation is based on single station data and therefore these problems do not occur. Additional advantages are: maximum portability of field recording system, non-destructive energy source that is environmentally acceptable (permitting not required in most areas), and it is economically cost effective. The groundnoise technique can compete in several applications with high resolution seismic reflection surveys at a fraction of the cost.

Applications of groundnoise techniques in oil and gas exploration include:

static corrections for reflection surveys, geophone design, and preliminary reconnaissance. With the onset of surface sources such as Vibroseis, the determination of overburden thicknesses for statics corrections need to be determined by means other than drill holes. The groundnoise technique ascertains the travel time of surface layers that can be used to correct reflection data. In this application velocity does not need to be determined since reflection data is also in travel time format. Hudson and Douglas (1975) have shown that Rayleigh wave spectral peaks occur at P-wave resonant frequencies. This information is easily derived from the groundnoise spectrum and is important in designing

geophone arrays to suppress surface wave motion. Normal faulting is easily detected by mapping changes in overburden thickness. The downthrown side of a fault would have a thicker surface layer and a corresponding shift in spectral peaks to lower frequencies.

It is the author's hope that this paper will stimulate interest in this most promising exploration tool.

References

- Aki, K. (1957). Space and time spectra of stationary stochastic waves, with special reference to microtremors, Bull. Earthquake Res. Inst., Tokyo Univ., 35, 415-456.
- Alcock, E. D. (1974). Comments on "comparison of earthquake and microtremor ground motions in El Centro, California" by F. E. Udvardi and M. D. Trifunac, Bull. Seism. Soc. Am. 64, 495.
- Asten, M. W. (1976). The use of microseisms in geophysical exploration, Ph.D. Dissertation, Macquarie University, North Ryde, N.S.W., Australia.
- Borcherdt, R. D. and J. F. Gibbs (1976). Effects of local geological conditions in the San Francisco Bay Region on ground motions and the intensities of the 1906 earthquake, Bull. Seis. Soc. Am., 66, 467-500.
- Crebs, T. J. and Cook, K. L. (1976). Gravity and ground magnetic surveys of the central mineral mountains, Utah: Dept. Geol. & Geophys. Univ. of Utah, NSF Report, Vol. 6.
- Frantti, G. E. (1963). The nature of high-frequency earth noise spectra, Geophysics 28, 547-581.
- Haskell, N. (1962). Crustal Reflections of plane P and SV waves, J. Geophys. Res. 67, 4751-4767.
- Hudson, J. A. and Douglas, A. (1975). Rayleigh wave spectra and group velocity minima, and the resonance of P-waves in layered structures: Geophys. J.R. astr. Soc., Vol. 42, p. 175-188.
- Kanai, K. and T. Tanaka (1961). On microtremors, VIII, Bull. Earthquake Res. Inst. 39, 97-114.
- Katz, L. J. (1976). Microtremor analysis of local geological conditions: Bull. Seis. Soc. Am., Vol. 66(1):45-60.
- Katz, L. J. and Bellon, R. S. (1978). Microtremor site analysis study at Beatty, Nevada: Bull. Seis. Soc. Am., Vol. 68, 757-765.
- Liaw, A. L. (1977). Microseisms in Geothermal Exploration: Studies in Grass Valley, Nevada, Ph.D. Thesis, Univ. of Calif./Berkeley, LBL-7002.

- Parry, W. T., Benson, M. L. and Miller, C. D. (1976).
Geochemistry and hydrothermal alteration at selected
Utah hot springs: Dept. Geol. & Geophys., Univ.
of Utah, NSF Report, Vol. 3.
- Sanford, A. R., Carapetian, A. G., and L. T. Long (1968).
High frequency microseisms from a known source,
Bull. Seis. Soc. Am., Vol. 58, 325-338.
- Udwadia, F. E. and M.D. Trifunac (1973). Comparison of
earthquake and microtremor ground motions in
El Centro, Calif., Bull. Seis. Soc. Am. 63, 1227-1253.
- Ward, S. H. and Sill, W. R., 1976, Dipole-dipole resis-
tivity surveys, Roosevelt Hot Springs KGRA: Dept.
Geol. & Geophys., Univ. of Utah, NSF Report Vol. 2.
- Weller, C. E. (1974). Seismic Exploration Method, U.S.
Patent 3,812,457.
- Whelan, J. A. (1977). Thermal gradient and heat flow
drilling: Dept. Geol. & Geophys., Univ. of Utah,
NSF Report, Vol. 5.

List of Figures

- FIG. 1. Approximate vertical section showing the instrument deployment and physical property data for the Beatty experiment.
- FIG. 2. Station 1, comparison of PSD estimate (solid) and single layer computer model (dotted). Layer thickness equals 41 meters. Hard rock PSD estimate (Station 8) also shown.
- FIG. 3. Station 2, comparison of PSD estimate (solid) and single layer computer model (dotted). Layer thickness equals 39 meters.
- FIG. 4. Station 5, comparison of PSD estimate (solid) and single layer computer model (dotted). Layer thickness equals 39 meters.
- FIG. 5. Location map Roosevelt Hot Springs, Milford, Utah.
- FIG. 6. Station 5W, comparison of groundnoise PSD estimate (solid) with computer model. Dotted curve is model contribution from layer 2 (788 meters) and dashed curve is contribution from layer 1 (34 meters).
- FIG. 7. Station 5E, comparison of groundnoise PSD estimate (solid) and two layer computer model (dashed). Layer 1 equals 48 meters and layer 2 equals 1.18 km.
- FIG. 8. Station 5S, comparison of groundnoise PSD estimate (solid) and two layer computer model (dashed). Layer 1 equals 53 meters and layer 2 equals 788 meters.
- FIG. 9. Station 5N, comparison of PSD estimate (solid) and two layer computer model (dashed). Layer 1 equals 76 meters and layer 2 equals 788 meters.
- FIG. 10. Interpretive two-dimensional model for gravity profile 4000N. Assumed density contrast is 0.5 gm/cc. From Crebs and Cook, 1976.

FIG. 11 Interpretive two-dimensional model for gravity profile baseline. Assumed density contrast is 0.5 gm/cc. From Crebs and Cook, 1976.

List of Tables

Table 1 Summary of drill hole data.

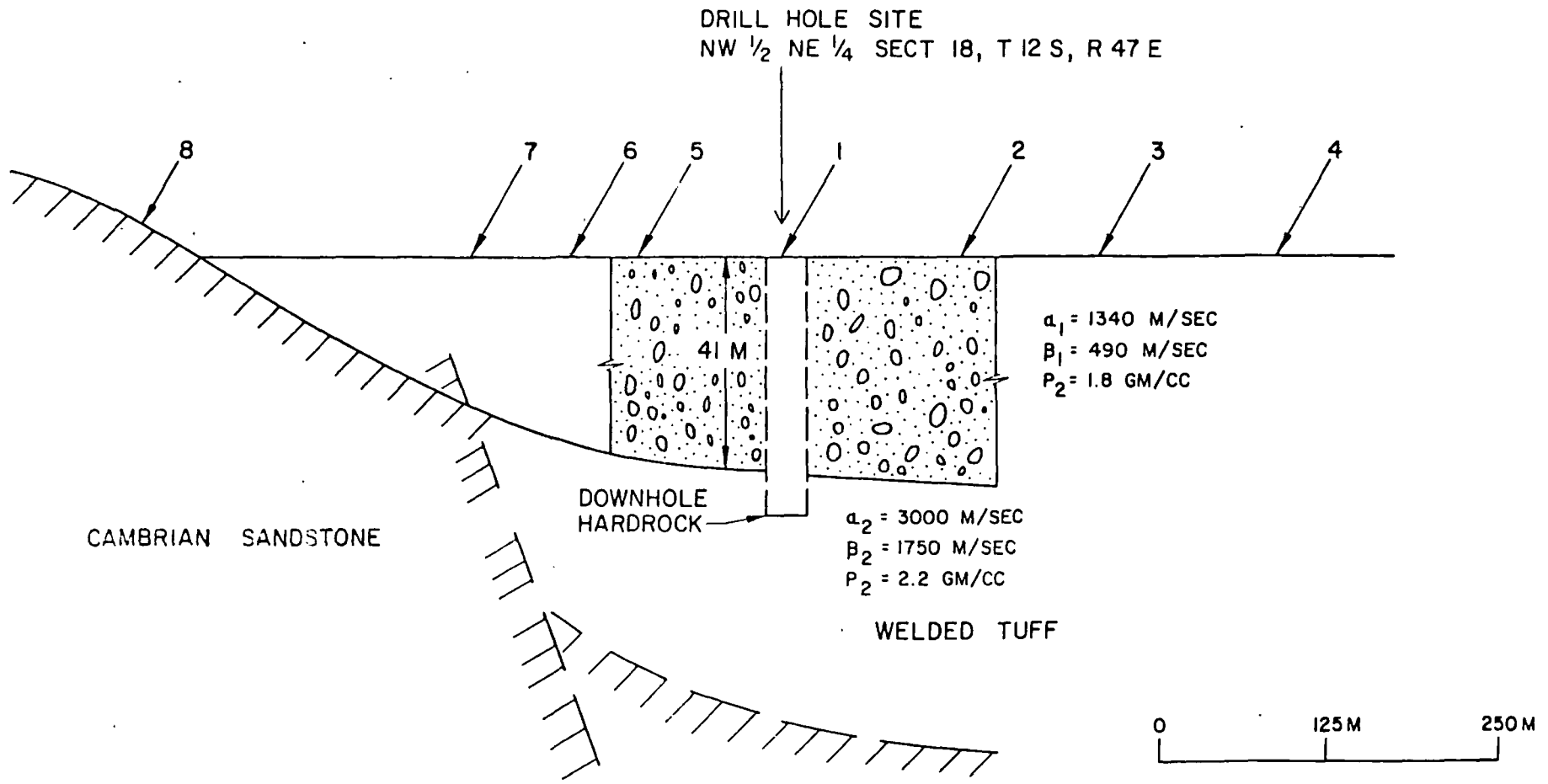
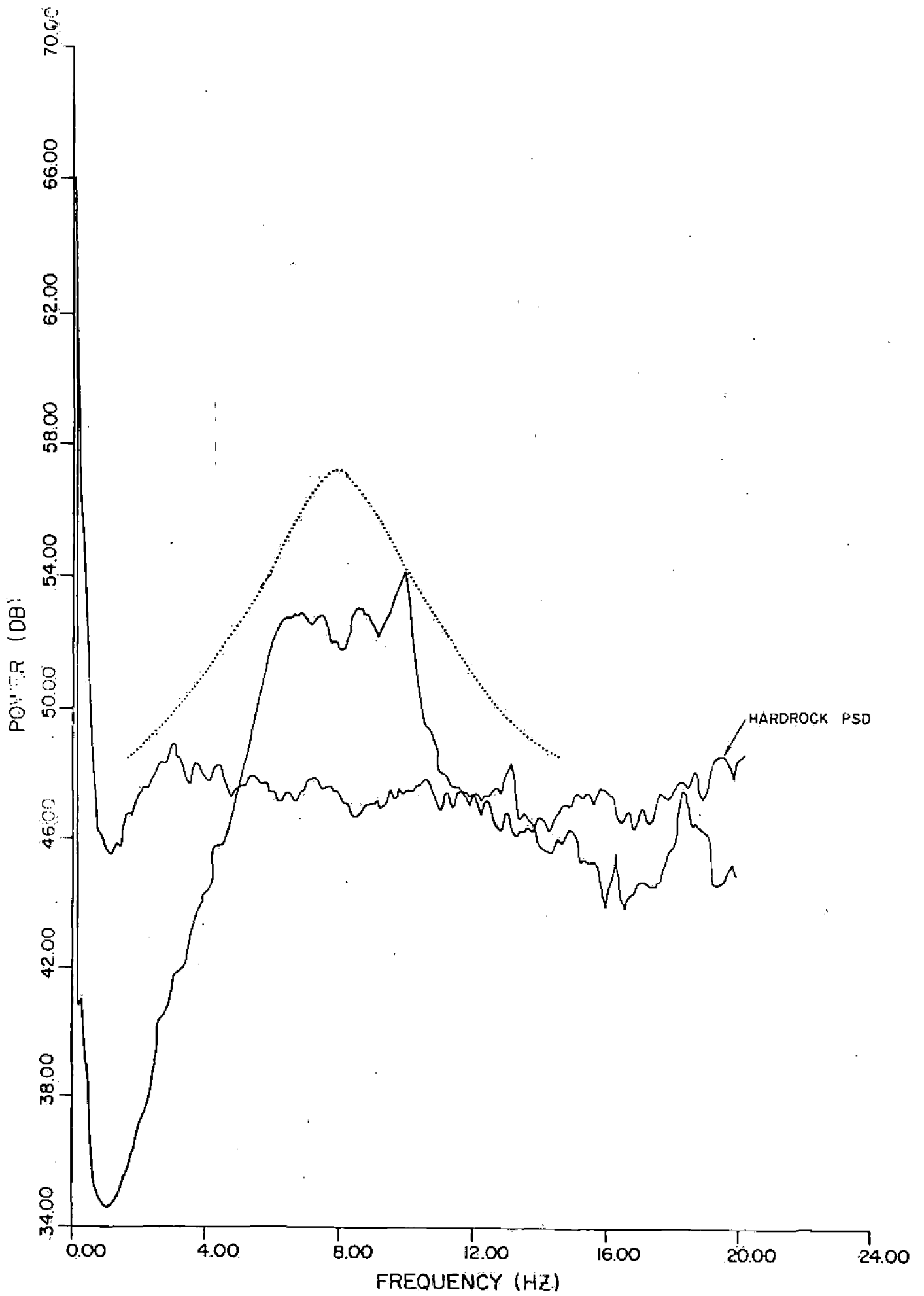
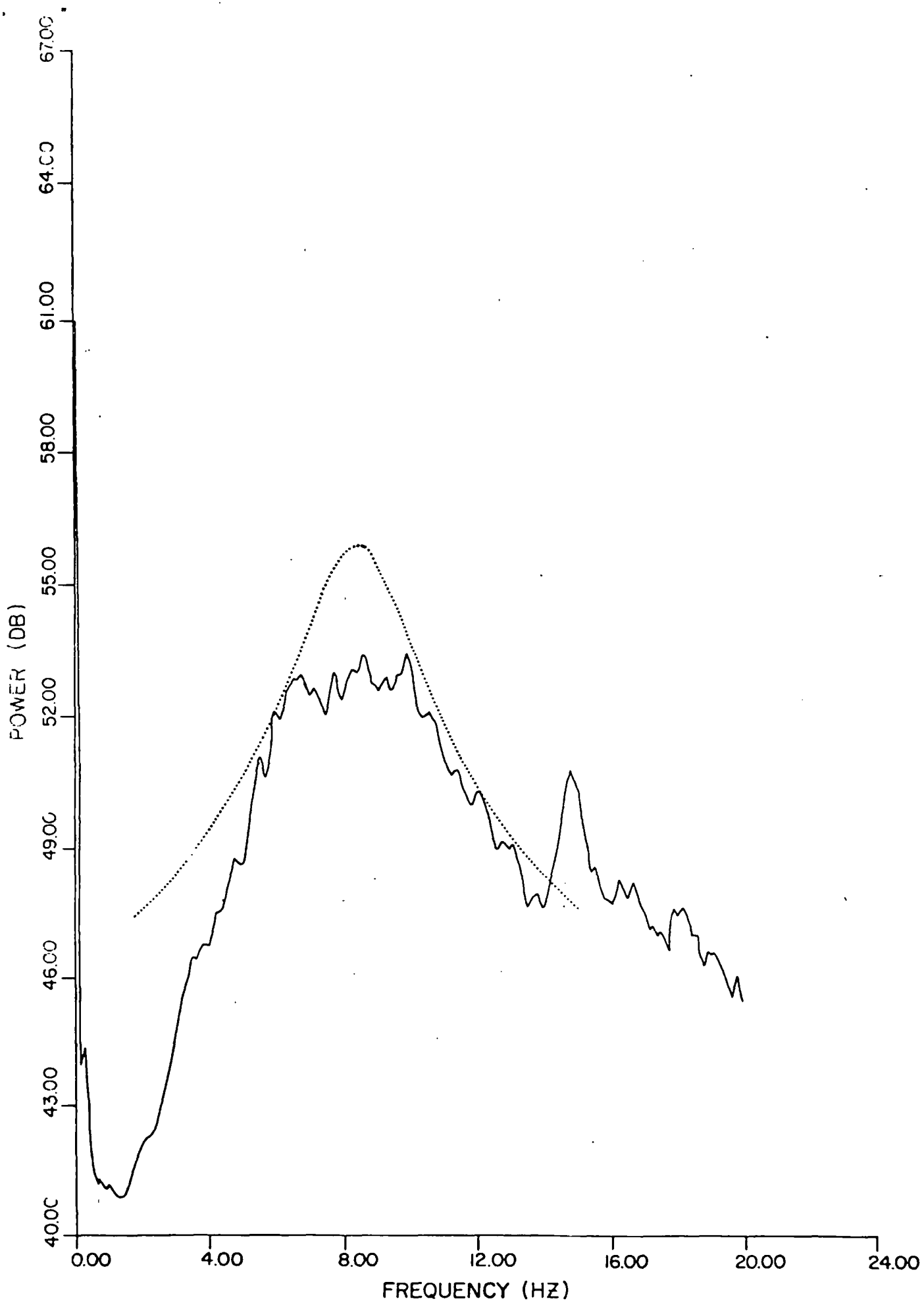
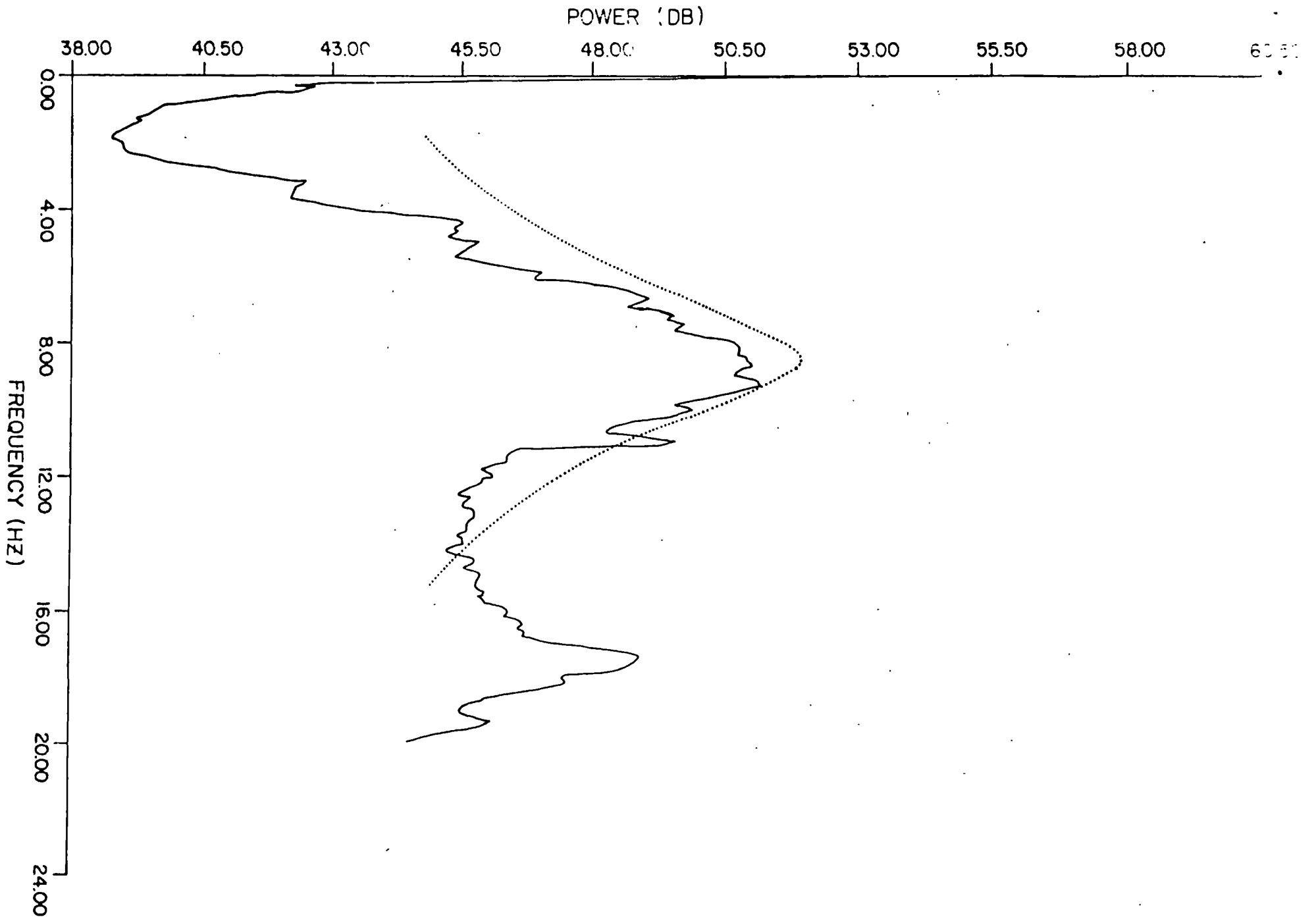
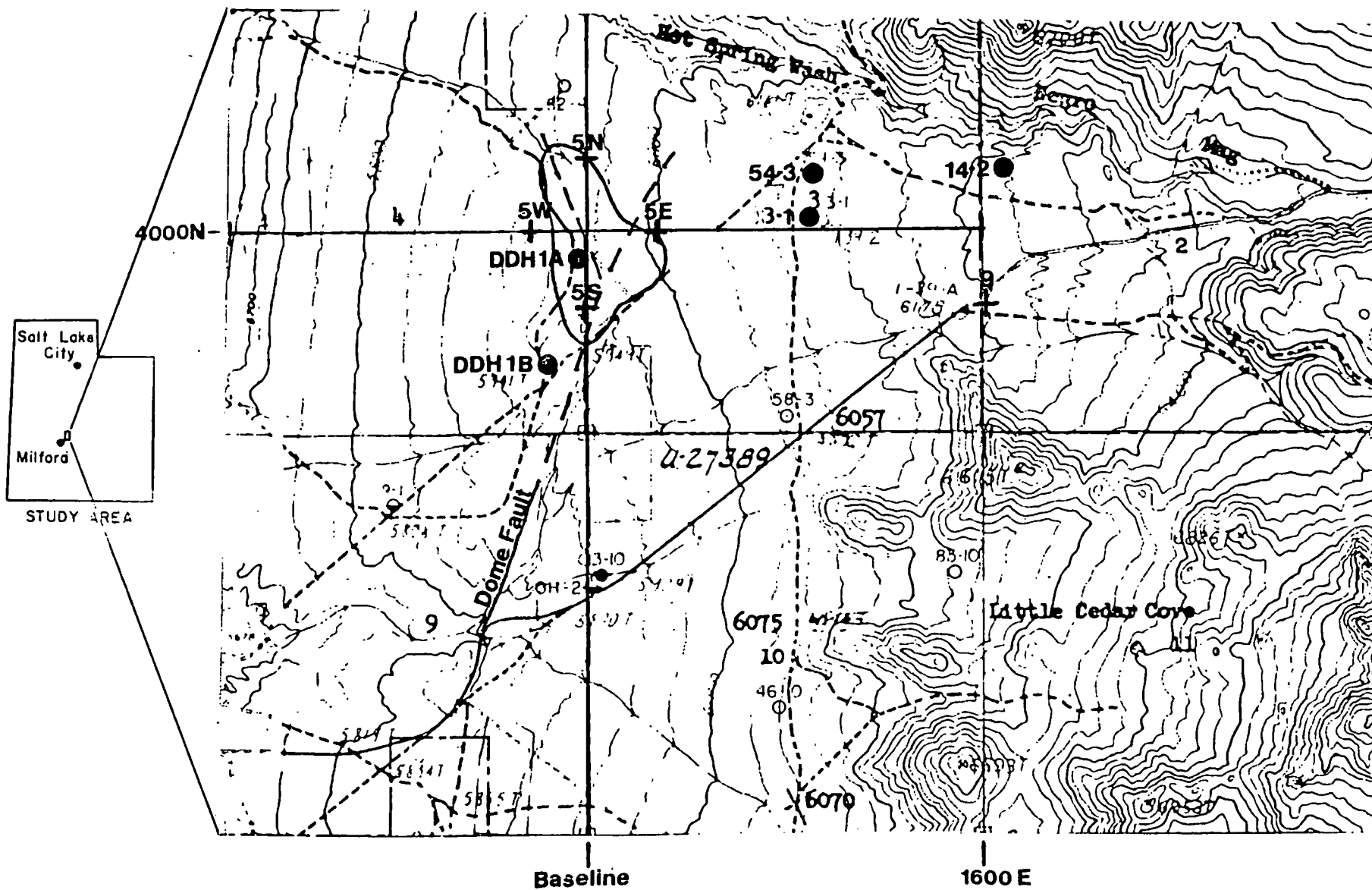


Fig 1









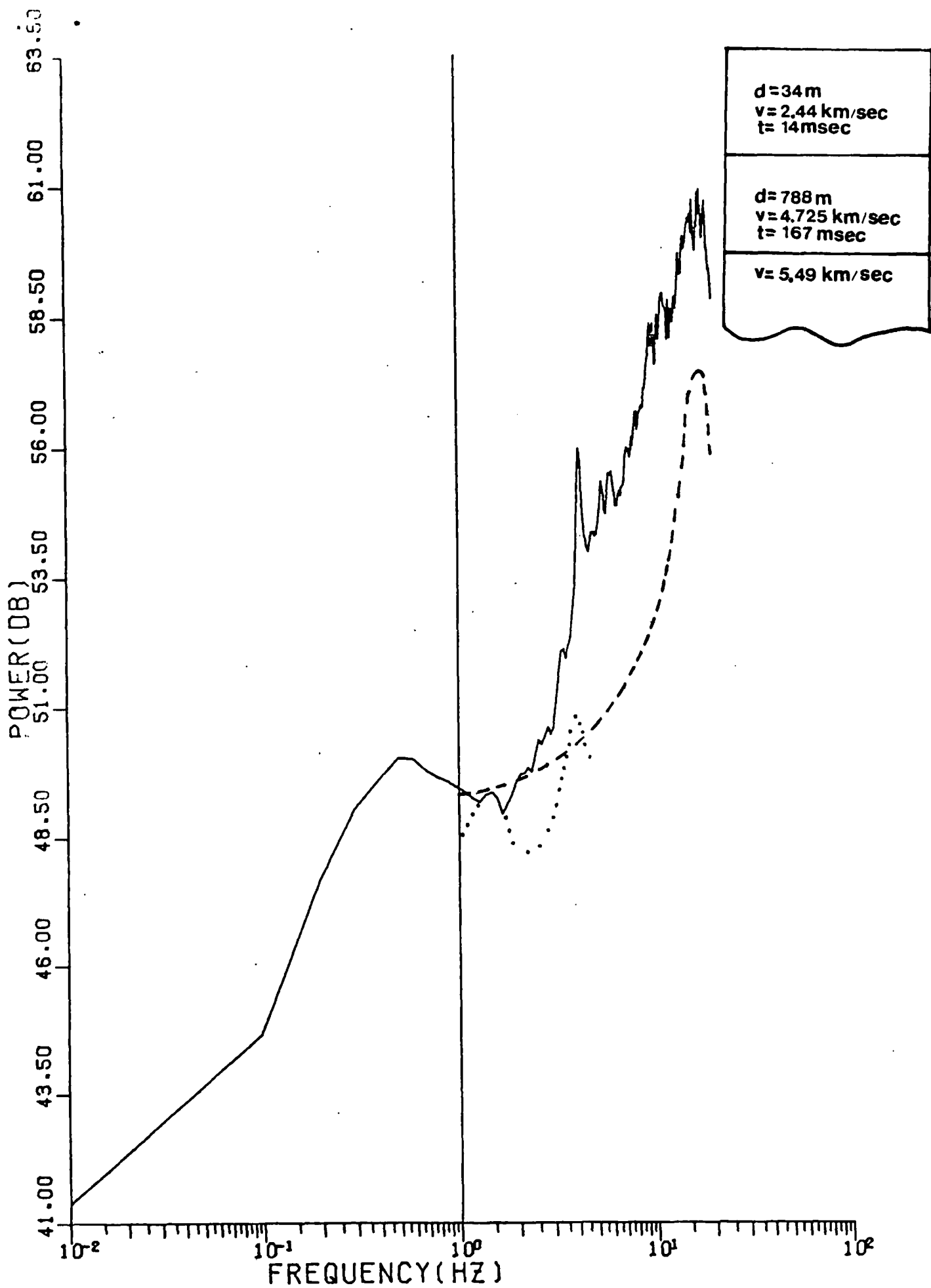
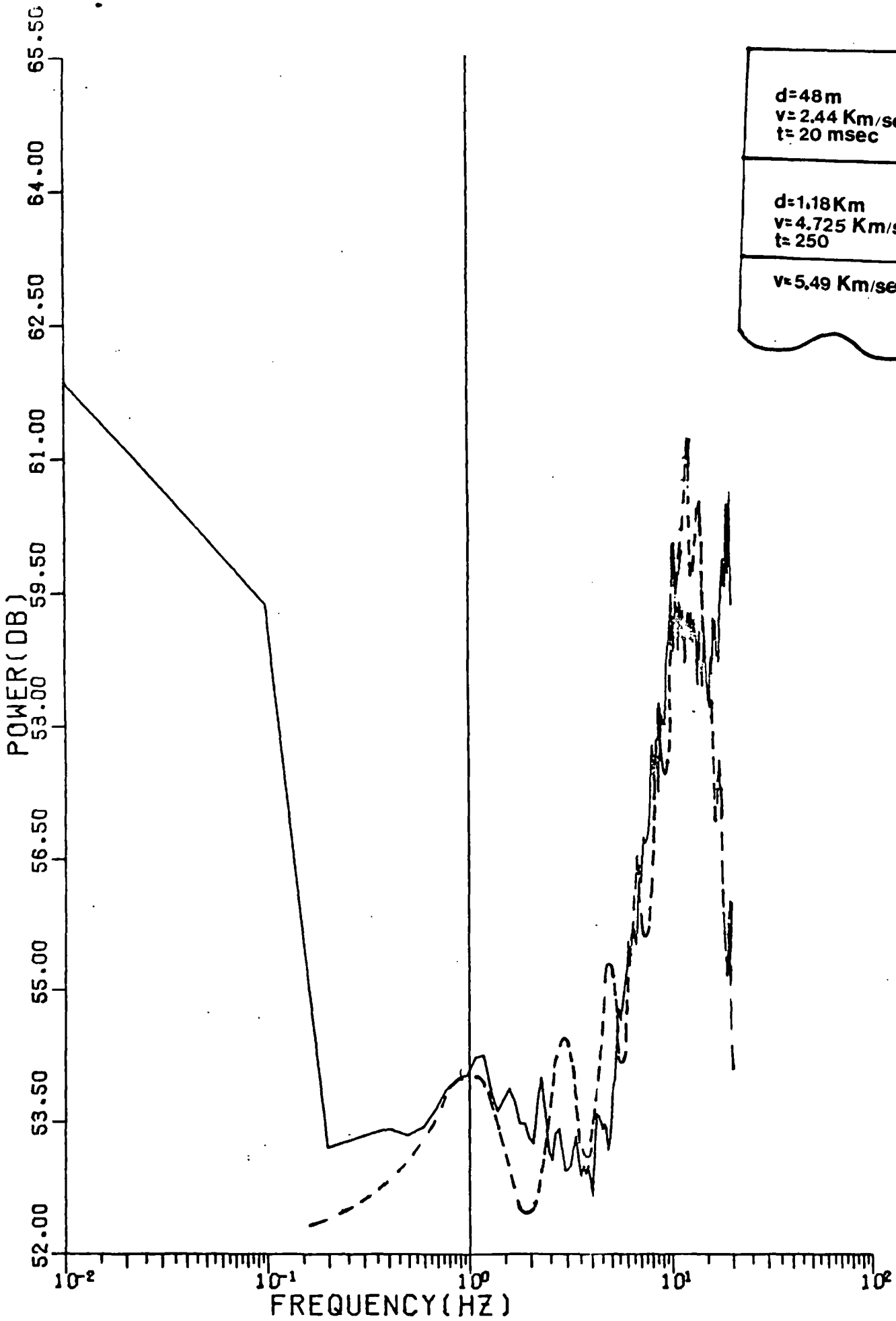


Fig 6

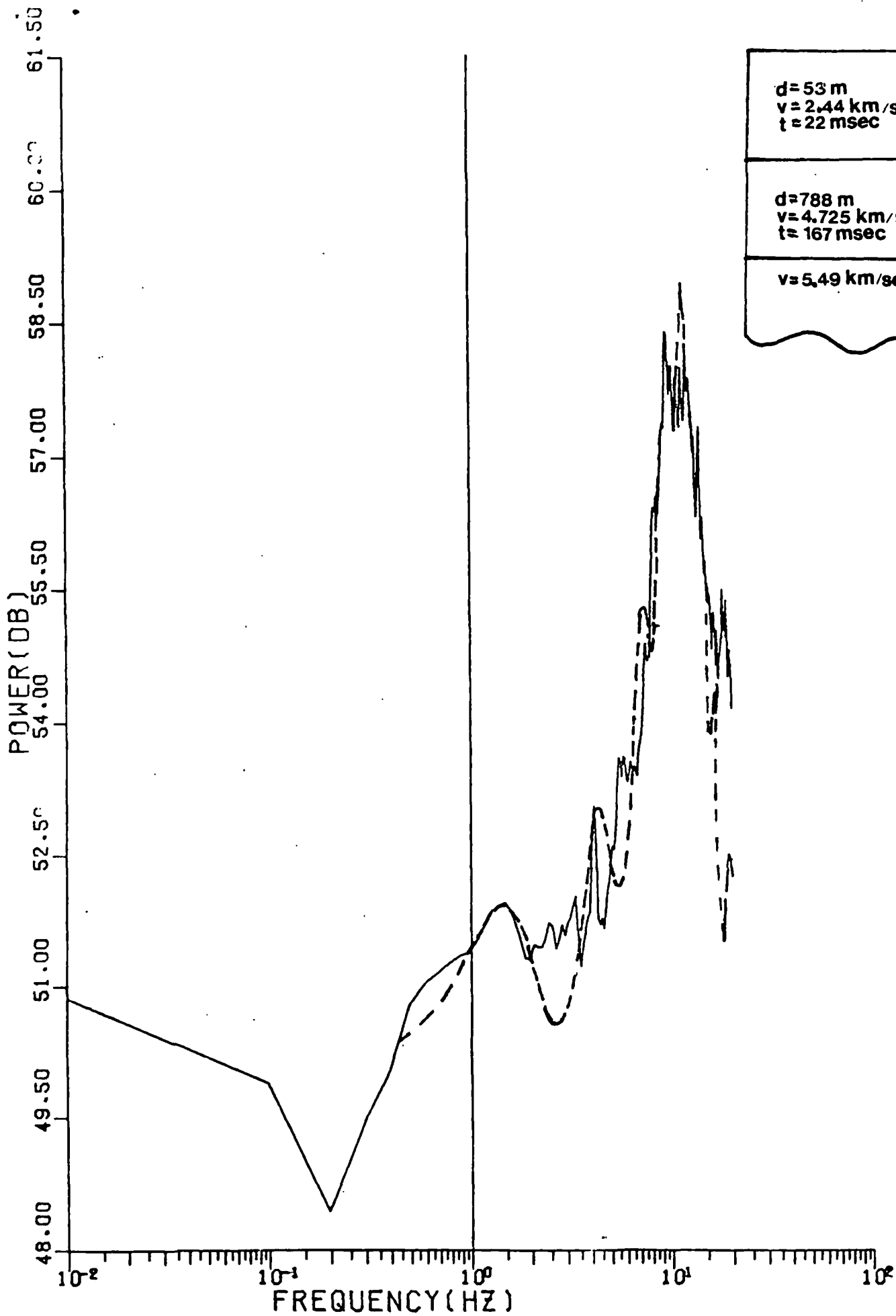
STATT AN 5W



<p>d=48m v=2.44 Km/sec t= 20 msec</p>
<p>d=1.18Km v=4.725 Km/sec t= 250</p>
<p>v=5.49 Km/sec</p>

F. >

STOTT AN 5E



<p>$d = 53 \text{ m}$ $v = 2.44 \text{ km/sec}$ $t = 22 \text{ msec}$</p>
<p>$d = 788 \text{ m}$ $v = 4.725 \text{ km/sec}$ $t = 167 \text{ msec}$</p>
<p>$v = 5.49 \text{ km/sec}$</p>

- Fig 8

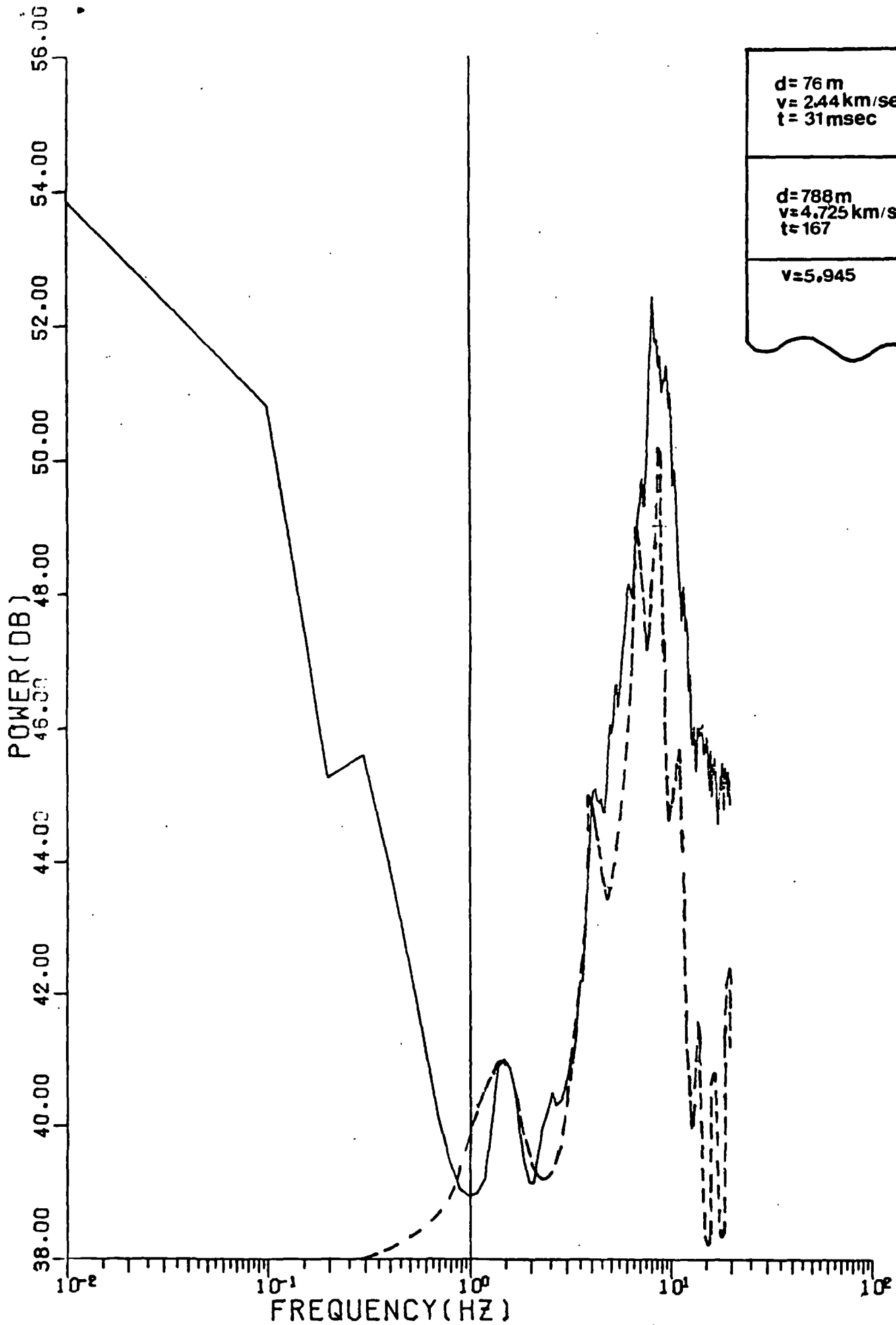


fig 9

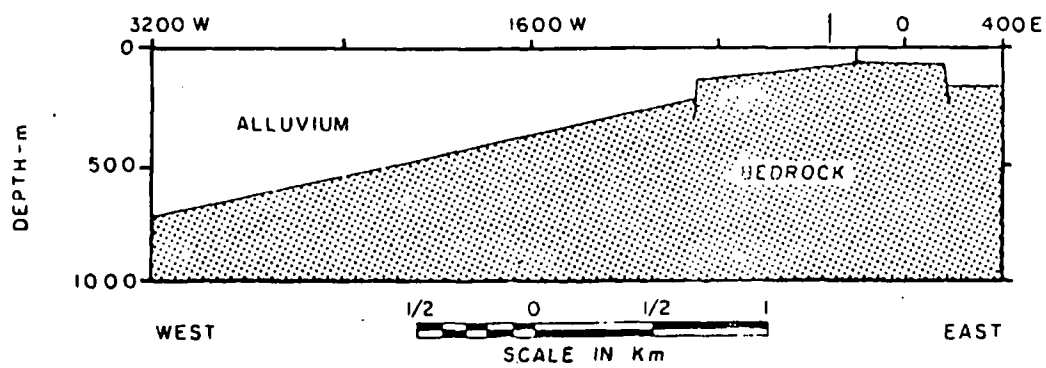
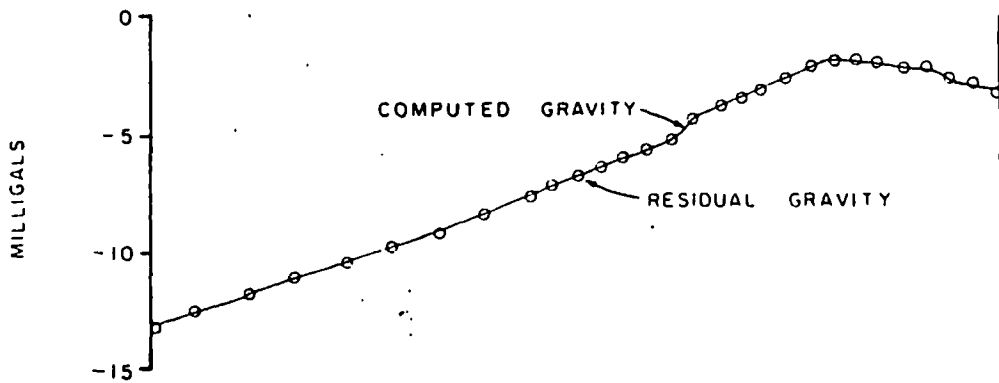
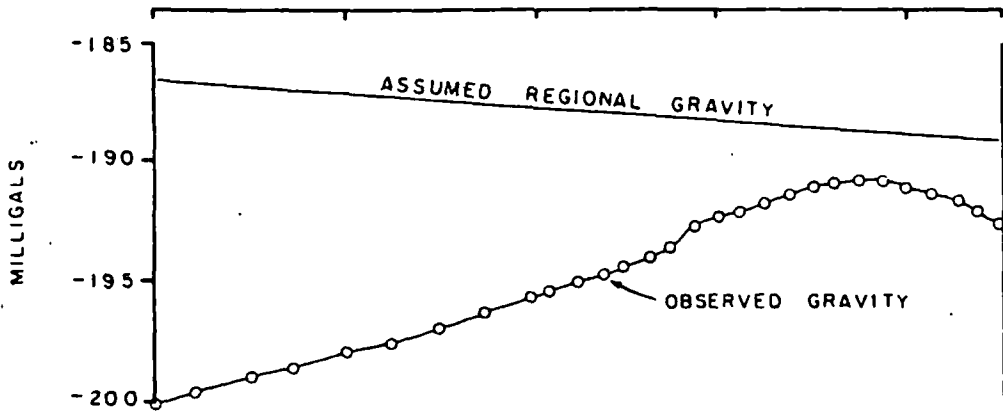


Fig 10

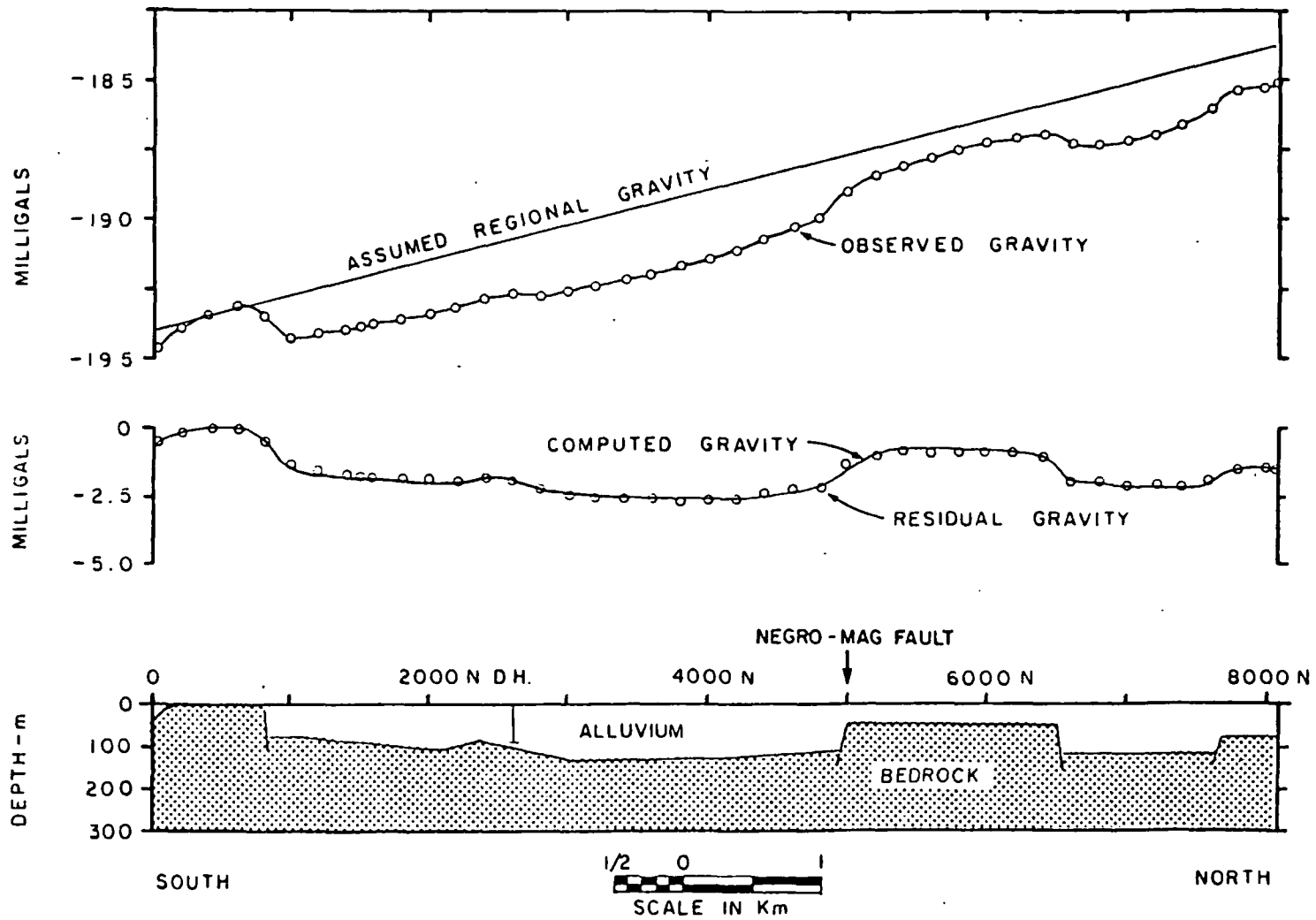


Fig 11

SUBJ
GPHYS
GIM

UNIVERSITY OF UTAH
RESEARCH INSTITUTE
EARTH SCIENCE LAB.

GEOPHYSICS IN MINING

A TOTAL CONCEPT OF THE MINING INDUSTRY

LECTURE OUTLINE AND ILLUSTRATIONS

by
Phillip M. Wright



BEAR CREEK MINING COMPANY
Salt Lake City, Utah

TABLE OF CONTENTS

INTRODUCTION

PHYSICAL PROPERTIES OF ROCKS

EXPLORATION STAGES

FORMATION OF A PORPHYRY COPPER OR MOLYBDENUM DEPOSIT

THE GRAVITY METHOD

THE MAGNETIC METHOD

THE INDUCED POLARIZATION METHOD

GEOPHYSICS IN PORPHYRY COPPER EXPLORATION

FORMATION OF A MASSIVE SULFIDE DEPOSIT

THE ELECTROMAGNETIC METHOD

GEOPHYSICS IN MASSIVE SULFIDE EXPLORATION

OTHER APPLICATIONS OF GEOPHYSICS

SUMMARY: PHYSICAL PROPERTIES, USES OF GEOPHYSICS, COSTS

INTRODUCTION

Each year more than \$30 million is spent in the free world on geophysical work related to mineral exploration. The included graph shows how and where this money is spent. Geophysical costs are, of course, only a portion of the total minerals exploration expenditure. Geological and geochemical costs, land acquisition costs and drilling costs, not included in the above figures, typically account for the lion's share of exploration costs. It would be safe to say that more than \$100 million is spent yearly in the free world on mineral exploration.

Professional earth scientists of a number of specialties (geology, geochemistry, geophysics) interact as a team in the typical exploration program. Support comes from lawyers and landmen (who obtain access and mineral rights), from research geoscientists (who develop new exploration concepts, techniques, and instrumentation), from deposit evaluation, mining and ore treatment experts (who judge whether or not a mineral discovery is indeed mineable), and from assistants and field technicians (who handle many of the routine aspects of exploration). Management welds the diverse groups into a (hopefully) working whole.

The mining geophysicist works closely with the geologist. They jointly plan geophysical surveys and jointly interpret the survey results. Good geological input is an absolute necessity to effective exploration use of geophysics. Of course the geophysicist should have a thorough educational background in geology. Other fields which the geophysicist uses are:

Physics

Mathematics

Electronics/Instrumentation

Computer Programming

Chemistry and Physical Chemistry

Economics/Business

Mineral Law

At this point it may be helpful to define what a geophysicist is.

A geophysicist is a person who makes measurements of physical properties of the earth and interprets these measurements in terms of the geological structure of the earth.

There are several specialties in the broad field of geophysics. Among them are:

Mining Geophysicist: A geophysicist who specializes in the exploration for mineral deposits.

Petroleum Geophysicist: A geophysicist who specializes in the exploration for petroleum.

Solid Earth Geophysicist: A geophysicist who studies processes within the earth by geophysical means.

Seismologist: A geophysicist who studies earthquakes.

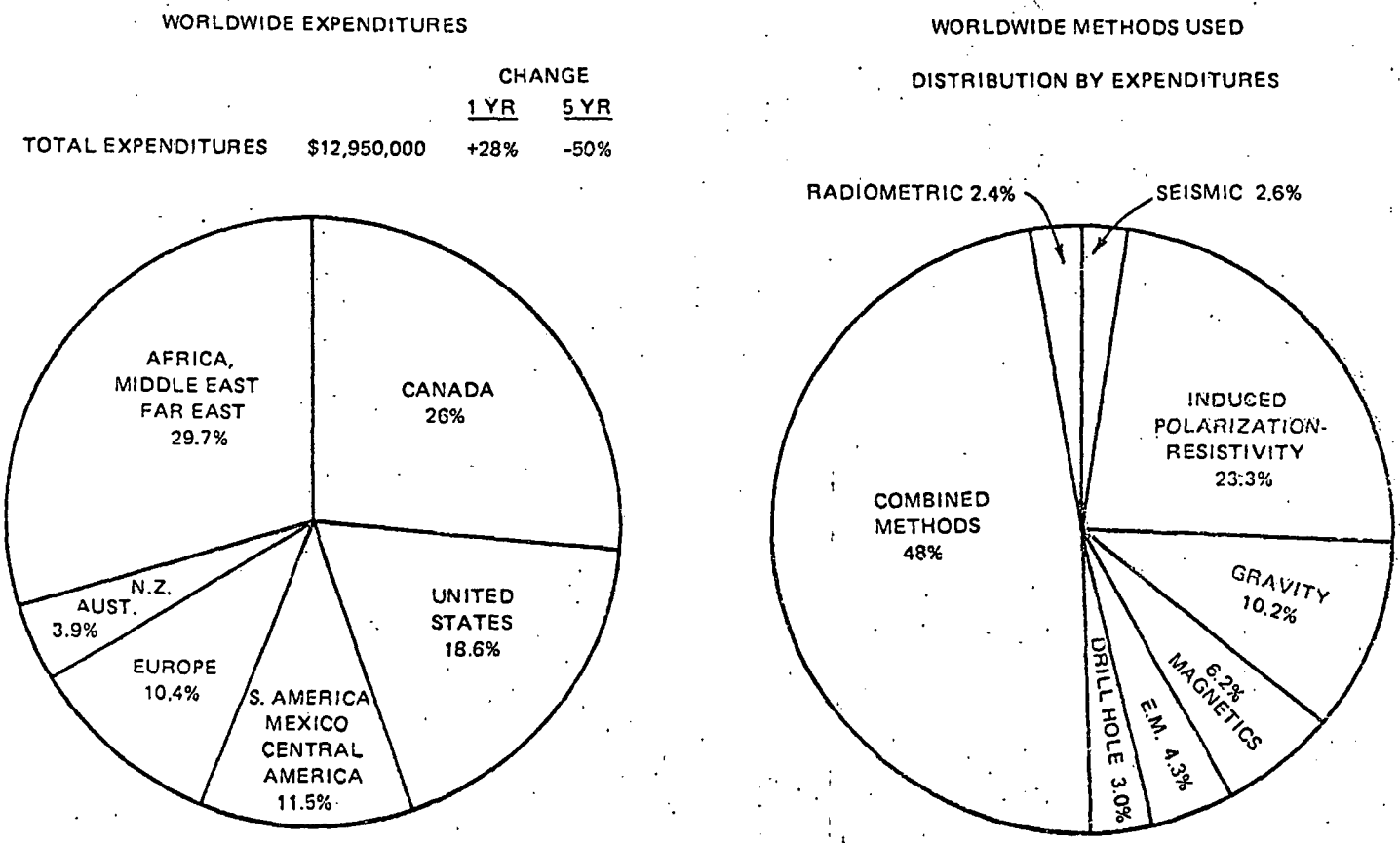


FIG. 18. Expenditures and methods used in 1972 in ground geophysics for minerals.

from the journal Geophysics, February, 1974

PHYSICAL PROPERTIES OF ROCKS

The geophysicist measures the physical properties of rocks at depth and interprets his measurements in terms of a geological picture. Although there are many physical properties which can be measured, geophysical prospecting techniques rely on the following to the greatest extent:

Useful Physical Properties of Rocks

Electrical

Magnetic

Gravity

Radiometric

Seismic

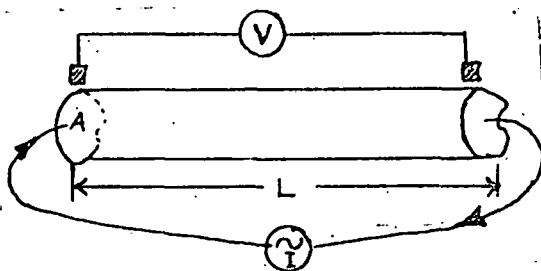
The following paragraphs discuss these physical properties in an introductory way. How they are used is the subject of all of the remaining material.

ELECTRICAL PROPERTIES OF ROCKS

I. The intrinsic rock properties are resistivity and induced polarization.

A. Resistivity. Apply Ohm's law to a hypothetical rod made from a rock as follows:

Ohm's Law: resistance (ohms) = $\frac{\text{voltage drop (volts)}}{\text{current (amperes)}}$ or $R = \frac{V}{I}$



A = end area of rod

L = length of rod

Results: 1) as A increases, R decreases in inverse proportion

2) as L increases, R increases indirect proportion

We can therefore define a rock parameter or physical property by the letter rho, ρ , which is the constant of proportionality.

$$\rho = \frac{RA}{L} = \frac{\text{ohms} \times \text{m}^2}{\text{m}} = \text{ohm-m} = \text{resistivity}$$

$$1/\rho = \sigma = \text{conductivity}$$

B. Induced Polarization. In the above experiment, let the frequency of the alternating current be variable. Then

$$\text{IP Effect} = \frac{\rho_{\text{DC}} - \rho_{\text{AC}}}{\rho_{\text{AC}}} \times 100\% = \text{percent frequency effect} = \text{pfe}$$

II. How do rocks conduct electricity? Most rock-forming minerals are good insulators but a few are conductors.

A. Rocks with no conducting minerals still carry electricity in water which fills tiny pore spaces between mineral grains.

B. Rocks with electrical conducting minerals conduct electricity both through the mineral grains and through pore water.

III. Classification of Rocks and Minerals

<u>Rock or Mineral</u>	<u>Electrical Resistivity, ρ</u>	
	good insulators $\rho = 10^7$ ohm-m	good conductors $\rho = 10^{-6}$ ohm-m
pure copper		—
pyrite (FeS_2)		—
graphite (carbon)		—
granite	—	
basalt	—	
limestone	—	
alluvium		—
calcite (CaCO_3)	—	
quartz (SiO_2)	—	

MAGNETIC PROPERTIES OF ROCKS

I. The intrinsic rock properties are magnetic susceptibility and remanent magnetization.

A. Magnetic Susceptibility. When a rock containing magnetic minerals is placed in an external magnetic field, it acquires an induced magnetization due to its susceptibility

$$\text{susceptibility, } k = \frac{\text{induced magnetic field strength}}{\text{external magnetic field strength}}$$

units of susceptibility are 10^{-6} cgs = μ cgs

Magnetic rocks have induced magnetization due to their presence in the earth's magnetic field.

B. Remanent Magnetization. When a rock containing magnetic minerals cools from high temperature or undergoes chemical change while in an external field such as the earth's magnetic field, it often acquires a remanent or permanent magnetization.

The ratio of remanent to induced magnetization in a rock is called the Koenigsberger ratio, or Q-factor.

II. The most common magnetic mineral in rocks is magnetite (Fe_3O_4). Magnetite accounts for almost all magnetic properties of rocks. The magnetic mineral pyrrhotite is often found in certain kinds of massive sulfide deposits. It is the only other important magnetic mineral.

III. Classification of Rocks and Minerals

<u>Rock or Mineral</u>	<u>Susceptibility (μ cgs)</u>			<u>Q-factor</u>		
	0	10^3	10^6	0	10	100
magnetite (Fe_3O_4)			_____		na	
pyrite (FeS_2)	_____				na	
quartz (SiO_2)					na	
igneous rocks	_____	_____		_____		
volcanic rocks	_____	_____		_____	_____	
sedimentary rocks	_____			_____	_____	
iron ore		_____		_____		

GRAVITATIONAL PROPERTIES OF ROCKS

I. The intrinsic rock property is density.

$$\text{Density} = \frac{\text{mass}}{\text{volume}} = \text{gm/cm}^3$$

II. Because all rocks have mass, they all have a density, and they all have a measurable gravity field. Density is measured by first weighing a rock in air, and then weighing the same rock while it is under water. The difference between these two weights gives the weight of water displaced and therefore the volume of the rock, since water has a known density of 1 gm/cm^3 .

$$\rho = \text{density} = \frac{\text{weight in air}}{\text{weight in air} - \text{weight in water}} = \text{gm/cm}^3$$

III. Classification of Rocks and Minerals

<u>Rock or Mineral</u>	<u>Density (gm/cm³)</u>
water	1.00
graphite	2.23
quartz	2.65
pyrite	5.02
magnetite	5.18
gold	19.3
alluvium	1.9-2.1
igneous rocks	2.5-2.7
volcanic rocks	2.2-3.0
sedimentary rocks	2.0-2.9
massive sulfide ore	3.0-6.0

RADIOACTIVE PROPERTIES OF ROCKS

I. Radioactivity is the spontaneous disintegration of the nucleus of one or more atoms with resulting emission of other particles and of energy.

II. Types of particles emitted and their penetration abilities are:

<u>Particle</u>	<u>Penetration</u>
Alpha particle (helium nucleus)	2 cm of air not paper or rock
Beta particle (electron)	0.2-0.4 cm rock
Gamma rays (electromagnetic radiation)	65 cm rock 7 cm lead

III. The main sources of terrestrial radiation cause gamma rays of various energies. The decaying series, elements measured, and energies are:

<u>Series begins with</u>	<u>Element Measured</u>	<u>Gamma Ray Energy</u>
K^{40}	K^{40}	1.35 to 1.58 Mev
U^{238}	Bi^{214}	1.65 to 1.88 Mev
Th^{232}	Tl^{208}	2.42 to 2.82 Mev
	Total count measurement 1.35 to 2.82 Mev	

SEISMIC PROPERTIES OF ROCKS

- I. The intrinsic property is the velocity of transmission of mechanical waves in the rock.
- A. Compressional Waves. These are ordinary sound waves in rocks-- the rock particle motion is in the same direction as the wave propagation.
- B. Shear Waves. These have no analogy with sound because fluids such as air and water will not transmit shear waves. The particle motion is at right angles to the direction of wave propagation, much as a wave traveling along a loose rope.
- II. Compressional waves are the ones commonly used in mining geophysics. The velocity of these waves in various rocks and minerals is as follows:

<u>Rock or Mineral</u>	<u>Velocity Range, ft/sec.</u>
alluvium	1,600-12,000
igneous rocks	13,000-20,000
volcanic rocks	10,000-18,000
sedimentary rocks	6,000-18,000
magnetite	18,200
massive sulfide ore	20,000-25,000

EXPLORATION STAGES

Most mineral exploration programs can be grouped into the following stages:

1. Business. Is there a market for the commodity sought and can it be mined at a profit from the deposits expected in a given area?
2. Reconnaissance. Large areas are first considered with the idea of locating much smaller portions within which chance of discovery is highest. Odds of making a discovery are determined mainly by: 1) odds of occurrence of a deposit, 2) odds of detecting the deposit by the methods employed.
3. Examination. Once a favorable small area has been identified, a closer and more detailed look is required for discovery.
4. Evaluation. When a mineral discovery is made it must be evaluated to determine whether or not a deposit exists which can be mined at a profit using existing technology. If the answer is "yes," then the deposit is called an "orebody," otherwise it is just a "mineral deposit" or a "mineral resource."

Geophysical surveys are used in stages 2, 3, and 4 above.

RECONNAISSANCE STAGE

● AREA SELECTION

● DATA ACQUISITION

● DATA ANALYSIS



AREAS FOR DETAILED EXAMINATION

EXAMINATION STAGE

● AREA SELECTION FROM RECONNAISSANCE

● LAND

● DATA ACQUISITION

● DATA ANALYSIS

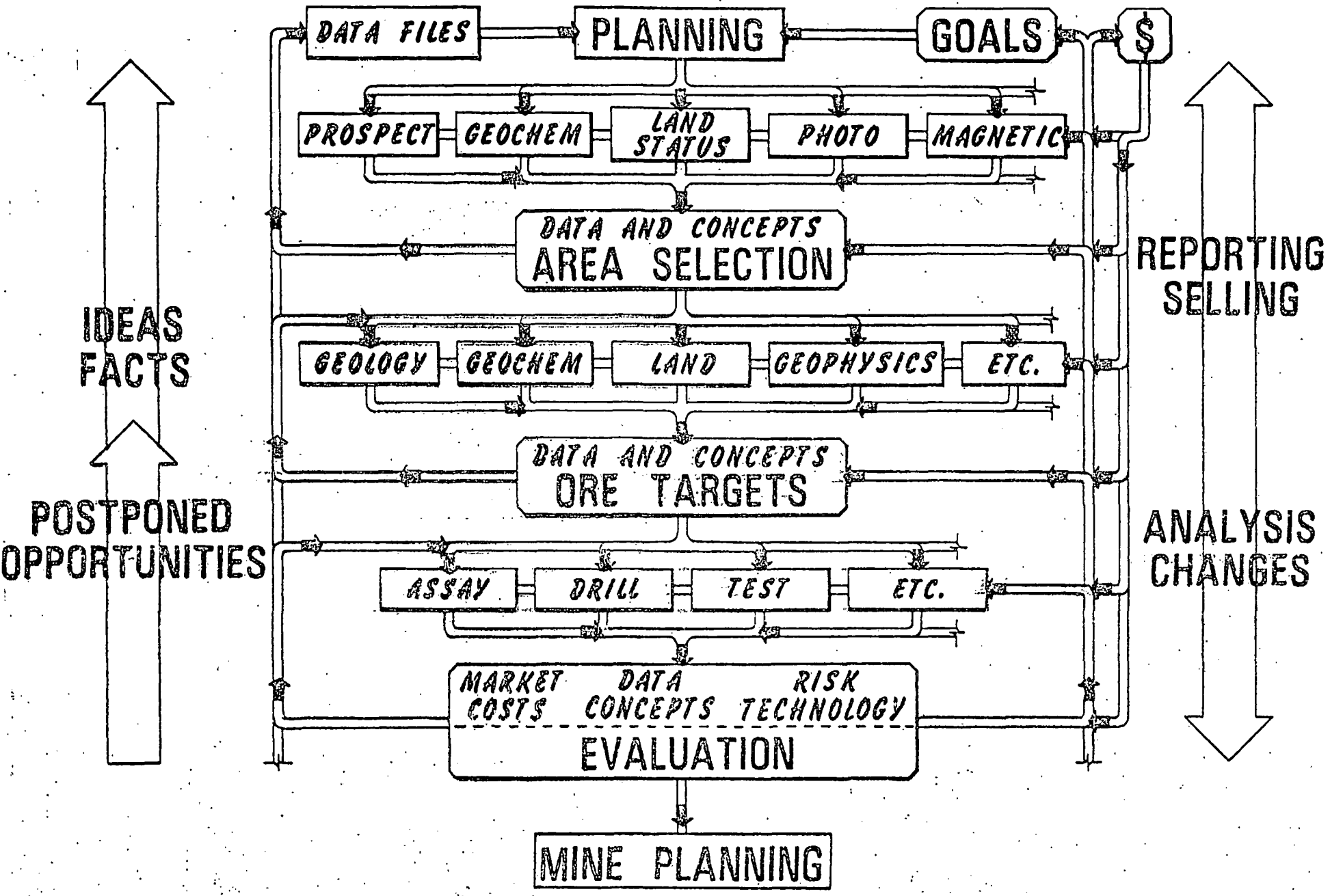


● ORE TARGET CONCEPT



● LAND

● DRILLING



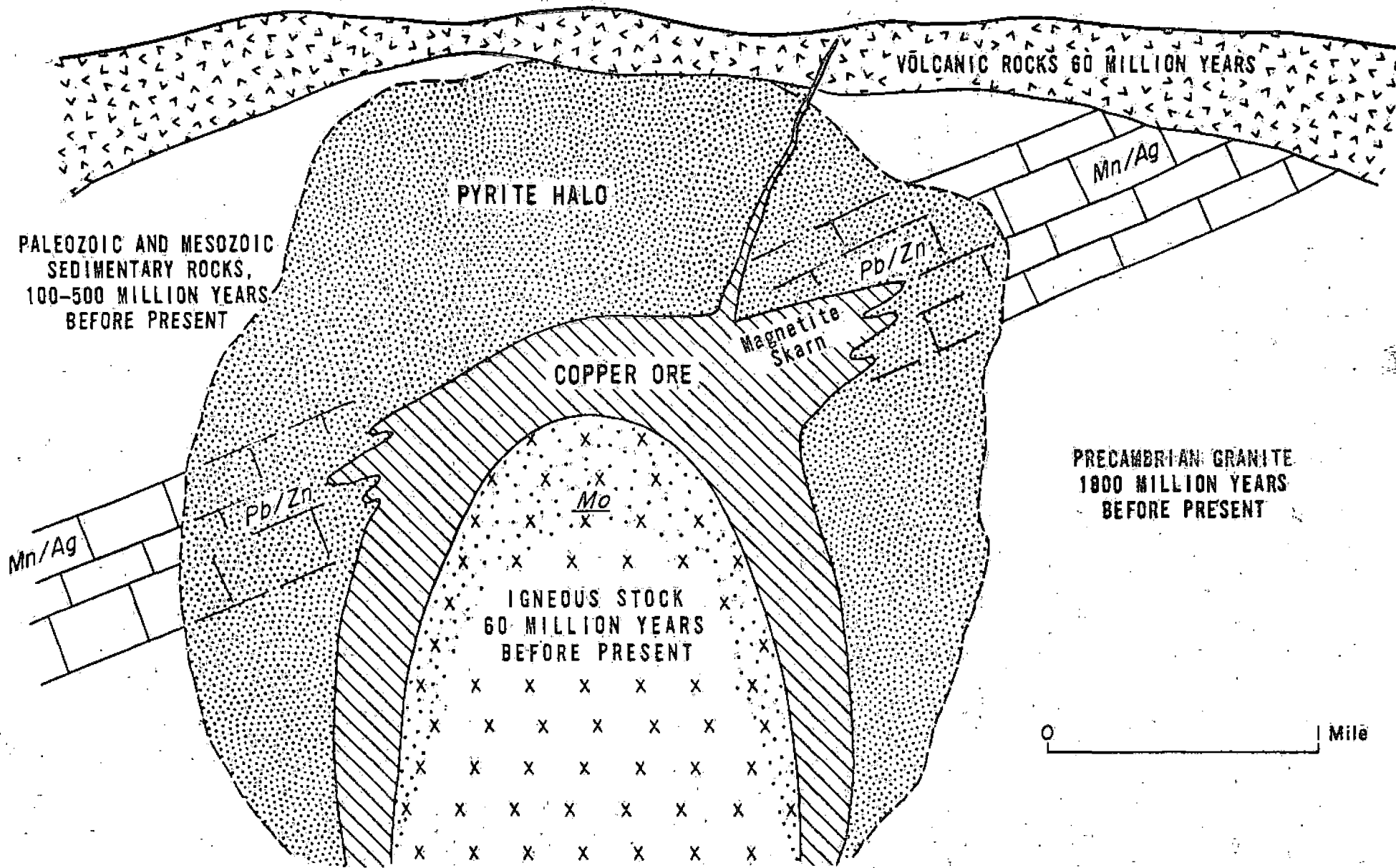
FORMATION OF A PORPHYRY COPPER OR MOLYBDENUM DEPOSIT

- (Fig. A) 1. A molten igneous stock of granite or quartz monzonite composition is emplaced in pre-existing rocks. Some of the molten material makes its way to the surface to form volcanoes and a covering layer of volcanic rocks results.
- (Fig. A) 2. The stock cools from its original temperature of more than 800°C ., and minerals begin to crystallize in the melt. Heat is carried away mainly by groundwater circulating in a large convection system around the stock. As more and more minerals crystallize in the melt, the residual fluid becomes enriched in volatiles which do not become part of the rock. These volatiles are composed mainly of water vapor, sulfur gas and compounds, and chlorine, with dissolved metals such as copper, molybdenum, lead, zinc, gold and silver.
- (Fig. A) 3. When the stock finally becomes solid, its outer margins fracture and the residual volatile fluids, which contain the metals, are released to the circulating groundwater convection system. The convection system distributes the metals in zones in both the host rocks and the parent stock. Copper and molybdenum ore are zoned inside of a pyrite (FeS_2) halo, with lead, silver and zinc ore further away. Gold usually occurs with the copper. Skarn deposits, often containing the magnetic mineral magnetite (Fe_3O_4) as well as copper minerals are sometimes formed in adjacent limestone if present. All of these processes are called mineralization.
- (Fig. A) 4. The convecting groundwater system also causes chemical changes to take place both in the stock and in adjacent host rocks. Feldspar minerals are altered to clays and micas and much quartz is introduced. This process is called alteration. Characteristic alteration minerals occur in zones around the stock, and the zonation of the alteration and mineralization processes often help geologists and geophysicists to locate the orebodies.
- (Fig. A) 5. The surface above a forming porphyry deposit is believed to show evidence of recent volcanism and geothermal activity such as we see at Yellowstone today.
- (Fig. B) 6. Erosion processes eventually strip off the top of the porphyry deposit, which has long since cooled. The upper part of the copper/molybdenum orebody and of the pyrite halo are exposed at the surface, and they undergo oxidation.

- (Fig. B) 7. Oxidation of pyrite (FeS_2) produces sulfuric acid (H_2SO_4), and the sulfuric acid dissolves copper minerals such as chalcopyrite (CuFeS_2) and bornite (Cu_5FeS_4). The dissolved copper minerals as chalcocite (Cu_2S) to form an enriched zone. The enriched zone contains all of its original copper plus what is added from above. As erosion and oxidation proceed downward through the deposit, the enriched zone moves downward also and becomes thicker and richer.
- (Fig. B) 8. Volcanism from a separate, unrelated volcano pours out volcanic rocks to cover the deposit and halt the oxidation and enrichment process.
- (Fig. C) 9. During ensuing time to the present the ore deposit is subjected to many geologic processes, among them tilting (rotation), faulting, and being covered by unconsolidated gravels. In this way many deposits are hidden from view, and geophysics helps to discover such hidden deposits.

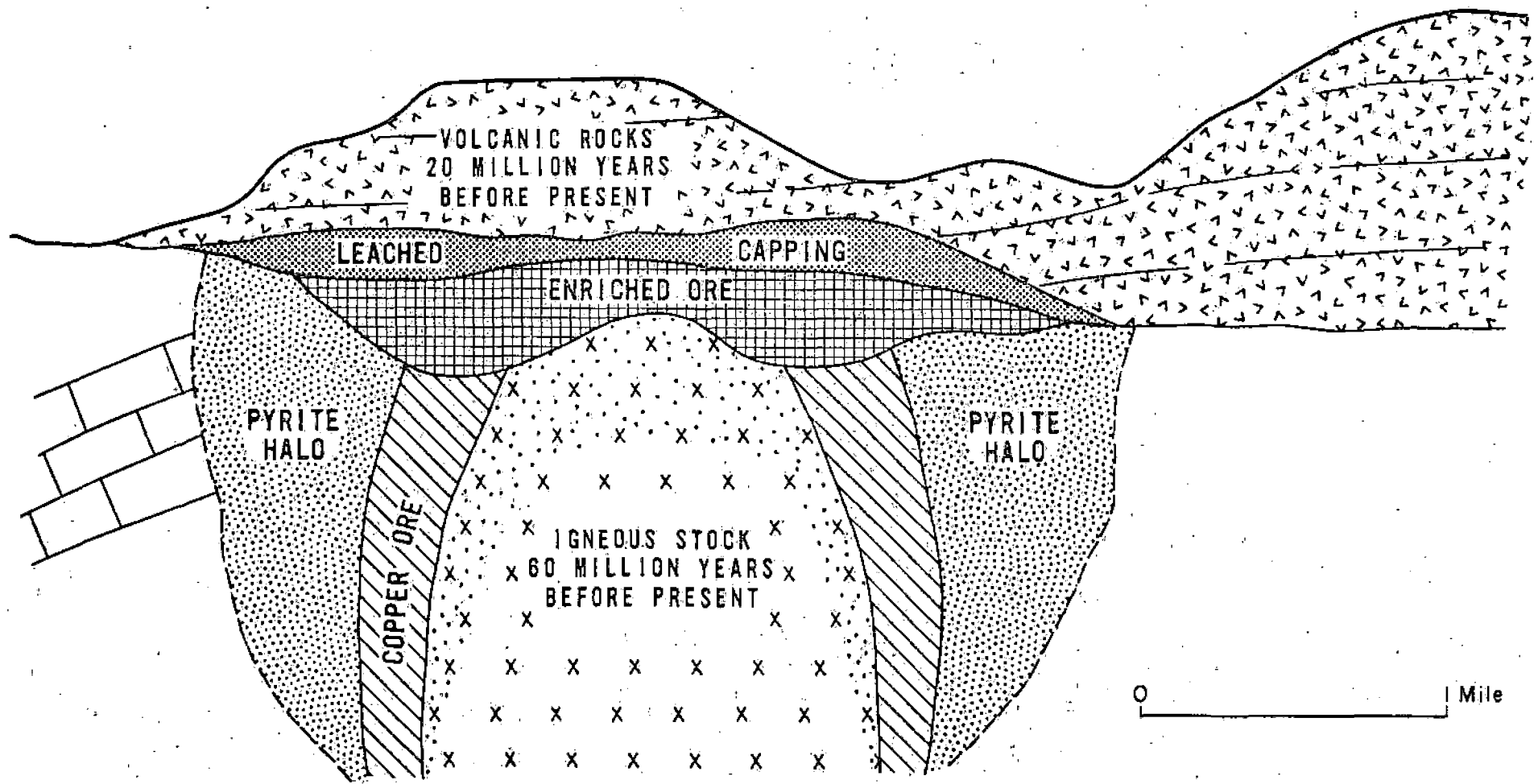
FORMATION OF PORPHYRY DEPOSIT

TIME: 50 MILLION YEARS AGO

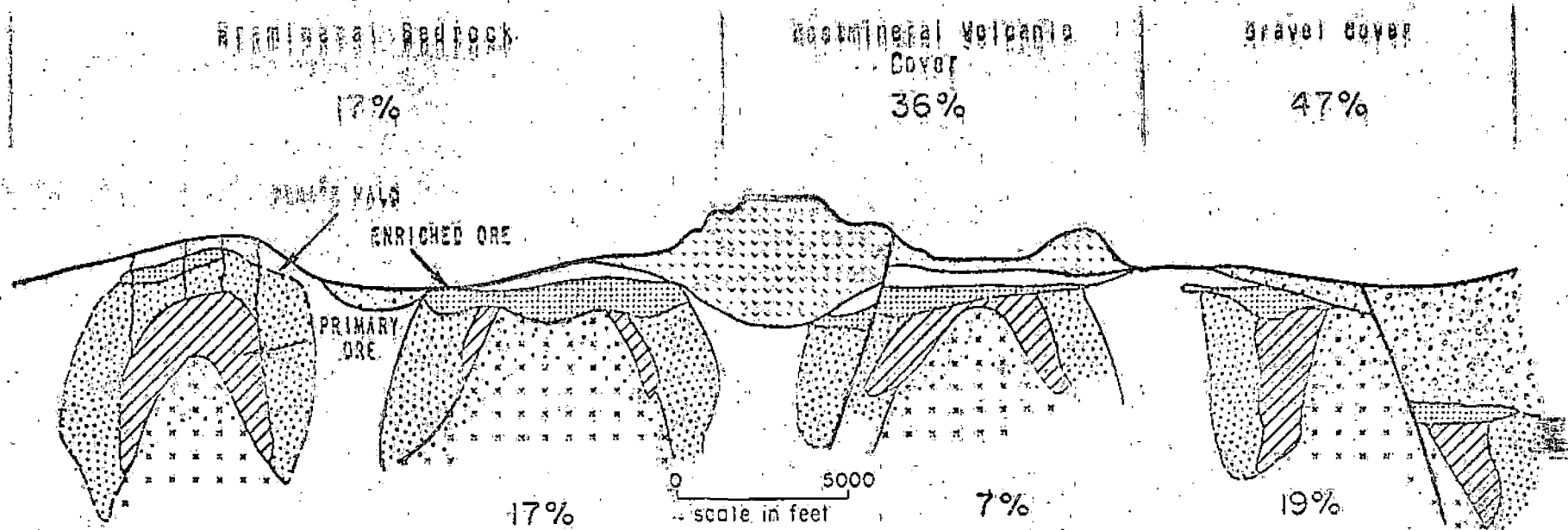


FORMATION OF PORPHYRY DEPOSIT

TIME: 10 MILLION YEARS AGO



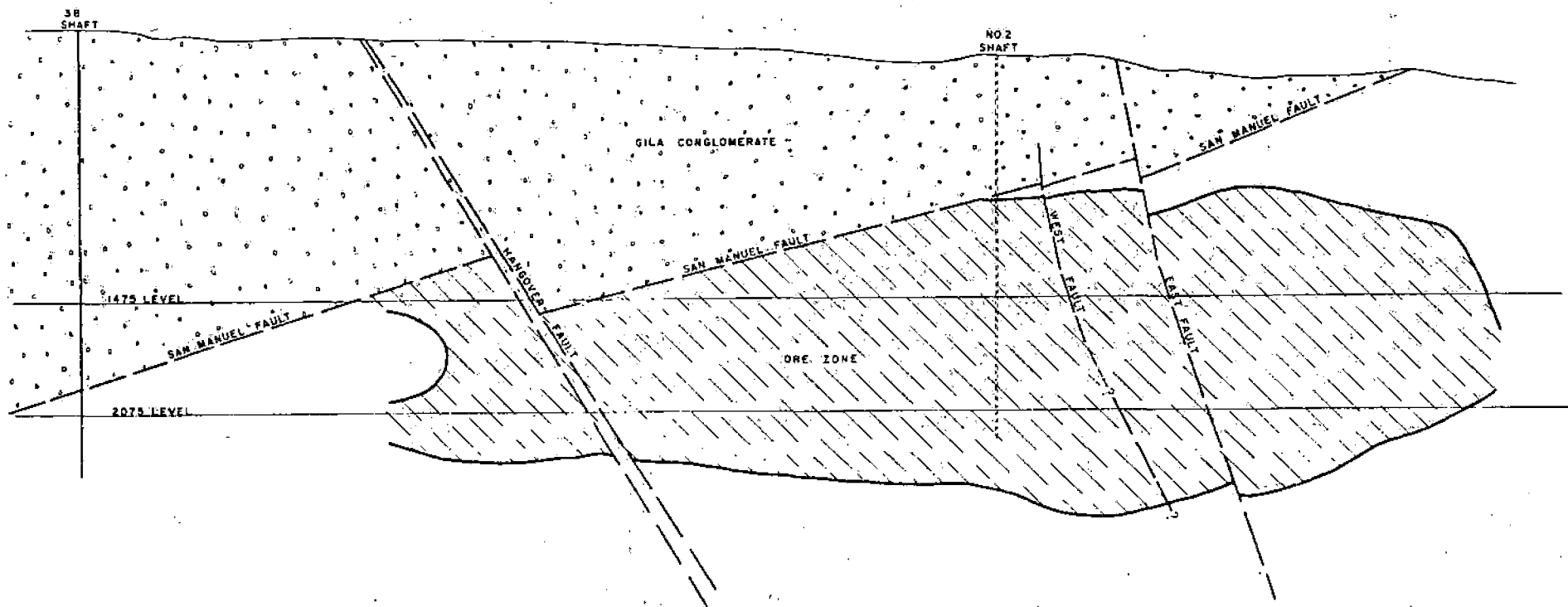
SIX EXPLORATION ENVIRONMENTS IN THE ARIZONA-NEW MEXICO PORPHYRY COPPER PROVINCE



MAJOR DEPOSITS FOUND	Blind		Exposed		Deep	Shallow		Shallow		Deep		
	Safford-RD.	'58	E Morenci	pre-'50	None	OX Safford	KCC	'58	San Manuel	'48		
	Kalamazoo	'65	E Ray	"				Pima-Mission	'52-'55			
	Pinto Valley	'67	E Miami-	"				Twin Buttes	'61			
	Red Mtn.	'70	Inspiration	"				E? Lakeshore	'67			
	Safford Annex	'71	E Chino	"				Poston Butte	'70			
	Deep Bisbee	?	Ajo	"				E Miami East	'20-'68			
	Chilico	?	E Bisbee	"								
			E Tyrone	"								
			E Silver Bell	'50								
			E Bagdad	'28-'68								
			E Helvetia	'61								
			Sierrita-	'55-'62								
			E Esperanza									

MAJOR DEPOSITS OR CLUSTERS FOUND	Districts with Blind Deposits	Exposed	Deep Volcanic	Shallow Volcanic	Shallow Gravel	Deep Gravel
FOUND	4	12	0	1	4	1
UNDISCOVERED	10-15	0*	many	4±	8±	many

*Possibly several deposits beneath structural cover



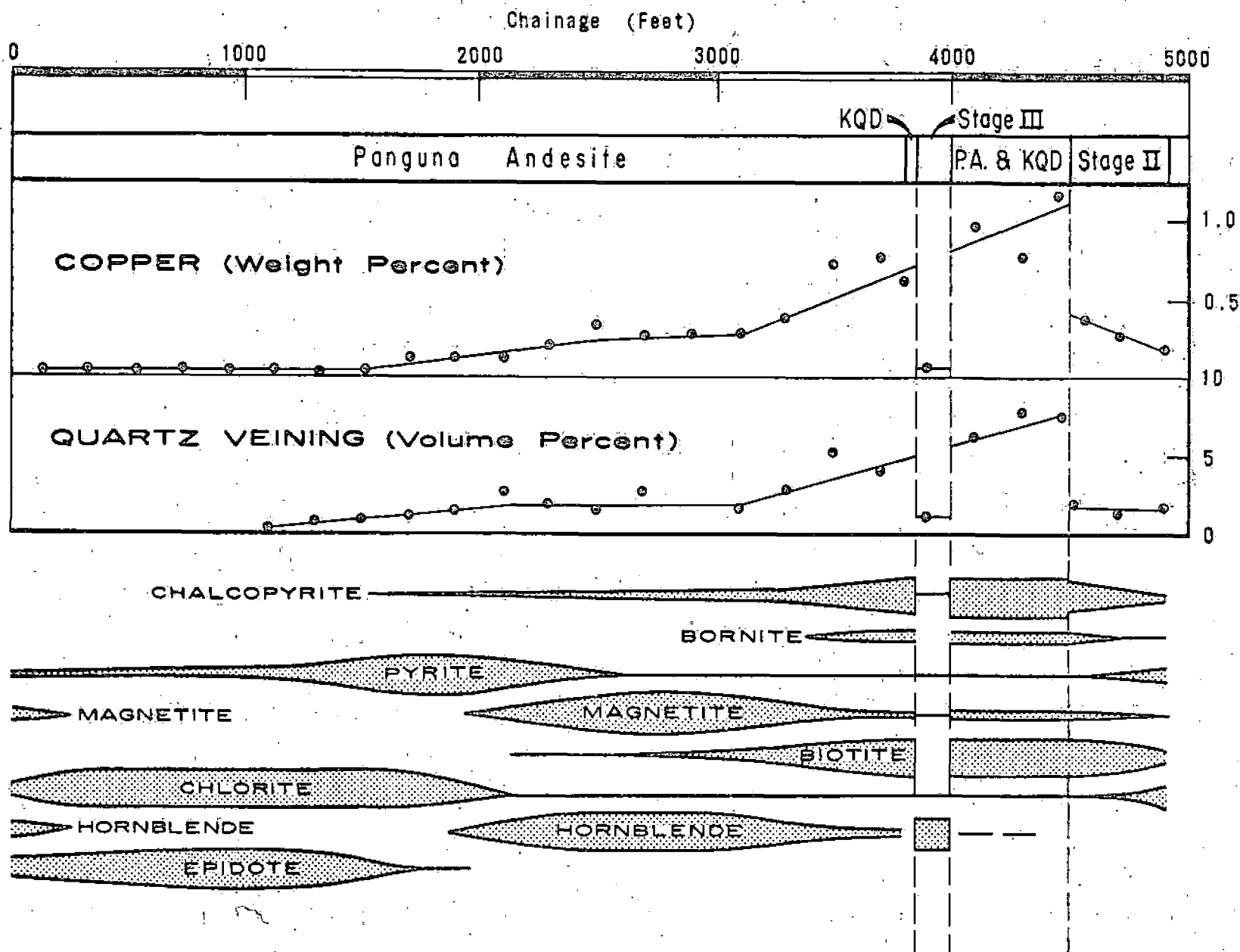
SECTION B'-B

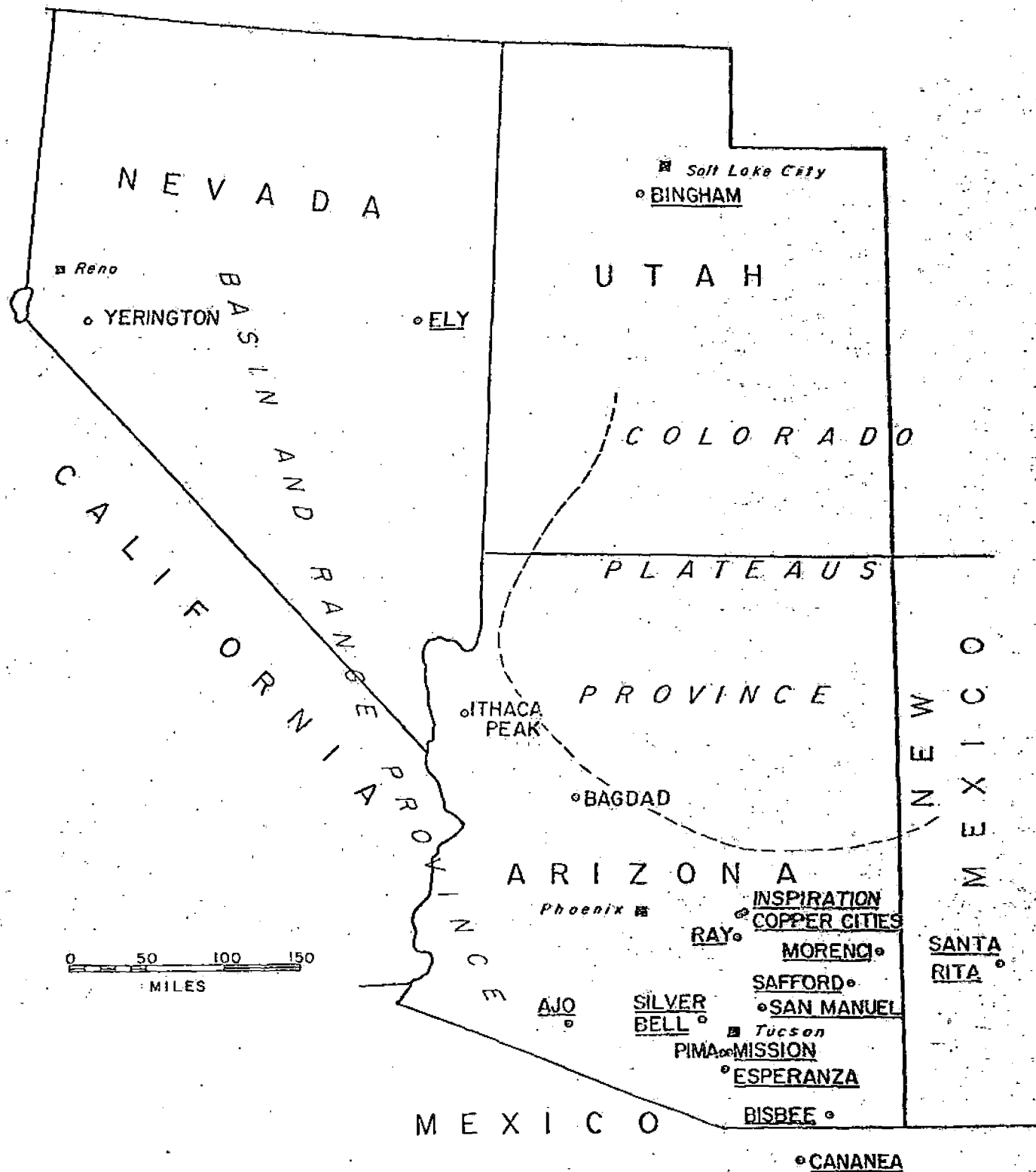


Idealized longitudinal section looking northwest.

Cross section through San Manuel mine, a porphyry copper deposit in southern Arizona. Note that the ore zone has been rotated from its original vertical position so that now it lies on its side.

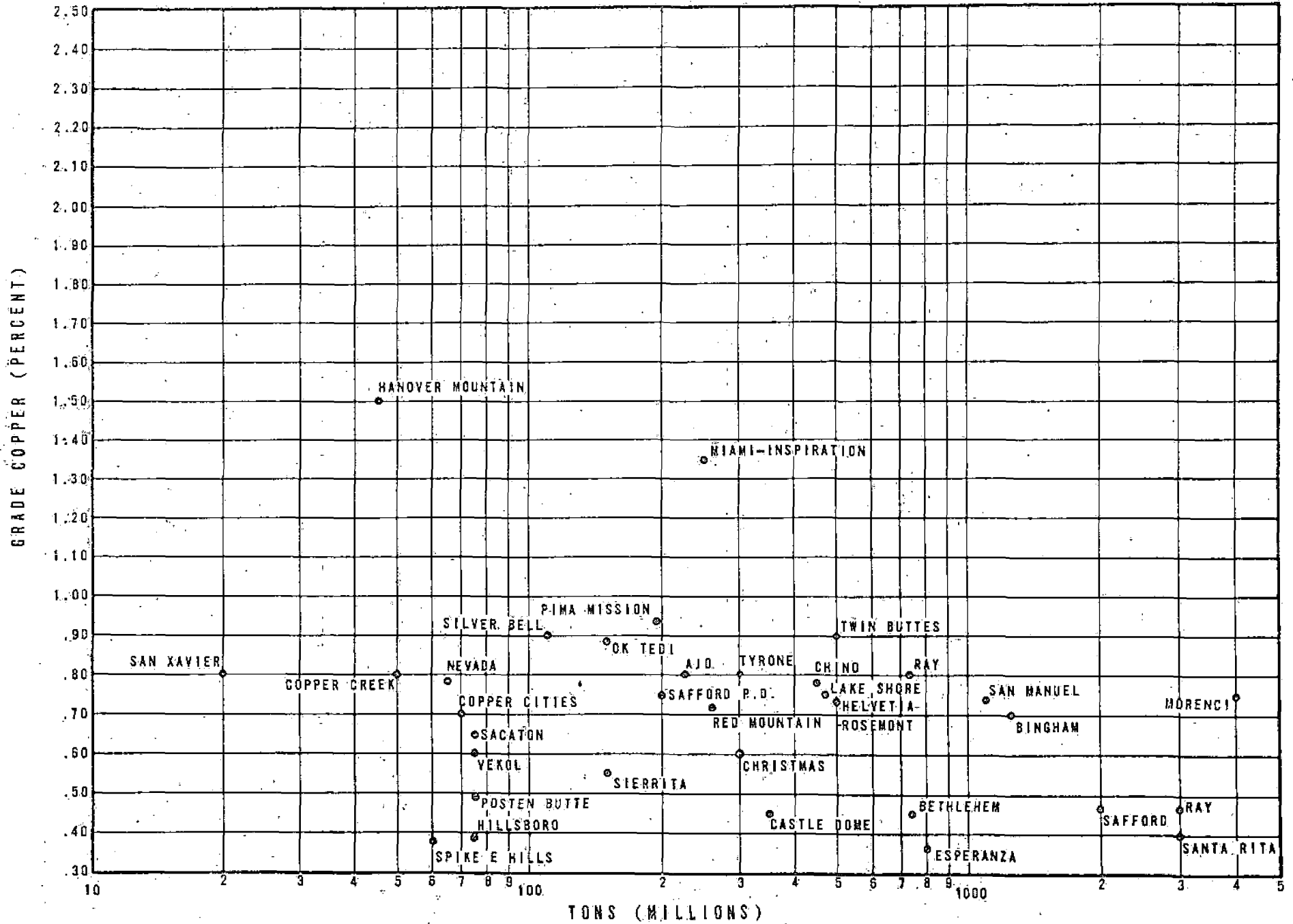
Distribution of Alteration Types, Panguna Deposit





Map of the southwestern United States and adjoining regions of Mexico showing the principal physiographic subdivisions and the location of the porphyry copper deposits. Names and locations underscored are the deposits described in this volume.

(from Geology of the Porphyry Copper Deposits - Southwestern North America by Titley and Hicks)



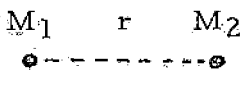
Copper grade and ore body size for some porphyry copper deposits, mostly U.S.



View of the Morenci operation from the southeast.

THE GRAVITY METHOD

For two masses, M_1 and M_2 , placed a distance r apart, the gravitational attraction is given by the equation:

$$F = \frac{\gamma M_1 M_2}{r^2}$$


where γ = universal gravitational constant

This is Newton's Law of Gravitation. We see that gravity varies directly with mass and inversely with the square of the distance.

The earth produces a gravitational field due to its mass (see accompanying figure) and the interaction between our body's mass and the earth's mass is what we call weight. Because the earth spins on its axis, it is not a true sphere, but is bulged outward at the equator. This makes a point on the equator further from the center of the earth than is a point near the north or south pole. Because of this, gravity is less at the equator than at the poles. Also the centrifugal force at the equator due to the earth's spin tends to try to fling a body off into space, thereby further decreasing the weight of a body at the equator relative to the weight of the same body at either pole.

Near-surface geology modifies the earth's gravity field because of the varying density of rocks. By measuring the earth's gravity field at many points, geophysicists are able to map density differences in near-surface rocks. Then by appropriate interpretation these density differences are visualized in terms of what they mean geologically.

The instrument used to perform a gravity survey is called a gravity meter or gravimeter. Modern gravity meters are among the most delicate and precise mechanical instruments ever made by man. They can detect the small decrease in gravity due to a 2-inch increase in elevation. Their cost is roughly \$10,000. They all work on the principle of measuring the change in weight of a small constant mass within the instrument. The measuring springs are made of fused quartz (SiO_2), an extremely stable substance (see accompanying figure).

During a gravity survey, the instrument is first setup and read at a base station. Then it is taken in turn to the survey stations, and after 2-6 hours it is returned to the base station. Changes in base readings are called drift and must be corrected for. Also survey station elevations and latitudes must be accurately known. Then a straightforward series of corrections is made, as indicated in the figure, before the data can be used for interpretation.

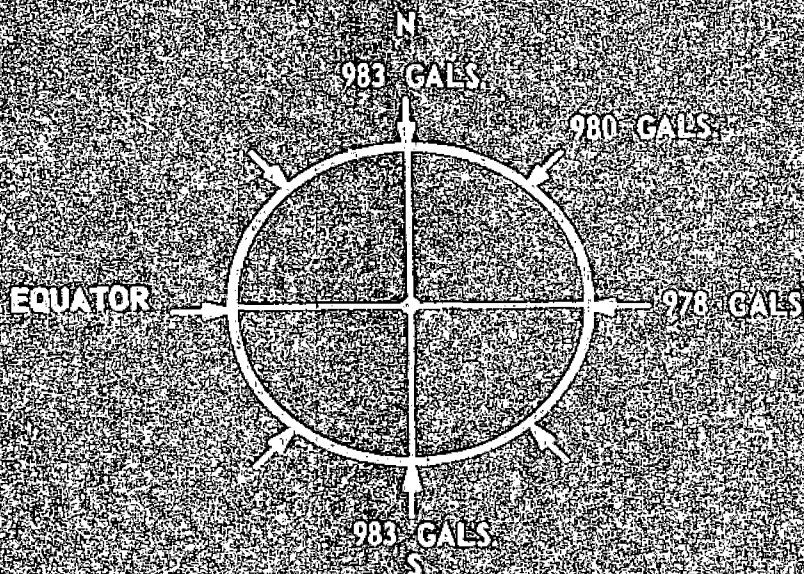
In porphyry copper exploration, gravity surveys are used to:

- 1) determine the thickness of gravel or volcanic cover over bedrock. Then if the cover is thin enough (less than 2,000 feet), other geophysical methods may be applied. In this application, the gravity survey does not detect ore directly;
2. locate and define dense skarn mineralization. In this case the ore may be directly detected;
3. map and project geology by mapping rock density differences.

NEWTON'S LAW OF GRAVITATION

$$F = \delta \frac{m_1 m_2}{r^2} \text{ (DYNES)}$$

$$\text{EARTH'S GRAVITY } g = \frac{66.7}{10^9} \frac{m}{r^2} = \text{(DYNES/UNIT MASS OR GALS)}$$



EQUATORIAL RADIUS = 3963 MILES

POLAR RADIUS = 3950 MILES

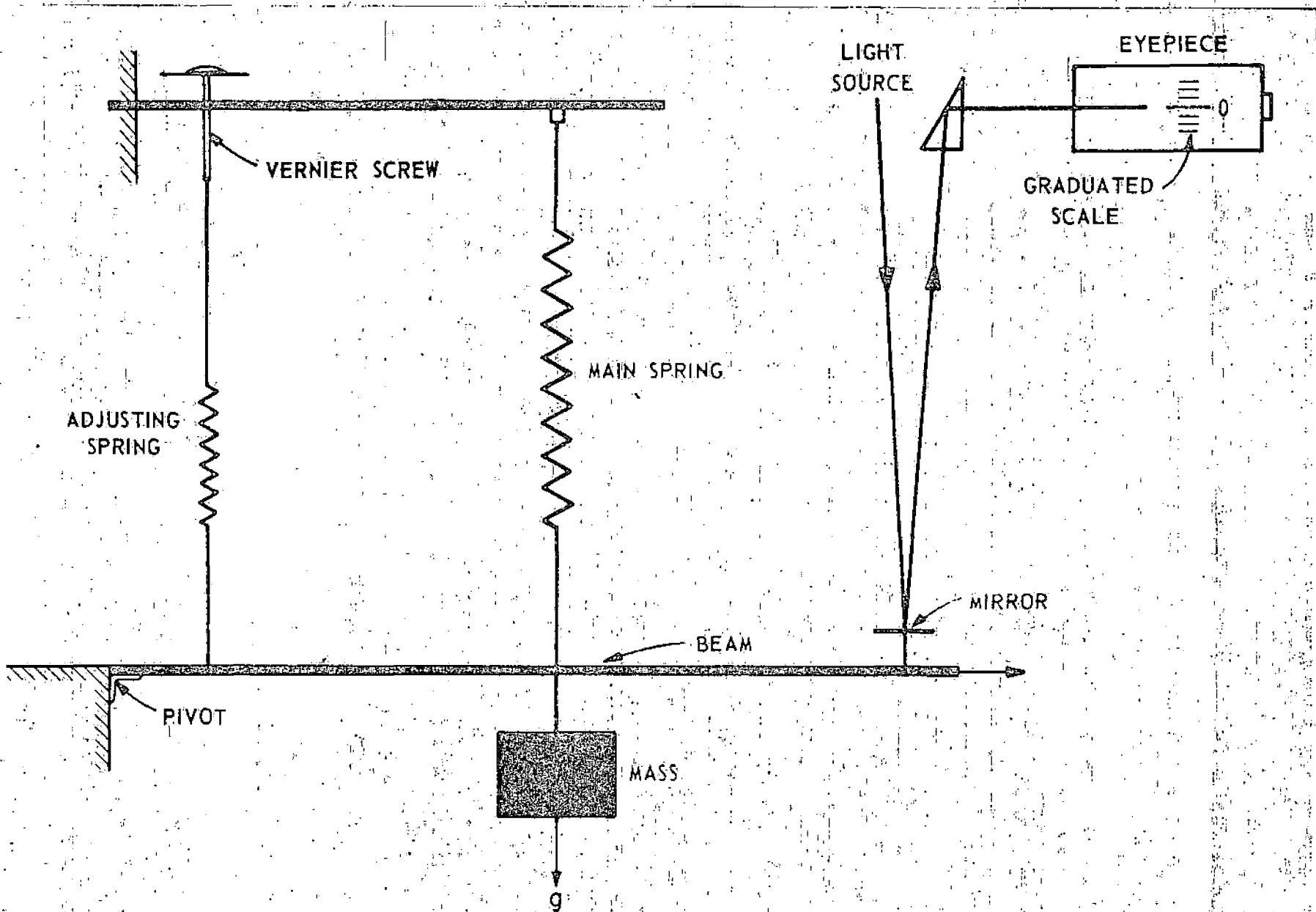
GRAVITY (45° LAT) = 980 GALS

GRAVITY (POLES) = 983 GALS

GRAVITY (EQUATOR) = 978 GALS

$$1 \text{ MILLIGAL} = .001 \text{ GAL} = \frac{.001}{980} = \frac{1}{1,000,000}$$

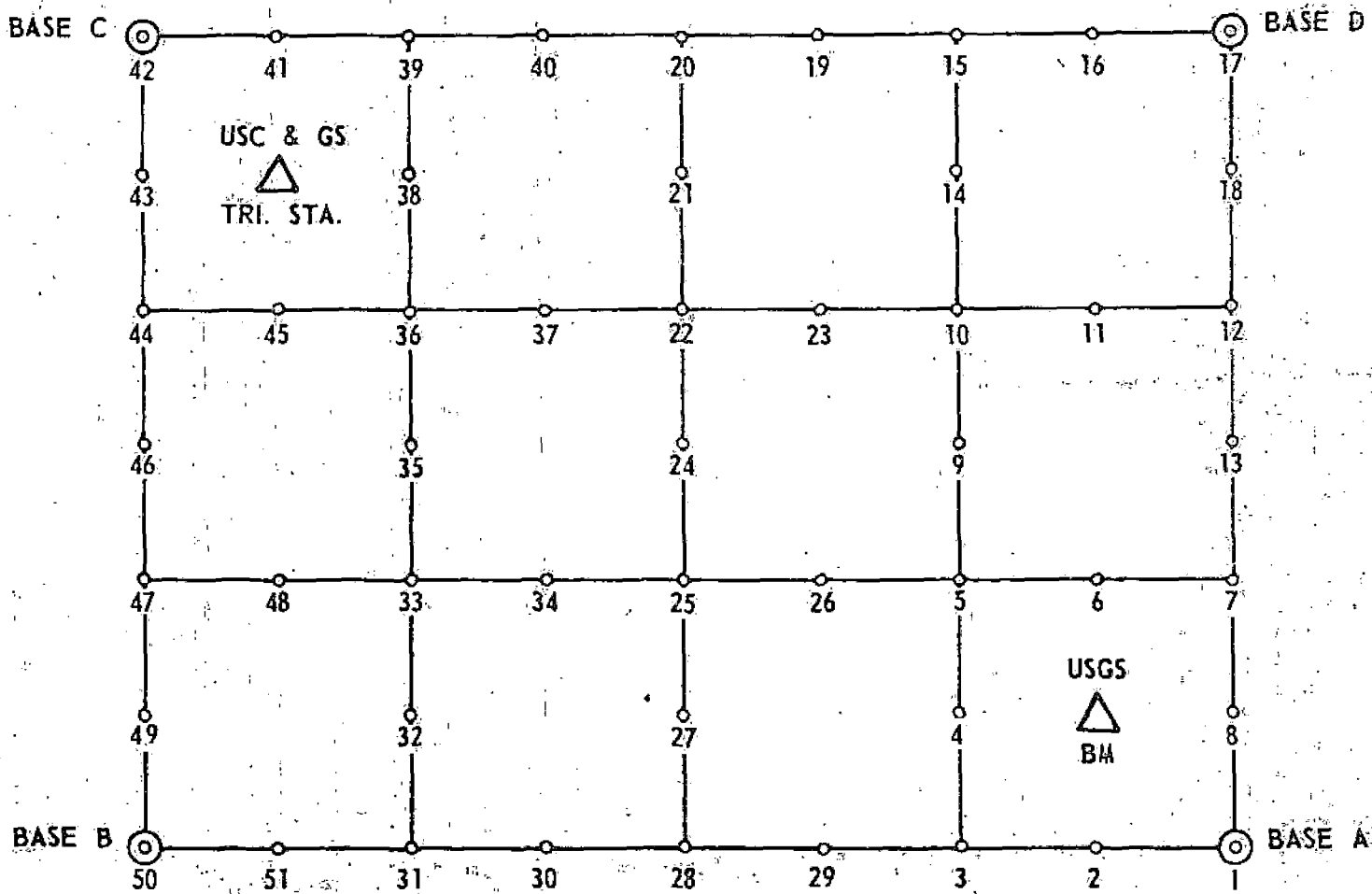
EARTH'S GRAVITY FIELD



HARTLEY GRAVITYMETER

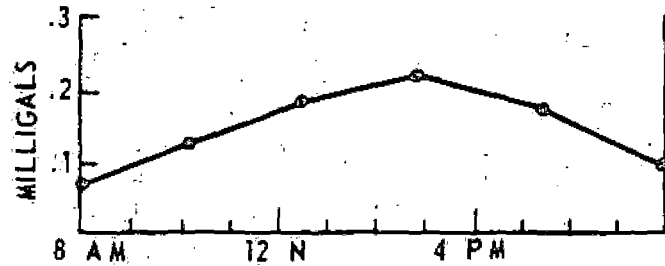
(AFTER DOBRIN.)

GRAVITY FIELD OPERATIONS

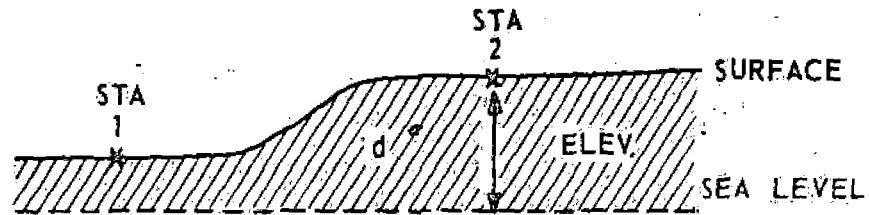


GRAVITY CORRECTIONS

2 HR. REPEAT READINGS ON BASE A

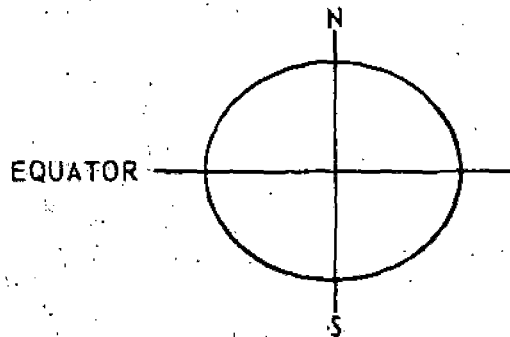


TIDAL & INST. DRIFT CORRECTIONS =
 $.3 \text{ mg} / 24 \text{ HRS}$

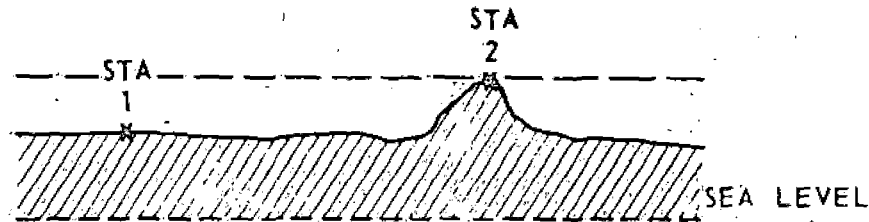


FREE AIR CORR. = $+ .094 \text{ mg} / \text{FT. ELEV.}$

BOUGUER CORR. = $- .013 d \text{ mg} / \text{FT. ELEV.}$

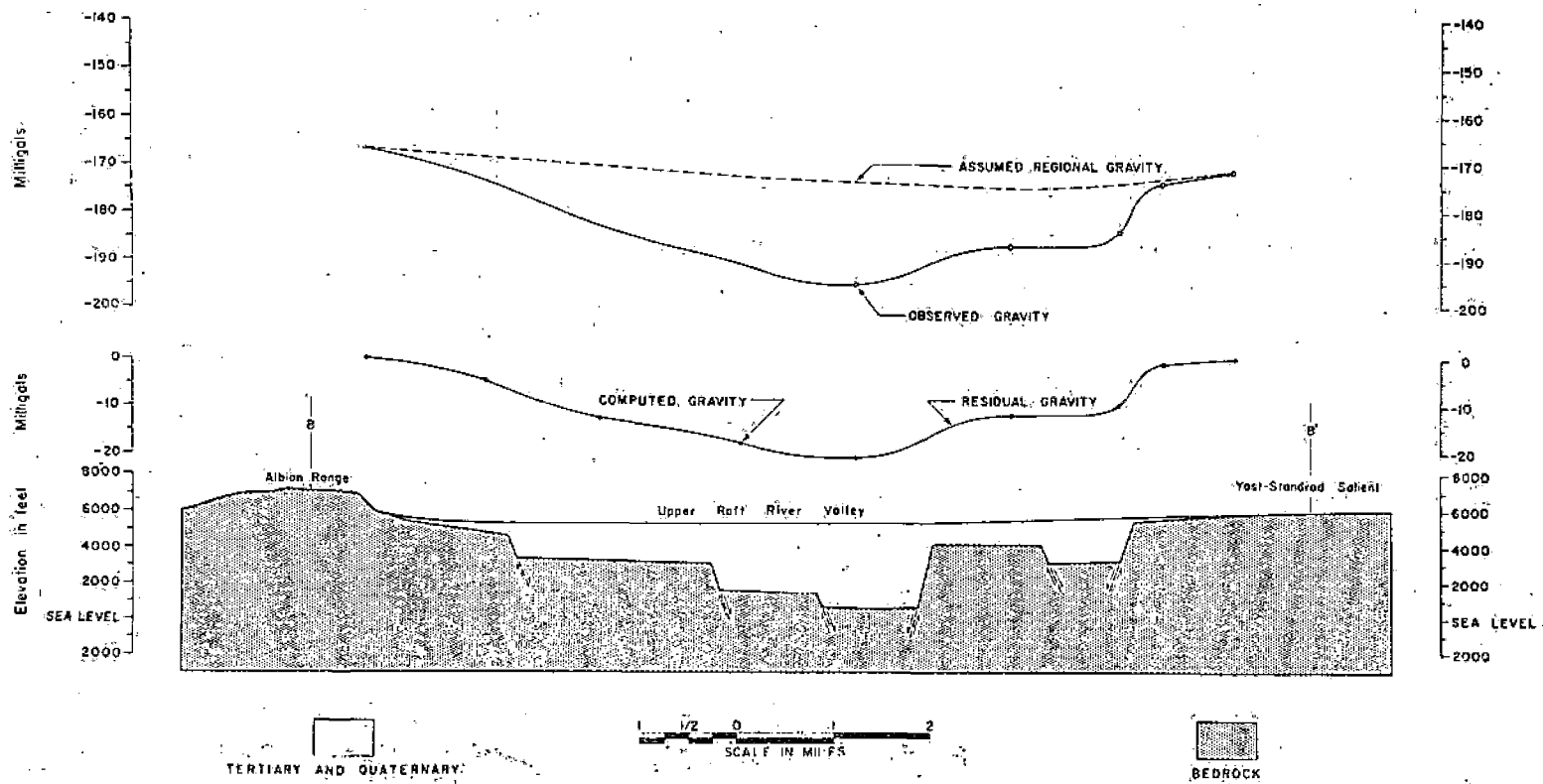


LATITUDE CORR. = $- 1.3 \text{ mg} / \text{MILE NORTH}$



TERRAIN CORR. = $+ \text{mg}$

BOUGUER GRAVITY (m_g) SEA LEVEL DATUM = OBS GRAVITY + TIDAL & DRIFT CORR. + LAT. CORR.
 + FREE AIR CORR. + BOUGUER CORR. + TERR. CORR.



Gravity and interpretive geologic cross-section along profile B-B' across Upper Raft River valley graben and northwestern part of Raft River Mountains. Assumed density contrast is 0.5 g/cc.

THE MAGNETIC METHOD

Rocks are magnetic by virtue of their contained magnetic minerals-- usually magnetite and/or pyrrhotite. Most rocks are usually only magnetic when they are placed in an external magnetic field, i. e., due to induced magnetization. Of course the external field which causes rocks to be magnetic is the earth's field.

The earth's magnetic field is like that due to a large bar magnetic placed deep within the earth. The origin of this field is probably explained by electrical currents circulating in the earth's core, which is believed to be composed of molten iron and nickel. The poles of the magnetic field, i. e., the spots on the earth where the magnetic field is vertical, are near, but not at the earth's rotation poles. Thus a compass does not point to true or geographic north, but rather to magnetic north (see the accompanying figure). The earth's field has a strength of about 25,000 gammas at the magnetic equator and about 75,000 gammas at the magnetic poles.

Many modern magnetometers measure the earth's field strength by measuring the frequency of precession of protons as they rotate around the earth's field direction. Field strength is directly proportional to this frequency. The source of protons is usually a container of kerosene about the size of a pint jar. Modern electronics has made magnetometers accurate, lightweight and trouble-free.

Magnetic surveys can be conducted either on the ground or from an aircraft. Ground surveys are performed in much the same way that gravity surveys (see above) are done. The modern magnetometer measures the value of the earth's local field to about 1 gamma. Corrections are applied for the regular daily variations in the earth's field which are caused by electrical currents in the ionosphere, high above the earth. During times of flares on the sun, the ionosphere becomes very disturbed, which disrupts the magnetic field as well as radio and telephone communications. Surveying is not possible until the magnetic storm subsides.

Magnetic surveys are also performed from an aircraft. In this case the instrumentation is more complex and may be somewhat more sensitive than ground magnetometers. Most surveys are fixed-wing, but the helicopter is also used. The magnetic data are recorded on a paper strip chart and perhaps also on digital magnetic tape. At the same time, 35-mm pictures are taken of the ground every 1-5 seconds by a camera mounted to look vertically downward. When these pictures are later developed, they are compared to larger air photos to recover the exact flight path, which is then posted on a map. During the survey flight a system called an interyolometer makes simultaneous fiducial marks on the magnetic record and on the flight path film so the two can be precisely tied together.

Once the survey has been flown, the flight path is recovered onto maps and some of the fiducial points are posted along the flight path. Then the magnetic profiles are read and posted onto the map, sometimes after a complex series of corrections. From the posted magnetic field values a contour map is constructed, and this contour map represents the final survey product which the geophysicist then uses for his interpretation.

Many factors must be considered in design of an aeromagnetic survey. These are listed on the accompanying chart. Once survey specifications are chosen, a contractor is usually selected to perform the survey, as few mining companies find it cost-effective to maintain their own aircraft.

The magnetic interpretation procedure is variable and complex. The magnetic survey has, of course, mapped changes in the earth's field caused by the varying distribution of magnetic minerals in the surface and near-surface rocks. The magnetic contour map becomes useful only after it has been interpreted, which usually means:

1. determining the size, location, depth and magnetic susceptibility of the various magnetic source bodies (done mainly by the geophysicist), and
2. interpreting the above source bodies in terms of a geologic picture (done by the geologist and the geophysicist).

Interpretation usually begins by quick rules-of-thumb to determine the source bodies and then proceeds to very complex modelling using the computer to calculate the theoretical effect of various source bodies for comparison with observed data. The accompanying figure shows the theoretical magnetic anomalies over a source body of size $4 \times 4 \times 2$ buried 2 units in an area where the earth's field is inclined at 60° to the horizontal and for a body with vertical sides and a susceptibility of 1000×10^{-6} cgs units. Many such models, using a number of source bodies in combination are usually necessary for a good fit to the observed data. The computer is a very valuable aid in this work. An accompanying figure shows the interpretive work for a simple anomaly on data we obtained in eastern Nevada.

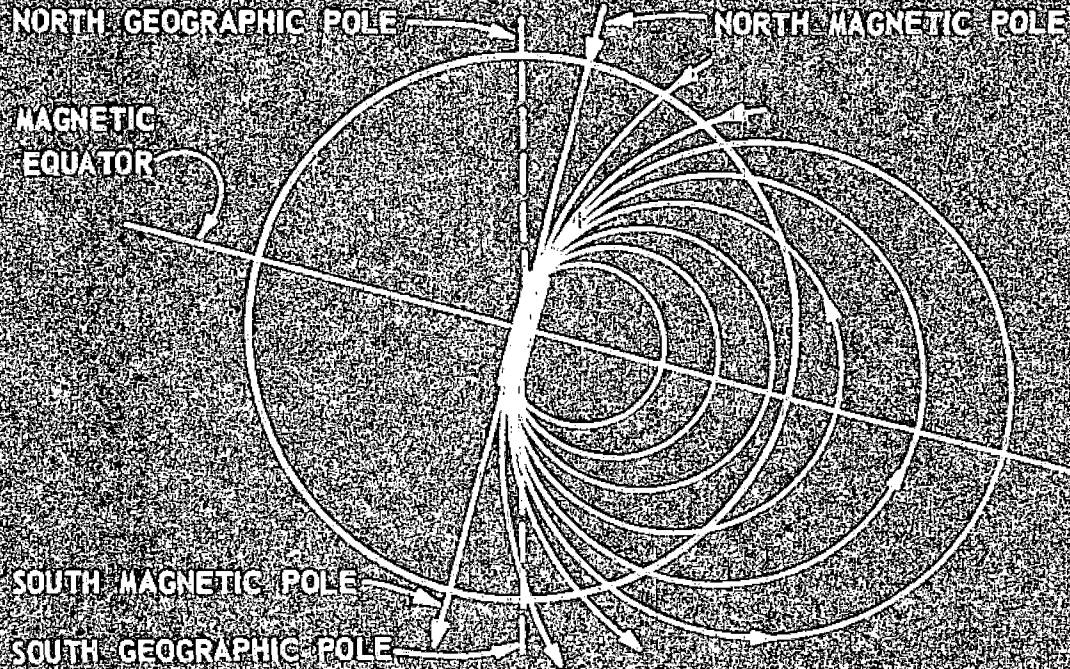
In porphyry copper exploration, the magnetic method is used to:

1. detect buried intrusions which are usually more magnetic than surrounding rocks,
2. detect buried magnetic skarns, which may be very magnetic,
3. detect magnetic lows associated with destruction of magnetite by the mineralization process, and
4. map and project geology.

COULOMB'S LAW OF MAGNETIC ATTRACTION

$$F = \frac{1}{\mu} \frac{P_1 P_2}{r^2} \text{ (DYNES)}$$

EARTH'S MAGNETIC FIELD $T = \frac{1}{\mu} \frac{P}{r^2}$ (OERSTEDS)



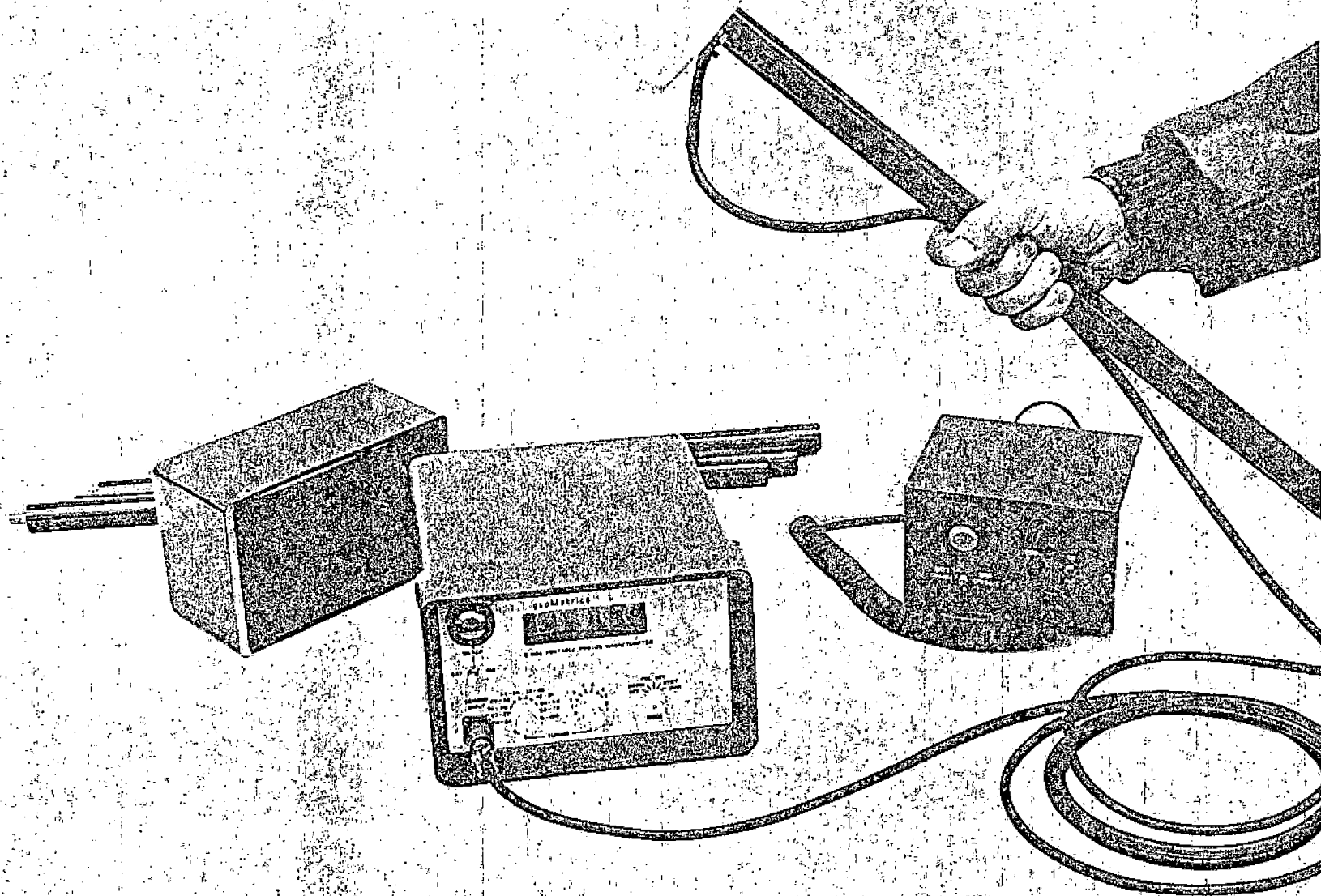
TOTAL MAGNETIC FIELD AT POLES = 0.7 OERSTED

TOTAL MAGNETIC FIELD AT EQUATOR = 0.25 OERSTED

$$1 \text{ GAMMA } (\gamma) = 0.0001 \text{ OERSTED} \quad \frac{0.0001}{7} = \frac{1}{70,000}$$

EARTH'S MAGNETIC FIELD

(AFTER JAKOSKY)



Model G-806 Portable Magnetometer.

AIRBORNE GEOPHYSICAL EXPLORATION SYSTEM
Instituto Nacional de Energia Nuclear

AIRCRAFT: Britten-Norman Islander, Model BN-2A-9R (STOL).
Twin turbo-charged 260 BNP engines with full IFR instrumentation.

Gross wt: 6300 lbs (2860 kg)
Empty wt: 3826 lbs (1737 kg)¹
Useful Load: 2474 lbs (1123 kg)
Operating Equipment: 2315 lbs (1051 kg)
Geophysical Instruments: 655 lbs (297 kg)
Operating Crew: 510 lbs (232 kg)
Fuel (U.S. gallons): 1150 lbs (522 kg)
Min. Survey Speed: 70 mph (113 km/hr)
Ferry Cruise Speed: 160 mph (267 km/hr)
Max. Cruise Range: 1263 st. miles

GAMMA RAY SPECTROMETER: Exploranium, Model DIGRS-3001
Four channel differential measurements of potassium, uranium, thorium and total count. Wt: 24 lbs (10 kg)

SPECTRUM STABILIZER: Exploranium, Model MSS-3002
Provides continuous automatic gain adjustment for each crystal and p.m. tube. Wt: 16 lbs (7.2 kg)

CRYSTAL DETECTOR: Exploranium, Model L100
Nine 6" dia. x 4" thk. (152 x 102 mm) sodium iodide crystals.
Total volume: 1018 ins.³ (16,683 cm³). Two containers.
Total wt: 297 lbs (134 kg)

PROTON MAGNETOMETER: GeoMetrics, Model G-803
Provides 0.25 gamma sensitivity, analog and digital outputs.
Stinger mounted sensor. Console wt: 14 lbs (6.35 kg)

ANALOG RECORDER: Exploranium, Model MARS-6
Provides six channels; two event markers, multiple chart speeds, inkless writing. Wt: 34 lbs (15.3 kg)

DIGITAL RECORDING SYSTEM: GeoMetrics, Model G-704
Sequentially scans, converts, formats, and records all digital and analog input data on magnetic tape for direct computer processing. Wt: 20 lbs (9.1 kg)

MAGNETIC TAPE RECORDER: Cipher, Model 70
Provides digital recording of 300 char/sec. at 200 bpi.
Wt: 30 lbs (13.6 kg)

VISUAL DATA DISPLAY: GeoMetrics, Model G-705
A digital data verification system (not shown) provides a 256 character visual display of all recorded survey data. Wt: 12 lbs (5.4 kg)

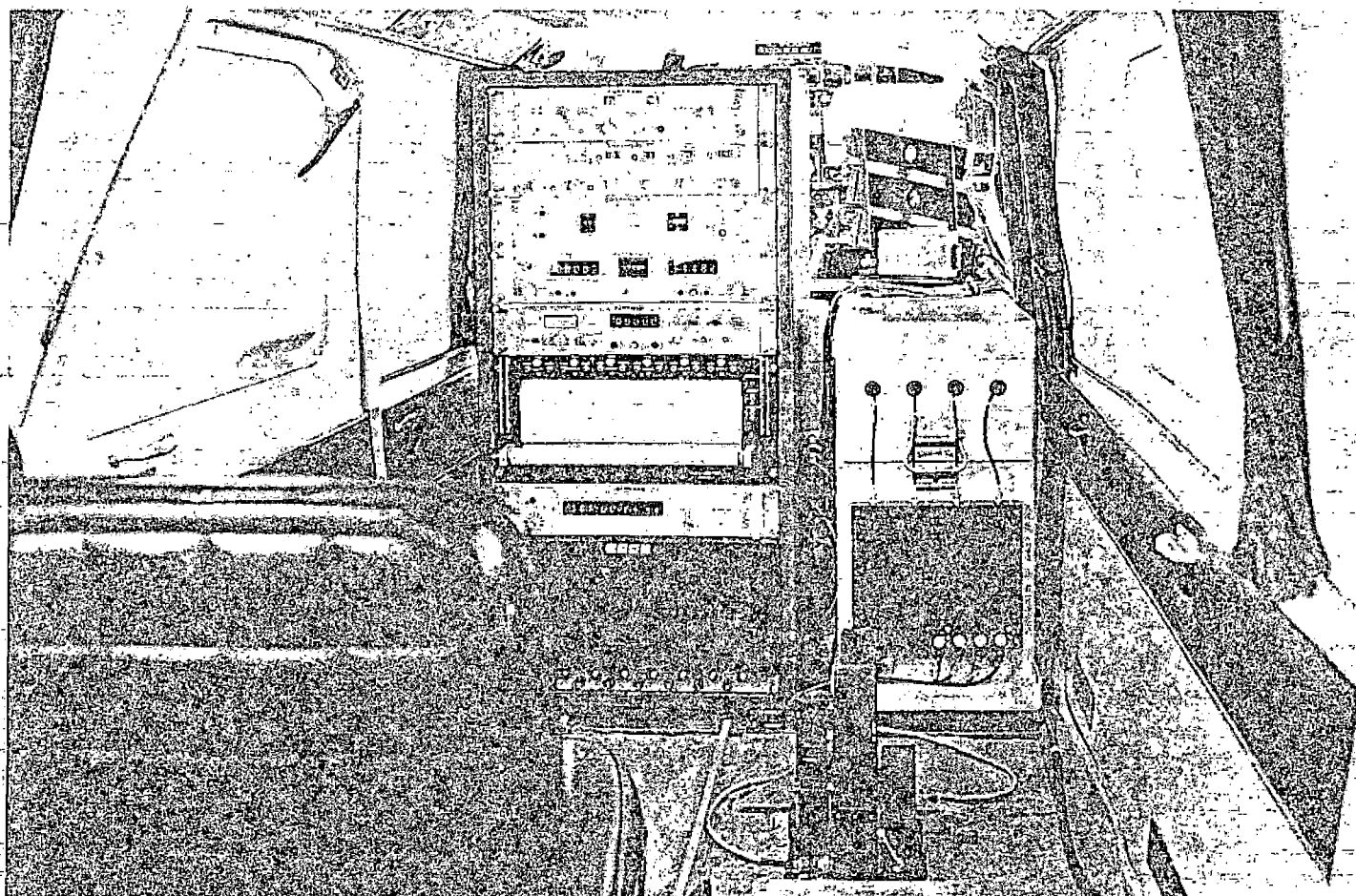
INTERVALOMETER: GeoMetrics, Model G-803-201
Provides pulse to navigation camera, fiducial counters and recorder event marker. Wt: 5 lbs (2.3 kg)

NAVIGATION CAMERA: Automax, Model G-2
35 mm system with twin optics, 400-ft. film magazine.
Wt: 25 lbs (9.1 kg)

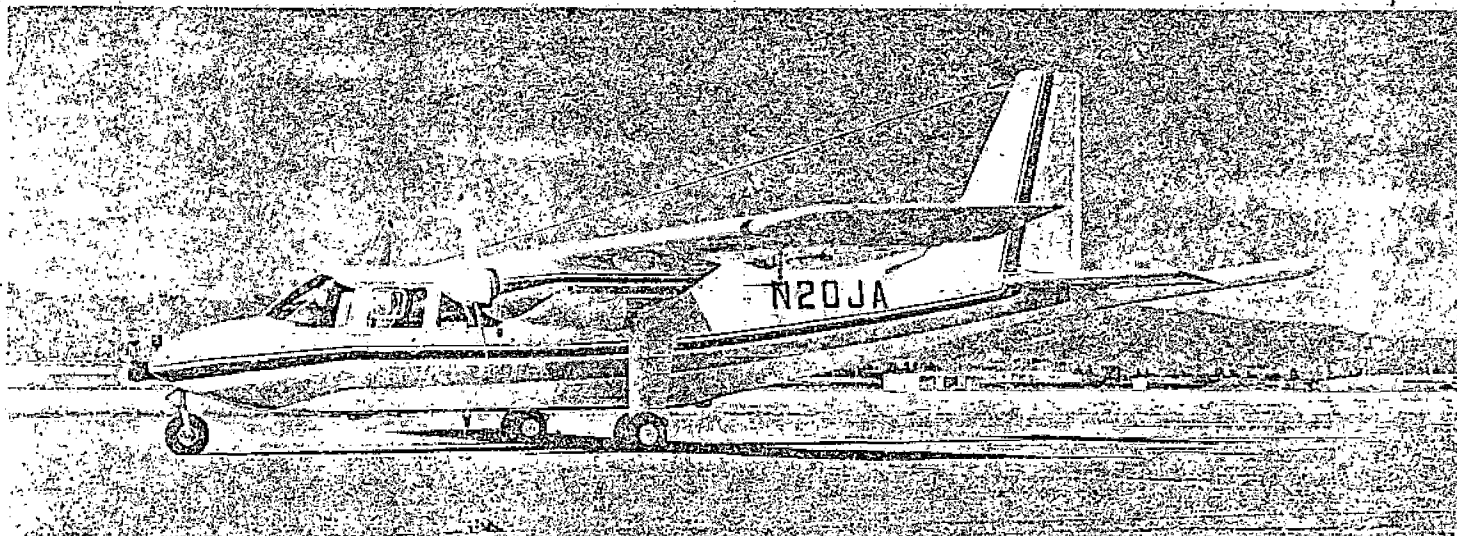
RADAR ALTIMETER: Honeywell, Model YG-7600
Provides 1% linear accuracy from 0 to 5,000 feet. Wt: 7 lbs (3.2 kg)

VLF NAVIGATION SYSTEM: Model GNS 300
Provides point-to-point radio navigational data over all terrain including water. Wt: 20 lbs (8.5 kg)

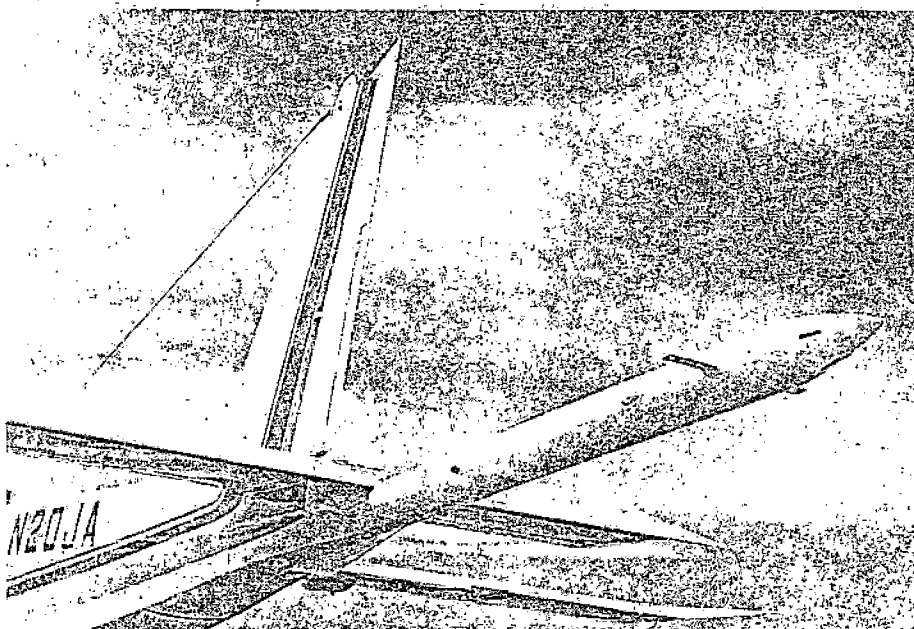
1. Includes basic equipment and standard avionics. ALL geophysical instruments are standard 19" rack mount with 24-32V DC power requirements (Islander power system is 28V DC.)



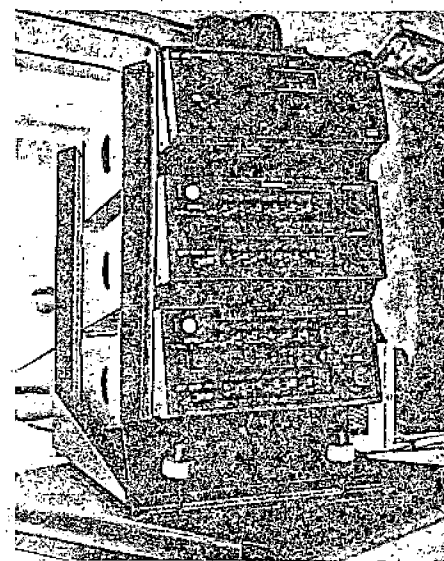
Complete geophysical survey installation (Islander aircraft)



Islander Survey Aircraft (Instituto Nacional de Energia Nuclear)



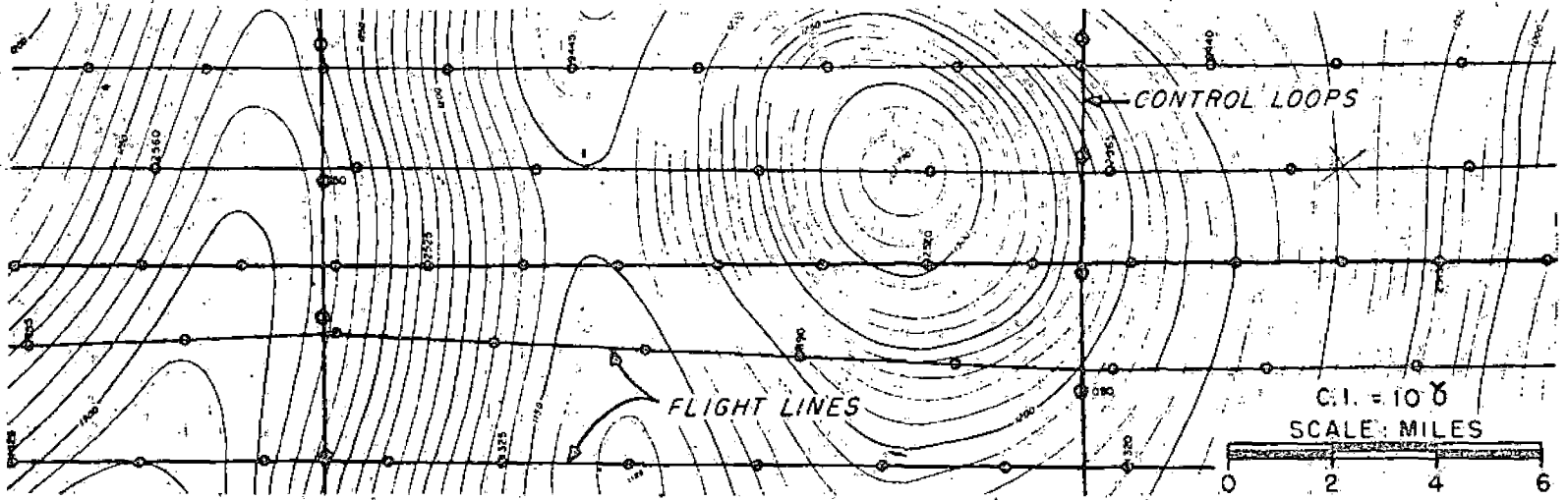
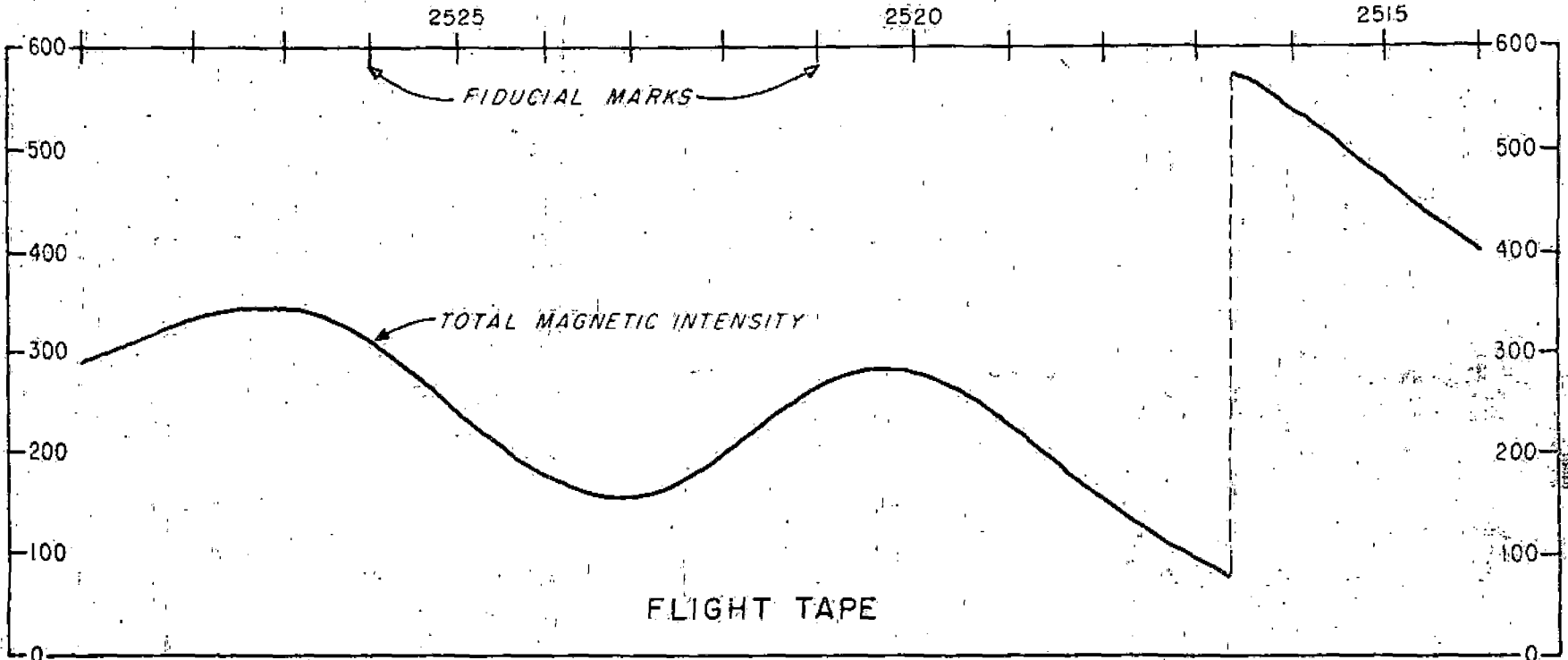
Magnetometer Stinger Sensor Installation

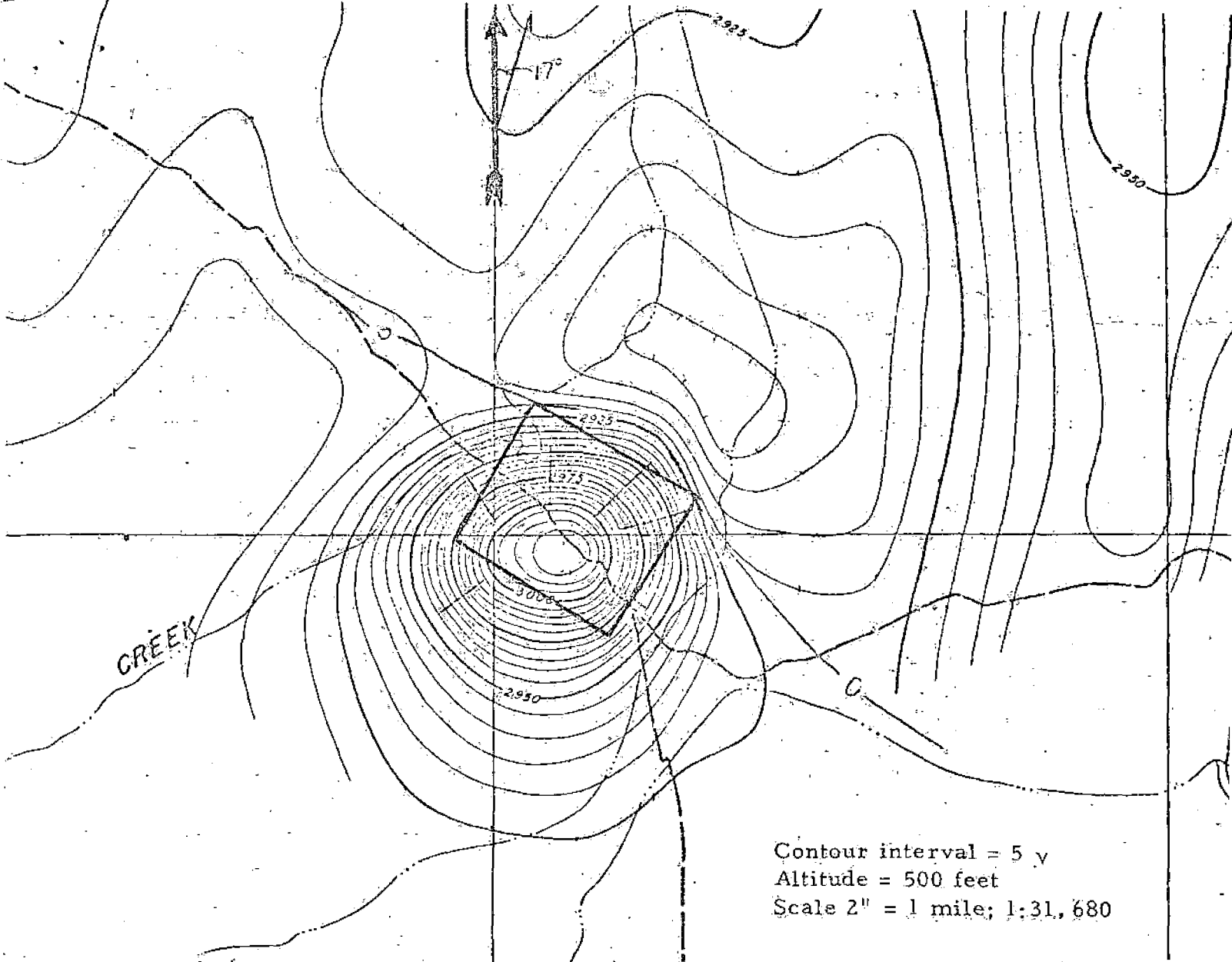


VLF Navigation System

GeoMetrics/Exploranium Instrument Division recently installed, tested and delivered a fully instrumented airborne survey exploration system to the Instituto Nacional de Energia Nuclear (National Institute of Nuclear Energy). The survey aircraft is the popular Britten-Norman Islander, offering installation convenience and stable survey characteristics. The exploration platform includes an Exploranium four channel digital Gamma Ray Spectrometer employing a large crystal volume (1018 ins.³) with fully automatic spectrum stabilization, a GeoMetrics Proton Magnetometer with stinger mounted sensor, and Digital Data Acquisition System for direct computer entry of all analog and digital survey data, as well as a six channel analog recorder, intervalometer, 35mm camera, radar altimeter, and a VLF radio navigation system. This sophisticated airborne system is an essential element of the Institute's newly established program to fully investigate and analyze the natural resources of the entire country of Mexico. While the primary emphasis is the discovery of radioactive sources to meet potential power requirements, capabilities also include reconnaissance mapping of geologic structures. To insure effective ground follow-up of selected areas of interest, GeoMetrics also provided a helicopter spectrometer platform complemented by truck-mounted spectrometer systems, base station magnetometers and portable instruments. During various phases of the Islander installation, GeoMetrics provided a comprehensive training program to familiarize the Institute's personnel with total instrument operation and maintenance, airborne and ground survey procedures, and modern compilation and interpretation techniques. Additional "on-site" training will continue to further insure that all survey objectives are achieved with optimum results.

AEROMAGNETIC DATA





Contour interval = 5 y
 Altitude = 500 feet
 Scale 2" = 1 mile; 1:31,680

Interpretation:

1. Establish background or 0 level (undisturbed field value) = 2915 to 2925
2. Establish anomalous maximum and minimum

maximum - 3018 → 98 γ
 background - 2920 → 0 ratio, $\frac{\min}{\max} = \frac{18}{98} = .18$
 minimum - 2902 → -18 γ
3. Determine depth; 1000-1500 feet below plane → 500-1000 feet deep
4. Draw a magnetic source body: ~2500' x 2500' → 2 x 2 depth units
5. Check prism models: Vacquier A58 = 2 x 2 at 60° inclination
6. Compute apparent susceptibility: $K_a \approx \frac{98}{1.7 \times 54,000} = \frac{98}{91.8 \times 10^3} = 1.07 \times 10^{-3} \approx 1000 \times 10^{-6}$ cgs (infinite body). Depth extent is between 2000' and ∞ $1000 < K_a < 2000 \times 10^{-6}$ cgs
7. Geologic explanation.

MAGNETIC INTERPRETATION PROCEDURE

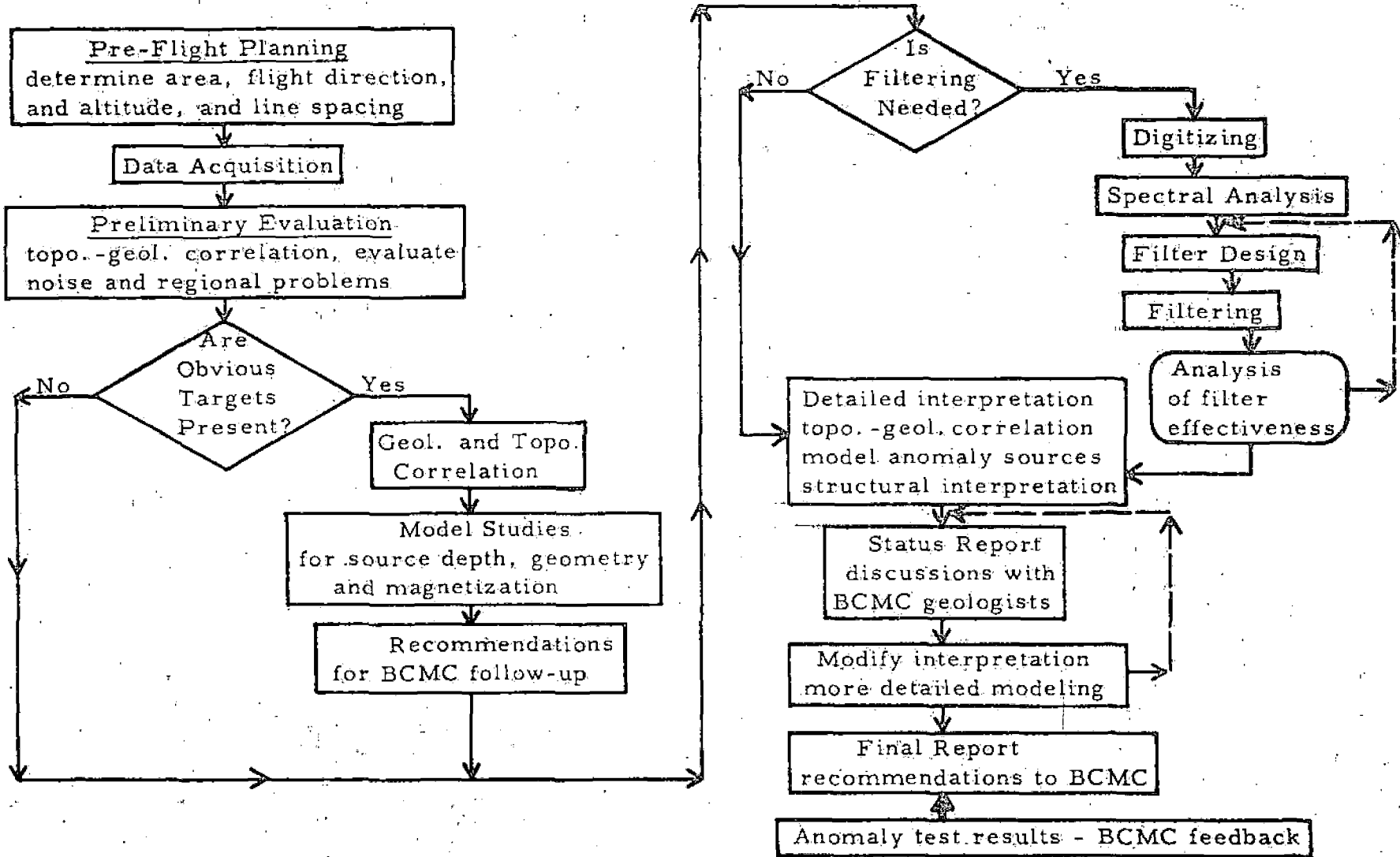
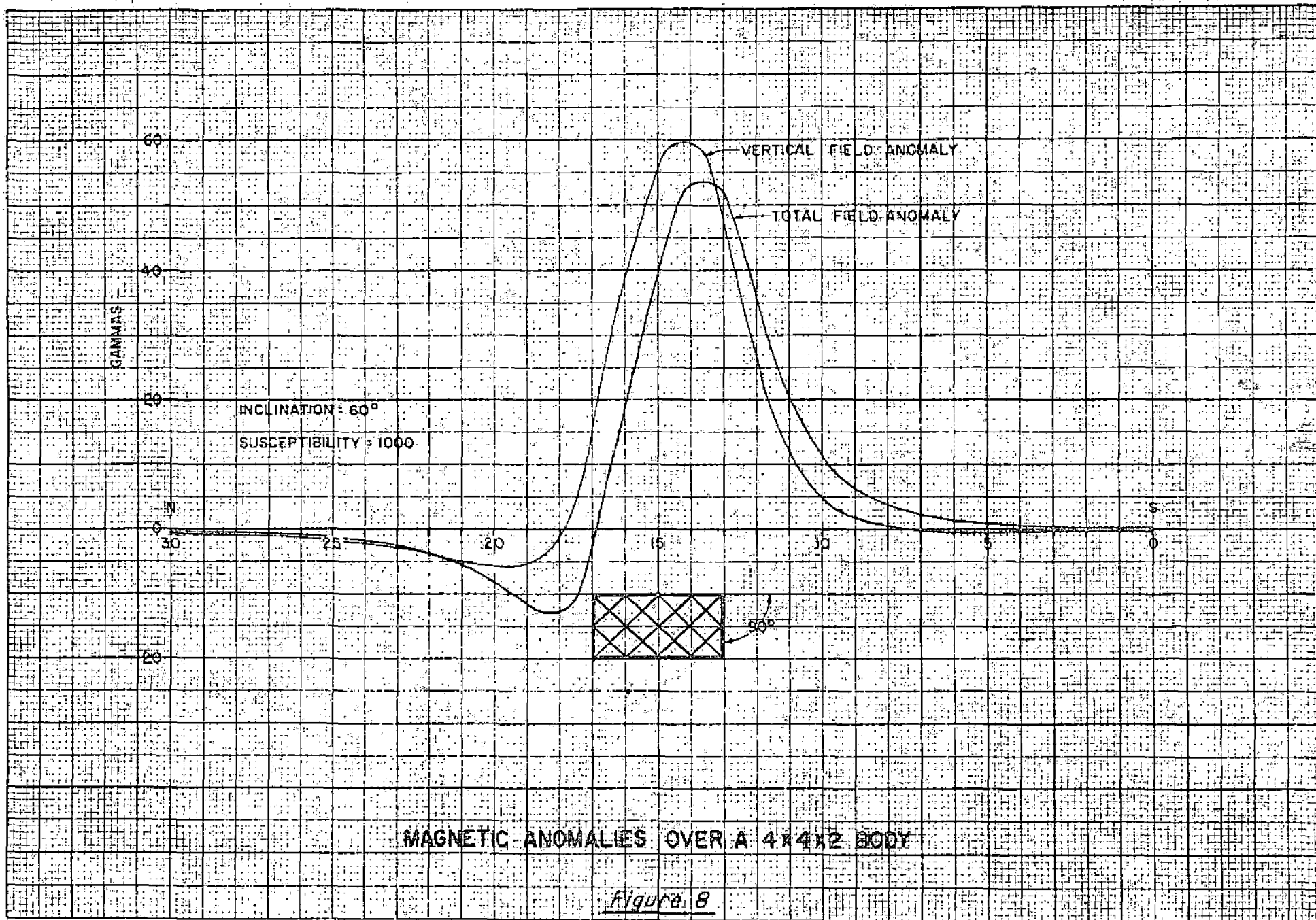
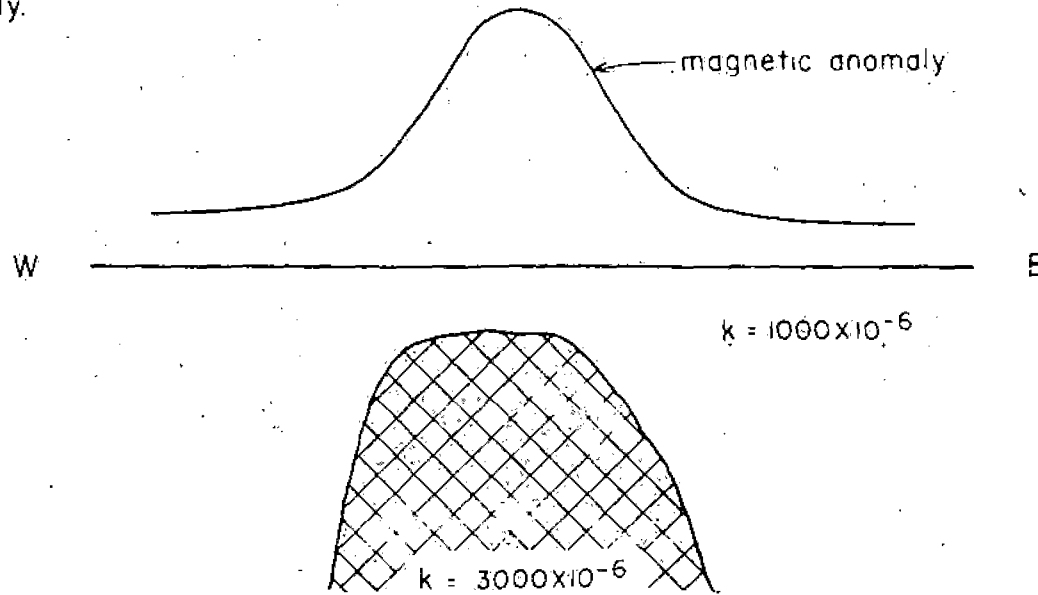


FIGURE 1. FLOW CHART OF MAGNETIC INTERPRETATION PROCEDURE



Horizontal changes in magnetic susceptibility are required to produce a magnetic anomaly.



Vertical changes in magnetic susceptibility are not detected by moving a magnetometer over or above the earth's surface.

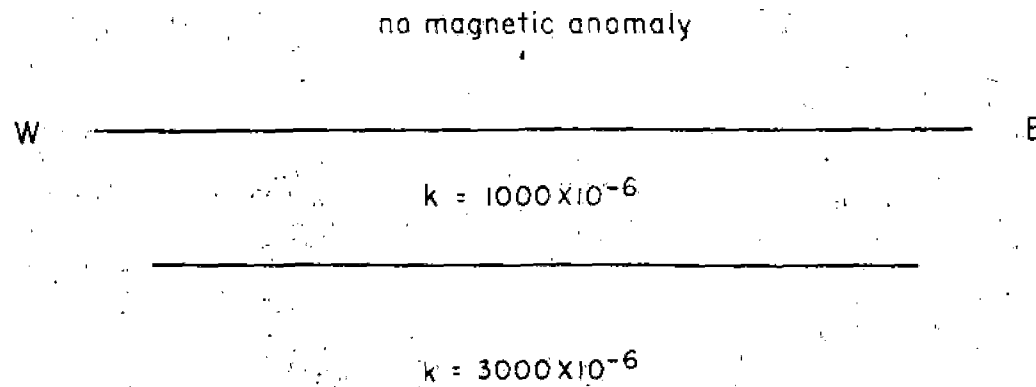
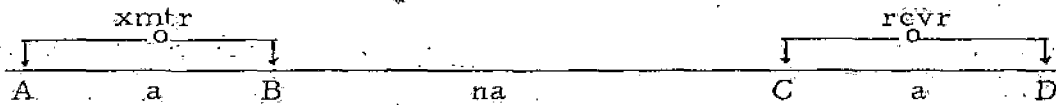


Figure 2

Horizontal Susceptibility Changes

THE INDUCED POLARIZATION METHOD

Induced polarization (IP) is an electrical method of geophysical prospecting. Current is injected into the ground and taken back out at points A and B,



respectively, a distance a apart. A special constant-current device called an IP transmitter (xmtr) does this. At some distance, na , away, the voltage difference is read between points C and D by an IP receiver (rcvr). From knowledge of the amount of current, I , injected by the transmitter and of the received voltage, v , as a function of transmitter frequency, f , two quantities are determined:

1. The resistivity of the ground, i. e., how well or how poorly the ground conducts electricity, and
2. the magnitude of the induced polarization effect, which is a measure of the amount of sulfide mineralization in the nearby ground.

In order to understand these two measurements, some background is needed. First, how does electricity go through the earth? Rocks at depth are composed mainly of minerals which are electrical insulators. But between the mineral grains are tiny pore spaces. The pore spaces are generally filled with groundwater and the groundwater contains dissolved salts, i. e., sodium, calcium, chlorine and sulfate ions. These ions, being electrically charged, move in response to an electric field and carry current through rocks.

The IP transmitter injects a square-wave alternating current, as shown on the accompanying figure. There are two types of IP measurement, 1) time domain and 2) frequency domain. In the time domain measurement the transmitter has a current-off period before each current reversal, whereas in the frequency domain measurement there is no current-off period. Because the origin of the IP effect is easier to understand in the time domain, we will consider it only.

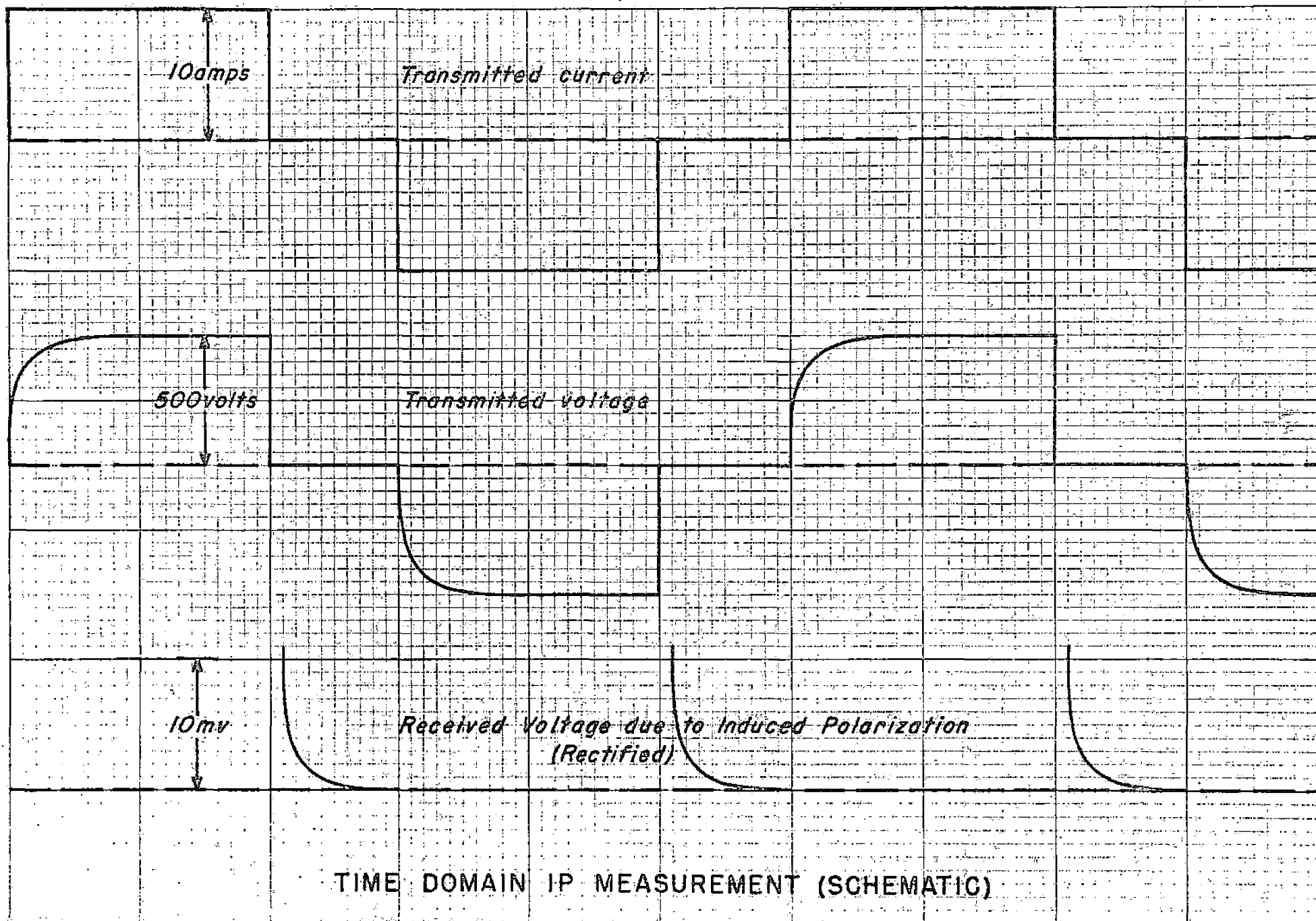
Imagine a square-wave alternating current as shown in the figure. It is important for the measurement that the edges of the current waveform be exactly square. In order to do this, complex electronic circuits in the transmitter constantly adjust the transmitter voltage so that the transmitter current is precisely regulated. The typical transmitter voltage is shown in the figure. The receiver measures only when the transmitter is off. It sees a voltage which decays rapidly with time. This decaying voltage is made up of 1) electromagnetic induction effects (not considered further), and 2) the induced polarization effect. If the receiver voltage tails off or decays more slowly, the IP effect is larger.

Now refer to the figure entitled "Rock Model for Electrode Polarization." On the right side is a microscopic view of a rock with two pore spaces magnified. One pore space is free while the other is blocked by a metallic (sulfide mineral) particle. The left side of the picture is a magnified view of the metallic particle-ionic solution interface in the blocked pore. While the IP transmitter is on, current flows via ion movement in the pore space, but the ions bump against the metallic particle and pile up there. These ions are discharged by electrons (or holes) moving in the metallic particle. There is thus a change in mode of electrical conduction across the metallic particle-ionic solution interface. In the solution electricity is carried by ions, whereas in the metallic particle electricity is carried by electrons and holes. Now when the transmitter current is shut off, the ions in the solution flow back away from the interface to an equilibrium position. It is this reverse ionic movement after current shutoff that causes the IP receiver to read a voltage. It occurs only in the blocked pores which have a metallic particle. Therefore the IP measurement tells us that there are metallic particles in the earth. Because most rocks do not contain metallic particles unless they are mineralized, the IP measurement detects mineralization.

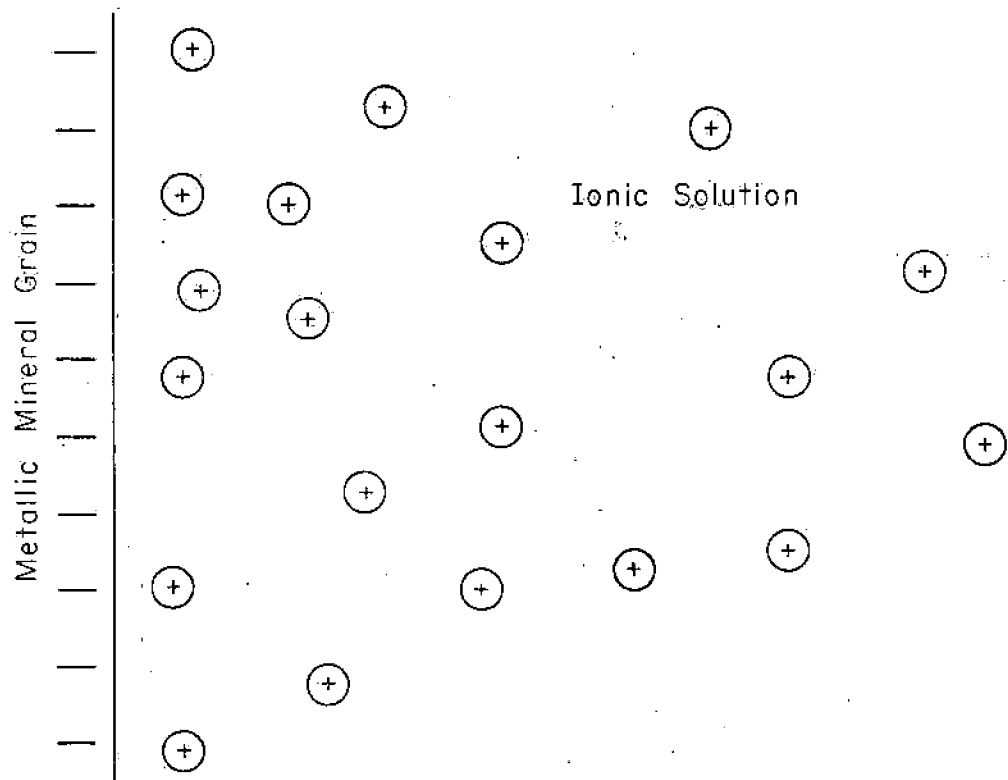
In practice a series of 7 electrodes is usually laid out at intervals of 1,000 feet in a line. The transmitter is stationed in a truck at the center of the line, and the truck engine runs a large generator which powers the transmitter. Some IP transmitters are capable of 20,000 watts. The IP receiver, which is a highly sophisticated electronic instrument, is connected to various electrode pairs as the transmitter is connected to various other electrode pairs and readings are taken. Each reading is plotted at the intersection of the 45° diagonals from the transmitter and receiver electrode pairs (see left side of figure entitled "Effect of Body Depth on IP Anomaly"). In this way a whole cross section of measurements is made. Resistivity is calculated from the measurements and is plotted on a similar cross section. Then begins the task of 1) interpreting these cross sections into the subsurface distribution of sulfide mineralization, and 2) converting this to a geologic picture.

The computer plays a big part in IP interpretation. The above referenced figure shows the effect on the IP anomaly of making an IP source body deeper. Note that the amplitude of the anomaly decreases, i. e. smaller numbers are read at the surface, for a deeper body. Note also the trapezoidal shape to the pattern of high numbers over the body. These are theoretical cross sections, calculated on a large computer.

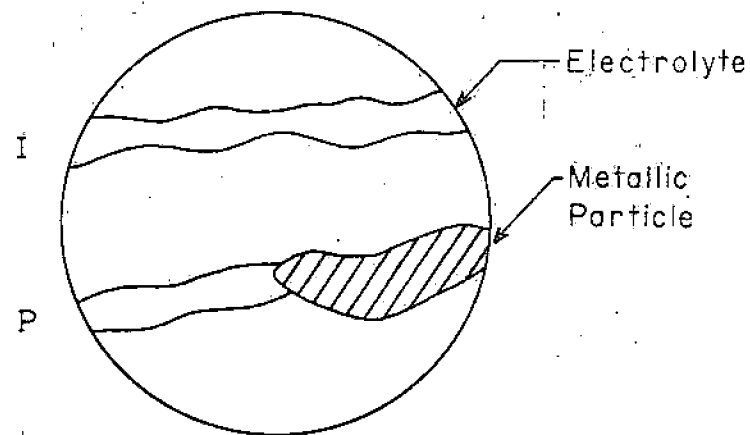
The geophysicist considers many factors in making an interpretation of one or more IP cross sections in terms of IP source bodies. Then the geologist and the geophysicist work together to determine the geological meaning of the source body distribution. The result of this effort may be a drill test of an ore target concept.



Rock Model For Electrode Polarization



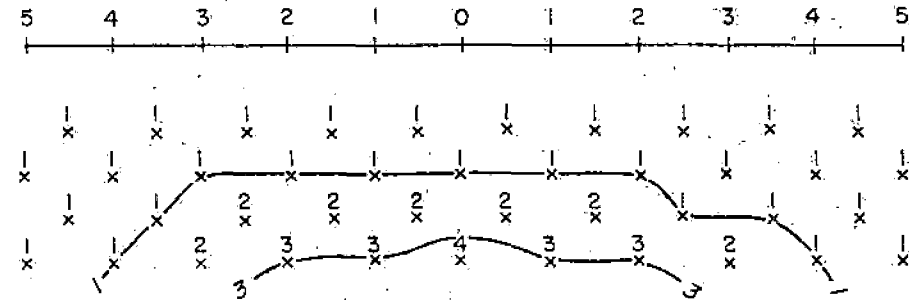
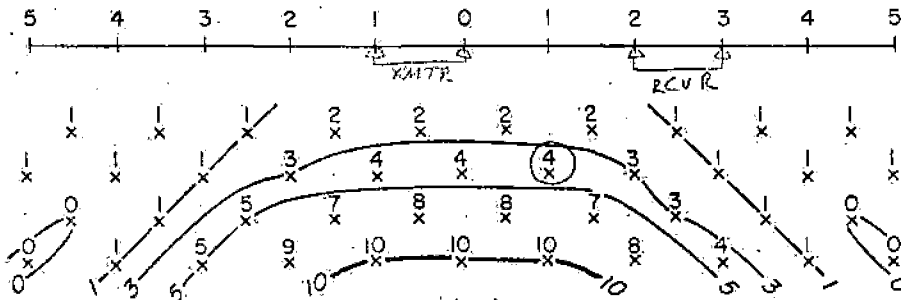
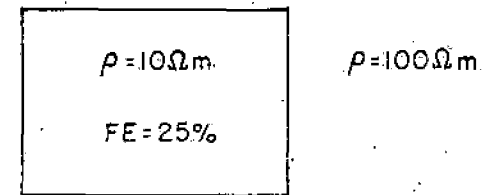
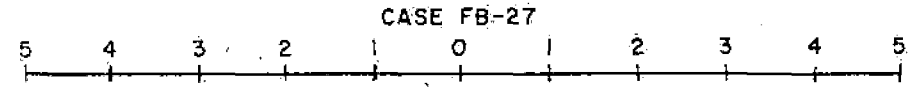
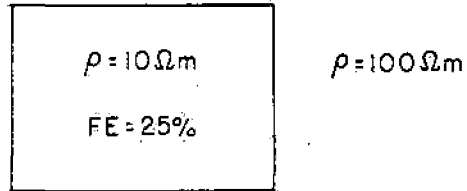
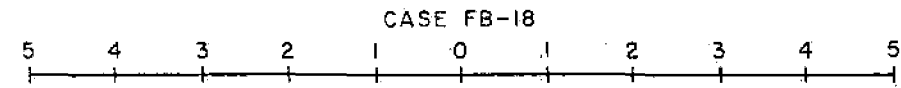
Simplified model of the *electrical double layer*, showing a negative surface charge balanced by cations in an electrode.



A simple model for conduction in a polarizable rock. I represents an ionic, or nonpolarizable path, while P represents a polarizable path.

Figure 1

Effect of Body Depth on IP Anomaly



Note that, for this particular model, doubling the burial depth causes the anomaly to decrease to one-third of its former value. The body buried 2000 feet deep is at the lower limit of our present detection capabilities.

GEOPHYSICS IN PORPHYRY COPPER EXPLORATION

The three most often used geophysical surveys in porphyry copper exploration and their uses are:

<u>Survey Type</u>	<u>Uses</u>
IP	1) locate sulfide mineralization 2) map details of sulfide distribution (zoning)
Magnetic	1) locate intrusions which may or may not have an associated deposit 2) locate magnetic skarns 3) detect magnetite distribution 4) map and project geology
Gravity	1) determine thickness of cover 2) detect skarns or massive sulfide mineralization

The accompanying figure shows typical responses for these geophysical techniques over the average porphyry copper deposit.

Exploration for porphyry copper deposits might follow the sequence below (other slants to exploration are also in logue):

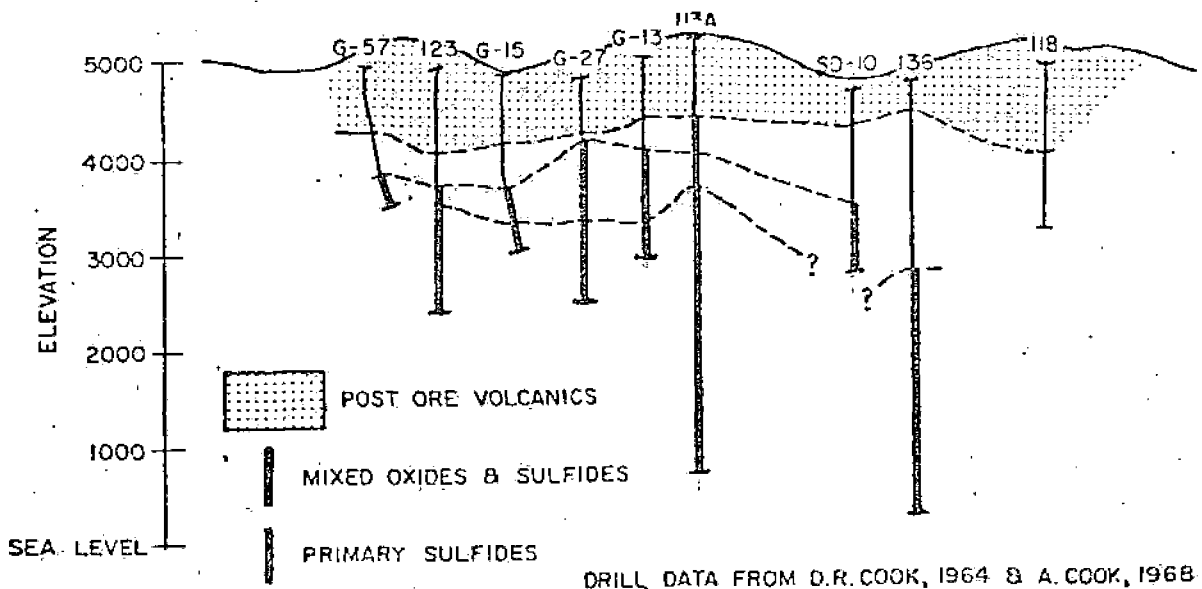
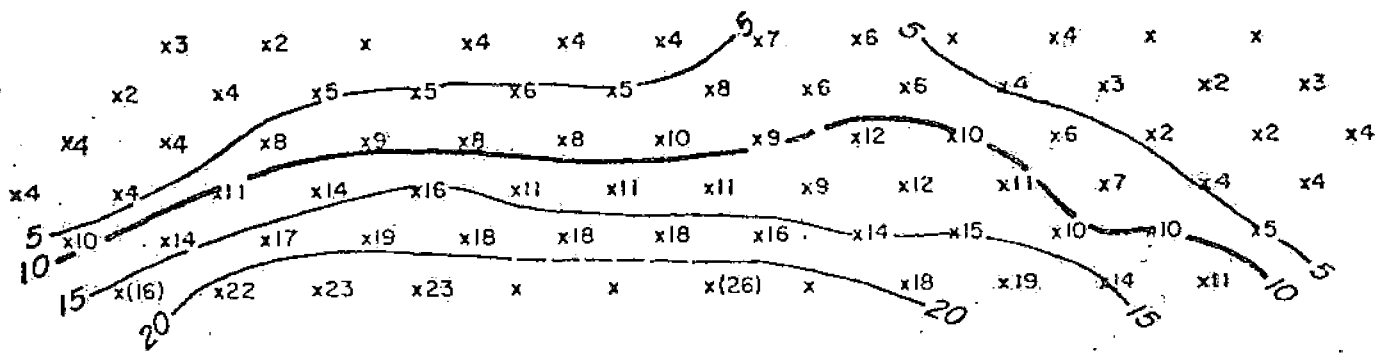
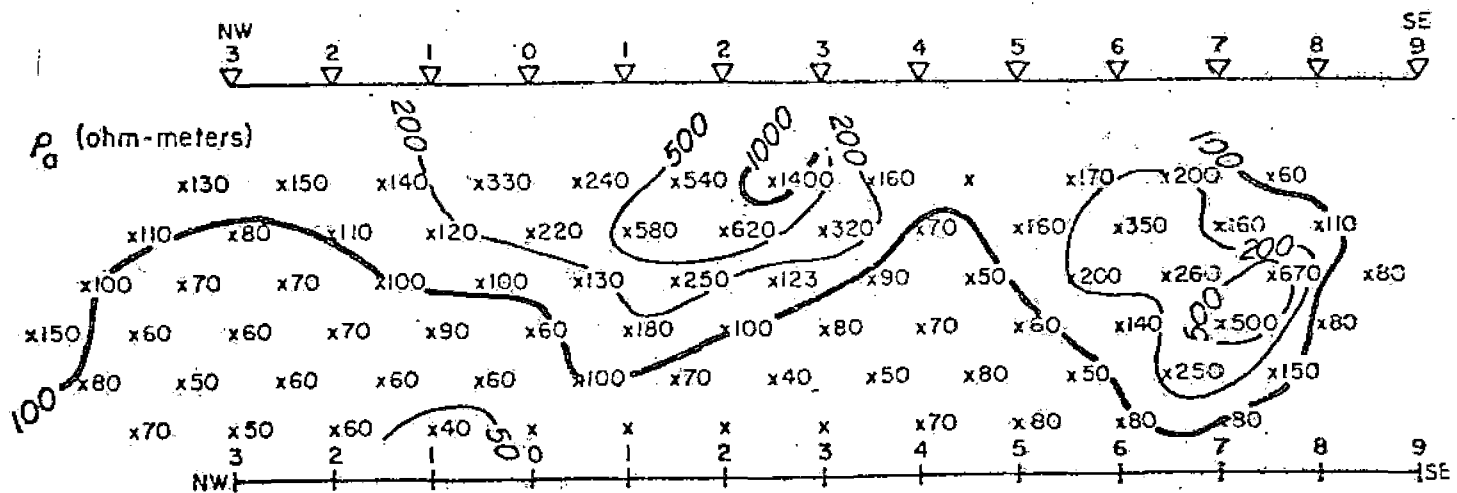
1. Generation of Areas of Interest
 - a) collect reconnaissance geological, geochemical and geophysical (magnetic, mainly) data
 - b) analyze data base in terms of chances for undiscovered ore deposits
 - c) select specific areas for further more detailed exploration.
2. Testing of Areas of Interest
 - a) map geology in detail
 - b) perform gravity survey if cover exists

- c) perform IP and detailed magnetic surveys if cover is thin
- d) analyze data base to determine chances for occurrence of undiscovered ore deposit-- i. e., formulate an ore target concept, if possible
- e) drill test

The following figures display aeromagnetic and IP data over select porphyry copper deposits.

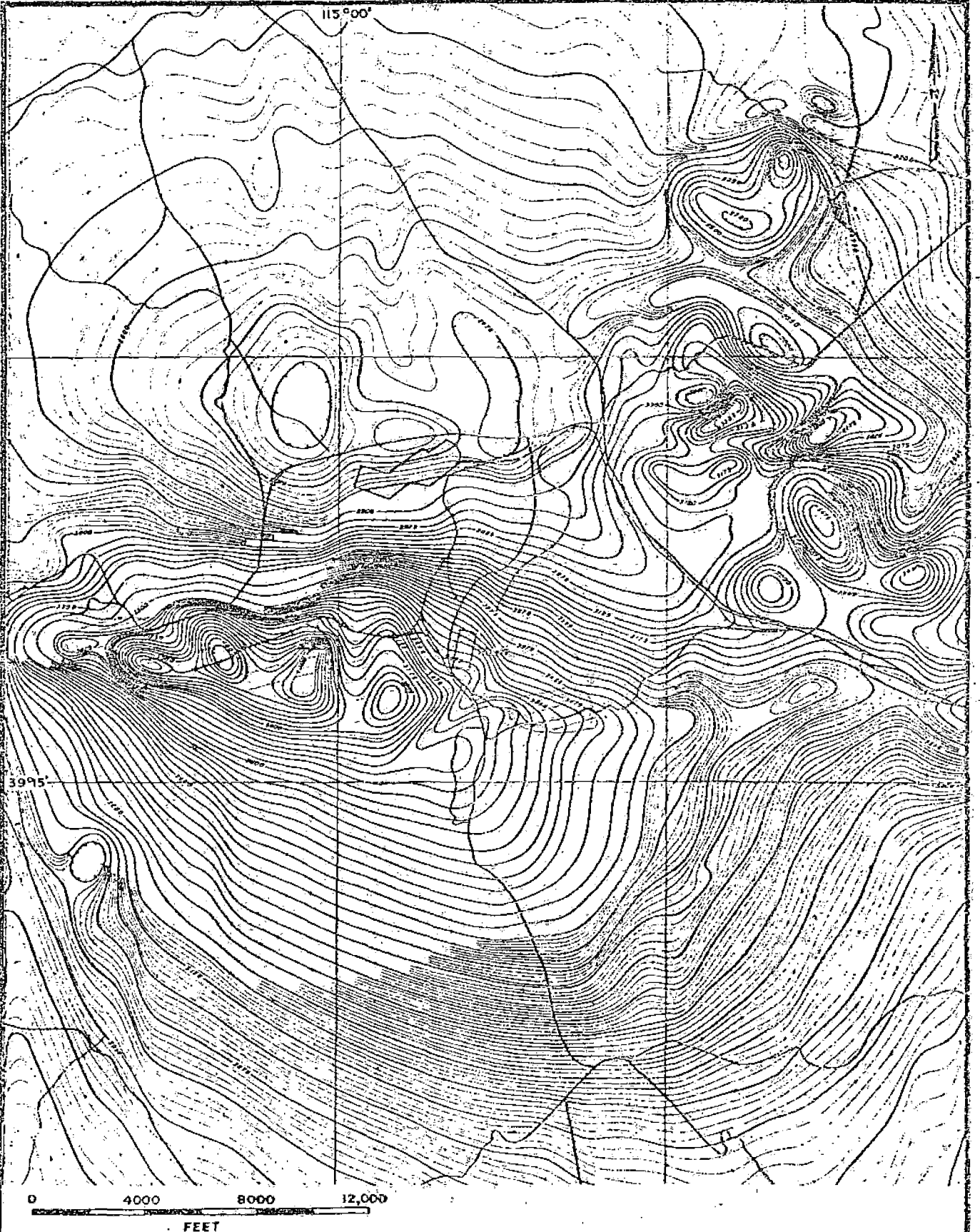
USEFUL GEOPHYSICAL RESPONSES PORPHYRY COPPER DEPOSITS

METHOD	RESPONSE/GEOMETRY	CAUSE
IP	0-3 pfe/ background 5 pfe / 4mi ² 6-15 pfe/ zones 500'-1500' wide	whole sulfide system pyrite halo-- internal sulfide geometry
RESISTIVITY	200 to 2000 Ω -m background 200 Ω -m/ 4mi ² 50 Ω -m/ zones 500'-1500' wide	whole sulfide system pyrite halo -- internal sulfide fracturing geometry
MAGNETIC	variable background 100 to 2000 γ -50 to -200 γ 3mi ² 100 to 5000 γ / 1/4 to 2mi ²	associated structures or intrusions magnetite destruction by sulfides skarn with magnetite
GRAVITY	variable background 0.02 to 1m gal / 0.1mi ²	associated massive sulfides



DRILL DATA FROM D.R. COOK, 1964 & A. COOK, 1968

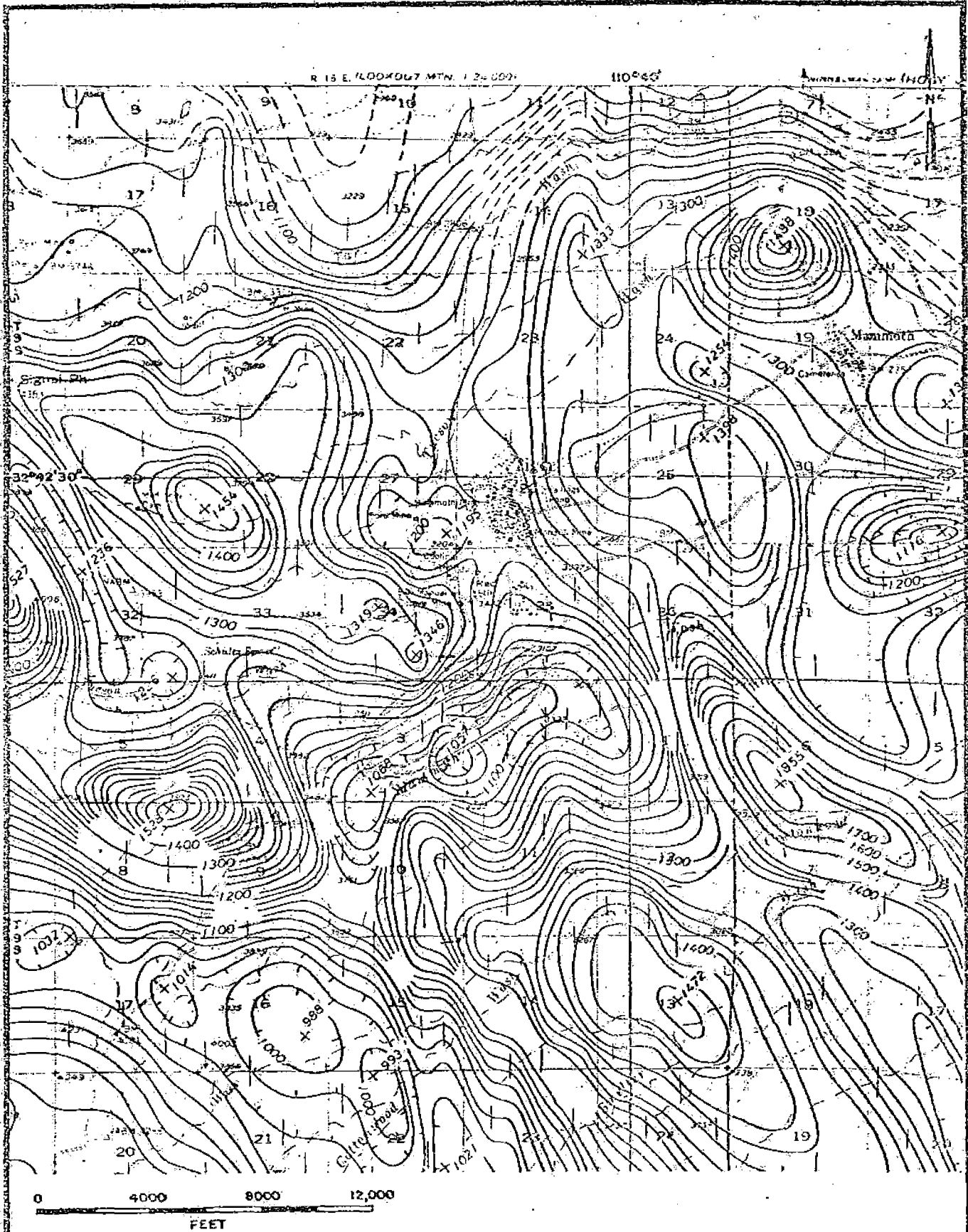
FIGURE 2. ELECTRICAL DATA AND DRILLING SECTION, LINE X-1, SAFFORD PROJECT, GRAHAM COUNTY, ARIZONA



	KENNECOTT COPPER CORPORATION — EXPLORATION SERVICES
	GEOPHYSICS DIVISION — U. S. OPERATIONS
	<i>Robinson District, Ely, Nevada</i>

SCALE: 1"=5000' C.I.: 5V DATA BY: A.S.C. DATE: 1960 NO.:

Aeromagnetic Map



SAN MANUEL

FORMATION OF MASSIVE SULFIDE DEPOSITS

Massive sulfide deposits occur in most of the shield areas of the world. The shields are those areas of ancient rocks (more than 600 million years old) which formed low (near sea level) but stable areas and around which the continents have grown. The particular type of deposit under consideration here is the volcanogenic massive sulfide, one which occurs in and is likely genetically related to ancient volcanic rocks. Volcanogenic massive sulfides are usually of three types: 1) barren pyrite (most abundant type), 2) copper-zinc with minor lead and precious metals, or 3) copper-nickel with minor other base and precious metals. By a massive sulfide we mean a deposit which consists of more than 40% sulfide minerals.

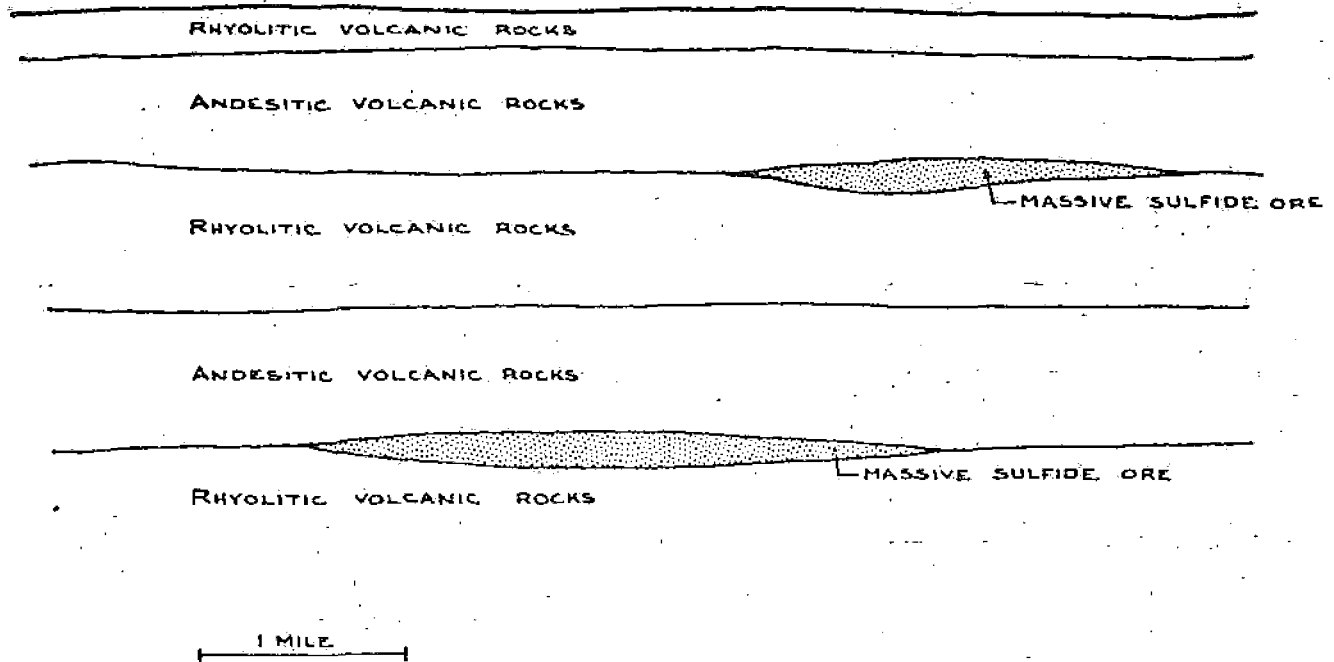
On this continent, massive sulfide deposits occur in Precambrian rocks of the Canadian Shield in central and eastern Canada and the northeastern U.S. One major massive sulfide, the United Verde deposit, occurred in the Southwest at Jerome, Arizona. Other more minor occurrences are scattered throughout northwestern Canada and Alaska. Much exploration potential remain throughout North America and throughout the world.

The accompanying figures show the evolution of a typical volcanogenic massive sulfide deposit. At the present time, these deposits are found within usually vertically standing belts of metamorphosed volcanic rocks which are surrounded by granite. Because the granite is not interesting, it is necessary to be able to distinguish volcanics (usually called greenstones) from granites. If these outcrop, the geologist can do this, but if there is a layer of glacial cover, this is usually done aeromagnetically.

The sulfide grains in most massive sulfide deposits are interconnected, and the entire deposit is therefore a good electrical conductor. This electrical conductivity is not due to pore water, but rather is due to electrons flowing through the sulfides. This property forms the basis of most geophysical exploration for massive sulfides, namely the electromagnetic (EM) method, considered next.

FORMATION OF MASSIVE SULFIDE DEPOSIT

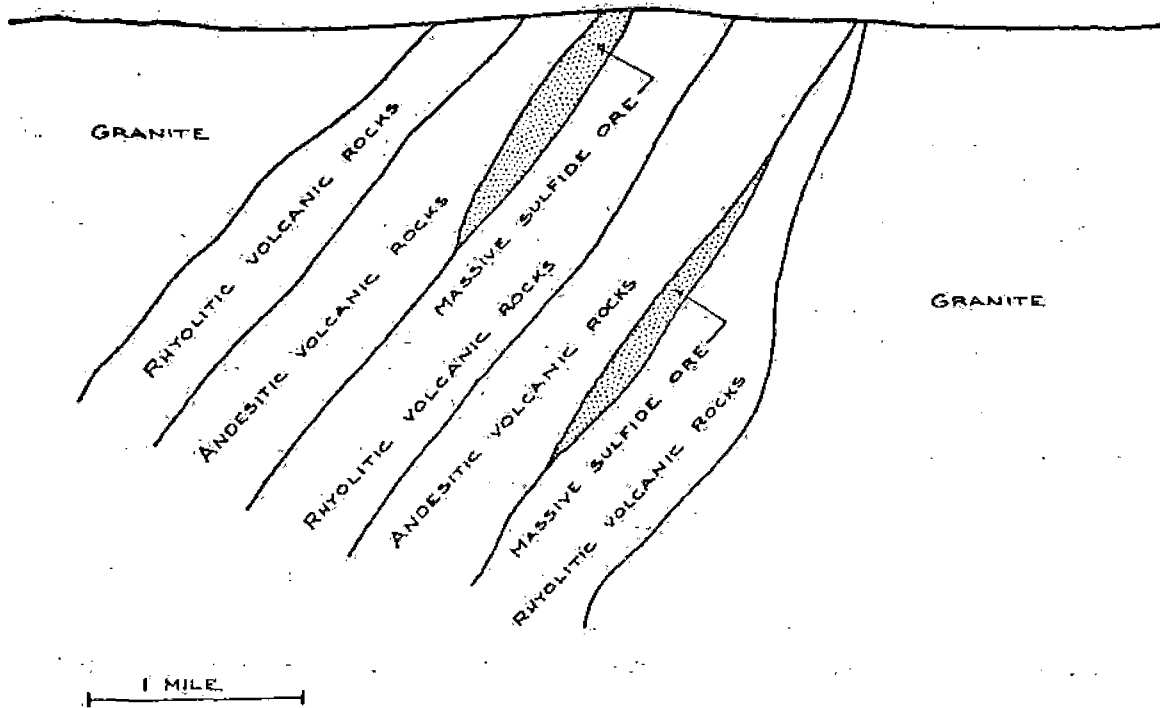
TIME: 3,000 MILLION YEARS AGO



1. Volcanic activity deposited layer of rhyolite.
2. Toward end of rhyolite phase, massive sulfide ore was deposited in a circular lens on surface of earth, probably under shallow water.
3. Later volcanism, often of andesitic composition covered massive sulfide ore.

FORMATION OF MASSIVE SULFIDE DEPOSIT

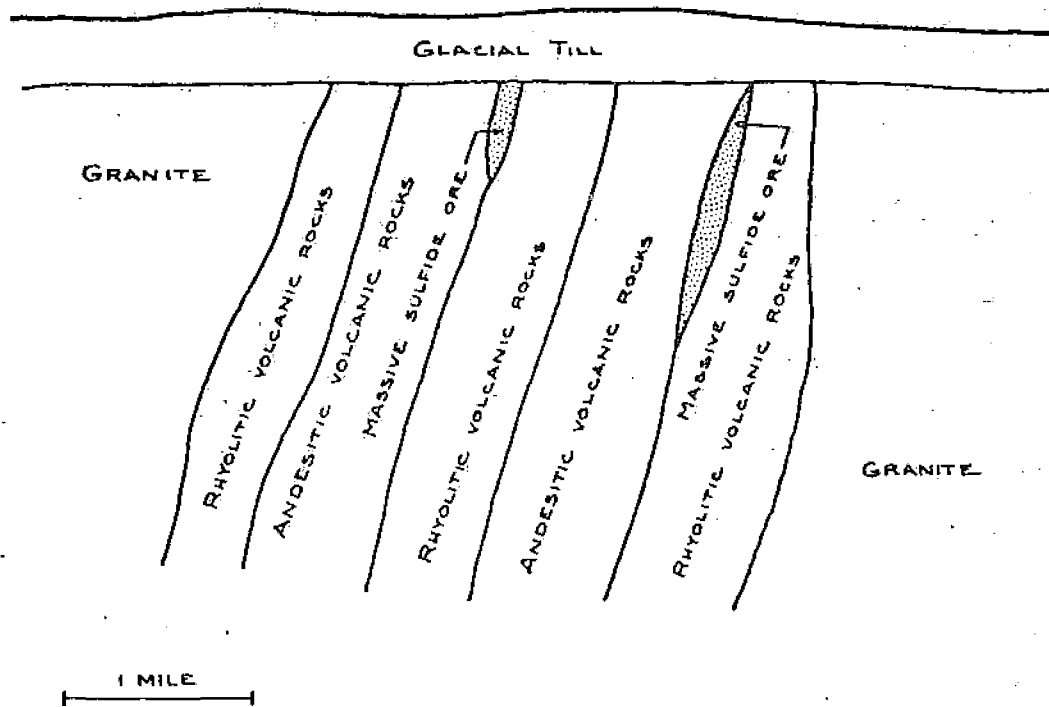
TIME: 2,000 MILLION YEARS AGO



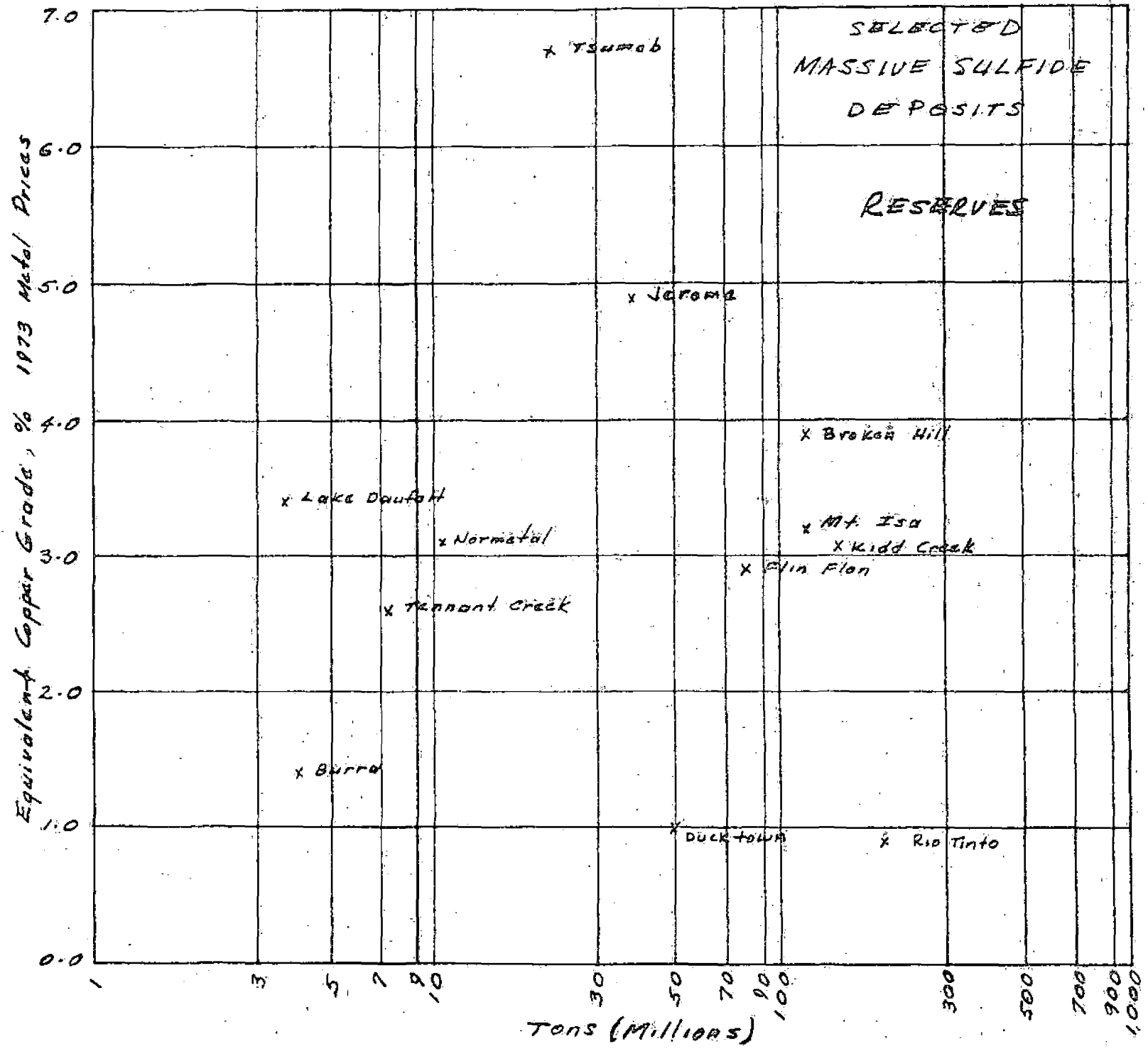
4. The alternating volcanic layers containing the massive sulfides were tilted and intruded by granites in the form of huge batholiths. The volcanic rocks were metamorphosed to "greenstones", and erosion of the surface occurred, leaving a flat peneplainé.

FORMATION OF MASSIVE SULFIDE DEPOSIT

TIME: PRESENT



5. Further, minor tilting of the greenstones and their enclosing granites occurred throughout geologic time.
6. Recent continental glaciers scoured the surface and left a cover of glacial till which hides the orebodies.



THE ELECTROMAGNETIC METHOD

The electromagnetic (EM) method detects areas of good electrical conductivity within the earth. Massive sulfides are only one type of good conductor, however. Water-filled fault zones, graphite layers within the greenstone belts, and man-made culture, such as railroads, power lines fences, etc. are all often good conductors, and are all detected.

To understand the principle of the EM method, refer to the figure entitled "A Generalized Picture, . ." The transmitter is a coil of wire through which an alternating current of a certain frequency, f, is passed. As the coil is energized with current, it sets up a magnetic field, called the primary field and shown by circular lines with arrows in the figure. The magnetic field also alternates with frequency f. The magnetic field permeates surrounding space, and some of it passes into the earth and intersects the buried electrical conductor. As the magnetic field links the conductor, it causes electrical currents to flow within the conductor. Of course, these currents would not flow so free if the body were not a good electrical conductor. Now the currents in the conductor are also alternating with frequency f, and they set up their own magnetic field, called the secondary field in the figure. This secondary magnetic field also permeates space, and some of it links with the receiving coil, which is a second coil of wire. The receiver coil thus sees two magnetic fields, and each cause current to flow in the coil. But the primary field has a known value, which is determined during calibration of the system, and so the current in the receiver coil due to the primary current can be nulled out. This leaves only the current due to the secondary magnetic field, i. e., the one due to the conductor. Therefore, if an EM reading is zero, no good electrical conductor exists near the EM system, whereas if a non-zero reading is obtained, a good electrical conductor is nearby. This same principle is used in land mine detectors and in the small metal detectors people use to find old coins in your lawn.

The EM method is actually available through a large number of techniques which all work on the same principle. Some systems are airborne, some are ground and some are semi-airborne, i. e., the transmitter is on the ground, whereas the receiver is in an aircraft. The accompanying pictures show both fixed-wing and helicopter-borne systems. The airborne systems are used to locate conductors, i. e., in a reconnaissance mode. After a conductor has been located, ground EM techniques are used for precise location and determination of electrical characteristics of the conductor.

One common airborne EM system, used to fly large shield areas for the purpose of locating conductors is the INPUT system. The letters stand for "induced pulse transient." An accompanying photo shows a PBY or Canso aircraft, an old World War II submarine chaser, with the INPUT transmitter coil stretched from nose to wing tip to tail to wing tip to nose. The receiver in this system flies in a bird which is hung 200 feet below the aircraft. A

magnetometer is also carried aboard the aircraft, and aeromagnetic data are collected at the same time as the EM data.

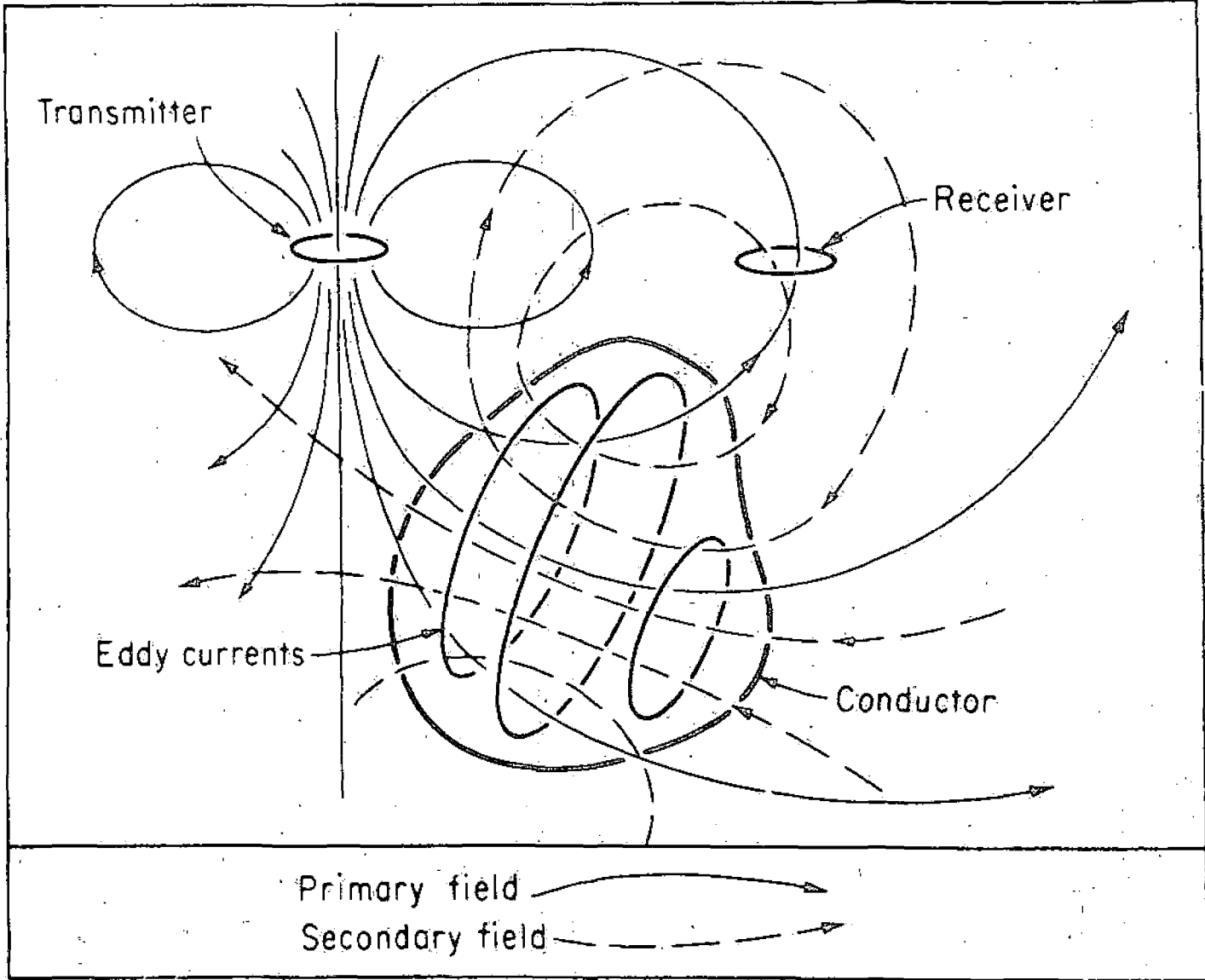
In the INPUT system the transmitter coil is pulsed with a half sine wave, as shown in the accompanying figure. In the absence of a conductor, the receiver sees only the primary field, also shown. If a conductor is present, the received waveform is altered. The receiver actually samples the received waveform during transmitter current-off periods at six different times after current shutoff. Thus six INPUT channels are displayed on a light sensitive paper, which is the data recording medium. The illustrations show anomalous excursions of either 3 or 4 channels, indicating an anomaly or a conductor.

When an area has been flown, the flight path is recovered by using the flight path tracking film in the same fashion as discussed under aeromagnetic surveys. The EM conductors are then plotted on a map in a fashion shown in the figure entitled "Typical INPUT Conductor Map." The next steps are:

- 1) check to see if a cultural source (fences, etc.) could account for the anomalies,
- 2) select anomalies for ground follow-up based on a) length of the conductor (most orebodies are short, whereas graphite horizons often go for miles), and b) conductivity (most orebodies show as very good conductors),
- 3) perform ground follow-up, which usually begins with ground EM.

There are a number of ground EM systems which are available to pinpoint a conductor. Some have better depth penetration, but are slower, whereas others may be faster but have less penetration. The geophysicist must make a cost-effective selection. The Turam technique, shown in an accompanying figure is sometimes his choice.

In the Turam method a large (2000' x 4000') loop of wire is laid out on the ground and is energized with alternating current at 200-1000 Hz. This sets up secondary fields in nearby conductors by the induction process already discussed. The receiver is a voltage-ratio and base-difference meter connected between two small coils which are 100 or so feet apart. One man carries each coil and the coils are moved along traverse lines perpendicular to one of the long sides of the coil. When the receiver setup passes over a conductor, both the field strength ratio and the phase difference between the two receiver coils changes. By measuring these changes precisely, the conductor location, width, depth and electrical conductivity can be approximately determined. These parameters are useful during the drill testing stage.



A generalized picture of electromagnetic induction prospecting.

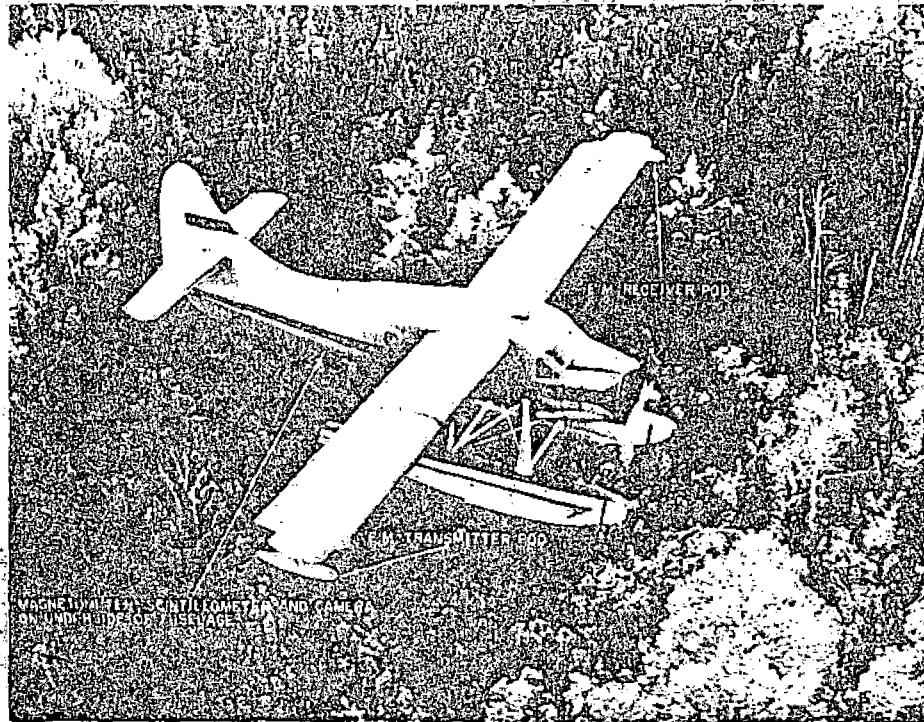


FIG. 14. Fixed-wing in-phase and out-of-phase installations on float equipped Otter aircraft operated by Canadian Aero Mineral Surveys, Ltd.

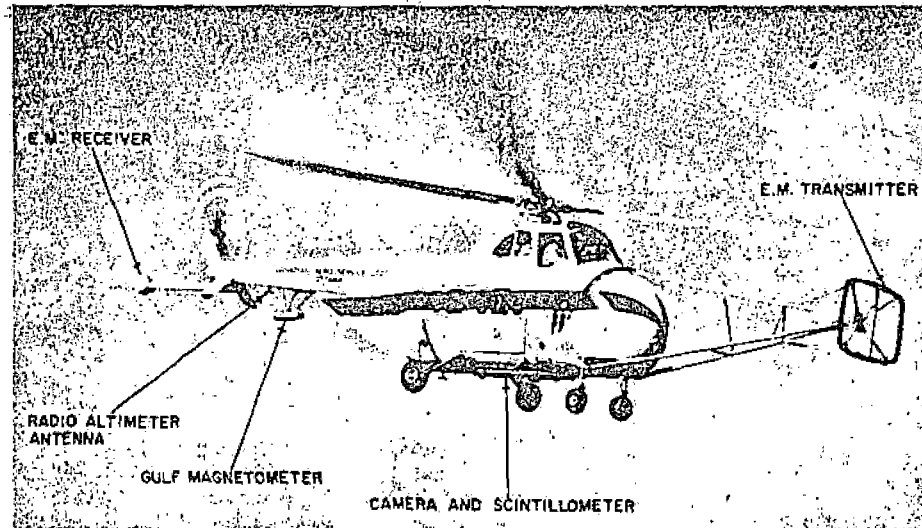


FIG. 10. Canadian Aero Service Sikorsky S-53 combined geophysical system showing location and types of instruments employed.

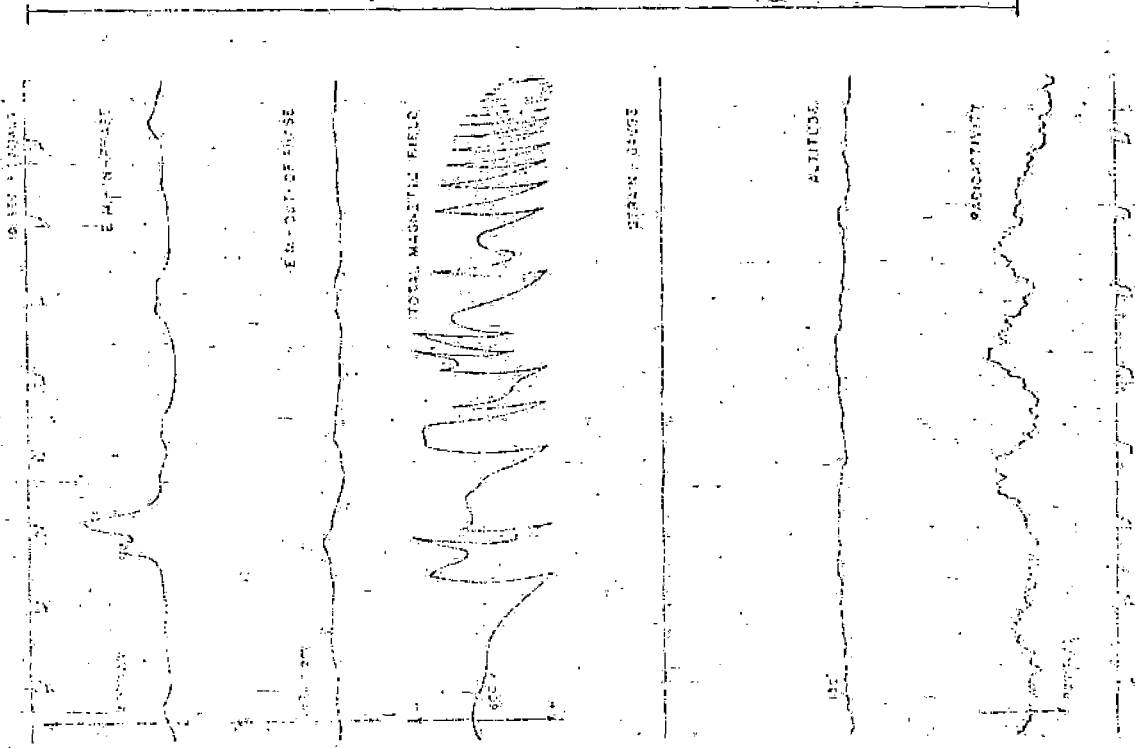


Fig. 40. Typical data recorded for Newfront/Aero Helicopter system.

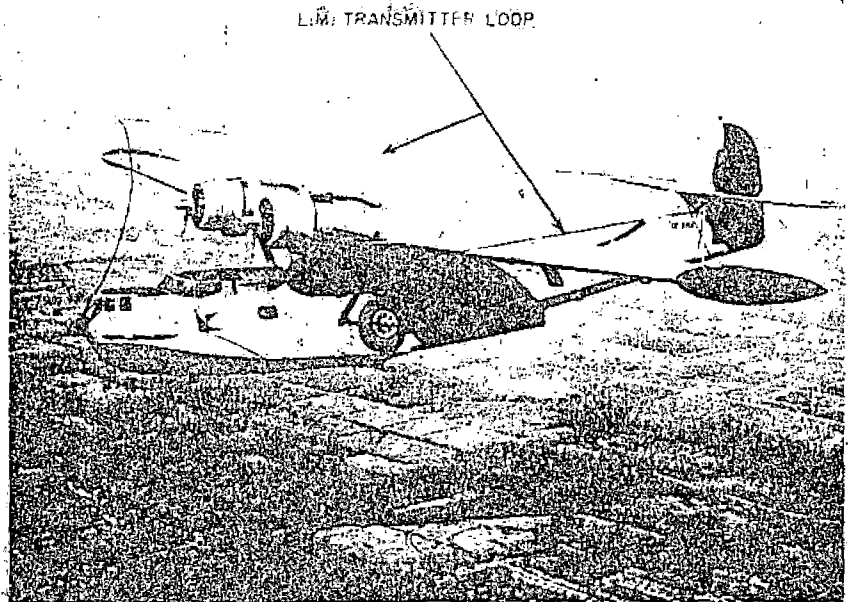


FIG. 15. Photo of Selco Explorations' Canso *EM* system showing transmitting loop of induced pulse transient system.

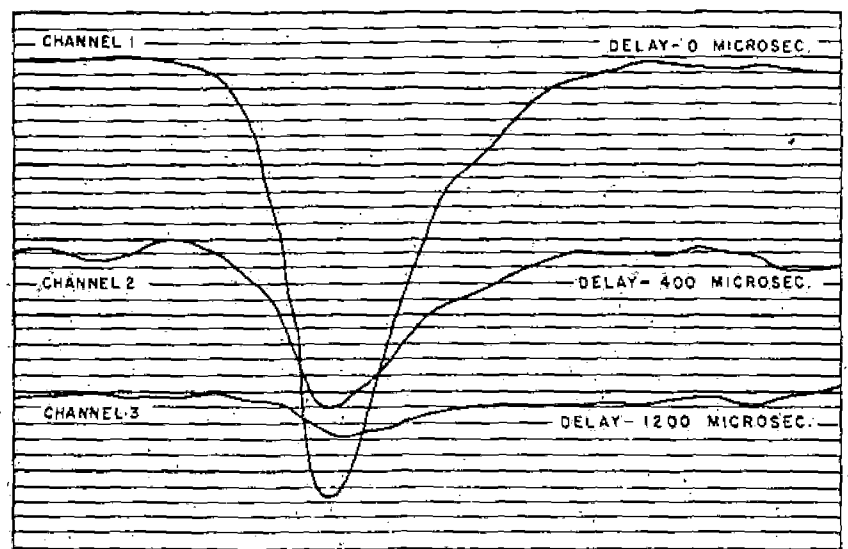


FIG. 16. Record showing *EM* responses from transverse receiver coil in Selco Input System at 0, 400, and 1,200 microsecond delay times.

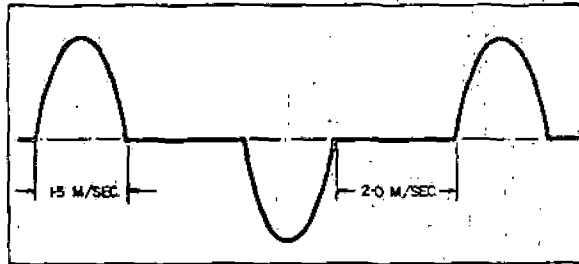


Figure 1.—Primary EM Field.

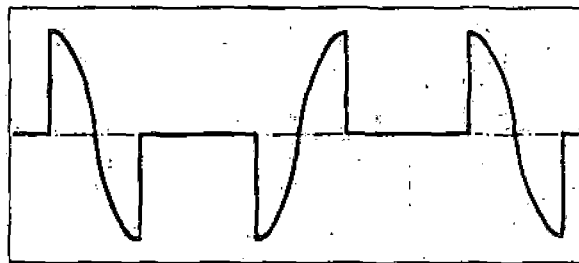


Figure 2.—Primary Field Detected in Bird.

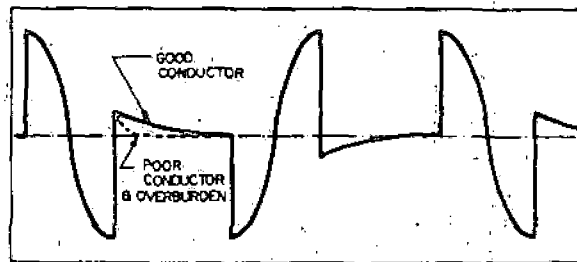


Figure 3.—Primary and Secondary Field Detected in Bird.

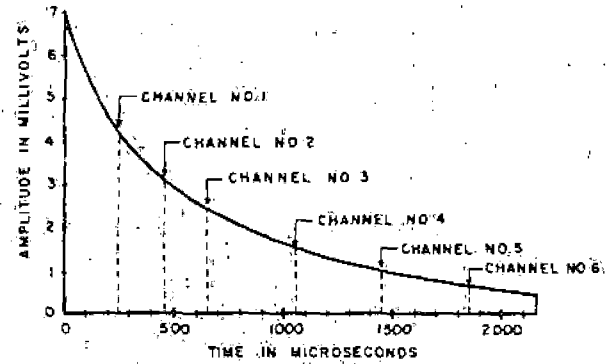


Figure 4.—Six-Channel Sampling Gate Centers of the Mark IV INPUT System.

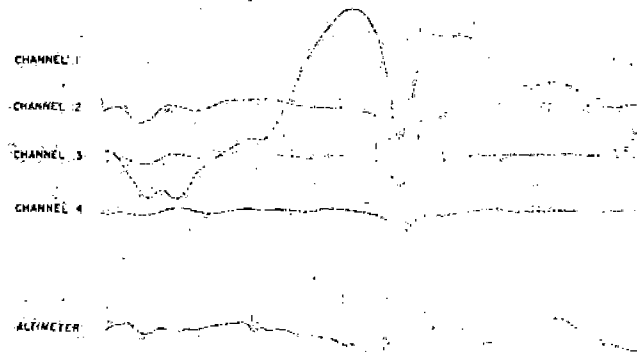
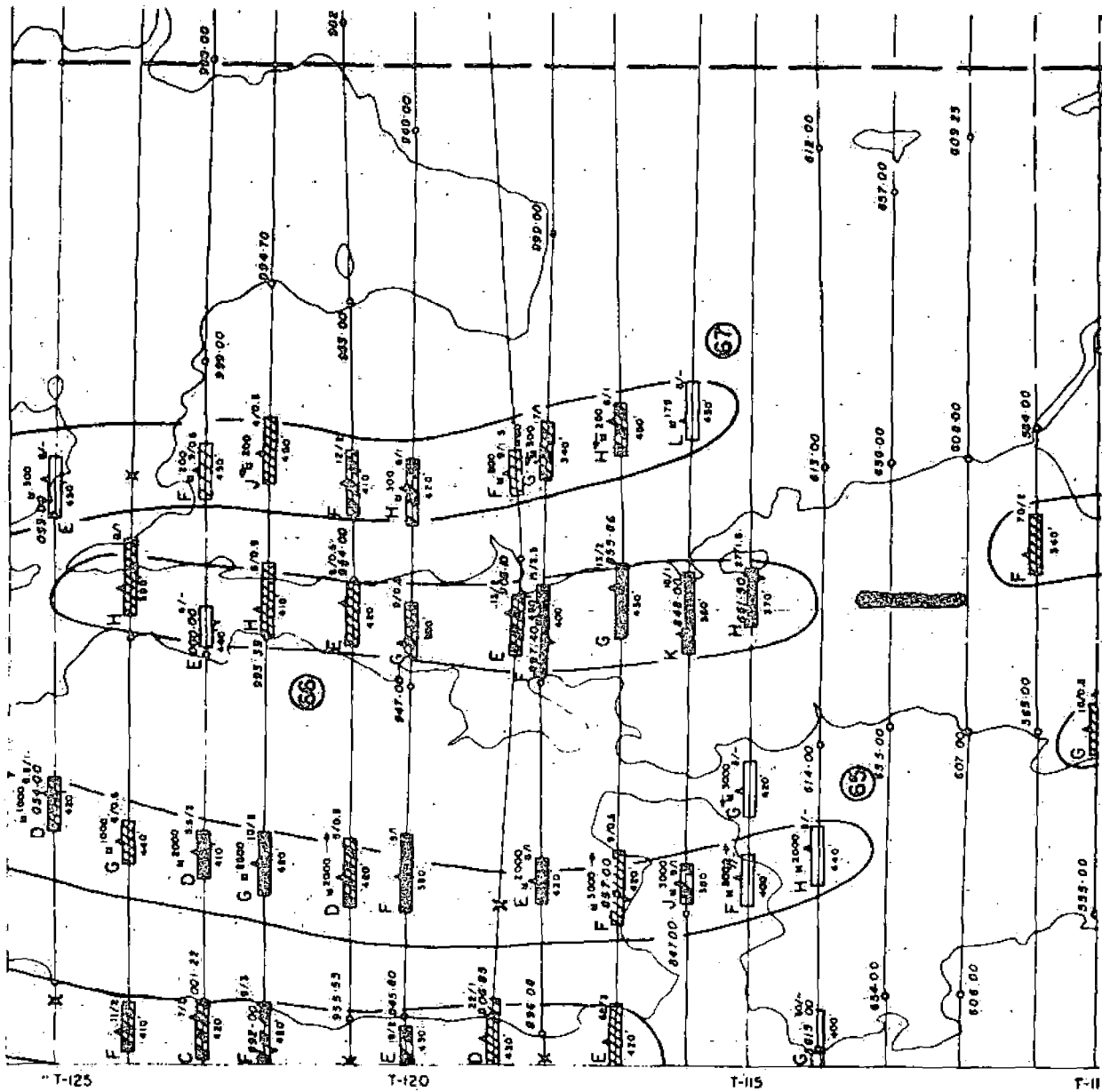
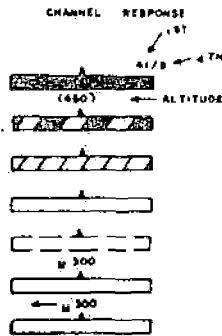


Figure 5.—Profile Over the Texas Gulf Sulphur Orebody, Timmins, Ontario.



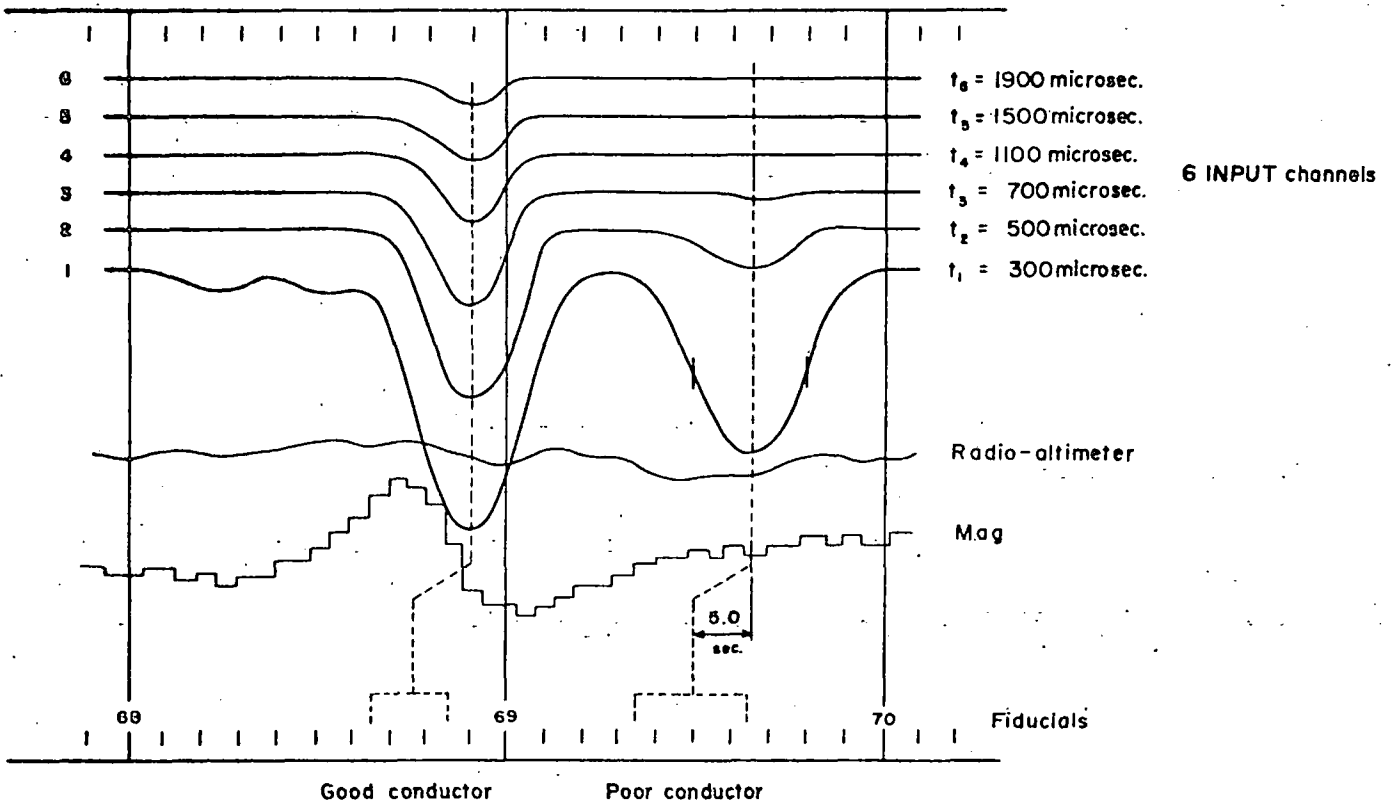
LEGEND

- 6 - CHANNEL ANOMALY
- 5 - CHANNEL ANOMALY
- 4 - CHANNEL ANOMALY
- 3 - CHANNEL ANOMALY
- 2 - CHANNEL ANOMALY
- E.M. AND COINCIDENT MAGNETICS
- INDIRECT MAGNETIC ASSOCIATION



TYPICAL INPUT CONDUCTOR MAP

TYPICAL INPUT RECORDING



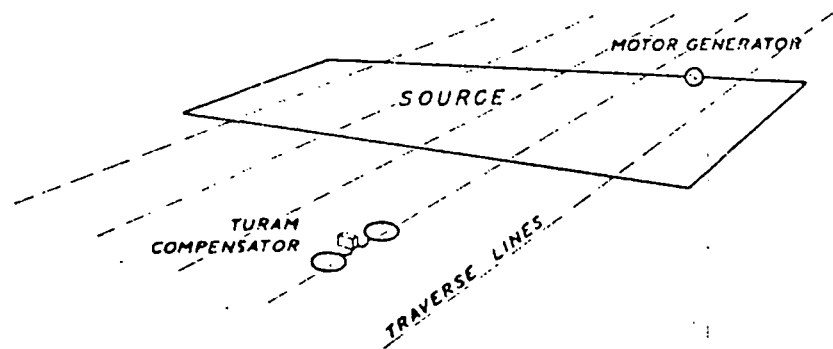


Fig. 1 The Turam method. General layout

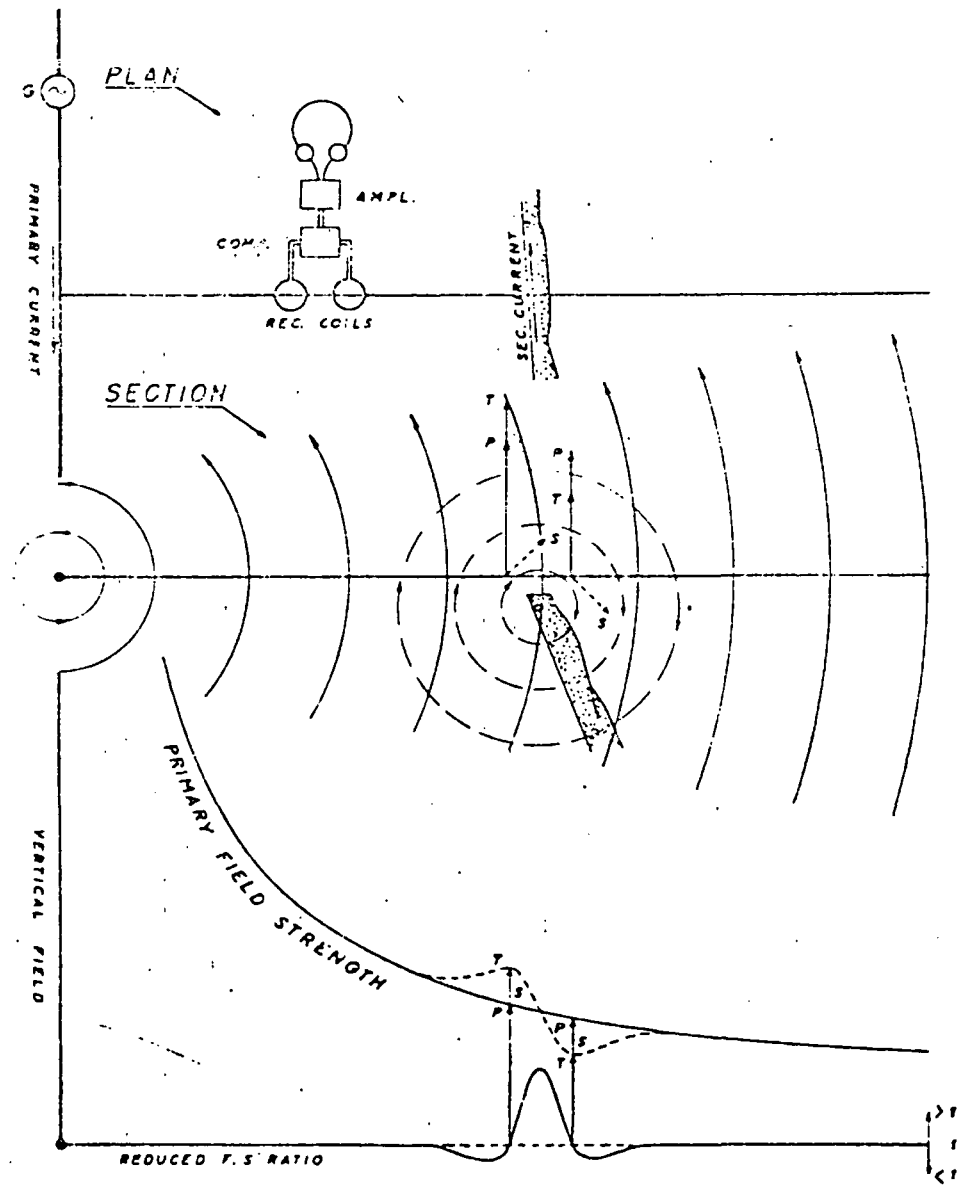


Fig. 2 Schematic presentation of primary and secondary fields

GEOPHYSICS IN MASSIVE SULFIDE EXPLORATION

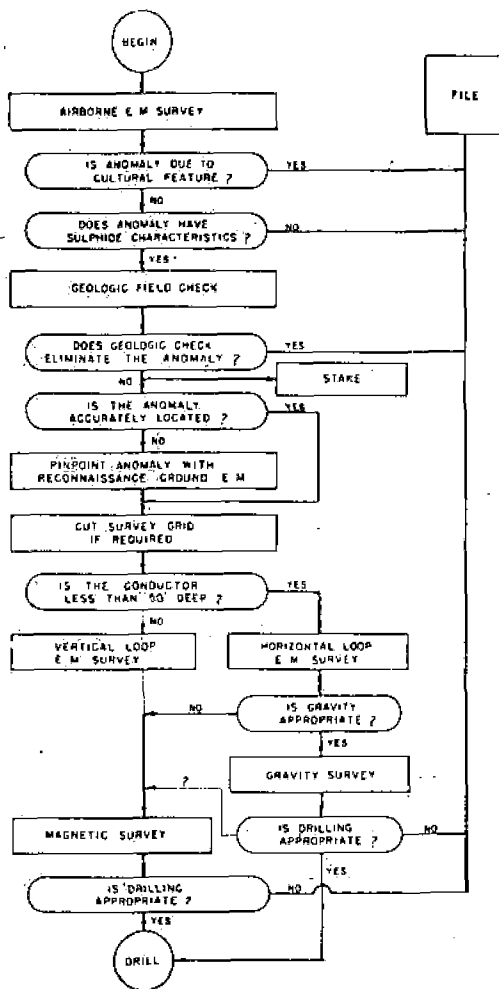
Geophysics is used in all stages of massive sulfide exploration. The aeromagnetic technique is often useful in mapping greenstone belts so that further exploration effort can be confined to these belts rather than to the surrounding, barren granite. The accompanying figure shows an interpretation of an aeromagnetic map in terms of occurrence of granite, schist, and greenstone. Such a map helps define areas for airborne EM surveys.

Once a flying area has been picked, the sequence shown on the accompanying figure is begun. The airborne EM is flown and ground checked with ground EM. Sometimes ground magnetic and gravity surveys are performed. Ground magnetic surveys are able to detect the magnetic mineral pyrrhotite which often accompanies copper-nickel deposits. Gravity surveys are able to detect the more dense massive sulfides if they are not too deep.

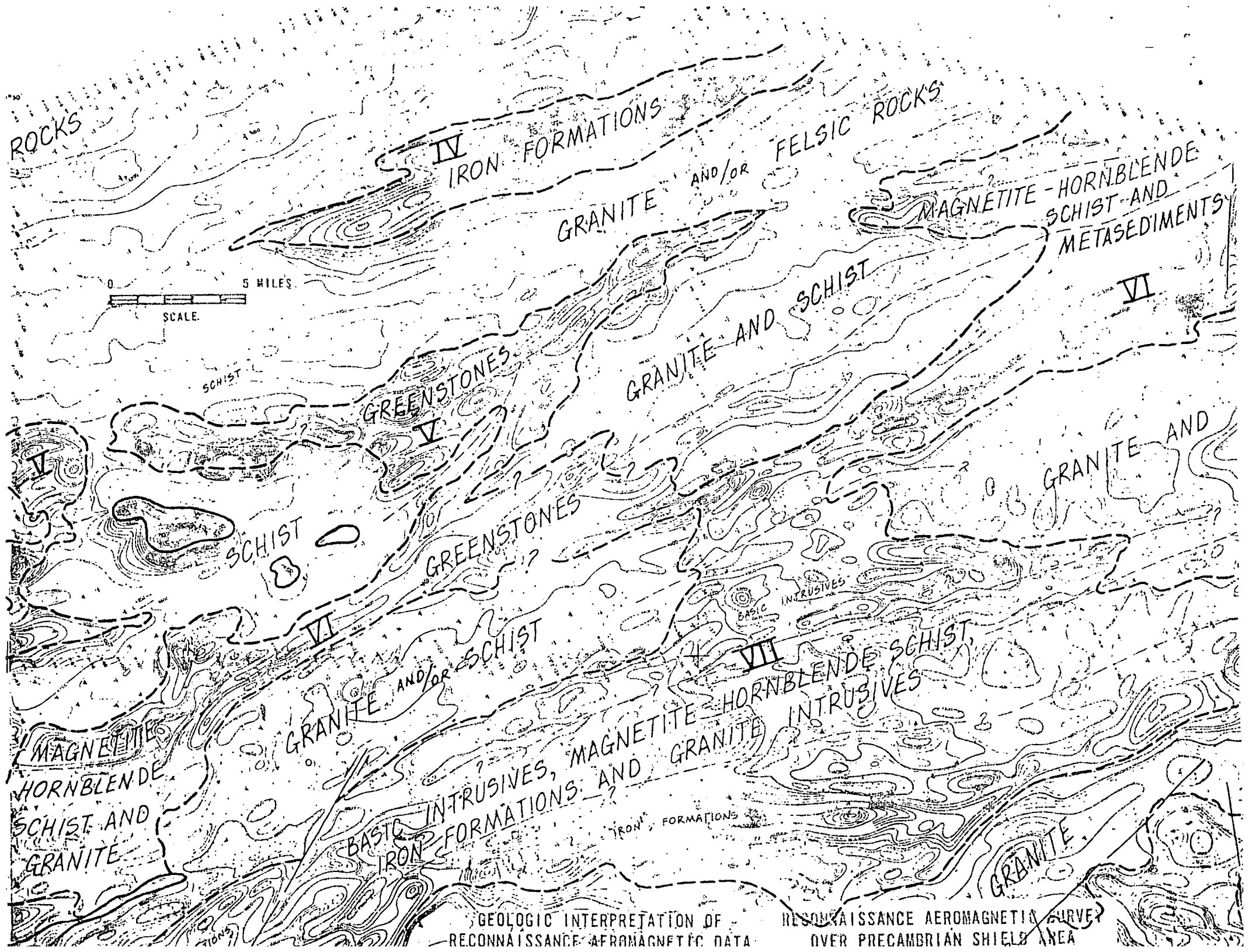
In summary, the geophysical techniques listed on the table entitled "Useful Geophysical Responses" are often used with the results shown.

The following diagrams show geophysical results for a massive sulfide orebody in Wisconsin discovered by Kennecott in 1968. Shown are:

- a) the INPUT profiles for the discovery flight lines,
- b) Slingram EM anomalies (a ground EM system) and gravity profiles which show a gravity high due to the massive sulfides,
- c) ground magnetic profiles (no anomaly) and Turam profiles (a big anomaly which goes off scale on these graphs, and
- d) a drilled section through the orebody.



Flow chart of the exploration sequence used in investigating the Muskeg.



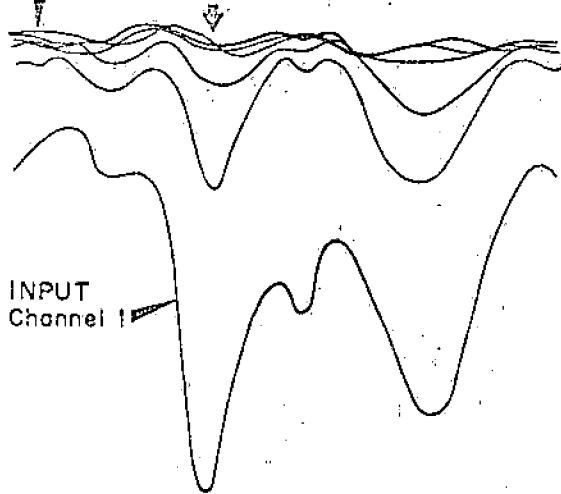
GEOLOGIC INTERPRETATION OF
RECONNAISSANCE AEROMAGNETIC DATA

RECONNAISSANCE AEROMAGNETIC SURVEY
OVER PRECAMBRIAN SHIELD AREA

**USEFUL GEOPHYSICAL RESPONSES
MASSIVE SULFIDE DEPOSITS**

METHOD	RESPONSE / GEOMETRY	CAUSE
EM	Variable Background & Noise Conductor 10' to 200' wide 200' to 5000' long	massive sulfides
IP	0 - 3 pfe Background 5 - 50 pfe 10' to 200' wide 200' to 5000' long 5 - 15 pfe 100' to 1000' wide 200' to 10,000' long	massive sulfides disseminated sulfides around massive sulfide zone
MAGNETIC	Variable Background 200 γ to >10,000 γ 10' to 1,000' wide 200' to 5000' long	pyrrhotite in massive sulfides or iron formation
GRAVITY	Variable Background 0.05 to 2 mgal 10' to 200' wide 200' to 5000' long	massive sulfides

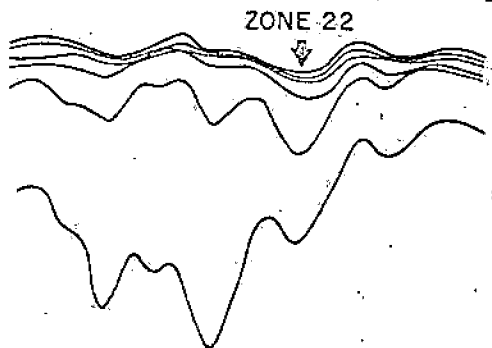
INPUT
Channel 6 ZONE 22



LINE A-



LINE B-N



LINE I-N

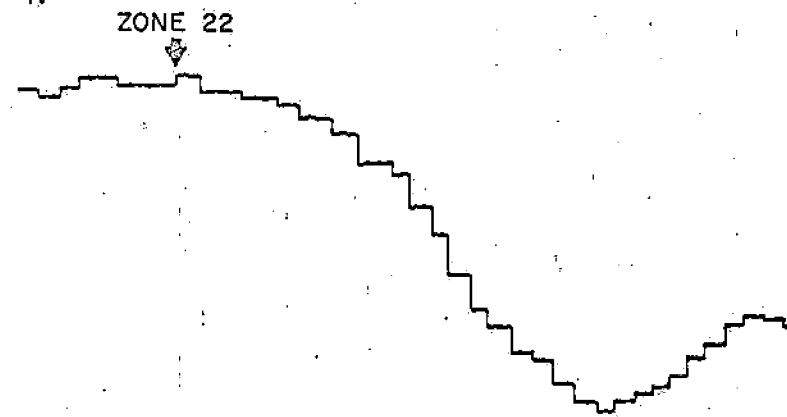
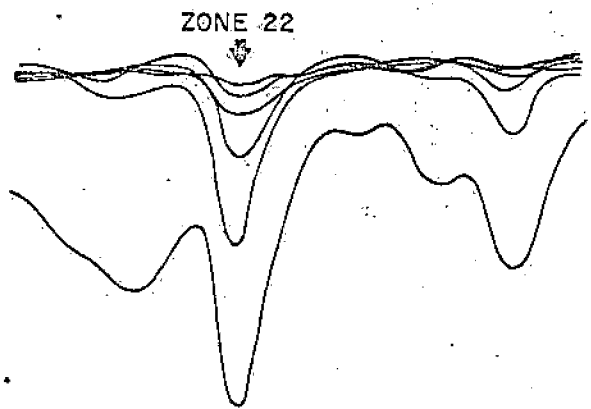


FIGURE 5. INPUT TAPES OVER ZONE 22.

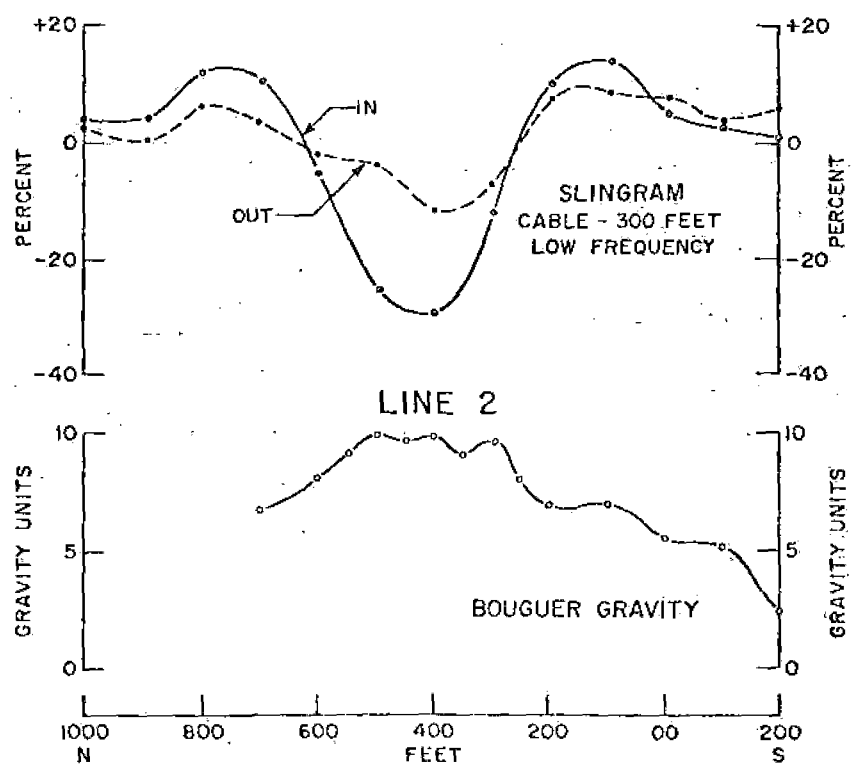
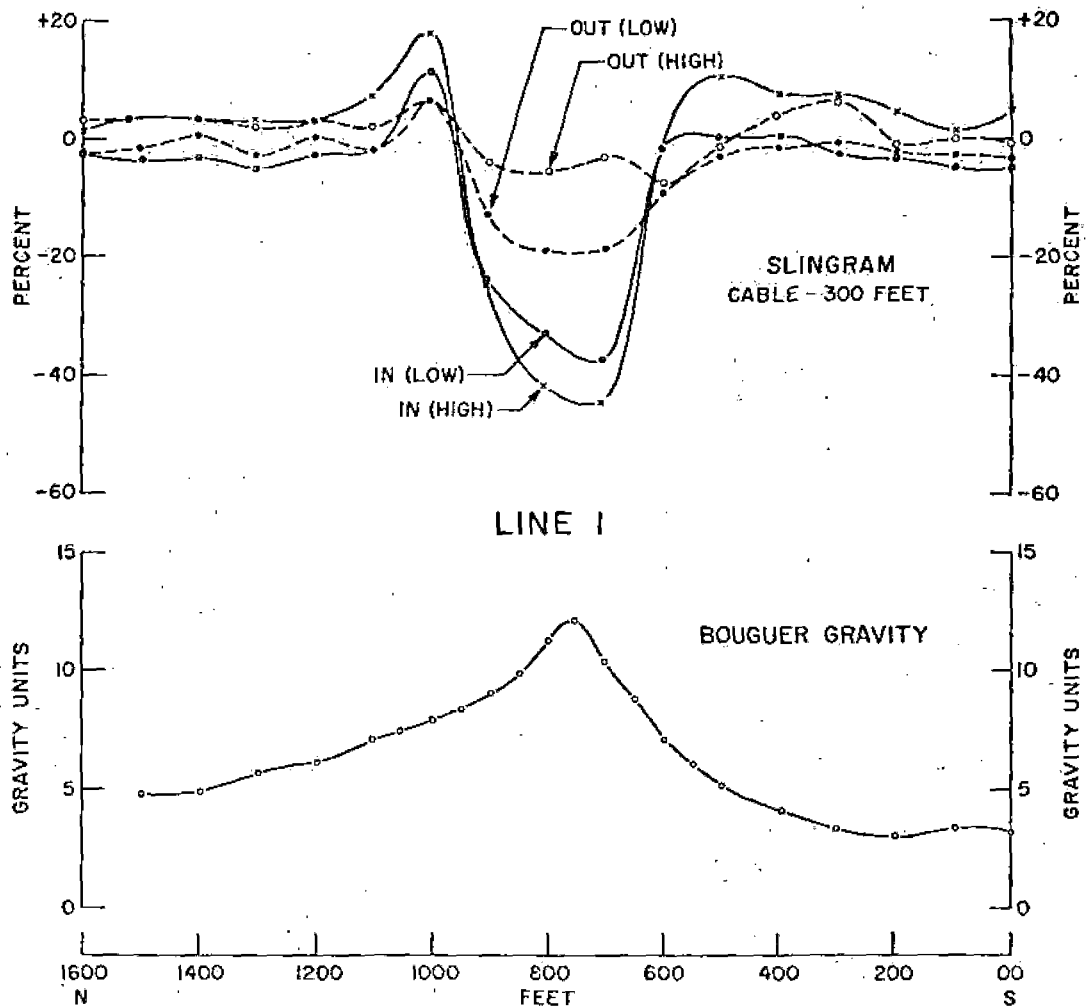


FIGURE 6. SLINGRAM AND GRAVITY PROFILES.

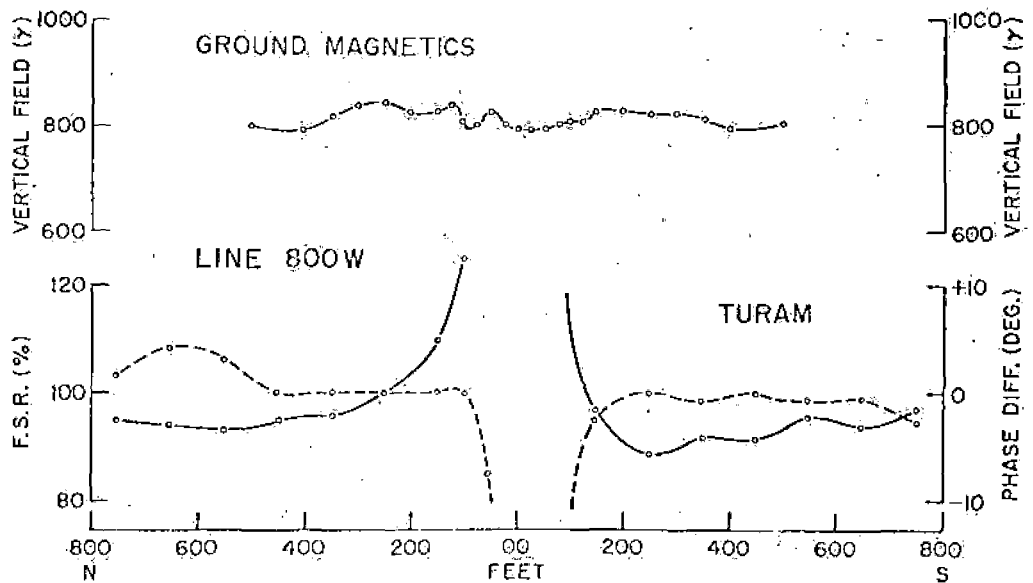
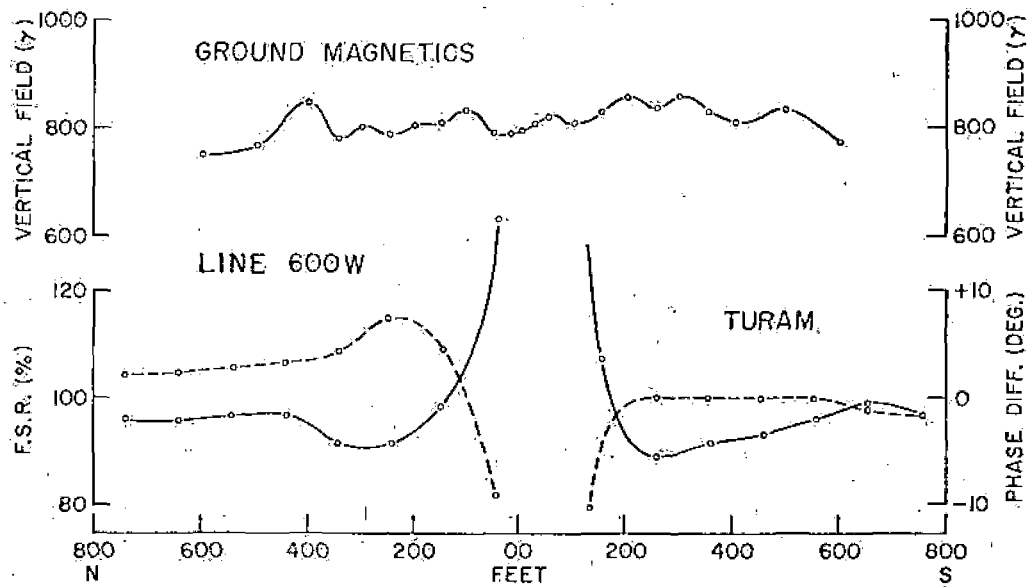
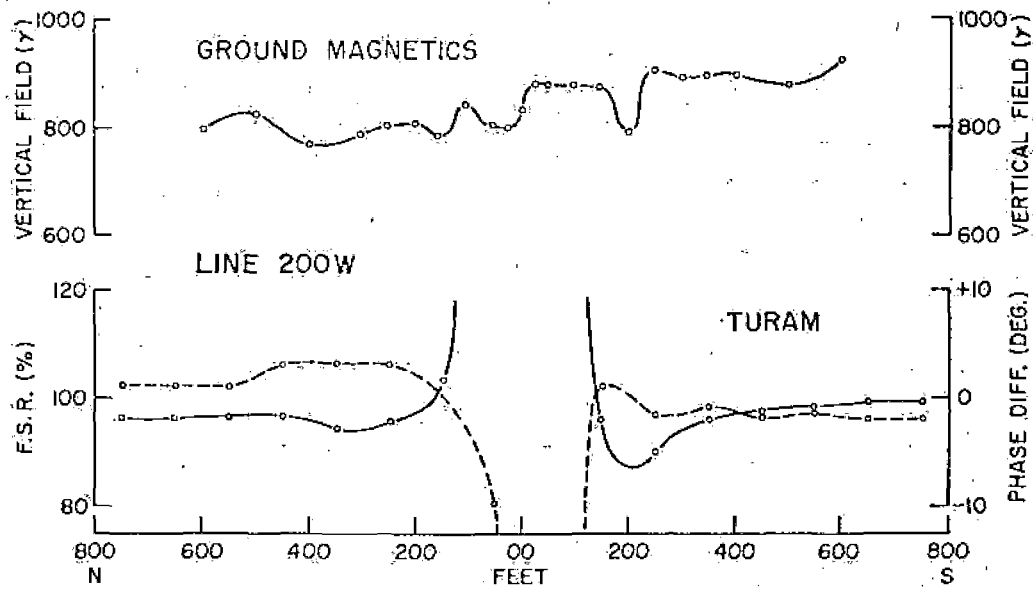


FIGURE 8. TURAM AND MAGNETIC PROFILES.

LINE 2000W

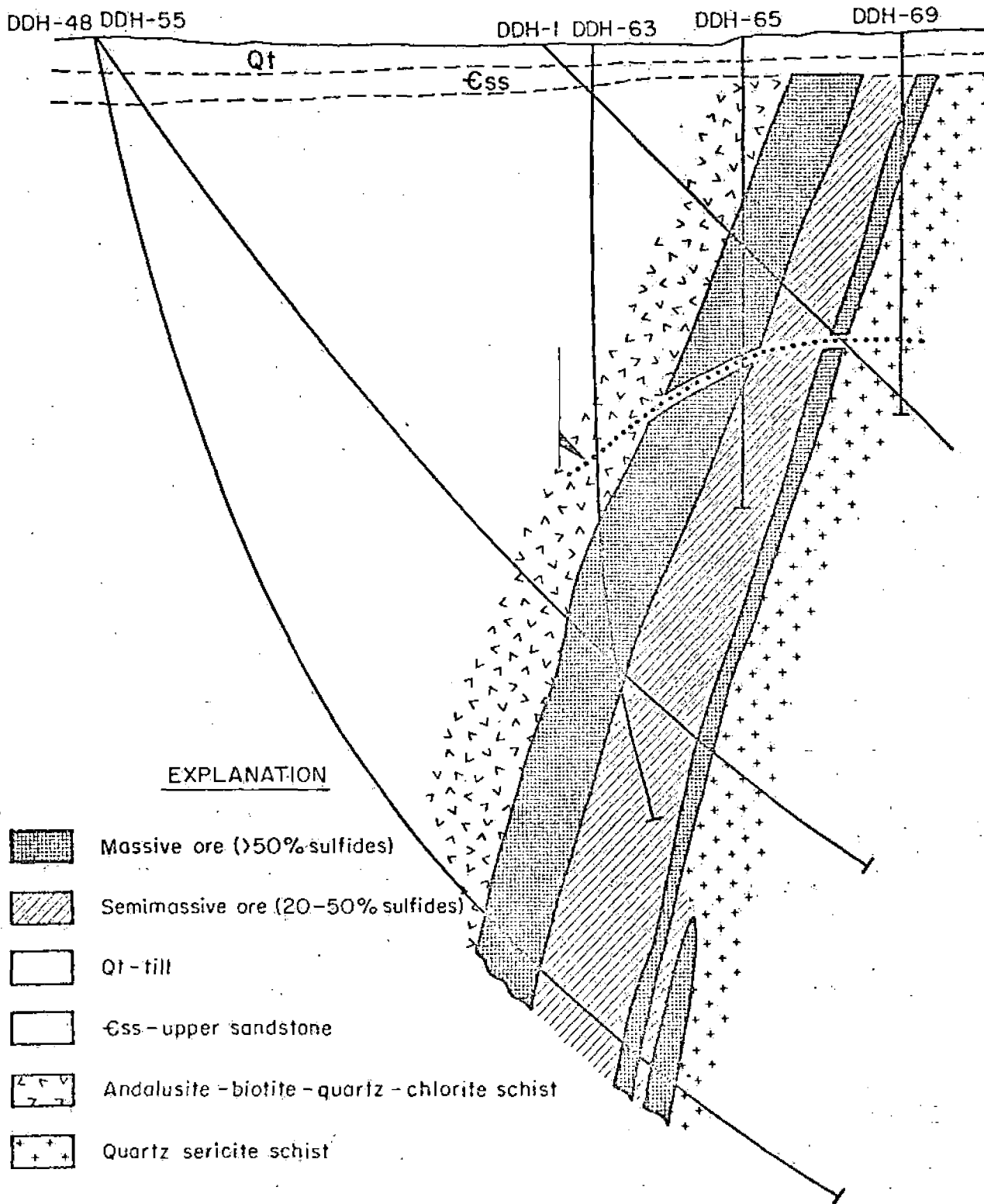
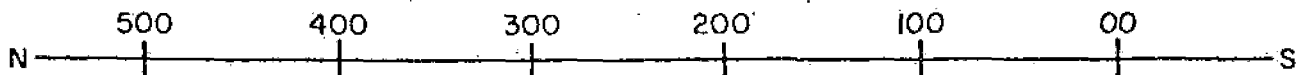


FIGURE 18. GEOLOGIC CROSS SECTION.

OTHER APPLICATIONS OF GEOPHYSICS

Iron Deposits

Many iron ore deposits are magnetic, and so the airborne and ground magnetometer find extensive use. Other geophysical methods can also be useful, although usually not in direct detection of ore.

Base Metal Vein Deposits (Pb, Zn, Ag)

These deposits are generally small, but are sometimes associated with porphyry copper deposits, i. e., they are zoned around porphyry copper centers. They are usually associated with an intrusion, and magnetic methods may be used to detect and map such intrusions. The IP techniques, used in detail are often useful in detecting these small deposits. EM methods may be applied to detecting veins.

Uranium Deposits

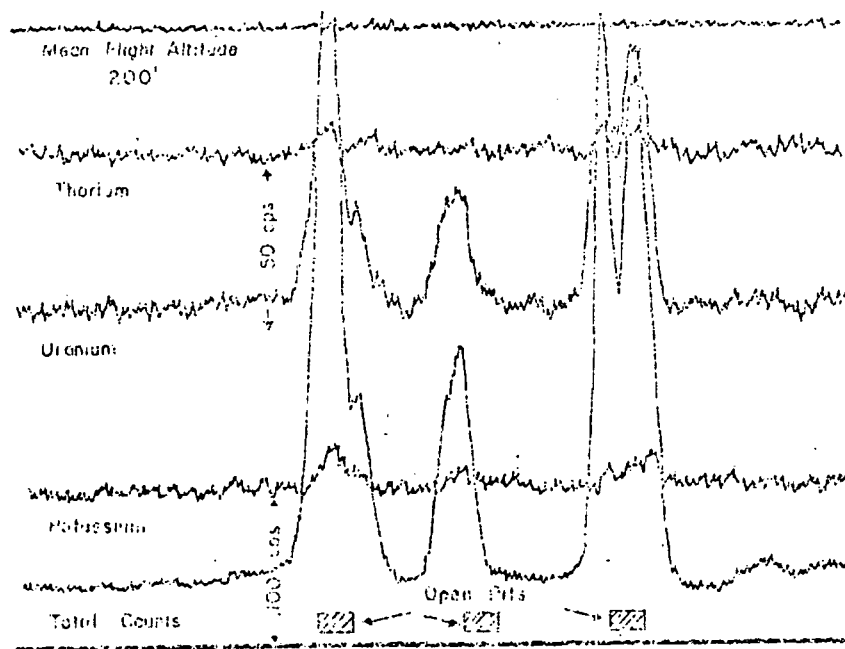
The radioactive methods are used to detect the ore directly. This may be done from the air, on the ground or in a drill hole. Also some uranium deposits have a small amount of associated pyrite (FeS_2), and so IP is sometimes used to trace the pyrite and the IP anomalies are then drill tested for uranium occurrence.

Coal Deposits

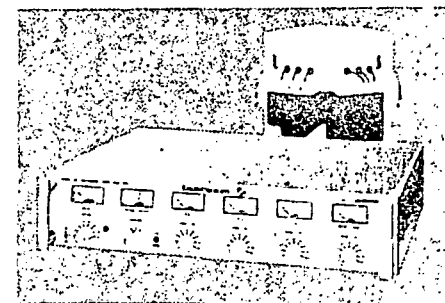
Geophysical applications to coal exploration are few. The seismic method is sometimes useful in tracing sedimentary beds and deciphering geologic structure, and so is indirectly useful. Some coal beds have associated pyrite, and can be traced by IP.

Geothermal Areas

Areas of hot steam which can be used for power generation can sometimes be found geophysically. Temperature surveys are useful but require drill holes to get away from the large daily and yearly near-surface temperature fluctuations which preclude accurate determination of deep temperatures. Resistivity surveying, using gear similar to IP gear, can often detect an area of better electrical conductivity at depth due to the hot, salty water.



Airborne radiometric four-channel GISA-4 profile over three uranium open pits Tordilla Hills area, Texas



GISA-4 four-channel airborne spectrometer

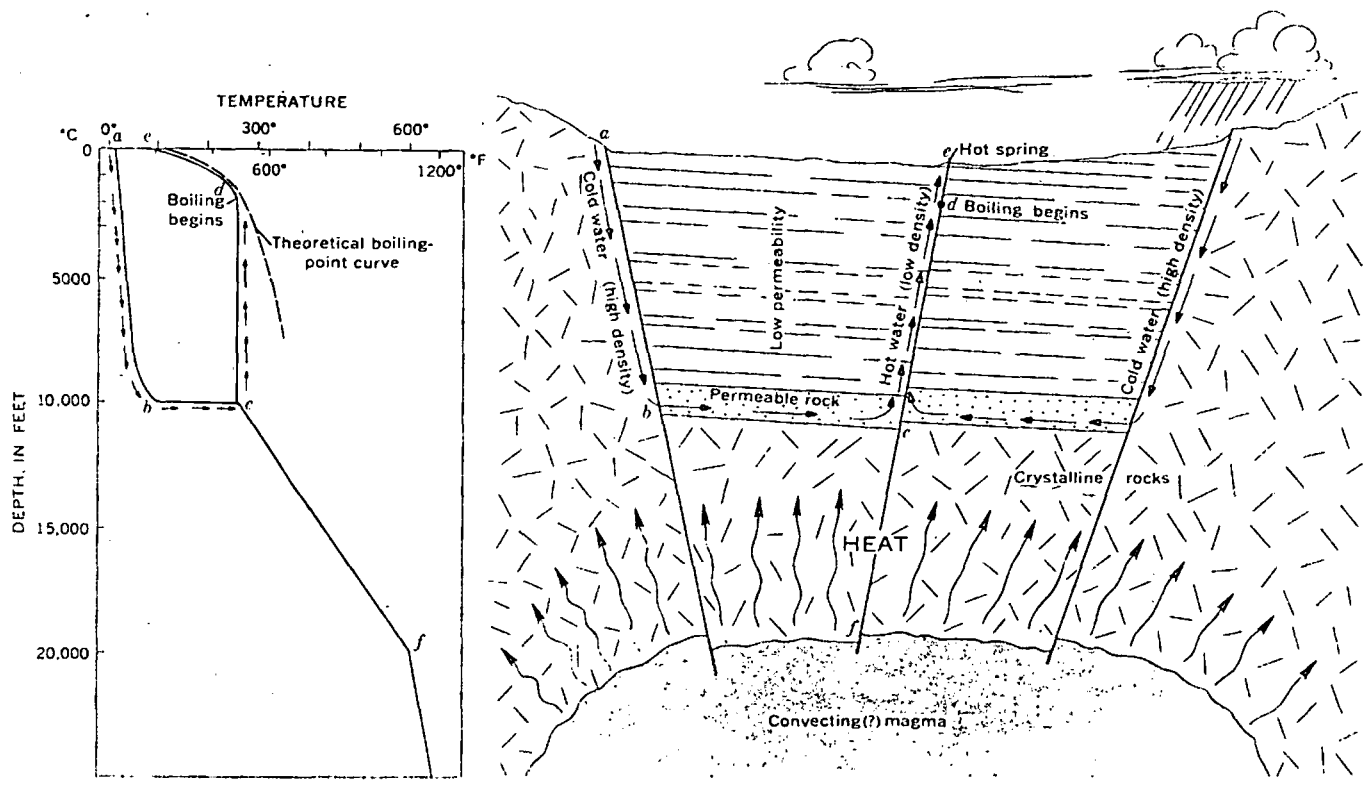


FIGURE 3.—Simple high-temperature hot-spring system with deeply circulating meteoric water assumed to be heated entirely by conduction.

PHYSICAL PROPERTIES OF SOME BASE METAL OREBODIES AND ROCKS

	Electr. Cond. <u>(1)</u>	IP Resp. <u>(2)</u>	Mag. Suscep. <u>(3)</u>	Spec. Grav. <u>(4)</u>	GP Meth. <u>(5)</u>
Disseminated Sulfide Orebodies	Low	Yes	No	Low	IP, Mag.
Unmineralized Intrusive Rocks	No	No	Yes	Av.	
Pyritic Halo	Mod.	Yes	No	Av. +	IP
Volcanic Flows	Var.	Var.	Var.	Av.	
Sedimentary Rocks	No	No	No	Av.	
Carbonaceous Limes and Shales	Mod.	Yes	No	Av.	
Alluvium-Southwest USA	High	Yes	Var.	Low	
Massive Sulfide Orebodies	High	Var.	Var.	High	EM, Mag., Grav.
Precambrian Shield Bedrock	Low	No	Var.	Av. +	
Graphite (Carbon), Clays	High	Var.	No	Low	
Glacial Drift	No	No	No	Av.	
Magnetite (Iron) Orebodies	Low	No	High	High	Mag., Grav.
Hematite (Iron) Orebodies	No	No	No	High	Grav.
Molybdenite Orebodies	Low	No	No	Av.	Mag.
Pyritic Halo	Mod.	Yes	No	Av. +	IP

- (1) Electrical Conductivity
- (2) Induced Polarization Response
- (3) Magnetic Susceptibility
- (4) Specific Gravity
- (5) Applicable Geophysical Methods

R. C. Holmer
June 1969

AVERAGE COSTS
MINING GEOPHYSICAL METHODS

	<u>Field Crew Size</u>	<u>Daily Cost of Crew</u>	<u>Production Rate</u>	<u>Unit Cost</u>	<u>Interpretation Cost</u>
IP	3-5	\$400-600	1-4 mi. /day	\$150-700 ¹ /mi.	\$50-300/mi.
Air Magnetics					
Fixed-Wing	2-4	\$800-1500	150-300 mi/day	\$6-10 ¹ /mi.	\$2-10/mi.
Helicopter	2-3	\$900-1500	50-150 mi/day	\$40 ¹ /mi.	\$5-20/mi.
Ground Magnetics	1-2	\$150-300	1-5 mi. /day	\$200-400 ¹ /mi.	\$25-200/mi.
Gravity	1-2	\$150-300	1-10 mi. /day	\$200-600 ¹ /mi.	\$25-200/mi.
Air EM					
Fixed-Wing	2-5	\$1000-1500	100-200 mi/day	\$15-40 ¹ /mi.	\$5-10/mi.
Helicopter	2-5	\$1000-1500	50-150 mi/day	\$60-100 ¹ /mi.	\$5-10/mi.
Ground EM	2-4	\$300-500	1-4 mi/day	\$200-600 ¹	\$50-100/mi

¹Includes office work involved in correcting field data, posting on a map, etc.

SUBJ
GPHYS
HF
HFUS

Reprinted from:

geophysical monograph 20

The Earth's Crust

Its Nature and Physical Properties

**UNIVERSITY OF UTAH
RESEARCH INSTITUTE
EARTH SCIENCE LAB.**

JOHN G. HEACOCK
editor

GEORGE V. KELLER

JACK E. OLIVER

GENE SIMMONS

associate editors

Copyright © 1977 by the American Geophysical Union.

GMAO

HEAT FLOW IN THE UNITED STATES AND THE
THERMAL REGIME OF THE CRUST

Arthur H. Lachenbruch and J. H. Sass

U.S. Geological Survey
Menlo Park, California 94025

Abstract. A contour map of heat flow based on 625 observations now available in the conterminous United States shows new detail. Subprovinces of exceptionally high heat flow (>2.5 HFU ($1 \text{ HFU} = 10^{-6} \text{ cal/cm}^2 \text{ s}$)) in the western states are beginning to emerge as regional features, but their boundaries are still largely unknown. The 'Battle Mountain High,' previously described in north central Nevada, probably extends northeastward to Utah and Idaho and westward almost to California. With the eastern Snake River Plain, a region that probably has large convective loss, it could form a zone of exceptionally high heat loss that extends almost continuously for 1000 km from the vicinity of Steamboat Springs near Reno, Nevada, to Yellowstone Park in Wyoming and possibly northward into the Idaho batholith. A sinuous high heat flow subprovince of comparable length is emerging in the Rio Grande Trough in New Mexico and southern Colorado. The linear relation between surface heat flow and radioactive heat production, so successful in the Sierra Nevada and eastern United States provinces, does not apply in the Basin and Range province. There the variations in heat flow caused by hydrothermal and magmatic convection are probably greater by a factor of 3 or 4 than those caused by crustal radioactivity, and heat flux into the lower crust is not uniform; it is probably controlled by the mass flux of intruding magma. Regional variations in this mass flux, probably associated with crustal spreading, can account for the high heat flow subprovinces, and more local anomalies and silicic volcanic centers as well. Although convective processes cause a large dispersion of heat flow in the Basin and Range province, modal values of reduced heat flow can be used to construct generalized crustal temperature profiles for comparison with profiles for more stable areas and with melting relations for crustal rocks. Theoretical profiles are consistent with the widespread magmatic manifestations observed in the Basin and Range province. Laterally extensive silicic partial melts are possible at midcrustal levels in 'hot' subprovinces like the Battle Mountain High. Effects of hydrologic convection (whether driven by thermal density differences or regional piezometric conditions) are important to an understanding of regional heat flow, especially in tectonically active areas. The 'Eureka Low,' a conspicuous subprovince ($\sim 3 \times 10^4 \text{ km}^2$) with anomalously low heat flow in southern Nevada, is probably caused by interbasin flow in deep aquifers fed by downward percolation of a small fraction of the annual precipitation. Heat flow observations in such areas provide useful information on regional hydrologic patterns.

Introduction

The net outward flow of heat across the earth's surface is a fundamental term in the energy balance of processes within the earth. Consequently, measurements of this quantity not only contain information about the state of the earth but also about processes associated with the generation, transport, and storage of heat within it. The number of heat flow data has increased tenfold in the last decade, and this has led to a more complete understanding of regional variation of heat flow and its causes. The observations often can be interpreted in terms of very simple, internally consistent models that give useful insights into processes of the lithosphere beneath both oceans and continents [see e.g., Birch et al., 1968; Roy et al., 1968a, b, 1972; Lachenbruch, 1970; Sclater and Francheteau, 1970]. This paper summarizes the data available on regional heat flow in the conterminous United States and discusses some of their implications for the thermal regime and processes within the crust.

A Heat Flow Map

The heat flow data available to us as of June 1976 are presented as coded symbols in Figure 1, and a contoured interpretation of them is shown as Figure 2. The heat flow unit (HFU) is 10^{-6} cal/cm² s (41.8 mW/m²). For continuity, we have included in Figure 1 heat flows measured in the Pacific Ocean near the coast; however, we have made no attempt to contour them. The 625 points from the conterminous United States include published results from many laboratories and 130 or so recent determinations in preparation for formal publication by the U.S. Geological Survey (USGS) (see Diment et al. [1975] and Sass et al. [1976a] for a complete bibliography of published values). Most of the published data are supported by tabulations of thermal gradient and conductivity, but a few of the points have been taken only from published graphs or maps. The quality of the data is quite variable, as many of the determinations were made in holes drilled for purposes other than heat flow measurement; some were made in shallow holes drilled primarily for geothermal energy prospecting, and some in holes (usually in crystalline rock) drilled for scientific studies of regional heat flow. The best and the worst determinations are generally from holes drilled for other purposes; the best because such holes may be drilled to much greater depths than can be justified by limited research budgets and the worst because such holes are sometimes sited poorly for heat flow measurements and they may be sampled inadequately to characterize thermal conductivity. Few determinations have been made in holes drilled for petroleum exploration because of the difficulty of obtaining adequate conductivity samples and undisturbed temperature measurements. In prospecting for geothermal energy, large local anomalies, often in surficial sediments, are the targets, and substantial uncertainties can be tolerated. Such holes, commonly drilled to depths of about 50 m, can, however, give valuable heat flows under favorable hydrologic and topographic conditions. Even in holes drilled for regional heat flow in crystalline rock, depths greater than 250 m rarely can be justified, and uncertainties regarding the regional significance of an individual determination can be substantial.

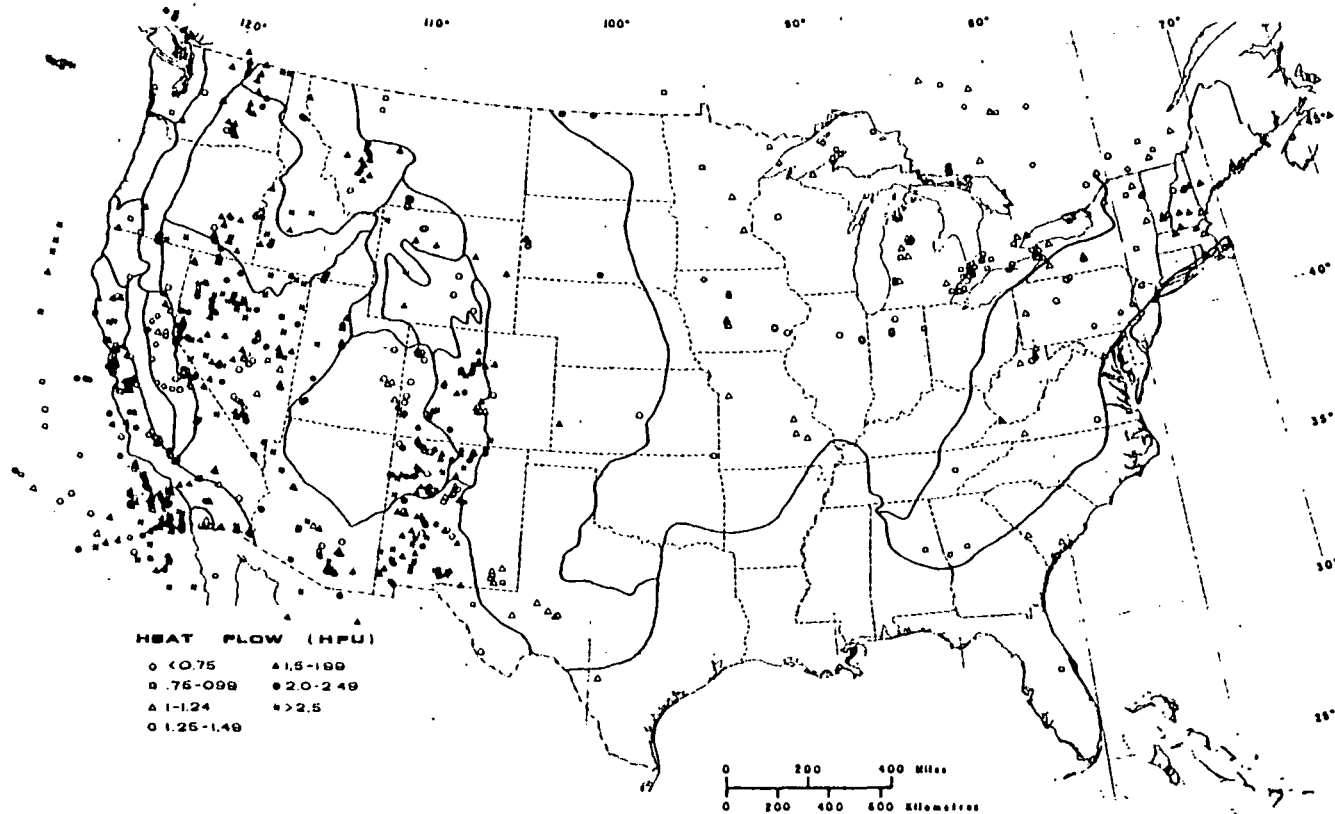


Fig. 1. Observed heat flow in the conterminous United States and some peripheral regions. Physiographic boundaries generalized from Fenneman [1946], (1 HFU = 10^{-6} cal/cm² s = 41.8 mW/m²).

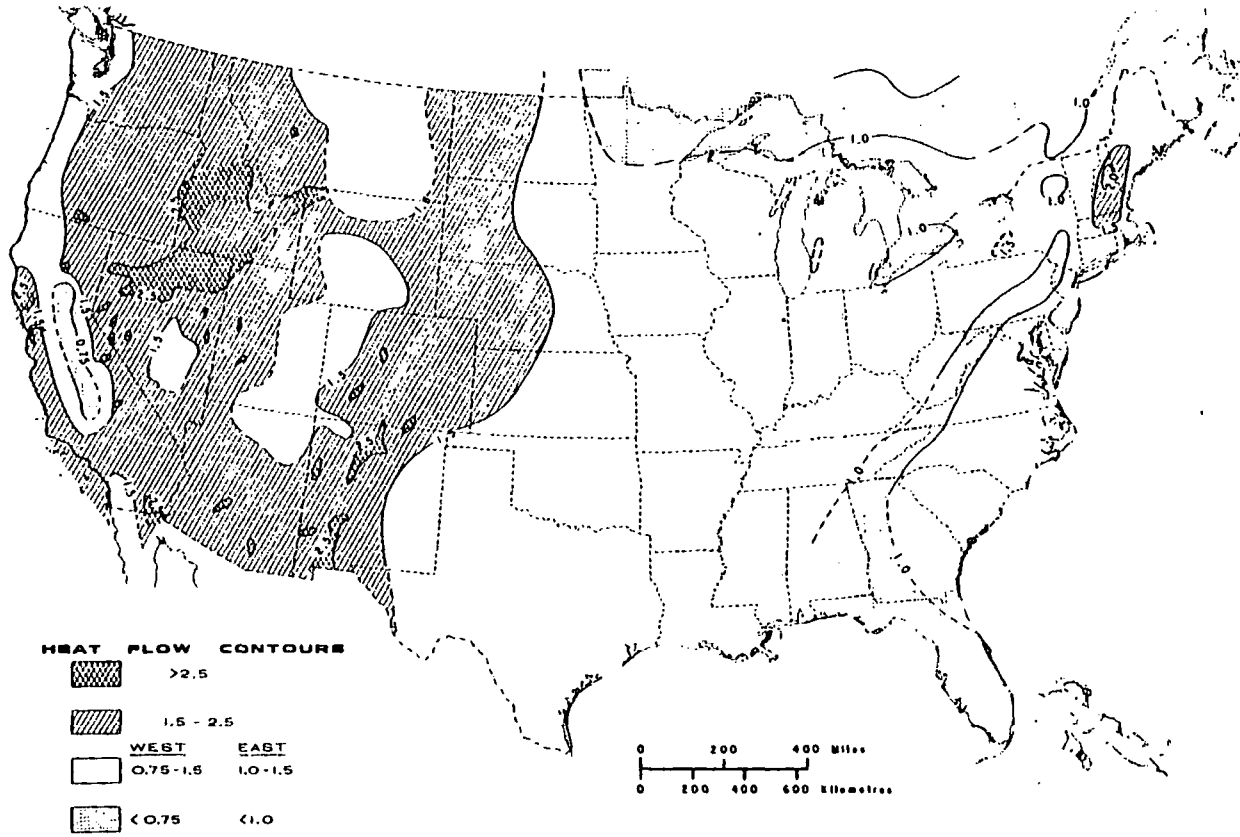


Fig. 2. A generalized heat flow contour map of the conterminous United States.

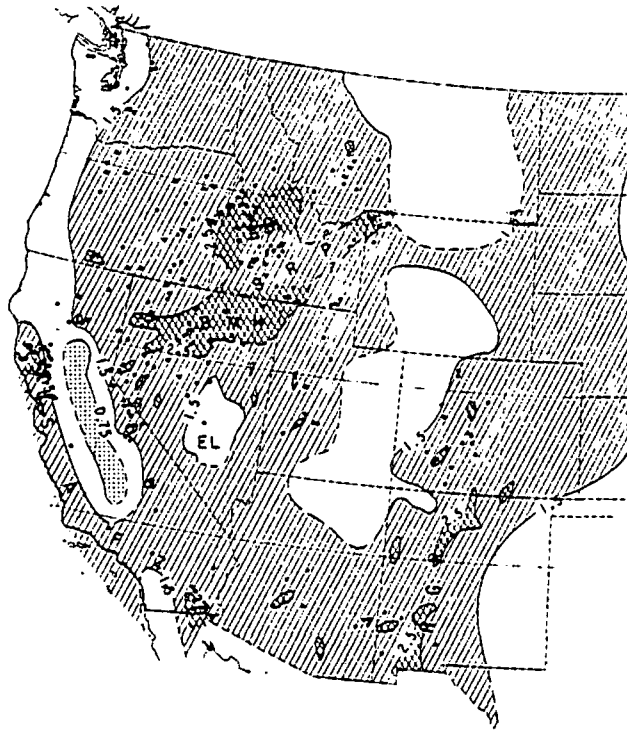


Fig. 3. Regional heat flow and distribution of hydrothermal systems. Dots show locations of hydrothermal systems in the conterminous United States with estimated reservoir temperatures greater than 90°C [Renner et al., 1975]. Abbreviations are BMH for Battle Mountain High, EL for Eureka Low, IB for Idaho batholith, SRP for eastern and central Snake River Plain, Y for Yellowstone thermal area, RGR for Rio Grande Rift, and SAFZ for San Andreas Fault zone.

In studies of regional heat flow it has been customary in the past to avoid regions of hot springs because of their local complexity. However, current interest in volcanic processes and the origin of geothermal energy resources requires that these hot spring areas be understood in relation to their regional thermal and tectonic settings. Figure 3 shows locations of the hotter known hydrothermal systems in the United States. Extending regional heat flow studies into these areas poses problems; the conductive flux at the surface can vary from zero to several hundred heat flow units over distances of a few kilometers, and substantial amounts of heat may be discharged convectively by lateral underflow in shallow aquifers into streams and lakes or at the surface by springs and fumaroles. Under these conditions there is some question about what we should define and map as 'heat flow.' In many regions we cannot feel confident, without hydrologic information, that heat transport in the upper few kilometers is exclusively conductive. However, hydrologic details are generally unknown; the heat flows selected for presentation in Figure 1 represent the upward conductive flux determined

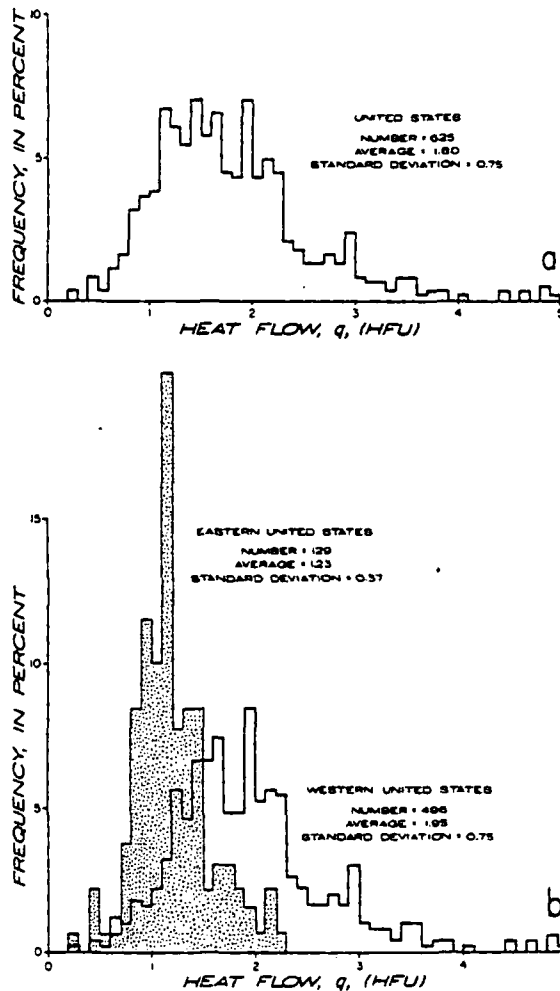


Fig. 4. Histograms of heat flow (a) for the conterminous United States as a single population and (b) for the portion east of the Great Plains (stippled) and the remainder of the conterminous United States (un-stippled), treated separately. (For location of the Great Plains, see Figures 1 and 14.)

in holes (usually to depths of at least 100 m) at all sites not obviously disturbed by local water movements. Figure 2 indicates the generalized distribution of heat flow we should expect for observations under these conditions. The data are summarized in histograms in Figure 4.

The gross features shown in earlier regional heat flow maps [Roy et al., 1972; Diment et al., 1972; Blackwell, 1971; Sass et al., 1971; Diment et al., 1975] persist in Figure 2. These are a generally low-to-normal heat flow in the eastern United States (1.5 HFU is approximately the world average) and a generally high heat flow in the west, with

zones of lower heat flow in the Colorado Plateau and near the Pacific Coast and very low values in the Sierra Nevada (for identification of the provinces, see Figure 14). The contours in the east are essentially unchanged from the map of Diment et al. [1972]. However, in the west, more information is now available from the work of Combs and Simmons [1973] in the Great Plains, Reiter et al. [1975] and Decker and Smithson [1975] in the Rio Grande Trough and Rocky Mountains, and by D. D. Blackwell, R. G. Bowen, and their associates [Blackwell, 1974; Bowen, 1973; Bowen et al., 1976; Brott et al., 1976] in the Pacific Northwest. Many new data from the USGS, largely in Nevada and the Pacific states, are also available [Lachenbruch and Sass, 1973; Diment et al., 1975].

In the map by Sass et al. [1971] a subprovince of exceptionally high heat flow, the 'Battle Mountain High,' was identified in the northern Great Basin, and one of normal and low heat flow, the 'Eureka Low,' was found in the southern Great Basin. The subsequent measurements tend to confirm the existence of both of these features. It now appears that the Battle Mountain High may be considerably larger than originally indicated, extending across northeastern Nevada at least to the Idaho and Utah borders. It is separated by the Snake River Plain from other regions of exceptionally high heat flow and hydrothermal activity in the Yellowstone, Wyoming, area to the northeast and the Idaho batholith to the north (Figure 3) [Blackwell, 1971; Urban and Diment, 1975; Morgan et al., 1977]. Recent volcanism and hot springs suggest that much of the Snake River Plain (particularly in the east) might have exceptionally large heat loss, although the surface heat flow is complicated by hydrologic conditions [Brott et al., 1976]. Hence a region of exceptionally high heat loss might extend northeastward almost continuously for 1000 km from the vicinity of Steamboat Springs near Reno, Nevada, to Yellowstone Park in Wyoming (see Figure 3). Another feature of the new map is the accumulating evidence for high heat flow in western California throughout a broad band that encloses the San Andreas Fault system [Lachenbruch and Sass, 1973].

The control is still poor in the western Colorado Plateau and eastern Great Basin (Figures 1 and 2); the boundaries drawn there are influenced by the distribution of hot springs and other geophysical data. Although heat flow data are accumulating in some volcanic regions such as parts of the Pacific Northwest [Bowen et al., 1976; Sass et al., 1976b; Brott et al., 1976], it is difficult to evaluate the regional significance of some of them because the rocks are often very permeable with temperatures influenced by hydrologic convection. In the Great Plains and much of the central and eastern United States the control is so poor that contours are rather arbitrarily drawn and a few new measurements could change them over large areas. Work is continuing at heat flow laboratories across the country, and better representations of the geographic distribution of heat flow are expected in the near future; good discussions of the major regional features have already been presented [Roy et al., 1972; Blackwell, 1971; Sass et al., 1971]. Therefore in this paper we shall focus on the general interpretation of heat flow within provinces that seem to have distinct regimes, rather than on the significance of the geographic distribution of the provinces themselves. In particular, we shall discuss the Sierra Nevada, the stable eastern and central United States, and the Basin and Range with its emerging subprovinces. The first represents the coldest crust in the United

States, and the Basin and Range subprovinces are probably among the hottest. Much of the discussion is general and applies to regions outside of these provinces where the heat flow is not as well known. In the San Andreas Fault zone of western California the crustal thermal regime may be unique; it has been discussed elsewhere [Lachenbruch and Sass, 1973; Brune et al., 1969; Henyey and Wasserburg, 1971].

In the next section we present some general background material as context for the discussions to follow. We hope it will make the paper more useful to readers not specialized in the study of terrestrial heat flow.

The symbols most frequently used in the text are as follows:

- θ temperature, °C;
- t time, s;
- K thermal conductivity, cal/°C s cm;
- ρ, ρ' density of static and moving material, respectively, g/cm³;
- c, c' heat capacity of static and moving material, respectively, cal/g °C;
- $\alpha = K/\rho c$, thermal diffusivity, cm²/s;
- q vertical conductive heat flux, HFU (10⁻⁶ cal/cm² s);
- q^* intercept value from heat flow-heat production curve, HFU;
- q_c vertical combined heat flux (convective plus conductive); HFU;
- q_r reduced heat flow, HFU;
- A^r heat generation, HGU (10⁻¹³ cal/cm³ s);
- A^o radioactive heat production in surface rock, HGU;
- v^o vertical (seepage) velocity or volume flux of water or magma, cm³/cm² s;
- $s = k/\rho'c'v$, characteristic length for groundwater convection, cm;
- k permeability, cm²;
- $\tau(z)$ conductive time constant for distance z ;
- $\lambda(t)$ conduction length for time t ;
- D characteristic depth for radioactivity or slope of heat flow-heat production curve, km;
- Γ thermal gradient for pure conduction, °C/km;
- z depth;
- h depth of circulation in hydrothermal system;
- H depth to top of magma
- θ_m magma temperature, °C.

Some General Considerations and Rules of Thumb

General

In discussing the geothermal regime it is useful to refer to the following general equation which relates the temperature and the processes that generate, transport, and store heat in the crust.

$$-\nabla \cdot \hat{q} \equiv \nabla \cdot (K\nabla\theta) \quad (1a)$$

$$-\nabla \cdot \hat{q} = -A + \rho'c'v \cdot \nabla\theta + \rho c \frac{\partial\theta}{\partial t} \quad (1b)$$

Here \hat{q} is the conductive flux vector, θ is the temperature, and K is the

thermal conductivity. The rate of heat generation per unit volume is denoted by A ; it could represent the effects of radioactive decay, frictional heating, phase change, or chemical reaction. The values ρ and c are the density and heat capacity of material at any point, and ρ' and c' are the corresponding properties for material (usually water or magma) moving with velocity \hat{v} . If the movement is through pores or fractures in a fixed framework, \hat{v} represents the volume flux ('seepage velocity') and not particle velocity. In general, all of the parameters in (1), including \hat{v} , are functions of x , y , and z , and some can have significant dependence on temperature or pressure.

Although three-dimensional effects must be kept in mind, useful simple interpretations generally involve quasi-one-dimensional models in which all of the quantities in (1) vary only with depth beneath the surface z . It is customary in geophysics to define the 'heat flow' q as the upward component of conductive flux and to reverse the sign convention; i.e.,

$$q \equiv K \frac{\partial \theta}{\partial z} \quad (2)$$

Unless otherwise specified, q will represent the conductive heat flow near the earth's surface $z = 0$. It is convenient also, in the one-dimensional models, to take the upward velocity v to be positive, although it is in the direction of negative z . With these conventions, (1) for the one-dimensional case reduces to

$$\frac{\partial q}{\partial z} = -A - \rho'c'v \frac{\partial \theta}{\partial z} + \rho c \frac{\partial \theta}{\partial t} \quad (3)$$

where q is the upward conductive heat flux, v is the upward volume flux of material with volumetric heat capacity $\rho'c'$, and ρc is the corresponding quantity in any stationary element.

Interpretation of regional heat flow in terms of crustal regime

Heat flow is determined from measurements of K and $\partial\theta/\partial z$ (equation (2)) in holes typically drilled to depths of 100-300 m. Whether the value is typical of conditions in the underlying crust must be judged on the basis of internal consistency of observations within each hole and among neighboring ones. Regionally significant heat flows are expected to vary only smoothly over lateral distances much less than a crustal thickness, and as a minimum condition there should be a substantial interval in each hole throughout which the measured heat flow is redundant, i.e., over which the right side of (3) vanishes (after correction, if necessary, for laterally variable temperature and topography at the earth's surface; see, e.g., Blackwell [1973], Birch [1950] and Lachenbruch et al. [1962]). As the earth's surface is a source of temperature change ($\partial\theta/\partial t \neq 0$) and hydrologic disturbance ($v \neq 0$) we generally have greater confidence in results from deeper holes. The internal consistency of measurements within and among holes in uniform granitic rocks at stations 30 km apart in the Sierra Nevada (Figure 5) provides some confidence that a regional condition is being measured there. By contrast, determination of the heat discharge and its regional significance in hydrothermal areas such as Long Valley, California (Figure 6) poses special problems.

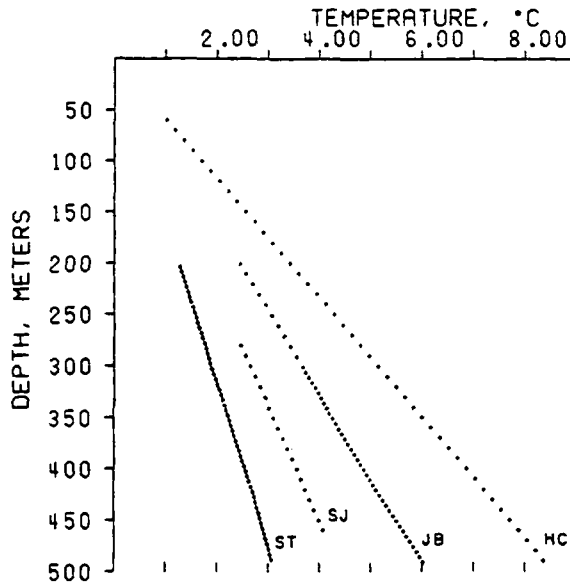


Fig. 5. Temperature measurements in granitic rocks of the Sierra Nevada province adjusted to a common temperature origin at the surface. Stations are about 30 km apart on a line from the western margin (ST) to the range crest (HC) [Lachenbruch, 1968].

The heat flow, normally measured in the upper 1% of the crust, provides only a boundary condition from which we should like to determine the thermal regime of the crust, i.e., to determine $q(z)$ throughout the entire crust. This requires a knowledge of how the terms on the right side of (3) vary throughout the crust. To provide meaningful constraints on these terms we must obtain insight into the physical processes that they represent. Interpretations of the crustal regime generally represent attempts to integrate (3) with simplifications believed to be appropriate for specific regions.

In our discussion, A will represent heat generated by radioactive decay of U, Th, and ^{40}K , elements present in minute amounts in crustal rocks. The process goes on steadily, irrespective of what else might be happening in the earth. The second term on the right in (3) represents effects of relative vertical movement of crustal (and upper mantle) masses; they may be solid blocks moving along faults or magmatic and aqueous fluids generally moving through fractures created by faulting or through pore spaces. As these movements are generally intermittent or short-lived, they generate transient disturbances represented by the last term in (3). Surface indicators of these mass movements are earthquakes, young volcanic rocks, and hot springs, which are shown with the heat flow distribution in Figures 3, 7, and 8. These manifestations are generally concentrated in the western regions of anomalously high heat flow, suggesting that the anomalies there are due primarily to convection and associated transients (i.e., to effects of the last two terms in (3)). The manifestations are rare in regions of low heat flow in the Sierra Nevada and the eastern half of the United States, and the crustal

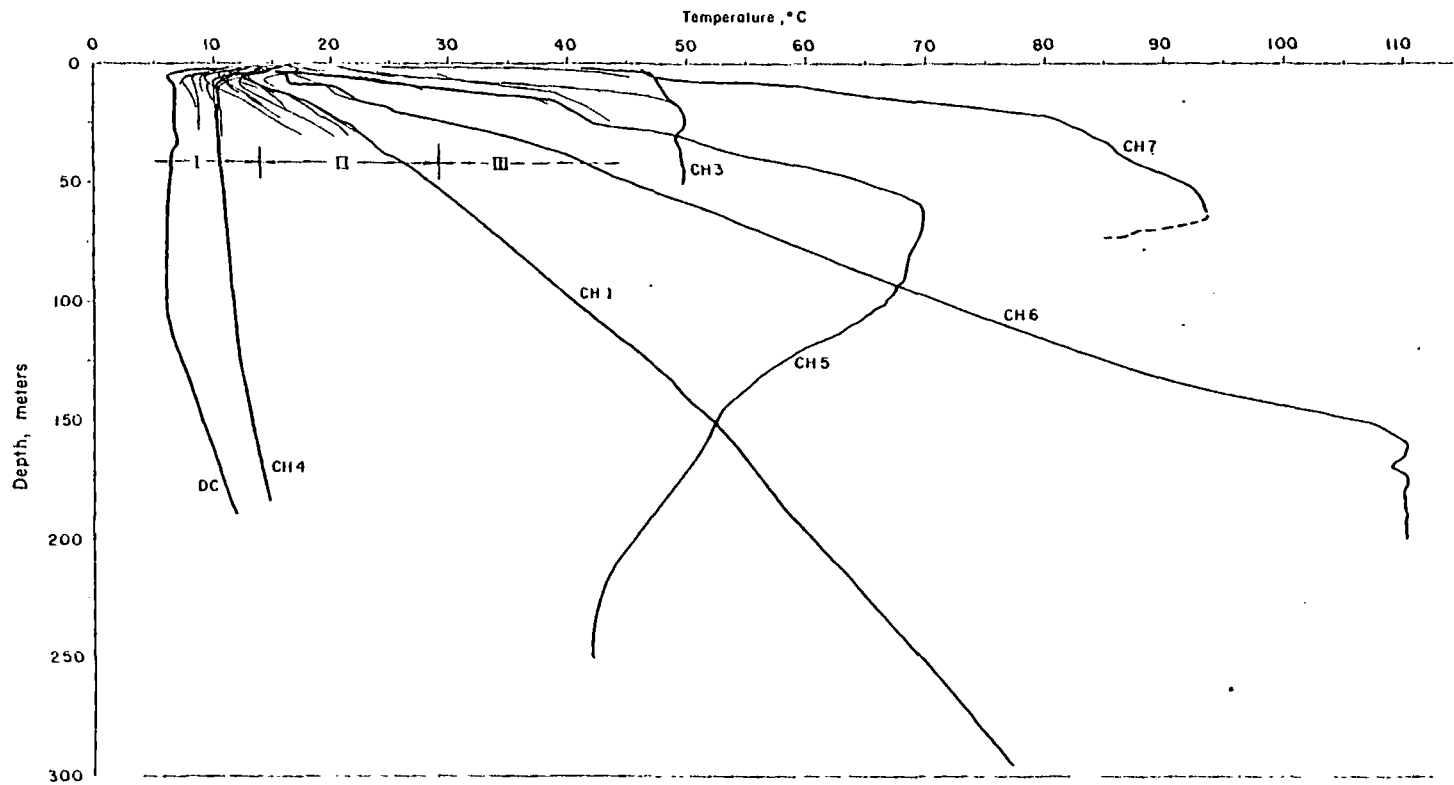


Fig. 6. Temperature measurements in the Long Valley caldera in California, a region with dimensions of about 20 km x 30 km [Lachenbruch et al., 1976b].

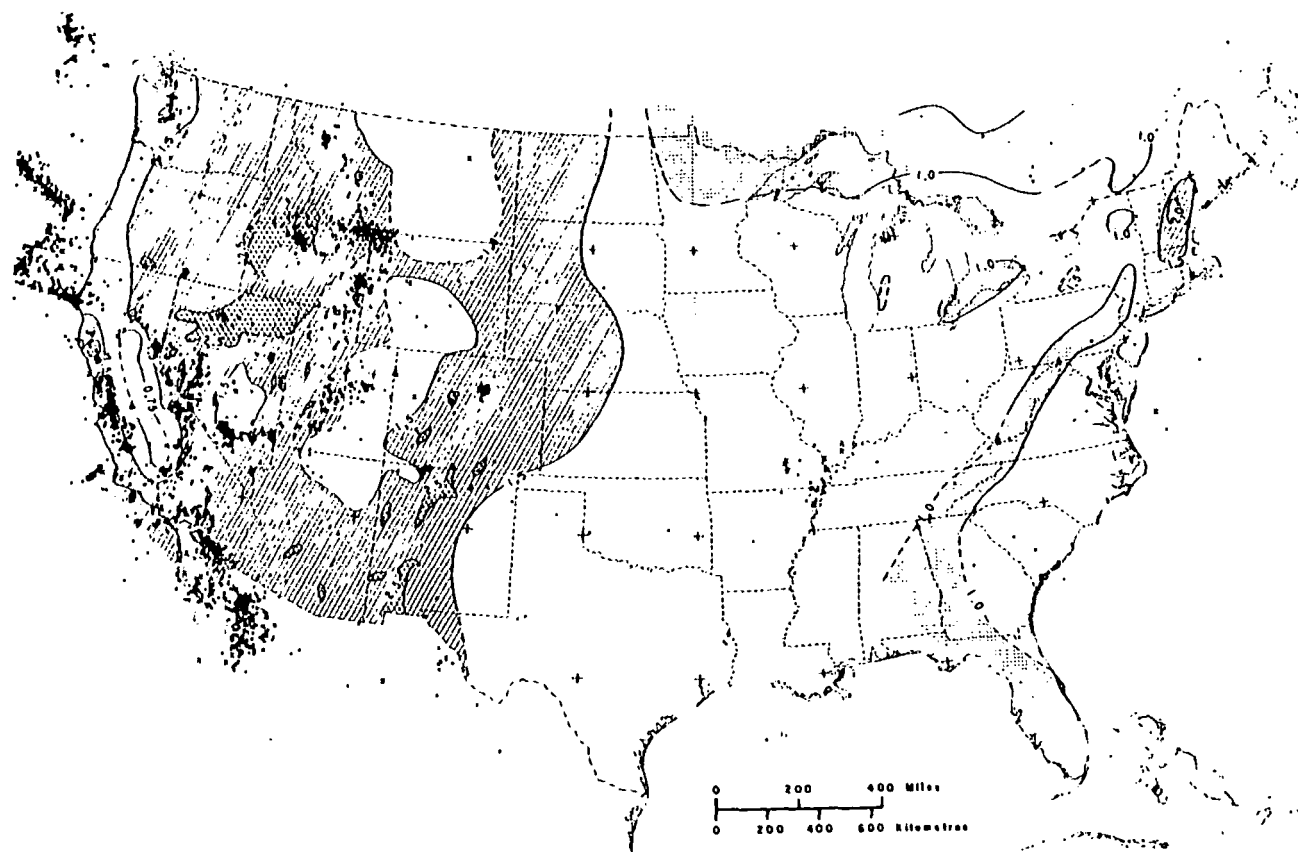


Fig. 7. Regional heat flow and distribution of seismic epicenters for the period 1961-1970. Dots represent earthquakes of magnitude about 3 to 5, crosses greater than 5. National Oceanographic and Atmospheric Administration epicenters have been replotted by J. C. Lahr and P. R. Stevenson of the USGS (personal communication, 1976).

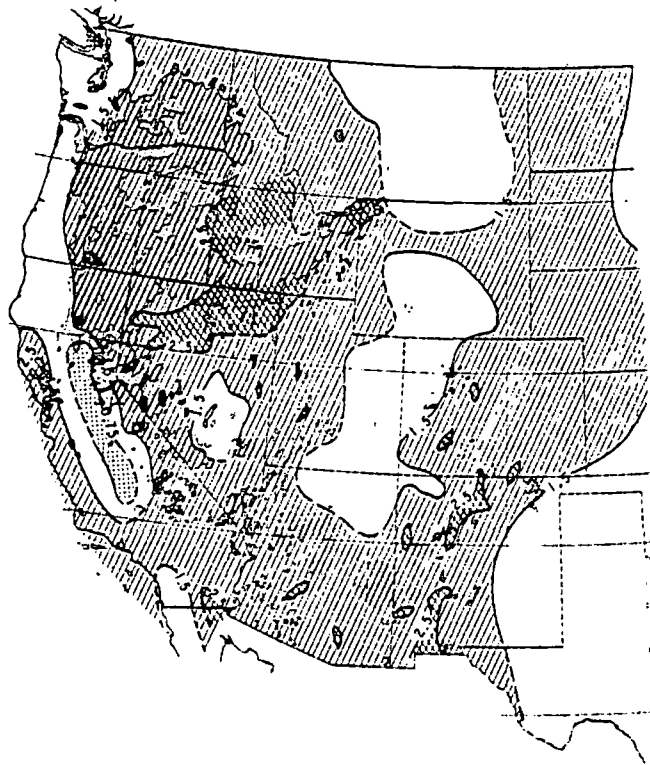


Fig. 8. Regional heat flow and the distribution of volcanic rocks erupted in the last 17 m.y. in the conterminous United States. Distribution of volcanic rocks adapted from Plate II of Stewart and Carlson [1977].

regime in these regions seems to be dominated by radioactivity (first term on the right in (3)).

Heat production and conductive transients

To estimate the relative importance of the terms in (3) we consider the contribution Δq to the surface heat flow that each term might make in a layer of thickness $\Delta z = z_2 - z_1$:

$$\Delta q = \int_{z_2}^{z_1} \frac{\partial q}{\partial z} dz \quad (4a)$$

$$\Delta q = A\Delta z + \rho'c'v\Delta\theta - \rho c \frac{\partial\theta}{\partial t} \Delta z \quad (4b)$$

where the parameters in (4b) are taken as appropriate average values and $\Delta\theta$ is the temperature difference across the layer.

If Δz represents a 30-km crust, then the contribution of the first term on the right can be written in dimensional form as follows:

$$\Delta q \text{ (HFU)} = 0.3A \text{ (HGU)} \quad (5)$$

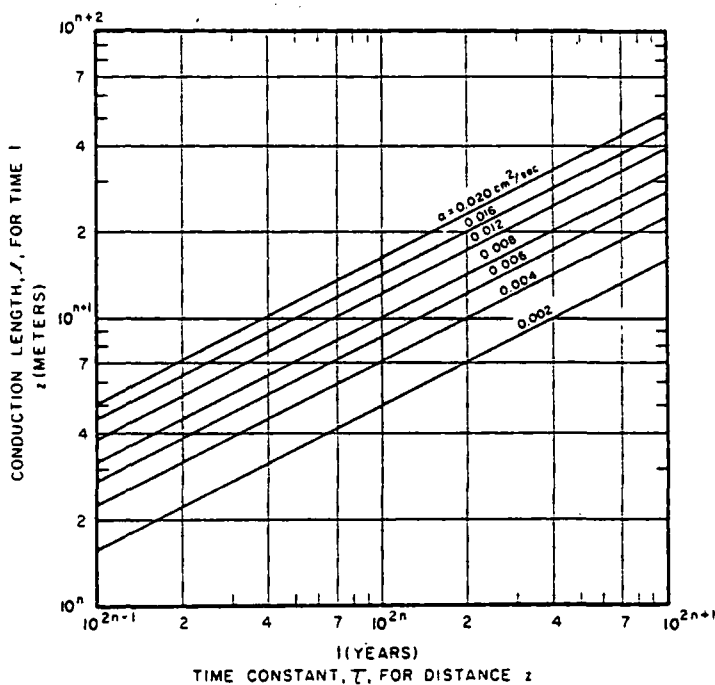


Fig. 9 Relation between conduction length z and time t , or between time constant τ and distance z , for the range of thermal diffusivities (α) of natural earth materials. The scale parameter n may be assigned any convenient value. (For example, if $\alpha = 0.008 \text{ cm}^2/\text{s}$ and $t = 1 \text{ m.y.}$, set $n = 3$ to obtain $z = 10 \text{ km}$. Conversely, given $z = 10 \text{ km}$, then $\tau = 1 \text{ m.y.}$).

Radioactive decay results in generation of heat at the rate of 1-10 HGU in most crustal rocks exposed at the surface. According to (5), if such rocks were distributed throughout the crust, they could account for much or all of the observed surface heat flow. Hence the distribution $A(z)$ is important to an understanding of the crustal regime, and it has been the subject of considerable study.

Skipping to the last term in (4b), we set $\rho c = 0.6 \text{ cal/cm}^3 \text{ }^\circ\text{C}$ and $\Delta z = 30 \text{ km}$ to represent the crust. The contribution of temperature change can be written

$$\Delta q \text{ (HFU)} \sim -0.6 \times 10^5 \times \frac{\partial \theta}{\partial \tau} \text{ (}^\circ\text{C/yr)} \quad (6)$$

Thus cooling of the entire crust at rates $\sim 10^{-5} \text{ }^\circ\text{C/yr}$ could contribute significantly to measured heat flow; a total of 20°C or 30°C of crustal cooling could account for heat flow at the observed rates for a million years with no other contributions. However, the rate at which the crust can cool is controlled by the mode of heat transfer within it. Hypothetical circulatory convection systems can be contrived to remove heat from the crust at almost any desired rate, but if the heat transfer is by conduction, the rate at which heat may be discharged or stored is severely constrained by the low conductivity and substantial volumetric

heat capacity of crustal materials. These constraints can be discussed in terms of simple limiting heat conduction models that can be reduced to convenient rules of thumb for the purpose of general discussion.

The solutions to many simple conduction problems can be expressed in terms of the single dimensionless ratio $z/\sqrt{4\alpha t}$. Normally, t is the time since some sort of disturbance occurred, z is a distance, usually from the source of disturbance, and α represents thermal diffusivity ($k/\rho c$). We define a characteristic 'conduction length' λ and a characteristic 'conduction time constant' τ as follows:

$$\lambda(t) \equiv \sqrt{4\alpha t} \quad (7a)$$

$$\tau(z) \equiv z^2/4\alpha \quad (7b)$$

Hence

$$\frac{z^2}{4\alpha t} \equiv \left(\frac{z}{\lambda(t)}\right)^2 = \frac{\tau(z)}{t} \quad (7c)$$

and the approach to steady conditions can be expressed in terms of how large t is in relation to τ or how large λ is in relation to z , depending on which variables are known. For convenient reference the conduction length λ can be found for any t , and the time constant τ can be found for any z for the range of diffusivities for natural earth materials in Figure 9. A reasonable average diffusivity for the entire crust may be around $0.01 \text{ cm}^2/\text{s}$.

Some convenient rules of thumb relevant to the measurement of heat flow or the interpretations to be presented are as follows:

1. A periodic temperature change with amplitude B and period P will have a negligible effect (a few percent of B) at depth $\lambda(P)$. Thus diurnal fluctuations ($P \sim 3 \times 10^{-3}$ years) are negligible in sediments ($\alpha \sim 0.002\text{--}0.008 \text{ cm}^2/\text{s}$) at depths of 30-50 cm (Figure 9, $n = -1$). The annual wave (Figure 9, $P = 1$ year, $n = 0$) penetrates about 5-10 m in poorly conducting sediments and 15 m in crystalline rock ($\alpha = 0.014 \text{ cm}^2/\text{s}$). The temperature pulsations due to repeated intrusion of a deep crustal layer with a period of 10^5 years would be negligible a few kilometers above (and below) the layer (Figure 9, $n = 3$). The process would therefore have the same effect at the surface as a continuous intrusion with a uniform (time averaged) temperature.

2. A rapid change in surface temperature at time $t = 0$ in the amount B perturbs the gradient at the surface by about $B/\lambda(t)$, and its effect on temperature may be appreciable ($\sim 15\%$ of B) to depth λ but is completely negligible ($< 1\%$ of B) beneath 2λ . Thus a 5°C post-Pleistocene warming 10,000 years ago (Figure 9, $n = 2$) could disturb the surface gradient of the order of $5^\circ\text{C}/\text{km}$ in crystalline rocks; temperature effects would be appreciable in holes to several hundred meters. The gradient disturbance would be greater in sediments, but because of the role of thermal conductivity the effect on heat flow would be less. Temperatures below an intruded layer maintained at constant temperature can be treated by these rules.

3. A rapid change in temperature at depth z will not be detectable in surface heat flow until times approaching $1/4 \tau(z)$, and the surface heat flow will be almost completely adjusted to the change for times exceeding $\tau(z)$. Thus a rapid (step) temperature change due to intrusion

at the base of a 30-km² crust ($\alpha \sim 0.01 \text{ cm}^2/\text{s}$) will not affect surface heat flow for about ~~3 or 4~~ m.y., but the entire crust will have equilibrated to the change in 8 m.y. or so (Figure 9, $n = 3$).

4. Heating (or cooling) by a constant heat source (or sink) at a depth z from time $t = 0$ will not affect heat flow at the surface until times approaching $\tau(z)$. The surface heat flow will not approach its steady value until $t \gtrsim 100\tau(z)$, but for $t > 3\tau(z)$ temperatures in the layer above depth z can be estimated (within about 10%) by assuming that conditions observed at the surface are steady, i.e., by assuming that heat flow is independent of depth in the layer. The constant source approximates long-term slow intrusion of a sill in which the melt does not survive between intrusive pulses or the thermal recovery of a layer of thickness z after extinction of a hydrothermal system within it. The constant sink approximates effects of a cooling sill after solidification [see Lachenbruch et al., 1976a].

Convection--general considerations

An understanding of regional heat flow in tectonically active areas requires at least a gross understanding of convective processes in the crust. We distinguish between two main types: convection by magma and convection by groundwater. The large-scale effect of magmatic convection on surface heat flow is caused by the upward transport of fluid at temperatures greater than ambient; it always results in a positive contribution to heat flow. The lateral extent of the positive anomaly will be comparable to that of the region intruded. In the steady state the intensity of the anomaly can be determined in terms of the rate (volume flux) of intrusion v from the second term on the right in (3), making allowance in the factor c' for the heat of crystallization. For present purposes, transient effects of convection by magma can be discussed adequately in terms of the rules of thumb presented in the last paragraph.

Groundwater convection is a more difficult problem; it generally involves some flows that are hotter than ambient and others that are colder, and it is mainly confined to the upper crust, close to the surface where heat flow is measured. With the search for geothermal energy it is becoming more important to understand groundwater convection in a regional context. As this process has generally been treated lightly in discussions of regional heat flow, we shall consider it here in somewhat more detail than the processes just discussed.

The magnitude of hydrothermal effects can be estimated by retaining only the second term on the right in (4b). The volumetric specific heat $\rho'c'$ for hot and cold water (and for melted rock as well) is generally from 0.7 to 1 cal/cm³ °C. Taking the latter value leads to the following dimensional relation for vertical one-dimensional steady convection

$$\Delta q \text{ (HFU)} = 10^6 v \text{ (cm/s)} \Delta\theta \text{ (}^\circ\text{C)} \quad (8a)$$

$$\Delta q \text{ (HFU)} \sim v \text{ (ft/yr)} \Delta\theta \text{ (}^\circ\text{C)} \quad (8b)$$

Equation (8b) is a useful rule of thumb. Seepage velocities of 1 ft/yr (0.3 m/yr) would result from Darcian flow under unit hydraulic gradient

in a medium with a permeability of only 1 mdarcy (10^{-11} cm²); they are not uncommon in hydrothermal areas. Such a flow rising across a layer with 10°C temperature difference would contribute 10 HFU to the surface flux.

A second useful relation for steady vertical flow is obtained by neglecting the first and third terms on the right in (3) and writing it in the form

$$\frac{\partial q}{\partial z} = - \frac{\rho'c'}{K} vq \quad (9)$$

Integration yields

$$q(z_1)/q(z_2) = e^{\Delta z/s} \quad (10)$$

where s is a characteristic distance with the sign of v .

$$s = K/\rho'c'v \quad (11a)$$

It is most easily expressed as a rule of thumb in terms of feet.

$$s \text{ (feet)} \sim \frac{100}{v \text{ (ft/yr)}} \text{ for 'sediment' (K = 3 mcal/cm s } ^\circ\text{C)} \quad (11b)$$

$$s \text{ (feet)} \sim \frac{200}{v \text{ (ft/yr)}} \text{ for 'rock' (K = 6 mcal/cm s } ^\circ\text{C)} \quad (11c)$$

According to (10) and (11b), steady vertical flow at 1 ft/yr through a 500-foot layer (Δz) would increase the gradient and conductive heat flow in the direction of water flow by the factor $e^5 \sim 150$. This can lead to very large (and short-lived) local fluxes and large temperature differences (equation (8)) unless the gradient on the inflow side is very small. Hence the flow will generally cause most of the layer to be nearly isothermal if $\Delta z \gg |s|$. Thus for downward flows (s negative) of 1 ft/yr the gradient near the surface and the measured heat flow will generally vanish if the layer is only a few hundred feet thick. Similarly, the surface heat flow will be 'washed out' by downward percolation of only 1 in./yr (a small fraction of annual precipitation) through a few thousand feet of porous rocks. This effect obviates the determination of regional heat flow by conventional means over large areas. Some such areas, mantled by permeable volcanic rocks, are of considerable interest as potential sources of geothermal energy.

Temperature in the layer of thickness Δz (equation (10)) is determined by specifying at least one of the boundary temperatures and the other boundary temperature or one of the boundary heat flows $q(z_1)$ or $q(z_2)$. To be consistent, any physical model must also conserve mass of the flowing water. A useful consistent solution for coupled heat and water flow is obtained by identifying $\theta(z_1)$ with the mean ground surface temperature and $q(z_2)$ with the regional heat flow. In this case, water flows horizontally along z_2 with no change in temperature, providing a source (or sink) for the vertical mass flow to (or from) the surface. The model yields a useful rule of thumb; viz., whether the surface heat flow ($q(z_1)$) is significantly different from the regional heat flow ($q(z_2)$) depends upon whether the depth of vertical water flow Δz is small or large in relation to $|s|$ (equation (10)). A second application

of (10) [Bredenhoeft and Papadopoulos, 1965] assigns both boundary temperatures $\Theta(z_1)$ and $\Theta(z_2)$. However, unless the assigned temperature $\Theta(z_2)$ is the value determined by uniform flux from below, $q(z_2)$, the water flowing horizontally along z_2 must be a source of heat as well as mass, its temperature must change horizontally, and the one-dimensional model is only approximate. It is useful to note, however, that from a transient solution for this case [Nathenson, 1977] it can be shown that the stationary condition described by (10) is generally approached after one conductive time constant ($\tau(\Delta z)$) for slow water flow between depths held at constant temperature and sooner if the vertical water flow is vigorous ($|s| \ll \Delta z$).

Equations (8), (10), and (11) give an indication of the enormous effects that hydrologic conditions can have on measured heat flow (see, e.g., Figure 6). In natural systems these effects can be extremely complex, involving variable upward and downward flows (with temperature and pressure dependent properties) in fractures and pore spaces [see, e.g., Sorey, 1975]. These systems may be in delicate balance, vulnerable to the effects of earthquakes or the drilling of wells. The pattern assumed by these flows depends upon the conditions that drive them. There are two distinct cases: (1) the flow is forced by the configuration of fractures and permeable formations and by regional piezometric conditions controlled by precipitation, evaporation, and topography, or (2) the flow results from the instability of groundwater heated from below in a permeable layer. (In general, elements of both driving mechanisms are present.) The second case tends to produce circulating cells with an aspect ratio close to unity [e.g., Sorey, 1975]; it should result in heat flow anomalies that change in sign over lateral distances of the order of the depth of circulation. No such condition applies to the first case, which in extreme circumstances could produce persistent anomalies in surface heat flow on a regional scale (e.g., possibly, the Eureka Low, to be discussed). The foregoing results can be applied to order of magnitude calculations for the first case. We shall now consider the second case, which we shall refer to as hydrothermal systems.

Hydrothermal systems

These systems are initiated when the Rayleigh number R exceeds a critical value [e.g., Lapwood, 1948]. Other things being equal, R increases linearly with the depth of the permeable zone, the permeability of the zone, and the temperature difference across it; increasing any of these could initiate a hydrothermal convection system. To investigate gross relations between these systems and the regional heat flow or magmatism that supplies their heat, we shall discuss some highly idealized quasi-one-dimensional models.

Consider a region near the earth's surface (Figure 10a, $z = 0$) in which the heat transfer is initially conductive and the temperature profile is linear with gradient Γ (Figure 10b, curve I). The heat flow q is then $K\Gamma$. Suppose that in a region of high heat flow at time $t = 0$, fractures open in a layer extending from the earth's surface to depth h and that this increases the permeability so much that the groundwater becomes unstable and starts to circulate. Above regions where the water is moving downward the surface heat flow will diminish, and above regions where it is moving upward the surface heat flow will increase.

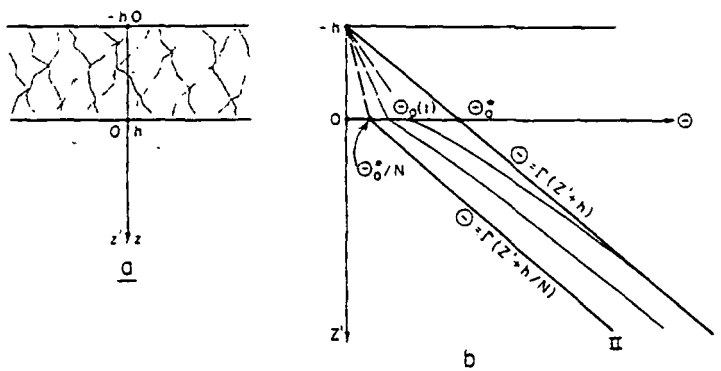


Fig. 10. Idealized one-dimensional model for hydrothermal convection in a surficial layer of thickness h ; the heat is supplied by steady regional heat flow (see text).

However, the total heat transport across the layer (integrated over the surface above the fractured region) must increase, as the initial conductive transport is now supplemented by convective transport. For simple one-dimensional order of magnitude calculations we assume that the net effect of convection is to increase the mean heat flux through the layer ($z < h$) by the factor $N > 1$ (e.g., for the layer with uniform vertical flow, upward over half the area and downward over the other half, (10) yields $N = [\exp(h/|s|) + \exp(-h/|s|)]/2$. When the system is in a stationary state and the lower and upper boundaries are held at constant temperatures, N would represent the Nusselt number; in real systems, neither surface would be at uniform temperature. We let $\Theta_0(t)$ be the average temperature at $z = h$ at time t and assume that it is uniform. The surface temperature is assumed to be uniform at the average ambient value taken as zero. This condition would be violated locally by hot springs, the convective discharge of which is included in the factor N . We neglect the change of N that would occur as the system evolves. (A useful discussion of the relation between heat flow and coupled heat and water flow in porous layers has been given by Donaldson [1962] and in isolated fractures by Lowell [1975] and Bodvarsson [1969].)

In this model the mean upward flux from $x = h$ will (initially) exceed the mean flux into $x = h$ by the factor N . After time t the basal temperature will drop from Θ_0^* to some value $\Theta_0(t)$, and the heat flux through the convecting layer will drop to $NK\Theta_0/h$. The convecting system will continue to mine heat from the earth until the flux through it is equal to the regional conductive flux $K\Gamma$ supplied from below, i.e., equilibrium will be established when

$$NK\Theta_0/h = K\Gamma \equiv K\Theta_0^*/h \quad (12a)$$

or

$$\Theta_0 = (\Theta_0^*/N) \quad t \rightarrow \infty \quad (12b)$$

To estimate the time required for stabilization, we first neglect the

heat capacity of the convecting layer $z < h$ and consider the underlying region $z > h$, which we denote by $z' > 0$ (Figure 10); heat loss from the surface $z' = 0$ is proportional to the temperature $\theta_0(t)$. The differential equation and conditions are

$$\frac{\partial^2 \theta}{\partial z'^2} = \frac{1}{\alpha} \frac{\partial \theta}{\partial t} \quad z' \geq 0 \quad (13a)$$

$$\theta = \theta_0^* + \tau z' \quad t = 0 \quad z' \geq 0 \quad (13b)$$

$$\frac{\partial \theta}{\partial z'} = \frac{N}{h} \theta_0(t) \quad z' = 0 \quad (13c)$$

The solution (modified from Carslaw and Jaeger [1959, p. 71]) for temperature θ_0 at the base of the slab is

$$\theta_0(t) = \theta_0^* - \theta_0^*(1 - 1/N) [1 - e^{-\beta^2} \operatorname{erfc} \beta] \quad (14)$$

where $\beta^2 = (N^2 \alpha / h^2) t$. Hence $\theta_0(t)$ approaches its equilibrium value θ_0^*/N after a time

$$t \sim h^2 / N^2 \alpha \quad (15)$$

which can be read from Figure 9. For $N = 2$ it is the same as the conductive time constant for the slab of thickness h , and for $N = 6$ it is an order of magnitude less.

The sensible heat lost by the slab as its base cools from θ_0^* to $(1/N)\theta_0^*$ (neglected in the above calculation) is roughly $\theta_0^*(1 - 1/N)h\rho c/2$. This heat could sustain the mean anomalous flux of $NK(\theta_0^*/h)(1 - 1/N)/2$ for a time

$$t \sim h^2 / N\alpha \quad (16)$$

The actual time for stabilization of the slab depends upon the complex behavior of coupled temperature and velocity fields; it will generally result in changing N and perhaps in an increase in h , if thermal contraction results in deepening fractures. However, for larger N (say, > 2) likely to be of interest we judge from the above that processes internal to the slab (16), not those beneath it (15), will be controlling and that a steady state is likely to be approached in times of the order of $\tau(h)$ (Figure 9) or less. For larger times the surface flux would still have extreme local variations, but perturbations would integrate to zero, and the average combined flux would equal the regional heat flow q . Stabilization times vary from 1,000 years for $h \sim 400$ m to 100,000 years for $h \sim 4$ km (Figure 9). More active systems (large N) probably stabilize more quickly. (For a layer in which circulation is confined to fractures separated by distance λ , the stabilization time will probably be controlled by $\tau(\lambda)$ if $\lambda > h$ [see, e.g., Bodvarsson and Lowell, 1972; Carslaw and Jaeger, 1959, Figure 12].)

Restoration of the steady regional heat flux at the surface after extinction of a hydrothermal system is a very slow process (governed by the conduction rule of thumb, number 4 above). It can be viewed crudely

as the conductive return of curve II, now the initial condition, to curve I, the final condition (Figure 10b). The heat flow anomaly Δq at the surface can be shown to be

$$\Delta q = -q(1 - 1/N) \operatorname{erf} \frac{h}{\sqrt{4\alpha t}} \quad (17)$$

where q is the steady regional heat flow. According to (17) the anomaly would be half its initial value when $t \sim h^2/\alpha$ (or $4\tau(h)$) and 10% of its initial value when $\tau \sim 110\tau(h)$.

We illustrate these results with a highly idealized numerical example. A 'one-dimensional' hydrothermal system with depth $h = 2$ km develops in a region with steady regional flux q of 2.5 HFU. Assume that $N = 5$ and (perhaps unrealistically) that this value and the depth h persist as the system ages. In early stages the average heat flow from the system will be Nq , i.e., 12 or 13 HFU. After some 25,000 years ($\tau(2$ km)) or less the average flux will fall to the regional value with 80% (i.e., $1 - 1/N$) or 2 HFU being supplied by convective transfer. If the circulation suddenly stopped (e.g., from earthquakes or sealing of fractures), the mean flux would fall to 0.5 HFU, producing a mean local anomaly of -2 HFU; negative anomalies of 0.5 and 0.2 HFU would still persist 1/2 and 3 m.y. after circulation stopped, respectively. Although the example is extreme, it serves to illustrate why the heat flow might be extremely variable in tectonically active provinces where hydrothermal convection systems are common; the relation of the anomalies to the systems that produced them may be obscure.

These highly simplified considerations suggest the following generalizations regarding hydrothermal convection systems supported by regional heat flow in permeable surface layers:

1. The heat flow q (and combined flux q_c) will vary over horizontal distances of the order of depth of circulation, h , during all phases.
2. During an initial phase which might last $\sim \tau(h)$ the mean combined flux from the surface will exceed the regional heat flow.
3. If the system survives, it will reach a stationary stable phase in which the mean combined flux will equal the regional heat flow.
4. In a waning or recovery phase, probably longer by a factor of 10^2 than the initial phase, the mean surface flux will be less than regional heat flow.
5. The mean combined flux at the surface integrated over all phases will equal the regional heat flow; if there was convective loss into surface drainage, the integrated conductive flux will be less than the regional value.

If we can view the Basin and Range province (which is $\sim 10^7$ m.y. old) as containing a random sample of such systems (with life cycles of $< 10^6$ years), the average combined flux will equal the regional heat flow, and the average conductive flux will be less. Similar generalizations apply to systems confined to widely separated fractures as long as they are sustained by regional heat flow (or a source of heat at depth that is uniform for times much larger than the stabilization time for the hydrothermal system).

In the foregoing discussion, hydrothermal instability was initiated by introducing fractures which increased the permeability k or depth of the fractured layer, h . We assumed a steady 'regional' conductive flux from great depth. Even in the Battle Mountain High the regional flux

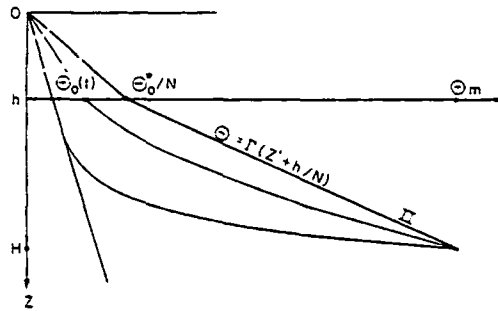


Fig. 11. Idealized one-dimensional model for hydrothermal convection in a surficial layer of thickness h ; the heat is supplied by upper crustal magma at depth H (see text).

does not exceed about 3 HFU, and it leads to regional gradients generally in the range of 50° - 100° C/km. Intrusions in the upper crust could, of course, produce much higher heat flows locally; if the melts persist long enough, they can generate a steady thermal condition in the overburden, heating the rock all the way to the surface. Under such conditions, hydrothermal instability could be initiated by raising the basal temperature Θ_0 of the fractured zone rather than by increasing its permeability. This condition is illustrated in Figure 11 for the simple one-dimensional case of intrusion at depth H with temperature Θ_m . If the magma supply is sufficient to maintain the isothermal condition at $z = H$ during the initial stages, a stationary thermal condition will be approached in the overlying rocks in about $\tau(H)$ (see Figure 9); otherwise, it will take longer [Lachenbruch et al., 1976a]. This stationary condition is represented by curve II in Figure 11, which, of course, is the same (mathematically) as curve II in Figure 10b. In this case, however, the mean surface flux from the developing system may be less than the flux in the steady state, and the steady flux may be much greater than the regional value. In the steady state the mean combined flux q_c from the system can be written

$$q_c = K\Gamma \quad (18a)$$

$$q_c = \bar{K}\Theta_m/H \quad (18b)$$

$$q_c = K\Theta_m/[H - h(N - 1)/N] \quad (18c)$$

where (18c) is obtained by substituting for \bar{K} the harmonic mean conductivity of the overburden (H), using the effective conductivity NK in the fractured zone. The expression in brackets in (18c) could be called the 'effective depth' of magma; it is the depth that would be implied by heat flow observations if convection were absent.

$$H - h\frac{N-1}{N} = K\frac{\Theta_m}{q_c} \quad (19)$$

At the Long Valley caldera in California the mean combined flux at the surface has been estimated by hydrochemical means to be greater than 10

HFU by Sorey and Lewis [1976] and about 16 HFU by White [1965]. The caldera has been a source of volcanism for 2 m.y., and hydrothermal activity has been in progress at least 300,000 years, more intense in the past [Bailey et al., 1976]. If we assume a stationary state and take $q_c \sim 13$ HFU, $\theta = 800^\circ\text{C}$, and $K = 5$ mcal/cm s $^\circ\text{C}$, we obtain for the effective depth of magma

$$H - h \frac{N - 1}{N} \approx 3 \text{ km}$$

This implies that hydrothermal convection must extend downward (to depth h) within 3 km of the magma with very high N or even closer if the circulation is less vigorous. Structural and seismic evidence [Bailey et al., 1976; Hill, 1976; Steeples and Iyer, 1976] suggests that if magma now exists beneath the caldera, it must be at a depth of at least 6 to 8 km. Thus at least 3 to 5 km is made 'transparent' by hydrothermal convection, and water must be circulating to very great depths.

It has been pointed out that hydrothermal systems supported by regional heat flow probably exhaust the sensible heat in time $\tau(h)$, say, 10^3 - 10^5 years, and if they survive thereafter, they do not result in anomalous heat loss. In volcanic areas such as Long Valley, hydrothermal systems are evidently supported by upper crustal intrusion, and they can persist for millions of years, discharging heat at an anomalous rate. This behavior imposes severe heat demands on the underlying magmatic system [see Lachenbruch et al., 1976a]. When the effective depth of magma exceeds 10 or 15 km (depending on the choice of K and θ in (18c)), the steady surface flux approaches the regional value characteristic of the Battle Mountain High (~ 3 HFU) and the time constant for the overburden becomes large in relation to the stabilization time for hydrothermal systems. Under these conditions the heat supply for hydrothermal systems would be considered as either regional heat flow or a local magmatic anomaly, depending upon whether or not the magmatic condition were widespread. Both situations probably occur in the Basin and Range province.

Convection and Regional Heat Flow

In general, convection by groundwater in upper crustal rocks poses the greatest obstacle to determining from surface observations the heat flow associated with crustal conditions at depth. Obvious effects can often be eliminated by judicious selection of study sites or by the criterion of internal consistency applied to measurements in deep holes and in neighboring holes. However, because hydrologic effects can be subtle, lingering uncertainties may persist. For regional interpretation it is important to know whether undetected hydrologic anomalies are likely to be the exception or the rule. It has already been pointed out that in some regions of porous volcanic and sedimentary rocks they may be the rule. Thus it is difficult to determine the regional significance of heat flow measurements throughout portions of the Pacific Northwest, including the Cascade volcanos, parts of the Columbia Plateau, and the important Snake River Plain [Brott et al., 1976], and in other recent volcanic areas such as the San Francisco peaks at the edge of the Colorado Plateau. Very detailed hydrologic studies and deep drilling might be required to detect heat from magmatic reservoirs



Fig. 12. Regional heat flow and the natural heat discharge of known hydrothermal systems with reservoir temperatures greater than 90°C . Each circle is centered at the location of the system it represents. A heat flow of 1 HFU through the circular area is equivalent to the rate of combined heat discharge estimated for the system. Systems with estimated discharge of less than 3×10^6 cal/s are not shown.

[Smith and Shaw, 1975] likely to underlie some of these regions. A similar problem often occurs in sedimentary basins, and for this reason, sites for regional heat flow studies are often chosen in less permeable rock, despite the more costly drilling.

In interpreting heat flow in the Basin and Range province it will be important to estimate the regional effects of hydrothermal convection systems. Figure 3 shows all the hydrothermal systems with estimated reservoir temperatures greater than 90°C that Renner et al. [1975] were able to identify in the conterminous United States in a recent study. From the data presented by them and from supplementary studies, chiefly those of Olmsted et al. [1975], Mariner et al. [1974], Bowen and Peterson [1970], and Fournier et al. [1976], we have attempted to summarize the natural heat discharge from each of these systems. This discharge comes in varying proportions from conductive loss from the reservoir and from conductive and convective losses from fluid discharged from the reservoir into shallow aquifers or surface drainage. Methods of estimating these discharges have been discussed by Olmsted et al. [1975], White [1965, 1968], Sorey and Lewis [1976], Fournier et al. [1976], and

Morgan et al. [1977]; the methods vary depending upon hydrologic conditions, and, of course, the estimates are subject to substantial uncertainty. Of the 255 systems listed by Renner et al. [1975], we judged that about three dozen had total combined natural discharges greater than about 3×10^6 cal/s; they are shown as circles in Figure 12. The area enclosed by each circle is the area through which an anomalous flux of 1 HFU would be equivalent to the total rate of combined (conductive and convective) heat discharge for the system. Typically, the anomalous regions have an area that is an order of magnitude smaller than the circles in which they are centered. The purpose of this representation is only to place some of the better known systems in a regional perspective. More detailed studies of these and other systems (some perhaps with high mass discharge at lower temperature) will surely change the picture.

Insofar as the 255 systems located in Figure 3 are concerned, the cumulative anomalous discharge is small in relation to the integrated regional flux; with the exception of the Yellowstone system, their effects on the thermal balance of the crust would be local. For the anomalous discharge to equal the integrated regional flux the circles (Figure 12) would have to overlap once on the average throughout most of the western United States. For those systems that might be stabilized above upper crustal intrusions the circle indicates the rate at which heat must be supplied by magmatic convection. For those systems that have stabilized and are supported by regional heat flow the circle represents the area over which a negative regional anomaly of 1 HFU would be sufficient to complete the heat balance.

These results offer some hope that we might be able to find a characteristic regional flux to identify with the crustal regime over large areas of the Basin and Range and similar regions; the most reasonable choice would be the most frequently occurring (or modal) value of the conductive flux. The mean would be biased toward large values by effects of undetected upper crustal intrusions, although the shallower ones would probably be identified by their hot springs and avoided in regional studies. In large regions of high heat flow, most of the local anomalies of unidentified origin are likely to come from hydrothermal convection supported by regional heat flow and modified by the forcing effects of variable topography, permeability, and precipitation. Although the combined anomalous flux from these systems might integrate to zero, the mean conductive flux would be biased toward lower values if there were appreciable convective discharge into surface drainage. (The mode and mean are not appreciably different for the Basin and Range data, possibly because internal drainage minimizes convective loss from shallow aquifers.) If the local convection systems were common, the dispersion of heat flow would be large, and the mode would be poorly defined, making the regional flux more difficult to identify. This is evidently the case in the Basin and Range (to be discussed further below), where highly fractured rocks are difficult to avoid and high heat flow and locally variable topography and precipitation favor small-scale convection systems [Olmsted et al., 1975].

A hydrologic anomaly on a regional scale seems to provide the most reasonable explanation of the Eureka Low subprovince of the Basin and Range (Figure 12). The average of 13 heat flows in this $30,000 \text{ km}^2$ region of south central Nevada is about 1.1 HFU, roughly 1 HFU less than

the heat flow believed characteristic of the surrounding Basin and Range province. The deeper holes generally showed thermal evidence of downward moving water; in the deepest hole this evidence persisted to depths greater than 3 km [Sass et al., 1971]. In a careful hydrologic synthesis, Winograd and Thordarson [1975] have shown that an 11,000 km² region, straddling the southern boundary of the Eureka Low, is hydrologically integrated into one groundwater basin, although the region contains 10 topographic basins. The interbasin flow occurs to depths up to 1 1/2 km beneath the surface in permeable fractured carbonate rocks underlying the region; discharge is concentrated along a fault line in the Armogosa Desert on the southwestern margin of the system. Eakin [1966] has described a similar system in a 20,000 km² region including much of the eastern portion of the Eureka Low; and Dinwiddie and Schroder [1971] report evidence for interbasin flows to depths greater than 2 km in valleys of the central portion of the Eureka Low. A general discussion of the problem has been given by Mifflin [1968], who summarizes evidence for large-scale interbasin flows in regions underlain by fractured carbonate rocks in southeastern Nevada. The observation of interbasin flow systems in this region makes it likely that the entire Eureka Low is caused by such systems and, in fact, that heat flow might be a useful means of studying them. As the heat flow is still poorly known in the Eureka Low, it is likely that the pattern is much more complex than indicated by the single contour that delineates it in Figure 12. Nevertheless, it is useful to make a very simple steady state order of magnitude calculation. Suppose water percolated downward uniformly in the Eureka Low at the average rate of 1 cm/yr, some 5-10% of the local annual precipitation. Then $s \sim 2$ km for 'rock' (equation (11c)). If the average depth of the interbasin conduit were ~ 1.4 km, according to (10), the surface heat flow would be roughly half the regional heat flow as required. If the recharge velocity ($-v$) were cut to 5 mm/yr, the regional depth of water flow would be 2.8 km. In the system studied by Winograd and Thordarson the average recharge rate required to supply the estimated annual discharge is about 2 mm/yr; for the system studied by Eakin it is about 5 mm/yr. These values seem consistent with the foregoing calculations, especially since the hydrologic systems studied each overlap the Eureka Low and may have somewhat higher mean heat flows. If the average heat flow anomaly in the Eureka Low is indeed about -1 HFU, the discharge required to complete the thermal balance can be compared to that of the hydrothermal systems by comparing the circles in Figure 12 to the mapped size of the Eureka Low. Next to the Yellowstone system the Eureka Low would have the greatest heat discharge. However, the temperature of the flow would be low, 30°-60°C above surface ambient according to (10) (when $-v = 1$ cm/yr and 5 mm/yr are used). Much of this heat is probably discharged convectively by warm springs; if it were not, it could cause a substantial positive heat flow anomaly. The possibility of interbasin flows on the scale suggested by the present configuration of the Eureka Low requires further investigation in connection with proposals for underground storage of nuclear wastes in such areas [see also Hunt and Robinson, 1960].

We shall return to the problem of convective transport in a later section; the next section considers the simpler crustal regime characteristic of regions where convection is unimportant.

Sierra Nevada and Eastern United States:
Effects of Radioactivity

It has been pointed out (5) that most crustal rocks seen at the surface contain enough radioactive uranium, thorium, and potassium to contribute appreciably to surface heat flow if such rocks were distributed uniformly through the crust. The cumulative contribution of crustal radioactivity must be known in order to determine from the surface heat flow the flux from the top of the mantle. Additionally, a knowledge of how crustal radionuclides are distributed vertically should lead to a better understanding of the thermal regime and geochemical evolution of the crust. Substantial progress has been made on these problems by studying the relation between surface heat flow and radioactive heat production of plutonic and highly metamorphosed crystalline rock exposed at the surface. Such rocks are the ones most likely to be related geochemically to the inaccessible material on which they rest.

Figure 13 is a plot of measured heat flow q versus radioactive heat production A_0 of crystalline drill core or outcrop material sampled at the heat flow site. The 150 or so points include all published results from the conterminous United States and adjacent Mexico and many new points of our own (heat productions were determined by our colleague, Carl Bunker, in Denver). Locations from which the data of Figure 13 were obtained are shown in Figure 14, to be discussed further below. Birch et al. [1968] discovered that a graph of heat flow versus heat production (q, A_0) for sites in New England yields a straight line, and Roy et al. [1968a] showed that the same line accommodated additional observations in the stable central region of the United States. Their line is shown in Figure 13 and labeled 'Eastern U.S.'; data from all of the locations east of the Great Plains (shown in Figure 14) lie close to this line (solid circles, Figure 13). Two other heat flow provinces were defined by (q, A_0) lines presented by Roy et al. [1968a], one for the Sierra Nevada and one for the Basin and Range province. Both lines are shown in Figure 13. The line for the Sierra Nevada province was confirmed by independent studies [Lachenbruch, 1968], and further confirmation has come from a value published more recently [Lachenbruch et al., 1976a]. Ten of the eleven points (crossed circles, Figure 13) interior to the Sierra Nevada physiographic province lie close to the Sierra line. The eleventh point for the Sierra Nevada (DP, near the top of Figure 13) lies far above the Sierra line, as was expected; the site is only 3 km from the Long Valley volcanic center. Most of the other points in Figure 13 are not close to any of these province lines, and they will be discussed later. However, it will be useful first to outline a simple interpretation of the linear relation for the Sierra Nevada and eastern United States; it provides general insight into conditions in the crust and mantle [Birch et al., 1968; Roy et al., 1968a; Lachenbruch, 1968, 1970].

The simplicity of the linear relation suggests a simple model. We assume one-dimensional steady state, nonconvective transfer and retain only the term for heat production $A(z)$ on the right side of (3).

$$\frac{dq}{dz} = -A(z) \quad (20)$$

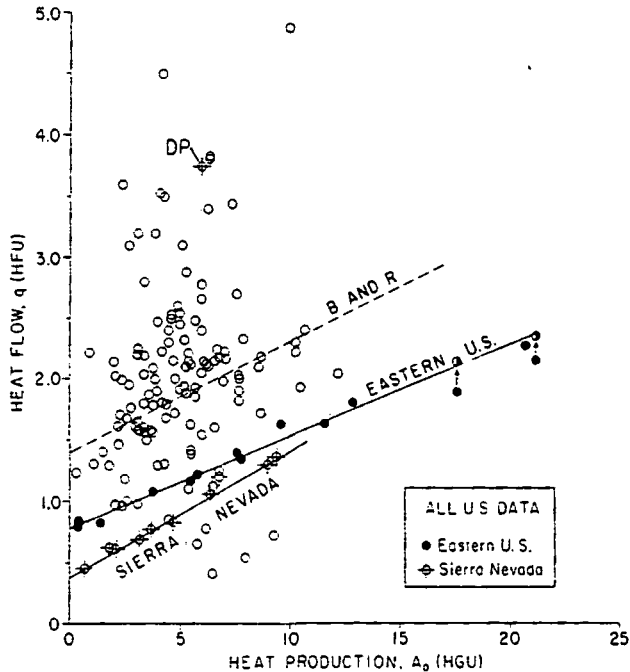


Fig. 13. Observations of heat flow q and radioactive heat production A_0 from crystalline rocks in the conterminous United States; linear regression lines are from Roy et al. [1968a] for the Basin and Range (dashed), eastern United States, and Sierra Nevada provinces. Solid circles represent points east of the Great Plains, and crossed circles represent points interior to the Sierra Nevada physiographic province. Vertical arrows represent corrections for finite size of plutons [Roy et al., 1968a]. Three of the open circles on the eastern United States curve at about 1 HFU are from the Klamath Mountains in northern California. The crossed circle slightly above the Sierra Nevada line ($q = 1.1$) has an uncertain heat production. DP is adjacent to the Long Valley volcanic center.

The linear relation for either province may be written

$$q = q^* + DA_0 \quad (21)$$

where q and A_0 are heat flow and heat production measured near the surface $z = 0_0$, and q^* and D are the intercept and slope parameters that define the heat flow province. Rocks at sites satisfying (21) vary greatly in age and have different histories of uplift and erosion; unless the relation (21) is an accident of the present, it should remain valid after erosion by an arbitrary amount z at any location. Thus if at any site a layer of thickness z is eroded away, A_0 will take on a new value $A(z)$ depending on how radioactivity is distributed with depth, and q will take on a new value $q(z)$, but (21) should still apply. Hence we let q be a function of z and replace A_0 by $A(z)$ in (21). Then substi-

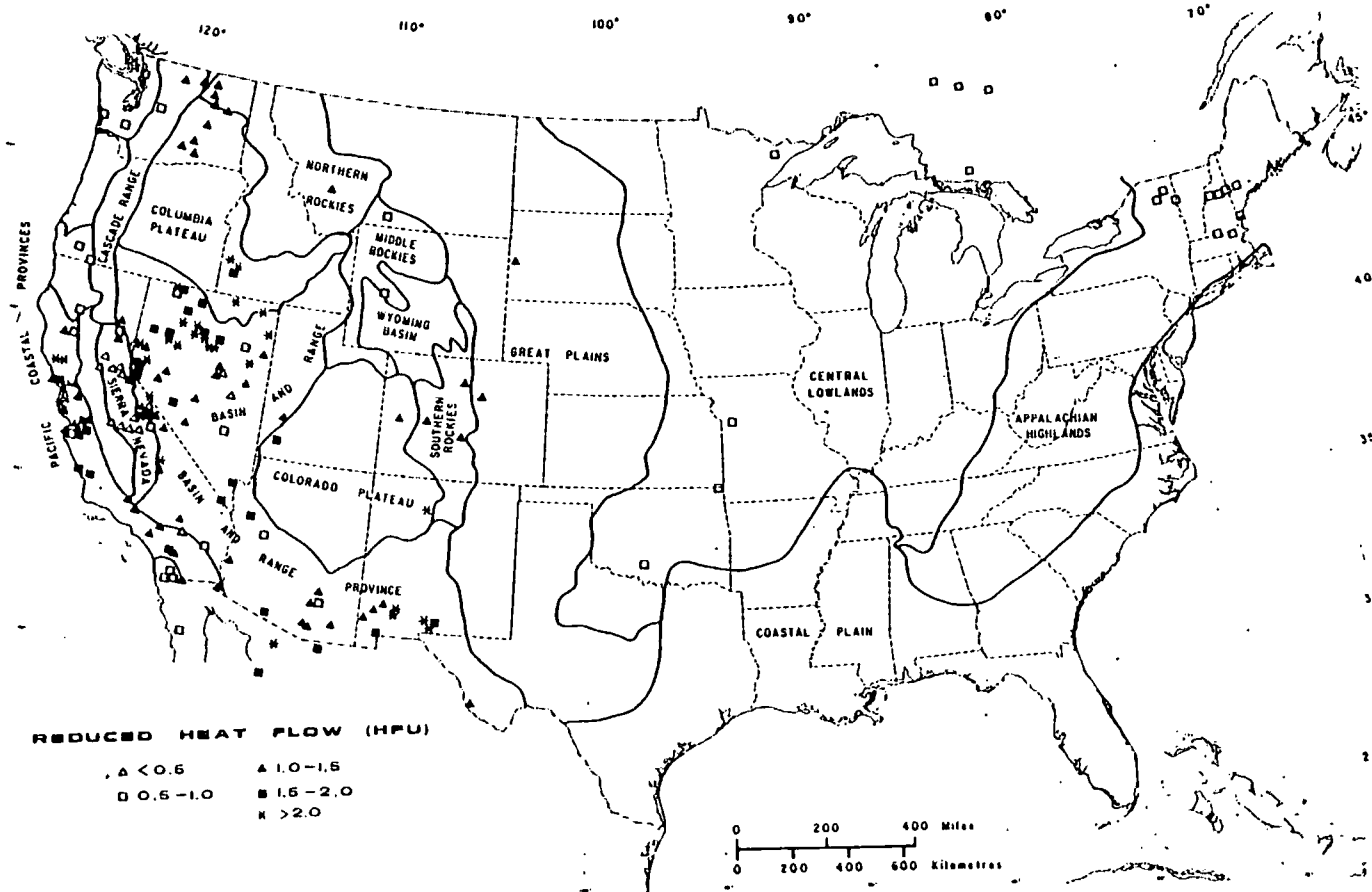


Fig. 14. Reduced heat flows and physiographic provinces (modified from Fenneman [1946].) Abbreviations are KM for Klamath Mountains, SAFZ for San Andreas Fault zone, and GV for Great Valley of California.

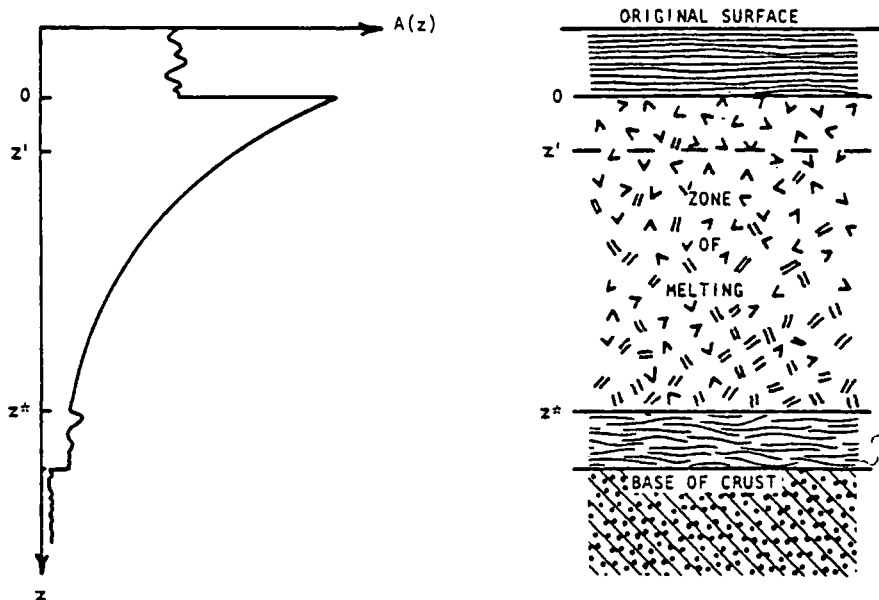


Fig. 15. Conceptual model for the distribution of heat production $A(z)$ in the continental crust (see text).

tuting (21) in (20) yields a unique result for heat production as a function of depth

$$A(z) = A_0 e^{-z/D} \quad (22)$$

where A_0 is the value on the presently exposed surface, $z = 0$. Suppose that this distribution extends to some depth z^* and that $q(z^*)$ is the heat flow at that depth. Then by using (22) the surface heat flow q is

$$q = q(z^*) + \int_{z^*}^0 A(z) dz \quad (23a)$$

$$q = [q(z^*) - DA_0 e^{-z^*/D}] + DA_0 \quad (23b)$$

The expression in brackets represents the empirically determined intercept q^* (equation (21)). The slope parameter D is about 7.5 km for the eastern United States and 10 km for the Sierra. Hence if the exponentially fractionated layer z^* extends throughout all or most of the crust ($z^* \gg D$), the exponential term in (23b) is small, and $q(z^*)$ corresponds approximately to q^* , which will probably be approximately the same as the mantle contribution. (For a more complete discussion, see Lachenbruch [1970].)

This simple model is illustrated conceptually in Figure 15. In the plutonic and highly metamorphosed rocks thought to make up most of the crust, U, Th, and K are fractionated upward exponentially, presumably by some process taking place during stages of partial melting or migration of metamorphic fluids [e.g., Lambert and Heier, 1967; Albarede, 1975].

The characteristic depth D is a parameter characterizing the fractionation process. If we assume that after equilibrium is established, heat flow into the lower crust q^* becomes uniform throughout the province, then subsequent measurements in exposed crystalline rocks would generally follow the linear relation observed (equation (21)).

Other assumptions regarding radioactivity of the lower crust are possible, and if the constraint imposed by differential erosion is set aside, source distributions in the upper crust other than (22) are permissible [see, e.g., Roy et al., 1968a; Lachenbruch, 1970; Blackwell, 1971]. Any simple source distribution model is, of course, approximate, as large variations are known to occur on all observable scales. Although direct observational evidence on the form of $A(z)$ is weak, statistical studies of heat production in deep boreholes [Lachenbruch, 1971; Lachenbruch and Bunker, 1971] and geologic studies of differentially eroded plutons [Swanberg, 1972] provide some support for the exponential model. In any case, as first pointed out by Birch et al. [1968], in provinces where the linear relation applies, local variations in heat flow are probably caused by variations in radioactivity strongly concentrated in the upper crust, and heat flow through the lower crust is evidently uniform. Important corollaries are that (1) convective heat transfer is probably insignificant in the crust in these provinces, for otherwise it would have to be uniform throughout each province, and (2) if transient conditions occur, they must be uniform throughout the province. This suggests a deep mantle origin for such transients; e.g., a cool subducted slab deep beneath the Sierra Nevada has been suggested to explain the very low q^* there [Roy et al., 1972; Blackwell, 1971].

For the exponential model described, crustal temperatures are given by [Lachenbruch, 1970]

$$\theta(z) = [q^*z + D^2A_0(1 - e^{-z/D})]/K \quad (24)$$

where K is thermal conductivity. Crustal temperatures for the appropriate province parameters (q^* , D) and for the ranges of heat production observed in each province are given for an assumed uniform conductivity ($K = 6 \text{ mcal/cm s } ^\circ\text{C}$) in Figure 16. Similar curves, some with different assumptions, can be found elsewhere [Roy et al., 1968a; Lachenbruch, 1968, 1970; Roy et al., 1972; Diment et al., 1975; Lachenbruch et al., 1976a; Blackwell, 1971]. However, in provinces where the linear relation is found to apply, crustal temperatures are severely constrained, and models more specialized than this simple one (equation (24)) do not give significantly different results. (The problem has been discussed by Blackwell [1971].) The chief uncertainty is in the choice of conductivity, which might be adjusted by $\pm 15\%$ with a proportional effect on the temperatures shown. For reference we have shown in Figure 16 the curves for the beginning of melting for granodiorite with pore water present (GSS) and without it (GDS); they are discussed further in the next section.

In the highly radioactive rocks of New England (shaded on map, Figure 2) crustal temperatures probably lie between the central and upper (eastern United States) curves ($A_0 = 10$ and 20 HGU) of Figure 16, whereas for most of the eastern United States, temperatures are expected to lie in the lower half of the range shown (between $A_0 = 0$ and $A_0 = 10 \text{ HGU}$). For the Sierra Nevada curves, temperatures in the upper range

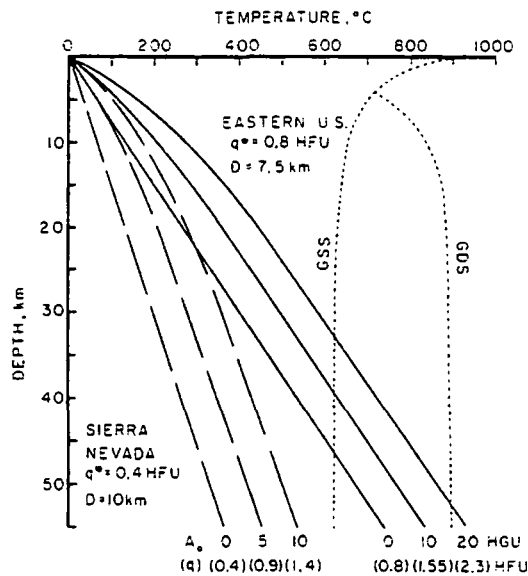


Fig. 16. Steady crustal temperature profiles based on the linear heat flow-heat production relation (equation (24)) for the Sierra Nevada (long-dashed curves) and the central and eastern United States (solid curves) for the range of heat production (A_0) observed in each province. Corresponding values of heat flow (q) are shown in parentheses. Assumed thermal conductivity is $6 \text{ mcal/cm s } ^\circ\text{C}$. Short-dashed curves GSS (granodiorite saturated solidus) and GDS (granodiorite dry solidus) from Wyllie [1971] show the beginning of melting for rock of intermediate composition.

($A_0 = 5$ to 10 HGU , Figure 16) are characteristic of the younger (Upper Cretaceous) plutons near the crest of the mountain system, and in the lower range ($A_0 = 0$ to 5 HGU) they generally represent conditions in the western foothills. For the same heat flow, temperatures are lower in the Sierra Nevada, where a smaller fraction of the heat originates at depth ($q^* = 0.4 \text{ HFU}$ in the Sierra and $q^* = 0.8 \text{ HFU}$ in the eastern United States).

The Basin and Range Province: Effects of Radioactivity and Convection

The third heat flow province defined by Roy et al. [1968a] is the Basin and Range province, for which all current (q , A_0) data are shown in Figure 17. The locations from which these data were obtained are indicated by the points within the Basin and Range province boundary in Figure 14 and those points in Mexico south of Arizona [from Smith, 1974]. The regression line (dashed, Figure 17) determined by Roy et al. [1968a] from 12 of 15 available data pairs had a slope D of $9.4 \pm 1.3 \text{ km}$ and intercept q^* of $1.4 \pm 0.09 \text{ HFU}$. It is clear from the scatter in Figure 17 that if the Basin and Range province is in some sense represented by this line, it is not in the same sense that the

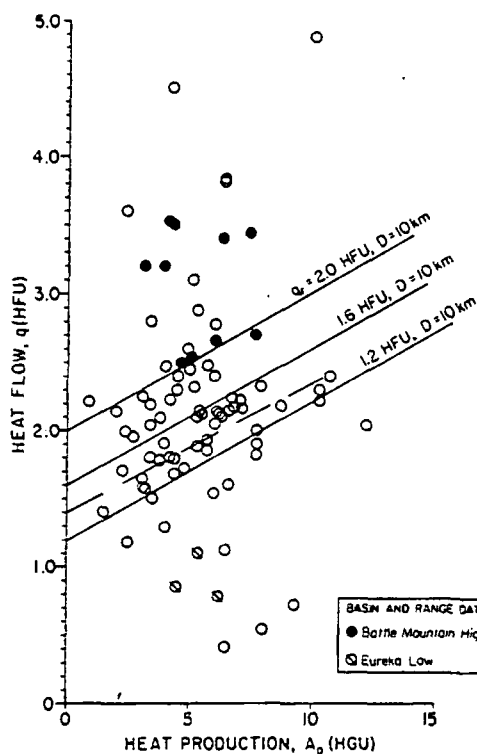


Fig. 17. Observations of heat flow q and radioactive heat production A_0 from crystalline rock of the Basin and Range province. Regression line from earlier studies is dashed.

Sierra Nevada and eastern United States provinces are represented by their lines (Figure 13). As the Basin and Range province now has by far the most observations, it could be argued that the linear regression lines will lose their significance in the other provinces, too, as more data are acquired. However, we consider this unlikely, as the density of observation is presently as great in the Sierra Nevada as it is in the Basin and Range, and it was recognized at the outset by Roy et al. [1968a] that the regression analysis was least significant in the Basin and Range province. A more discriminating use of the variable quality data shown in Figure 17 might provide justification for a linear relation in the Basin and Range or parts of it, and this is under study. For the present, however, it appears that the linear regression of q on A_0 has little significance in the Basin and Range province, and the question arises whether insights from the foregoing simple model of the linear relation can be applied usefully there.

According to the simple model the steady state contribution from crustal radioactivity is DA_0 , where D is a geochemical characteristic of the crust describing its fractionation. This physical interpretation does not depend upon the constancy of lower crustal heat flow (q^*) and is reasonable whether or not the linear relation applies. On this basis, we might subtract the term for crustal radioactivity from the

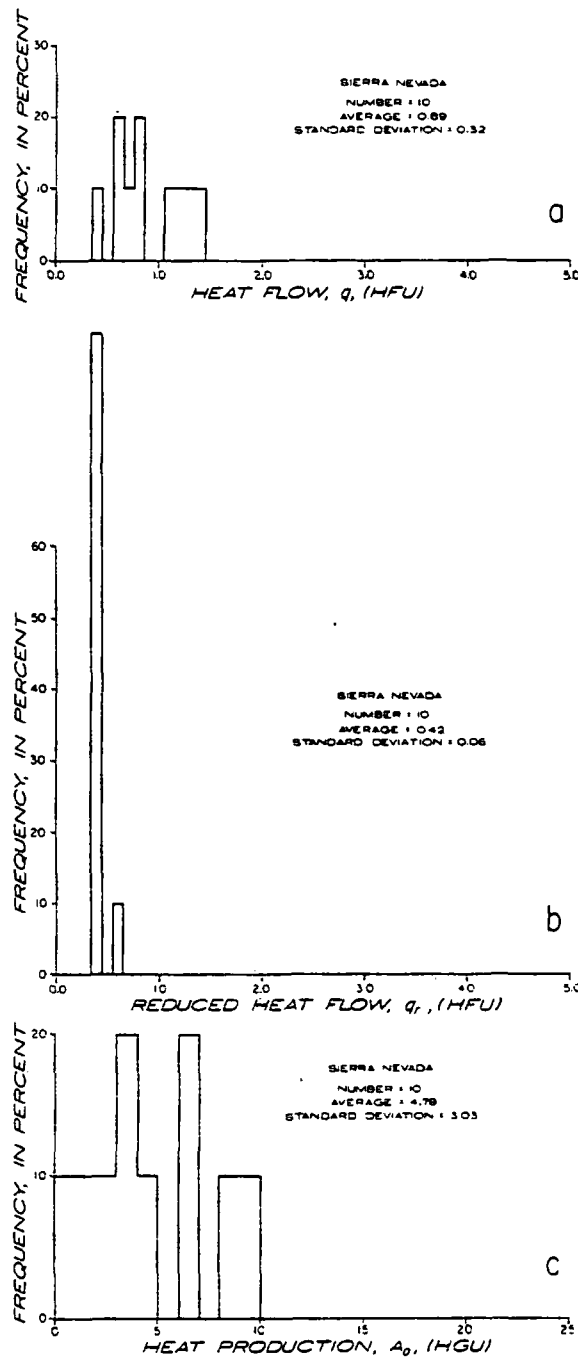


Fig. 18. Histograms of (a) heat flow, (b) reduced heat flow, and (c) radioactive heat production for stations at which both q and A_0 were measured in the Sierra Nevada province.

observed heat flow to obtain the 'reduced heat flow' q_r employed by Roy et al. [1972].

$$q_r = q - DA_o \quad (25)$$

Although D is not known directly for the Basin and Range, we might reasonably assume it to have the constant value of 10 km, firmly established in contiguous rocks of the adjacent Sierra Nevada province (granitic rocks in the western Basin and Range province are part of the Sierra Nevada batholith).

Histograms of the three variables in (25), heat flow q , reduced heat flow q_r , and heat production A_o , are shown in parts a, b, and c, respectively, of Figures 18-20 for the three provinces. For a province in which the linear relation applied in a deterministic sense, q_r would be identical to q^* , a constant (equation (21)). It is seen from Figures 18 and 19 that this is nearly the case for the Sierra Nevada and eastern United States. In such provinces the simple interpretive model gives q_r a clear-cut physical meaning; it is the uniform flux q^* from the mantle or at least the lower crust. No such interpretation is possible for the Basin and Range, where q_r is widely dispersed (Figure 20b). A second distinctive feature of the Basin and Range data (Figure 20b) is the large mean value for q_r , about 1.6 HFU or twice the value for the stable eastern United States usually considered as normal. On the basis of an earlier discussion we believe that the large dispersion results primarily from convection by groundwater, and the large mean, from convection by magma. Before discussing implications of these two inferences we shall consider how widespread the conditions represented by the sample in Figure 20 might be.

In brackets in Figures 20a and 20b, statistics are given for the Basin and Range province excluding determinations in the anomalous subprovinces (10 values from the Battle Mountain High and 3 values from the Eureka Low). For comparison, we show in Figure 21 the corresponding results for the complete population of heat flow measurements in the Basin and Range province; again the brackets enclose statistics determined with the two subprovinces excluded (20 values from the Battle Mountain High and 13 values from the Eureka Low). The fact that the principal mode, the mean, and the standard deviation are essentially the same for data in brackets in Figures 20a and 21 adds a note of generality to the analysis of data in Figure 20. However, without a more careful study of the individual sites than we have yet undertaken, more refined statistical treatment is not warranted. Reduced heat flows reported from the northern and southern Rocky Mountains and the Columbia Plateau (Figure 14) seem commonly to fall in the modal range (1.2-1.6 HFU) characteristic of the Basin and Range data, and those provinces are expected to have similar crustal regimes [see Blackwell, 1969, 1971; Roy et al., 1972]. We have focused on the Basin and Range province because it seems to represent a fairly continuous tectonic unit, and the heat flow coverage there is relatively dense.

The reduction for crustal radioactivity in the Basin and Range province does not significantly reduce the dispersion, and we should be little better off in estimating the heat flow with a knowledge of local radioactivity than without it. This does not mean that the reduction (25) for crustal radioactivity in the Basin and Range is not valid. The

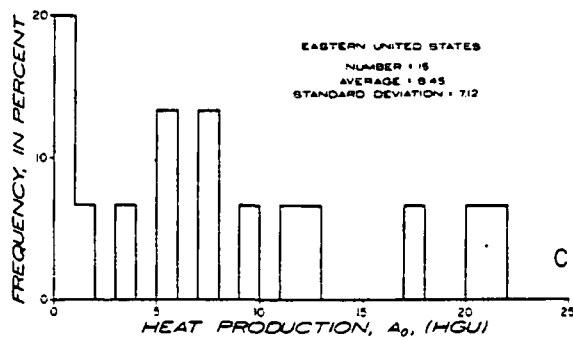
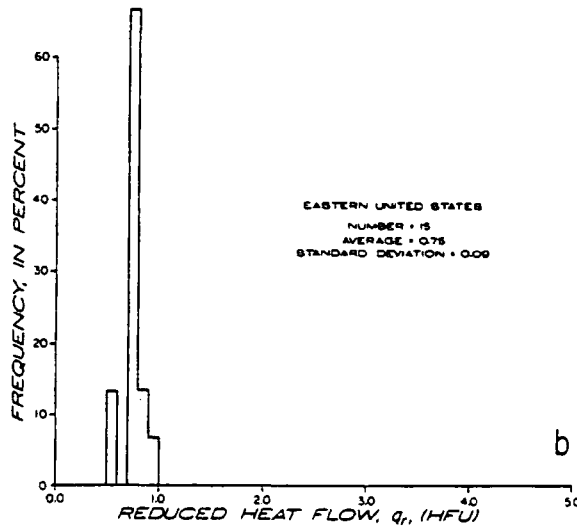
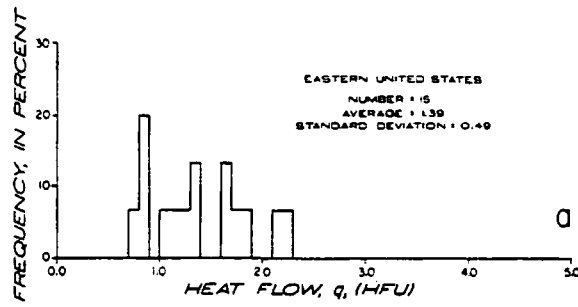


Fig. 19. Histograms of (a) heat flow, (b) reduced heat flow, and (c) radioactive heat production for stations at which both q and A_0 were measured in the eastern United States province (i.e., east of the Great Plains).

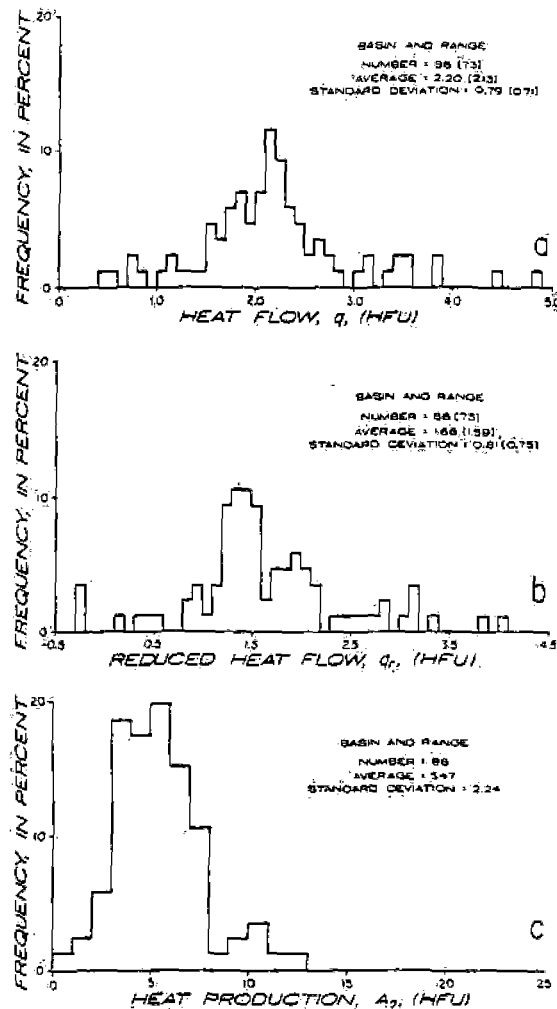


Fig. 20. Histograms of (a) heat flow, (b) reduced heat flow, and (c) radioactive heat production for stations at which both q and A_0 were measured in the Basin and Range province. Statistics in brackets in (a) and (b) were determined with data from Battle Mountain High and Eureka Low deleted.

standard deviation of the crustal correction (DA , with $D = 10$ km, Figure 20c) is only 0.22 HFU, about one fourth of the standard deviations for both q and q_r . If q and A_0 were normally distributed, the reduction from q to q_r (equation (25)) would have an insignificant effect on the standard deviation (≈ 0.03 HFU). The statistics do suggest that three-dimensional effects, thermal transients, and convection, neglected in the simple theory (equation (20)), are substantially greater (generally by a factor of 3 or 4) than the effects of variable crustal radioactivity. As three-dimensional effects are evidently unimportant in the other provinces, it is likely that the dispersion of

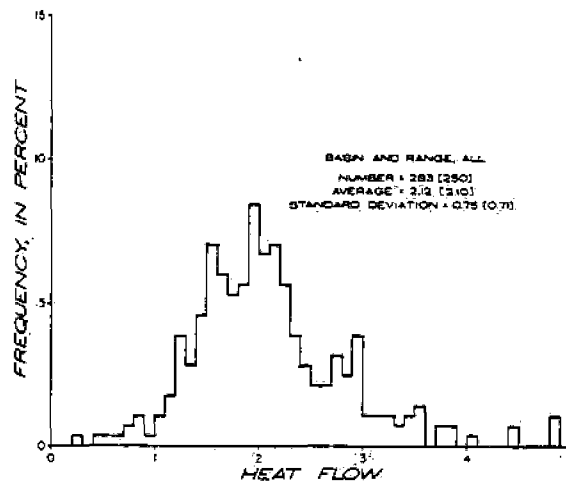


Fig. 21. Histogram of all heat flow data from the Basin and Range province. Statistics in brackets were determined with data from the Battle Mountain High and Eureka Low deleted.

reduced heat flow in the Basin and Range is due primarily to hydrothermal and (to a lesser extent) magmatic convection, including, of course, their time dependent effects, as discussed in an earlier section.

We have mentioned that in the Basin and Range province the mean conductive flux reduced for crustal radioactivity is about twice as large as would be expected in stable regions. We naturally associate this large and variable reduced heat flow with the present pattern of extensional deformation, magmatism, and hot spring activity that has probably characterized the province for the past 17 m.y. [Thompson and Burke, 1974]. It has been shown that convective processes operating solely within the crust over this time (twice the conductive time constant for the crust) would probably reduce the mean conductive flux, not increase it. Hence the excess heat is probably supplied convectively by magma rising across (and possibly beneath) the base of the crust. Regional variations in the intensity of this magmatic upflux are probably responsible for high heat flow subprovinces like the Battle Mountain High and the Rio Grande Trough, and for local silicic volcanic centers like the Long Valley caldera as well. It is likely that these variations are, in turn, caused by local variations in the rate of crustal extension [Lachenbruch et al., 1976a] (A. R. Lachenbruch and J. H. Sass, unpublished models).

It is useful to assume that over large areas the crust is in a quasi-steady state, receiving as much heat by conduction and convection across its base as it gives off by conduction and convection at its surface. As q_c is normally estimated from the conductive heat flow, the actual mantle contribution would be larger than q_c by the amount of convective loss from hot and warm springs and volcanoes. However, the heat delivered by post-Oligocene extrusive rocks in the Great Basin is negligible in relation to the conductive heat flow, and judging from Figure 12, the net effect of the hotter known springs might not be important on a regional scale. Nevertheless details of the total hydrologic heat loss

are poorly known, and we shall neglect them although they could be significant. In regions where the convective flux is known, it can be accommodated in the computation of q_r (by using combined surface flux q_c instead of q in equation (25)) if the steady state assumption seems to warrant it.

If there is a characteristic flux into the lower crust of the Basin and Range, it is likely that it is represented by the modal value of q_r , with the nonmodal values generally representing superimposed anomalous convective effects. Excluding the two subprovinces, almost half the values of q_r fall in the modal range 1.2-1.6 HFU (Figure 20b). (Interestingly, the value of q^* originally determined from linear regression by Roy et al. [1968a] was 1.4 HFU.) The Battle Mountain High, a positive anomaly with lateral dimensions of many crustal thicknesses, has been defined as a region with $q > 2.5$, but it is essentially unchanged if defined as the region $q_r > 2$. Figure 22 shows crustal profiles (equation (24)) for a steady conductive mantle flux q_r of 1.2 and 1.6, which might bracket the 'characteristic' conditions in the Basin and Range province, and of 2.0 and 2.5, which are intended to represent (lower) limiting and typical conditions in the Battle Mountain High. (The mean for the 20 heat flows in the Battle Mountain High is 3.0 ± 0.4 standard deviation; the mean for the 10 reduced heat flows is 2.5 ± 0.4 standard deviation.) As such large variations in q_r (from 1.2 to 2.5) have a far greater effect on temperature than variations in radioactivity, the curves are shown only for the near-average A_0 of 5 HGU (Figure 20c). Likely variations in A_0 (of ± 3 HGU, Figure 20c) would change the deep crustal temperatures by only $\pm 50^\circ\text{C}$. Variations in thermal conductivity of $\pm 15\%$ from the assumed value of $6 \text{ mcal/cm s } ^\circ\text{C}$ would change the temperatures in Figure 22 by $\pm 15\%$. Shown also in Figure 22 is the curve for the Sierra Nevada ($q^* = 0.4$ HFU) and the curve for $q^* = 0.8$ HFU, which is similar to that for the stable eastern United States except that it is drawn for $D = 10 \text{ km}$ (instead of 7.5 km) for consistency. The latter is a useful (if somewhat arbitrary) reference for conditions one might expect in the Basin and Range crust if it were underlain by a stable mantle; it differs from the corresponding curve ($q^* = 0.8$ HFU, $D = 7.5 \text{ km}$) for the stable eastern United States by less than 45°C .

Although the curves in Figure 22 are drawn as if all of the mantle flux q_r were conducted from the base of the crust, this condition is not required nor is it expected to apply in the hotter regimes. Insofar as our observations at the surface are concerned, the anomalous source may be produced by repeated intrusion at any depth; if the source persists long enough to establish a steady state, the temperatures above it will fall on the appropriate curve of Figure 22. The time $\tau(z)$ required for a sill-like constant temperature source to equilibrate the overburden is shown on the depth axis in Figure 22. (A sill-like source whose strength does not change with time takes about three times as long. During the slow cooling following solidification the average gradient anomaly in the overburden will remain rather close to that measured at the surface, provided that the original source persisted for many τ .) Thus a continuing intrusive process that maintained the 20-km temperature at 900°C for more than 3 m.y. would cause a conductive regime above it as indicated by curve F (Figure 22); thereafter, downward extrapolation from surface observations would correctly identify the 20-km temperature.

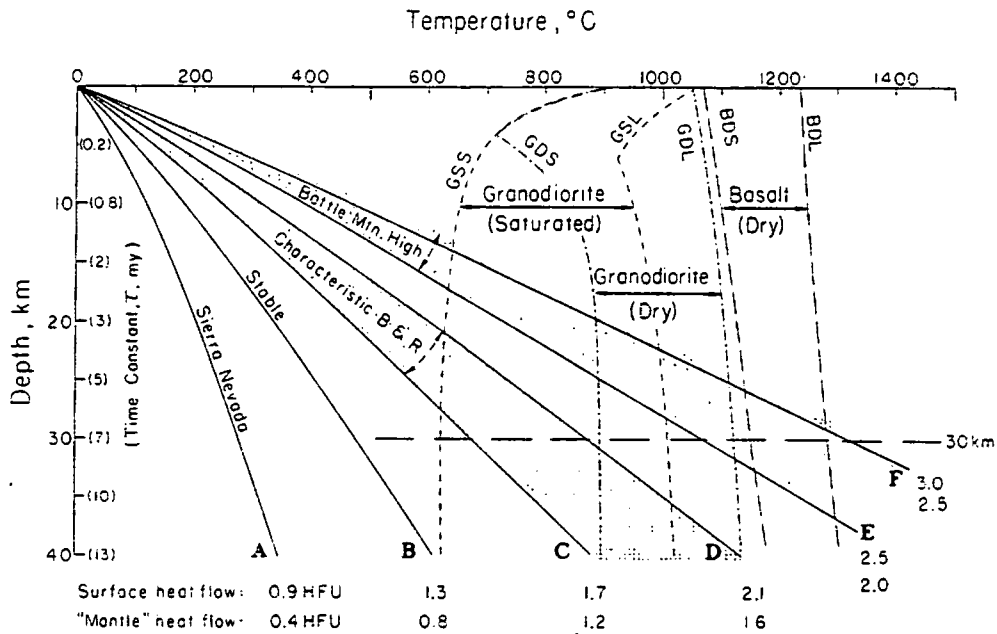


Fig. 22. Generalized conductive temperature profiles for the Sierra Nevada crust (A), a stable reference crust (see text) (B), the characteristic Basin and Range crust (C to D), and lower limiting (E) and typical (F) conditions in the crust of the Battle Mountain High. All curves are drawn for a surface heat production (A_s) of 5 HGU and thermal conductivity (K) of 6 mcal/cm s °C (equation (24)). Corresponding surface heat flow and reduced or 'mantle' heat flow are shown at the bottom of each curve. Melting relations [after Wyllie, 1971] are shown for intermediate crustal rock by the curves GSS (granodiorite saturated solidus), GDS (granodiorite saturated liquidus), GSL (granodiorite dry solidus), and GDL (granodiorite dry liquidus) and for basalt by BDS (basalt dry solidus), and BDL (basalt dry liquidus). In parentheses on the depth axis is shown the time required for the overburden to approach thermal equilibrium after intrusion by a sill maintained at constant temperature.

Above the intrusion we would measure a surface heat flow of 3 HFU and a reduced heat flow of 2.5, and (relative to curve B, Figure 22) the contribution of anomalous convected flux would be 1.7 HFU. The actual anomalous flux into the lithosphere at the time might be greater or less than 1.7 HFU, depending upon whether the lower portion was absorbing or releasing heat, i.e., whether its temperature was approaching the new stationary state from below or above. Convective transfer by magma rising in the lower crust (below 20 km in this example) would cause mean temperatures there to be less than indicated by the conductive curve F (A. H. Lachenbruch and J. H. Sass, unpublished models). Convection in this lower region might involve no more than the upward movement of basalt in narrow conduits en route to the 20-km depth, or it could

involve complex networks of basaltic intrusion and secondary diapiric movements of silicic melts and adjustments of solid rock.

In Figure 22 we have shown [from Wyllie, 1971] some limiting melting relations for materials likely to be involved in convective heat transport to and through an anomalously hot crust. The most probable source of anomalous heat is upward migration of basalt (or possibly other mantle-derived magma) beneath or into the base of the crust. For reasonable water contents, most of the crystallization and hence most of the latent heat release will have occurred by the time the basalt cools past its dry solidus (BDS, Figure 22) [Wyllie, 1971; Peck et al., 1966]. Heat introduced by the basalt could raise the temperature and melt fractions of the indigenous crustal material, assumed to have an intermediate (granodiorite) composition. In the presence of excess water ('vapor present condition'), such rocks would begin to melt along the curve GSS (granodiorite saturated solidus) (Figure 22), and melting would be complete at GSL (granodiorite saturated liquidus). If no water occurred in the crustal rock except that bound in hydrous minerals, melting would not begin until temperatures exceeded GDS (granodiorite dry solidus), and it would not be complete until they reached GDL (granodiorite dry liquidus). If a trace of pore water were present, it would dissolve preferentially in a melt (of rhyolite composition) that would begin to form along GSS. With further increase of temperature the increasing melted fraction would become more and more undersaturated, making the residual crystals more difficult to melt; complete melting would not occur until temperatures approached GDL. As the radioactive elements, like the water, move preferentially into the melt, upward migration of the melt might produce the condition illustrated schematically in Figure 15 and at the same time dehydrate the lower crust. Wyllie [1971] has pointed out that unless the lower crust were somehow rehydrated, a second cycle of lower crustal melting would be more difficult, as it would require temperatures in excess of GDS. If repeated cycles did occur, however, we might expect more complete upward fractionation of radioelements. This would appear in surface observations as a decrease in the value of the characteristic depth D (equation (21)).

It is seen from Figure 22 that at the base of a 30-km crust in the Battle Mountain High, basalt melt could be stable, and dry intermediate crustal rock could be completely melted. Hence some heat is probably transferred by magmatic intrusion in the lower crust of the Battle Mountain High, for if it were not, the thermal regime would be conductive, and the base would be nearly or quite all melted. Substantial amounts of melting of most crustal rocks in the presence of pore water could occur near the base of a 30-km crust in the 'characteristic Basin and Range' regimes. Hence 'first cycle' (wet) crustal fractionation could be initiated under the Basin and Range regimes, and 'second cycle' (dry) fractionation could occur under the Battle Mountain High regime. Convection by quasi-steady upward migration of a melted fraction could, of course, convert one regime to the other.

Typically, the upper 20 km of the Basin and Range crust has a seismic velocity ($V_p \approx 6.0$ km/s) characteristic of silicic rocks, including granite, and the lower 10 km or so has a higher velocity ($V_p \approx 6.7$ km/s) characteristic of denser (and presumably more refractory) materials, including basalt [e.g., Hill and Bakiser, 1966]. As temperatures in the Battle Mountain High and similar regions can be in the range 700°-900°C

at depths of 15-20 km (curve F, Figure 22), laterally extensive partial silicic melts could occur at midcrustal levels in such regions. Convective transfer attending stretching and intrusion of the extending lithosphere could, however, reduce these temperature estimates by 100°C or so (A. H. Lachenbruch and J. H. Sass, unpublished).

In summary, we have found that the linear relation between heat flow and surface radioactivity does not apply generally in the Basin and Range province. For the linear relation to apply, crustal contributions to heat flow should be exclusively from radioactivity, and the mantle flux should be uniform. We believe that the relation fails in the Basin and Range province because both conditions are violated there. Variations in surface heat flow caused by hydrothermal and magmatic convection overshadow variations caused by crustal radioactivity (they are probably greater by a factor of 3 or 4), and the anomalously large mantle flux is not uniform. Mantle heat flux is probably controlled by magmatic mass flux (into or beneath the base of the crust) which varies in intensity, creating subprovinces like the Battle Mountain High and the Rio Grande Rift, and more local heat flow anomalies and volcanic centers as well (Figure 3). Frequently occurring values of reduced heat flow suggest that the mantle flux throughout much of the province might have characteristic values in the range 1.2-1.6 HFU. These considerations form the basis for construction of generalized crustal temperature profiles which can be discussed in terms of melting relations for crustal rocks. Theoretical temperatures are consistent with the extensive manifestations of magmatic activity observed in the province.

Discussion and Summary

Our knowledge of regional heat flow in the United States has been acquired only recently. In his review of the status of geothermal investigations in 1954, Birch [1954a] was able to cite only three 'reasonably adequate' determinations (0.93 HFU in northern Michigan [Birch, 1954b], 1.7 HFU in the Colorado Front Range [Birch, 1950], and 1.29 HFU in the Central Valley of California [Benfield, 1947]). Although we now know that each of these values is quite representative of its geologic province, little could be deduced about regional patterns from three determinations. In a review about a decade later, Lee and Uyeda [1965] listed heat flow from about 40 distinct sites in the conterminous United States; the data indicated that heat flow was generally higher in the tectonically active western United States than in the more stable eastern and central portions. A few years later, publication of over 100 new values [Roy et al., 1968b; Blackwell, 1969] revealed correlations between heat flow and higher-order tectonic and geologic features, chiefly, high heat flow in New England and in the Basin and Range province, the northern and southern Rockies, and the Columbia Plateau and a band of lower heat flow near the Pacific Coast, features shown in the maps of Roy et al. [1972] and Blackwell [1971]. A map by Diment et al. [1972] showed the systematic variations of heat flow in the Appalachian Mountain region. Sass et al. [1971] presented 100 or so additional values revealing the strong correlation of heat flow with the major N-S trending tectonic provinces of California, including the San Andreas Fault zone. They also defined subprovinces of high and low heat flow in the Basin and Range province, to which an-

other, the Rio Grande Rift, has more recently been added [Decker and Smithson, 1975; Reiter et al., 1975]. Further detail is shown in the map presented here, and we can, of course, expect the trend to continue.

Our understanding of these heat flow observations was increased substantially in 1968 by the discovery of the linear relation between heat flow and surface radioactivity in New England [Birch et al., 1968], its application to other provinces [Roy et al., 1968a], and its independent confirmation for the Sierra Nevada [Lachenbruch, 1968]. Curiously, 8 years later we still do not know how general this relation might be. It has been shown above that in one of the provinces where the relation was formerly thought to apply approximately (the Basin and Range province), it does not apply. Although the relation is now supported by studies in crystalline rocks of Canada [Cermak and Jessop, 1971], Australia [Jaeger, 1970; Sass et al., 1976c], India [Rao et al., 1976], and Norway [Swanberg et al., 1974], the most convincing results remain those from the provinces in which the relation was first discovered, the eastern United States and the Sierra Nevada. As anticipated by Roy et al. [1968a], data from the Canadian Shield [Cermak and Jessop, 1971] and to a lesser extent those from central Australia are accommodated reasonably well by the line for the stable eastern United States, but the parameters determined from these areas independently are somewhat different; in particular, the values $q^* = 0.64$ HFU and $D = 11.1$ km for nine points in central Australia [Sass et al., 1976c] seem significantly different. Several isolated determinations such as the three from the Klamath Mountains in northern California (Figure 13 and Lachenbruch and Sass [1973]) and two from Precambrian rocks in southern India [Rao et al., 1976] fall on the eastern United States curve. The data from southern Norway [Swanberg et al., 1974] lie rather close to the Sierra Nevada line; the linear regression analysis there yielded $q^* = 0.48$ HFU and $D = 8.4$ km. However, nine points from Precambrian rocks of western Australia [Sass et al., 1976c] yield $q^* = 0.63$ and $D = 4.5$ km, a line quite different from those observed elsewhere, and four points from northern and central India [Rao et al., 1976] yield $q^* = 0.92$ HFU and $D = 14.8$ km. Judging from our experience with the Basin and Range province, many more observations will be needed in all of these areas, and others, to establish the general significance of the relation between heat flow and radioactivity in crystalline rocks. As we have remarked, the importance of this relation is the requirement it places on the vertical distribution of crustal radioactivity and to a lesser extent on the total contribution of crustal radioactivity to surface heat flow. These requirements relate to the processes responsible for evolution of the continental crust. In order for the linear relation to obtain, several other special requirements must be met [Lachenbruch, 1970]; i.e., three-dimensional conductive effects and magmatic and hydrothermal convection must be negligible in the crust, and crustal transients and mantle heat flow must be uniform throughout the province. Thus the linear relation can be expected to apply only in more stable regions, and even there, only under rather special circumstances. Nevertheless, the insight obtained from the relation can provide a basis for estimating the contribution of crustal radioactivity elsewhere on the continents. Thus the 'reduced heat flow,' obtained by subtracting the estimated crustal contribution from observed heat flow [Roy et al., 1972], might be used to interpret continental heat flow

where the linear relation does not apply. As the reduction depends upon the value of D , which varies around the world by a factor of 3, according to presently available studies, the reduction must be applied with caution. The justification for using $D = 10$ km in the Basin and Range province is provided by the linear relation observed in the Sierra Nevada and the observation that granitic rocks in the western Basin and Range at least are part of the Sierra Nevada batholith. Reasonably confident reductions can sometimes be made in regions where crystalline rock is not exposed if enough information on crustal composition is available from other sources. Examples are the California coast ranges, where the thickness of the Franciscan formation (of known radioactivity) is estimated from seismic studies [Lachenbruch and Sass, 1973], and the Pacific Northwest coastal provinces, where the basement rock is believed to be largely mafic [Blackwell, 1971; Sass et al., 1971] and hence to have rather low radioactivity. It is seen from Figure 14 that reduced heat flow estimated for sites along the Pacific Coast is generally in the range characteristic of the eastern United States except in the band through western and south central California enclosing the San Andreas Fault, where it is generally similar to values in the Basin and Range province.

A rather complete description of regional heat flow in the United States and a thorough understanding of its implications for thermal state and processes in the crust will probably be needed for a comprehensive assessment of our geothermal energy resource and the formulation of rational plans for exploring it and exploiting it. As we have seen, even in regions where the heat flow is low and the likelihood of an exploitable resource is slight, the understanding obtained from heat flow studies can be important for unraveling the more complex thermal problems in high heat flow areas. It is seen from Figures 1-3 that only now, with more than 600 determinations, are the areas of extremely high heat flow beginning to emerge as regional features; their boundaries are generally unknown, however, and few areas are sampled adequately for an understanding of hydrothermal systems in a crustal context. Large areas of the heat flow control map (Figure 1) are blank. Ironically, many of these are oil-producing areas where every year more than 10,000 holes are drilled and temperatures are measured. It is likely that a knowledge of regional heat flow in these areas would increase our understanding of the widely discussed 'geopressured' energy resources of the Gulf Coast [see, e.g., Jones, 1969; Jones and Wallace, 1974; Papadopoulos et al., 1975] and of the general problem of thermal evolution of sedimentary basins and the maturation of hydrocarbons. A comprehensive compilation of temperature gradient from some 25,000 sites in oil-producing areas of North America has recently been published by the American Association of Petroleum Geologists in cooperation with the USGS [American Association of Petroleum Geologists-U.S. Geological Survey, 1976]; it contains much useful regional information. However, as was emphasized by Birch [1954a], the principal variable affecting temperature gradient in the outer layers of the crust is thermal conductivity (and locally, water movement). Hence a compilation of the temperature gradient alone can be expected to tell us much more about the variations in conductivity (and locally, water movement) than about variations in the more fundamental quantity, heat flow. Regional heat flow studies are proceeding at a modest pace (limited by the avail-

ability of drill holes) at a handful of research laboratories across the country. In view of the importance of regional studies to the energy industries and the enormous amount of drilling they undertake, more interaction between these groups should hold substantial advantage for all.

Heat convected by moving groundwater requires careful attention in heat flow studies; it can perturb or completely dominate the regional flux associated with the crustal regime at depth. In tectonically active regions, open fractures, permeable volcanic rocks, and high heat flow may result in circulatory convection systems driven primarily by thermal density differences. Such systems are expected to produce perturbations to surface heat flux which change sign over lateral distances of the order of the depth of circulation, probably up to many kilometers. If the system is sustained by upper crustal magmatic intrusion, the combined flux at the surface might be much greater than the regional value for millions of years. If the system is sustained by regional heat flow, the combined flux will probably fall to the regional value after 10^3 - 10^5 years (depending on circulation depth), but a lingering conduction anomaly will persist long after the circulation stops. Perturbations caused by these systems create large dispersion in conductive flux from tectonically active regions, making it difficult to identify and interpret the regional heat flow without a dense network of observations [see, e.g., Blackwell and Baag, 1973; Blackwell et al., 1975; Brott et al., 1976; Combs, 1975; Lachenbruch et al., 1976b; Sass and Sammel, 1976; Sass et al., 1976b, d]. Hydrothermal convection systems constitute most of the targets under investigation as potential sources of geothermal energy, and much will no doubt be learned about their inner workings in the next few years. We expect that the increased understanding of the dynamics of these systems will help in the interpretation of regional heat flow and that the better understanding of regional heat flow will, in turn, increase our general understanding of the broader crustal conditions that generate hydrothermal systems. In regions like the Battle Mountain High, where the average heat flow is about 3 HFU, the steady gradient in poorly conducting sediments is typically about $100^\circ\text{C}/\text{km}$, and under favorable conditions a commercial energy resource could exist beneath deep sedimentary basins, even in the absence of hydrothermal convection [see, e.g., Diment et al., 1975].

Large disturbances to regional heat flow can also be caused by groundwater circulation forced by the distribution of precipitation, topography, and permeable formations. In some regions mantled by permeable volcanic rocks, downward percolation can completely 'wash out' the conductive flux, making it impossible to study regional heat flow by conventional means. In other regions like the Eureka Low, effects can be more subtle. Evidence there suggests that a negative heat flow anomaly over an area $\sim 3 \times 10^4 \text{ km}^2$ might be caused by interbasin flow in deep aquifers fed by downward percolation of a small fraction of the annual precipitation. Heat flow results of this sort can provide useful information on regional hydrologic patterns with important implications for underground disposal of radioactive waste.

Acknowledgments. We are grateful to our colleagues, R. L. Christiansen, W. H. Diment, D. R. Mabey, L. J. P. Muffler, M. Nathenson, F. H. Olmsted, M. L. Sorey, D. E. White, and D. L. Williams, for helpful

comments on the manuscript and to B. V. Marshall, S. P. Galanis, Jr., and R. J. Munroe for assistance with computations and illustrations.

References

- Albarede, F., The heat flow/heat generation relationship: An interaction model of fluids with cooling intrusions, *Earth Planet. Sci. Lett.*, 27, 73-78, 1975.
- American Association of Petroleum Geologists-U.S. Geological Survey, Geothermal gradient map of North America, scale 1:5,000,000, U.S. Geol. Surv., Reston, Virginia, 1976.
- Bailey, R. A., G. B. Dalrymple, and M. A. Lanphere, Volcanism, structure, and geochronology of Long Valley caldera, Mono County, California, *J. Geophys. Res.*, 81, 725-744, 1976.
- Benfield, A. E., A heat flow value for a well in California, *Amer. J. Sci.*, 245, 1-18, 1947.
- Birch, F., Flow of heat in the Front Range, Colorado, *Geol. Soc. Amer. Bull.*, 61, 567-630, 1950.
- Birch, F., The present state of geothermal investigations, *Geophysics*, 19, 645-659, 1954a.
- Birch, F., Thermal conductivity, climatic variation, and heat flow near Calumet, Michigan, *Amer. J. Sci.*, 252, 1-25, 1954b.
- Birch, F., R. F. Roy, and E. R. Decker, Heat flow and thermal history in New England and New York, in Studies of Appalachian Geology: Northern and Maritime, edited by E. Zen, W. S. White, J. B. Hadley, and J. B. Thompson, Jr., pp. 437-451, Interscience, New York, 1968.
- Blackwell, D. D., Heat flow determinations in the northwestern United States, *J. Geophys. Res.*, 74, 992-1007, 1969.
- Blackwell, D. D., The thermal structure of the continental crust, in The Structure and Physical Properties of the Earth's Crust, *Geophys. Monogr. Ser.*, vol. 14, edited by J. G. Heacock, pp. 169-184, AGU, Washington, D. C., 1971.
- Blackwell, D. D., Surface ground temperature variations in mountainous regions and a new topographic correction technique for heat flow measurements (abstract), *Eos Trans. AGU*, 54, 1207, 1973.
- Blackwell, D. D., Terrestrial heat flow and its implications on the location of geothermal reservoirs in Washington, *Wash. Div. Mines Geol. Inform. Circ.*, 50, 21-33, 1974.
- Blackwell, D. D., and C. G. Baag, Heat flow in a 'blind' geothermal area near Marysville, Montana, *Geophysics*, 38, 941-956, 1973.
- Blackwell, D. D., M. J. Holdaway, P. Morgan, D. Petefish, T. Rape, J. L. Steele, D. Thorstenson, and A. F. Waibel, Results and analysis of exploration and deep drilling at Marysville geothermal area, in The Marysville, Montana Geothermal Project, Final Report, pp. E.1-E.116, Battelle Pacific Northwest Laboratories, Richland, Wash., 1975.
- Bodvarsson, G., On the temperature of water flowing through fractures, *J. Geophys. Res.*, 74, 1987-1992, 1969.
- Bodvarsson, G., and R. P. Lowell, Ocean floor heat flow and the circulation of interstitial waters, *J. Geophys. Res.*, 77, 4472-4475, 1972.
- Bowen, R. G., Progress report on geothermal measurements in Oregon, *Ore Bin*, 35, 6-7, 1973.
- Bowen, R. G., and N. V. Peterson, Thermal springs and wells, *Oreg. Dep. Geol. Miner. Ind. Misc. Pap.*, 14, 1970.

- Bowen, R. G., D. D. Blackwell, D. A. Hull, and N. V. Peterson, Progress report on heat-flow study of the Brothers fault zone, central Oregon, Ore. Bin, 38, 39-46, 1976.
- Bredehoeft, J. D., and I. S. Papadopoulos, Rates of vertical groundwater movement estimated from the earth's thermal profile, Water Resour. Res., 1, 325-328, 1965.
- Brott, C. A., D. D. Blackwell, and J. C. Mitchell, Heat flow study of the Snake River Plain region, Idaho, Geothermal Investigations in Idaho, Water Inform. Bull. 30, part 8, 195 pp., Idaho Department of Water Resources, Boise, 1976.
- Brune, J. N., T. L. Henyey, and R. F. Roy, Heat flow, stress, and rate of slip along the San Andreas Fault, California, J. Geophys. Res., 74, 3821-3827, 1969.
- Carstlaw, H. S., and J. C. Jaeger, Conduction of Heat in Solids, 2nd ed., Oxford University Press, New York, 1959.
- Cermak, V., and A. M. Jessop, Heat flow, heat generation and crustal temperature in the Kapuskasing area of the Canadian Shield, Tectonophysics, 11, 287-303, 1971.
- Combs, J., Heat flow and microearthquake studies, Coso geothermal area, China Lake, California, Final Report, Order Number 2800, contract N00123-74-C-2099, 65 pp., Advan. Res. Proj. Agency, Washington, D. C., 1975.
- Combs, J., and G. Simmons, Terrestrial heat flow determinations in the north central United States, J. Geophys. Res., 78, 441-461, 1973.
- Decker, E. R., and S. B. Smithson, Heat flow and gravity interpretation across the Rio Grande Rift in southern New Mexico and west Texas, J. Geophys. Res., 80, 2542-2552, 1975.
- Diment, W. H., T. C. Urban, and F. A. Revetta, Some geophysical anomalies in the eastern United States, in The Nature of the Solid Earth, edited by E. C. Robertson, pp. 544-572, McGraw-Hill, New York, 1972.
- Diment, W. H., T. C. Urban, J. H. Sass, B. V. Marshall, R. J. Munroe, and A. H. Lachenbruch, Temperatures and heat contents based on conductive transport of heat, U.S. Geol. Surv. Circ., 726, 84-103, 1975.
- Dinwiddie, G. A., and L. J. Schröder, Summary of hydraulic testing in and chemical analyses of water samples from deep exploratory holes in Little Fish Lake, Monitor, Hot Creek, and Little Smoky Valleys, Nevada, Central Nevada-40, Tech. Lett. 474-90, 70 pp., U.S. Geol. Surv., Denver, Colorado, 1971.
- Donaldson, I. G., Temperature gradients in the upper layers of the earth's crust due to convective water flows, J. Geophys. Res., 67, 3449-3459, 1962.
- Eakin, T. E., A regional interbasin groundwater system in the White River area, southeastern Nevada, Water Resour. Res., 2, 251-271, 1966.
- Fenneman, N. M., Physical divisions of the United States, U.S. Dep. of the Interior, Washington, D. C., 1946.
- Fournier, R. O., D. E. White, and A. H. Truesdell, Convective heat flow in Yellowstone National Park, in Proceedings of the Second United Nations Symposium on the Development and Use of Geothermal Resources, pp. 731-739, U.S. Government Printing Office, Washington, D. C., 1976.
- Henyey, T. L., and G. J. Wasserburg, Heat flow near major strike-slip faults in California, J. Geophys. Res., 76, 7924-7946, 1971.
- Hill, D. P., Structure of Long Valley caldera, California, from a seismic refraction experiment, J. Geophys. Res., 81, 745-753, 1976.

- Hill, D. P., and L. C. Pakiser, Crustal structure between the Nevada Test Site and Boise, Idaho, from seismic refraction measurements, in The Earth Beneath the Continents, Geophys. Monogr. Ser., vol. 10, edited by J. S. Steinhart and T. J. Smith, pp. 391-419, AGU, Washington, D. C., 1966.
- Hunt, C. B., and T. W. Robinson, Possible interbasin circulation of ground water in the southern part of the Great Basin, U.S. Geol. Surv. Prof. Pap., 400-B, B273-B274, 1960.
- Jaeger, J. C., Heat flow and radioactivity in Australia, Earth Planet. Sci. Lett., 8, 285-292, 1970.
- Jones, P. H., Hydrodynamics of geopressure in the northern Gulf of Mexico basin, J. Petrol. Technol., 21, 803-810, 1969.
- Jones, P. H., and R. H. Wallace, Jr., Hydrogeologic aspects of structural deformation in the northern Gulf of Mexico basin, J. Res. U.S. Geol. Surv., 2, 511-517, 1974.
- Lachenbruch, A. H., Preliminary geothermal model of the Sierra Nevada, J. Geophys. Res., 73, 6977-6989, 1968.
- Lachenbruch, A. H., Crustal temperature and heat production: Implications of the linear heat flow relation, J. Geophys. Res., 75, 3291-3300, 1970.
- Lachenbruch, A. H., Vertical gradients of heat production in the continental crust, 1, Theoretical detectability from near-surface measurements, J. Geophys. Res., 76, 3842-3851, 1971.
- Lachenbruch, A. H., and C. M. Bunker, Vertical gradients of heat production in the continental crust; 2, Some estimates from borehole data, J. Geophys. Res., 76, 3852-3860, 1971.
- Lachenbruch, A. H., and J. H. Sass, Thermo-mechanical aspects of the San Andreas, in Proceedings of the Conference on the Tectonic Problems of the San Andreas Fault, pp. 192-205, Stanford University Press, Stanford, Calif., 1973.
- Lachenbruch, A. H., M. C. Brewer, G. W. Greene, and B. V. Marshall, Temperatures in permafrost, in Temperature—Its Measurement and Control in Science and Industry, pp. 791-803, Reinhold, New York, 1962.
- Lachenbruch, A. H., J. H. Sass, R. J. Munroe, and T. H. Moses, Jr., Geothermal setting and simple heat conduction models for the Long Valley caldera, J. Geophys. Res., 81, 769-784, 1976a.
- Lachenbruch, A. H., M. L. Sorey, R. E. Lewis, and J. H. Sass, The near-surface hydrothermal regime of Long Valley caldera, J. Geophys. Res., 81, 763-768, 1976b.
- Lambert, E. B., and K. S. Heier, The vertical distribution of uranium, thorium, and potassium in the continental crust, Geochim. Cosmochim. Acta, 31, 377-390, 1967.
- Lapwood, E. R., Convection of a fluid in a porous medium, Proc. Cambridge Phil. Soc., 44, 508-521, 1948.
- Lee, W. H. K., and S. Uyeda, Review of heat flow data, in Terrestrial Heat Flow, Geophys. Monogr. Ser., vol. 8, edited by W. H. K. Lee, pp. 87-190, AGU, Washington, D. C., 1965.
- Lowell, R. P., Circulation in fractures, hot springs, and convective heat transport on mid-ocean ridge crests, Geophys. J. Roy. Astron. Soc., 40, 351-365, 1975.
- Mariner, R. H., J. B. Rapp, L. M. Willey, and T. S. Presser, The chemical composition and estimated minimum thermal reservoir temperatures

- of selected hot springs in Oregon, open file report, 27 pp., U.S. Geol. Surv., Menlo Park, Calif., 1974.
- Mifflin, M. D., Delineation of ground-water flow systems in Nevada, *Hydro. Water Resour. Publ.* 4, 111 pp., Desert Res. Inst., Reno, Nevada, 1968.
- Morgan, P., D. D. Blackwell, R. E. Spafford, and R. B. Smith, Heat flow measurements in Yellowstone Lake and the thermal structure of the Yellowstone caldera, *J. Geophys. Res.*, in press, 1977.
- Nathenson, M., The effects of a step change in water flow on an initially linear profile of temperature, in Proceedings of the Geothermal Reservoir Engineering Workshop, vol. 2, Stanford Geothermal Program, Stanford, California, in press, 1977.
- Olmsted, F. H., P. A. Glancy, J. R. Harrill, F. E. Rush, and A. S. VanDenburgh, Preliminary hydrogeologic appraisal of selected hydrothermal systems in northern and central Nevada, *Open File Rep.* 75-56, 267 pp., U.S. Geol. Surv., Menlo Park, Calif., 1975.
- Papadopoulos, S. S., R. H. Wallace, Jr., J. B. Wesselman, and R. E. Taylor, Assessment of onshore geopressured-geothermal resources in the northern Gulf of Mexico basin, *U.S. Geol. Surv. Circ.*, 726, 125-146, 1975.
- Peck, D. L., T. L. Wright, and J. G. Moore, Crystallization of tholeiitic basalt in Alae lava lake, Hawaii, *Bull. Volcanol.*, 29, 629-656, 1966.
- Rao, R. U. M., G. V. Rao, and H. Narain, Radioactive heat generation and heat flow in the Indian shield, *Earth Planet. Sci. Lett.*, 30, 57-64, 1976.
- Reiter, M., C. L. Edwards, H. Hartman, and C. Weidman, Terrestrial heat flow along the Rio Grande Rift, New Mexico and southern Colorado, *Geol. Soc. Amer. Bull.*, 86, 811-818, 1975.
- Renner, J. L., D. E. White, and D. L. Williams, Hydrothermal convection systems, *U.S. Geol. Surv. Circ.*, 726, 5-57, 1975.
- Roy, R. F., D. D. Blackwell, and F. Birch, Heat generation of plutonic rocks and continental heat flow provinces, *Earth Planet. Sci. Lett.*, 5, 1-12, 1968a.
- Roy, R. F., E. R. Decker, D. D. Blackwell, and F. Birch, Heat flow in the United States, *J. Geophys. Res.*, 73, 5207-5221, 1968b.
- Roy, R. F., D. D. Blackwell, and E. R. Decker, Continental heat flow, in The Nature of the Solid Earth, edited by E. C. Robertson, pp. 506-543, McGraw-Hill, New York, 1972.
- Sass, J. H., and E. A. Sammel, Heat flow data and their relation to observed geothermal phenomena near Klamath Falls, Oregon, *J. Geophys. Res.*, 81, 4863-4868, 1976.
- Sass, J. H., A. H. Lachenbruch, R. J. Munroe, G. W. Greene, and T. H. Moses, Jr., Heat flow in the western United States, *J. Geophys. Res.*, 76, 6376-6413, 1971.
- Sass, J. H., W. H. Diment, A. H. Lachenbruch, B. V. Marshall, R. J. Munroe, T. H. Moses, Jr., and T. C. Urban, A new heat-flow contour map of the conterminous United States, *Open File Rep.* 76-756, 24 pp., U.S. Geol. Surv., Menlo Park, Calif., 1976a.
- Sass, J. H., S. P. Galanis, Jr., R. J. Munroe, and T. C. Urban, Heat-flow data from southeastern Oregon, *Open File Rep.* 76-217, 52 pp., U.S. Geol. Surv., Menlo Park, Calif., 1976b.
- Sass, J. H., J. C. Jaeger, and R. J. Munroe, Heat flow and near-surface

- radioactivity in the Australian continental crust, Open File Rep. 76-250, 91 pp., U.S. Geol. Surv., Menlo Park, Calif., 1976c.
- Sass, J. H., F. H. Olnsted, M. L. Sorey, H. A. Wollenberg, A. H. Lachenbruch, R. J. Munroe, and S. P. Galanis, Jr., Geothermal data from test wells drilled in Grass Valley and Buffalo Valley, Nevada, Open File Rep. 76-85, 43 pp., U.S. Geol. Surv., Menlo Park, Calif., 1976d.
- Sclater, J. G., and J. Francheteau, The implications of terrestrial heat flow observations on current tectonic and geochemical models of the crust and upper mantle of the earth, *Geophys. J. Roy. Astron. Soc.*, 20, 509-542, 1970.
- Smith, D. L., Heat flow, radioactive heat generation, and theoretical tectonics for northwestern Mexico, *Earth Planet. Sci. Lett.*, 23, 43-52, 1974.
- Smith, R. L., and H. R. Shaw, Igneous-related geothermal systems, U.S. Geol. Surv. Circ., 726, 58-83, 1975.
- Sorey, M. L., Numerical modeling of liquid geothermal systems, Open File Rep. 75-613, 66 pp., U.S. Geol. Surv., Menlo Park, Calif., 1975.
- Sorey, M. L., and R. E. Lewis, Convective heat flow from hot springs in the Long Valley caldera, Mono County, California, *J. Geophys. Res.*, 81, 785-791, 1976.
- Steeple, D. W., and H. M. Iyer, Low-velocity zone under Long Valley as determined from teleseismic events, *J. Geophys. Res.*, 81, 849-860, 1976.
- Stewart, J. H., and J. E. Carlson, Generalized maps showing distribution, lithology, and age of Cenozoic igneous rocks in the western United States, scale 1:5,000,000, in *Cenozoic Tectonics and Regional Geophysics of the Western Cordillera*, Spec. Pap., edited by R. B. Smith and G. P. Eaton, Geological Society of America, Boulder, Colorado, in press, 1977.
- Swanberg, C. A., Vertical distribution of heat generation in the Idaho batholith, *J. Geophys. Res.*, 77, 2508-2513, 1972.
- Swanberg, C. A., M. D. Chessman, G. Simmons, S. B. Smithson, G. Gronlie, and K. S. Heier, Heat-flow-heat-generation studies in Norway, *Tectonophysics*, 23, 31-48, 1974.
- Thompson, G. A., and D. B. Burke, Regional geophysics of the Basin and Range province, *Annu. Rev. Earth Planet. Sci.*, 2, 213-238, 1974.
- Urban, T. C., and W. H. Diment, Heat flow on the south flank of the Snake River Rift (abstract), *Geol. Soc. Amer. Abstr. Programs*, 7, 648, 1975.
- White, D. E., Geothermal energy, U.S. Geol. Surv. Circ., 519, 17 pp., 1965.
- White, D. E., Hydrology, activity, and heat flow of the Steamboat Springs thermal system, Washoe County Nevada, U.S. Geol. Surv. Prof. Pap., 458-C, 109 pp., 1968.
- Winograd, I. U., and W. Thordarson, Hydrogeologic and hydrochemical framework, South-Central Great Basin, Nevada-California, with special reference to the Nevada Test Site, U.S. Geol. Surv. Prof. Pap., 712-C, 126 pp., 1975.
- Wyllie, P. J., Experimental limits for melting in the earth's crust and upper mantle, in *The Structure and Physical Properties of the Earth's Crust*, *Geophys. Monogr. Ser.*, vol. 14, edited by J. G. Heacock, pp. 279-301, AGU, Washington, D. C., 1971.

SUBJ
GPHYS
HE
HGP

EARTH AND PLANETARY SCIENCE LETTERS 5 (1968) 1-12. NORTH-HOLLAND PUBLISHING COMP., AMSTERDAM

vol 5 No 1

HEAT GENERATION OF PLUTONIC ROCKS AND CONTINENTAL HEAT FLOW PROVINCES *

Robert F. ROY, David D. BLACKWELL

Seismological Laboratory, California Institute of Technology, Pasadena, California

and

Francis BIRCH

Hoffman Laboratory, Harvard University, Cambridge, Massachusetts

UNIVERSITY OF UTAH
RESEARCH INSTITUTE
EARTH SCIENCE LAB.

Received 7 September 1968

Combined radioactivity and heat flow measurements in plutonic rocks at 38 localities in the United States define three heat flow provinces; the eastern United States, the Sierra Nevada, and a zone of high heat flow in the western United States which includes the Basin and Range province. In each of these provinces heat flow (Q) and heat production (A) are related by an equation of the form $Q = a + bA$. The simplest interpretation of this linear relation is that the radioactivity measured at the surface is constant from the surface to depth b but varies from place to place. Thus the fraction of heat flow from the lower crust and upper mantle, a , remains constant within a heat flow province while the variable upper crustal radioactivity generates the variable heat flow observed at the surface. In the eastern United States $b = 7.5$ km and $a = 0.79 \mu\text{cal}/\text{cm}^2 \text{ sec}$, in the Sierra Nevada $b = 10.1$ km and $a = 0.40 \mu\text{cal}/\text{cm}^2 \text{ sec}$, and in the Basin and Range province $b = 9.4$ km and $a = 1.4 \mu\text{cal}/\text{cm}^2 \text{ sec}$. The line characteristic of the eastern United States may have broad applicability to stable portions of continents and thus be considered the reference curve for normal continental heat flow. The similarity of all the slopes indicates that most local variability of heat flow is due to sources in the uppermost 7-11 km of the earth's crust, and that the contribution from the lower crust and upper mantle is quite uniform over large regions. The intercept values can be used to infer the proportion of heat flow from the mantle and to map provinces with different mantle heat flow. These heat flow provinces correlate closely with surface geological provinces.

1. INTRODUCTION

A major problem in the interpretation of heat flow data is the wide variation in observations only a few tens of kilometers apart. In most cases the variations are unexplained and interpretations are based on regional values which are obtained by some method of averaging, for example over squares of latitude and longitude or geological provinces. If the variations are not random the averaging methods suppress much important information contained in the unsmoothed data.

In recent studies in New England and New York Birch, Roy and Decker [1] found that lateral variations in heat flow could be correlated with the radioactivity of the plutonic rocks in which the measurements of heat flow were made. The data plot close to a line of the form $Q = a + bA$, where Q is the heat flux at the surface and A is the radioactive heat production of the surface rocks. Their interpretation of this linear relation is illustrated in fig. 1. It is assumed that the radioactivity measured at the surface is constant to depth b , but varies from pluton to pluton. The heat flow from beneath the pluton (a), consisting of a component from the lower crust (cA_3) and a component from the upper mantle (Q_m), remains

* Division of Geological Sciences Contribution No. 1555, California Institute of Technology, Pasadena, California 91109.

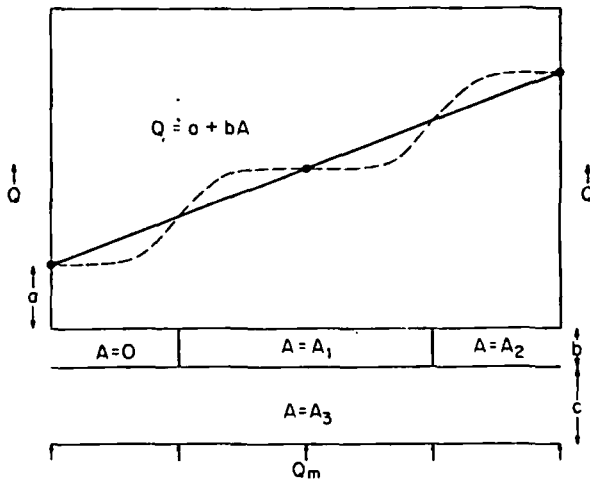


Fig. 1. Surface heat flow (Q) as a function of heat productivity (A) of the surface rocks for an ideal case. The intercept (a) is the flux from the upper mantle (Q_m) plus the heat generated in the lower crust (cA_3). The variable heat flow observed at the surface is due to variations in heat productivity in the surface layer. The vertical scale of the model is exaggerated for clarity. The horizontal scale for the solid line is in units of heat production. The horizontal scale for the dashed line is in units of distance and shows the effect on surface heat flow of lateral variations in heat productivity.

constant throughout the region and the variable radioactivity of the upper crust generates the variable heat flow observed at the surface.

The data from New England and New York imply a surface layer of variable heat production 6 to 7 km thick. This thickness is much smaller than the limits which can be derived from lateral variability by the usual geophysical arguments as the horizontal interval between stations is some tens of kilometers. With many new measurements of radioactivity reported in this paper, it is now possible to define several heat flow provinces based on the relationship of heat flow to basement radioactivity.

2: DATA

The data of this study are measurements of heat flow and radioactive heat generation in large plutons. Gravity studies suggest that such bodies typically have a thickness of 5 to 15 km [2, 3]. Studies of the radio-

element distribution in some plutonic rocks [4, 5] suggest that each intrusive has a fairly uniform heat production on the exposed surface and over a vertical range of 1–2 km. Thus there is some justification for the assumption that the heat generation measured on core from shallow holes near the present surface has some relation to that in the rest of the pluton.

The steady state heat flux due to the radioactive heat sources in plutonic bodies can be calculated by analogy with their gravity field [6]. Unless the diameter of a plutonic body is many times its thickness or the heat production contrast with the country rock is small, the amplitude of the anomaly will be significantly less than that of an infinite sheet. Consequently, corrections for the finite size of the pluton have been applied to several of the heat flow values.

Radioelement concentrations were determined by gamma ray spectrometry for localities where Th contents are recorded. The apparatus and technique are described by Adams [7]. The measurements are considered accurate to $\pm 5\%$. At localities where Th is not listed, equivalent uranium (eU) was determined by counting alpha particles from 50 g samples of core crushed to -400 mesh (less than 37 microns). The powders were packed in aluminum pans 22 cm in diameter and placed 2 mm from a ZnS (Ag) alpha particle detector. Scintillations were counted with a 23 cm diameter photomultiplier tube (57 AVP) and appropriate electronics. A sample with 1 ppm eU has the alpha activity of 1 ppm U [15]. However, for samples with a Th/U ratio of 4 the average energy per alpha particle is about 5% greater than for ordinary uranium, thus the 5% higher conversion factor from eU to heat generation in table 1. Because the average energy per alpha particle in the thorium series is only 10% larger than in the uranium series, use of

Table 1
Conversion factors for heat generation

Element	Heat generation (cal/cm ³ sec)
1 ppm U (ordinary)	0.62×10^{-13}
1 ppm Th	0.17×10^{-13}
1 ppm eU	0.66×10^{-13}
1% K (ordinary)	0.23×10^{-13}

Heat flow
in the refe
[9] and [1

New En
Kanca
Water
North
Casco
Chelm
Fitzwi
North
Durha

Central
Picher
Riverv
Levasy
Ely, M
Sarana
Wadha
Elizab

Sierra N
Helms

Loon l

Blodge
Wright
Grass
Loomi
San Jo

Basin ar
Quartz
Ajo, A
Cresce
Milfor
Tyronc

Orogra
Hualap
Sierrita
Oracle
Schurz
Ruth, l
Helveti
Lucern
Bagdad
Dragoc

Northern
Butte,

HEAT GENERATION OF PLUTONIC ROCKS

3

Table 2

Heat flow and heat generation data for 38 localities in the United States. *N* is the number of radioactivity samples. The numbers in the reference columns are the references for the heat flow (H. F.) and radioactivity (Rad.) data. The heat flow values from [1], [9] and [10] have been corrected for steady-state topography; heat flow values by all other investigators are preliminary.

Locality	Reference		<i>N</i>	Th (ppm)	U (eU) (ppm)	K (%)	<i>A</i>	<i>Q</i>
	H. F.	Rad.					$\frac{10^{-13} \text{ cal}}{\text{cm}^3 \text{ sec}}$	$\frac{10^{-6} \text{ cal}}{\text{cm}^2 \text{ sec}}$
New England								
Kancamagus, N. H.	1	1	557	59	15.8	4.0	20.7	2.27
Waterville, N. H.	1	1	349	61	15.9	4.1	21.2	2.15 (2.35)
North Conway, N. H.	1	1	145	52	12.6	4.3	17.6	1.89 (2.15)
Casco, Maine	1	1	32	40	8.2	4.3	12.9	1.80
Chelmsford, Mass.	1	1		(30)	9	(4)	(11.6)	1.63
Fitzwilliam, N. H.	1	1	145	23.5	7.6	3.9	9.6	1.63
North Haverhill, N. H.	1	1	24	26.7	4.0	3.2	7.8	1.34
Durham, N. H.	1		10	8.4	2.8	2.8	3.8	1.08
Central Stable Region								
Picher, Okla.	9		13		10.0	4.3	7.6	1.46
Riverview, N. Y.	1		72	15.0	3.3	5.2	5.8	1.22
Levasy, Mo.	9		16		6.9	4.1	5.5	1.17
Ely, Minn.	9		7		1.4	2.2	1.4	0.82
Saranac Lake, N. Y.	1		6		<0.3	<1.0	<0.4	0.81
Wadhams, N. Y.	1		6		<0.3	<1.0	<0.4	0.79
Elizabethtown, N. Y.	1		6		<0.3	<1.0	<0.4	0.81
Sierra Nevada								
Helms Creek, Calif.	11	12	72	21.5	7.2	2.9	8.8	1.3
Loon Lake, Calif.	9		14		5.1	2.8	4.0	1.25
Blodgett, Calif.	9		6		13.3	(3.5)	9.6	1.25
Wright's Lake, Calif.	9		92	16.1	4.3	4.5	6.4	1.06
Grass Valley, Calif.	10		109	12.6	3.4	2.0	4.7	0.83
Loomis, Calif.	9		7		4.2	2.0	3.2	0.73
San Joaquin, Calif.	9		153	3.2	1.6	1.2	1.8	0.62
	11	12	71	5.2	1.6	1.5	2.2	0.6
Basin and Range Province								
Quartzsite, Ariz.	9		6		15.0	(3.5)	10.7	2.4
Ajo, Ariz.	9		10		7.6	4.2	6.0	2.4
Crescent Peak, Nev.	9		9		10.4	4.5	7.9	2.3
Milford, Utah	9		11		14.3	3.6	10.3	2.22
Tyrone, N. M.	13		20		9.5	3.4	7.1	2.2
Orogrande, N. M.	13		10		8.9	3.5	6.7	2.2
Hualapai Mtns., Ariz.	9		5		1.7	3.9	2.0	2.14
Sierrita Mtns., Ariz.	9		9		9.9	4.9	7.7	2.0
Oracle, Ariz.	13		15		7.5	3.2	5.7	1.9
Schurz, Nev.	9		9		7.1	2.8	5.3	1.88
Ruth, Nev.	9		10		10.4	3.6	7.7	1.82 (2.0)
Helvetia, Ariz.	9		8		4.7	2.9	3.8	1.78
Lucerne Valley, Calif.	15	15	10		3.9	2.1	3.1	1.65
Bagdad, Ariz.	9		7		9.0	2.7	6.6	1.64 (1.84)
Dragoon, Ariz.	13		20		3.7	2.8	3.1	1.6
Northern Rocky Mountains								
Butte, Mont.	14	14	19	22.8	6.3	3.4	8.6	2.2

the eU conversion factor implies an error of $\leq 5\%$ for Th/U ratios from 0 to ∞ (Birch [8]). Potassium concentrations which accompany the eU values were determined by X-ray fluorescence. The accuracy of heat productivity measurements by combined alpha counting and X-ray fluorescence is estimated to be $\pm 15\%$ based on comparisons with gamma ray measurements by H. A. Wollenberg at the Lawrence Radiation Laboratory.

The conversion factors from radioelement concentration to heat production are given in table 1, after Birch [8]. A density of 2.67 g/cm^3 was assumed in converting from cal/g sec to $\text{cal/cm}^3 \text{ sec}$.

The heat flow and heat productivity values used are listed in table 2. Heat flow values in parentheses are corrected for the finite size of the pluton. The standard errors of the heat flow values are usually less than 5%, but may be as large as 10% in a few cases for values in the Basin and Range province.

In the interest of brevity throughout this paper the units of heat flow, $10^{-6} \text{ cal/cm}^2 \text{ sec}$, will be replaced by the abbreviation HFU; and the units of heat generation, $10^{-13} \text{ cal/cm}^3 \text{ sec}$, by HGU.

3. NEW ENGLAND

The data from New England are located in the crystalline Appalachians as defined by King [16]. The last major metamorphic and igneous activity was in the Devonian. The last significant thermal event was a milder episode of epizonal magmatism in the Triassic. Birch et al. [1] discuss the interpretation of heat flow data in this region, including significant corrections for geological evolution, and the reader is referred to that paper for further analysis of the problem. In this paper only steady-state heat flow values are used because geological corrections have not been made at any localities in the other regions. The New England data, solid circles in fig. 2, determine a line with a slope of 7.2 km and intercept of 0.84 HFU.

4. CENTRAL STABLE REGION

The area between the Appalachian and Rocky Mountains, largely covered by a thin layer of sedimentary rocks, has been subjected to only mild disturbances

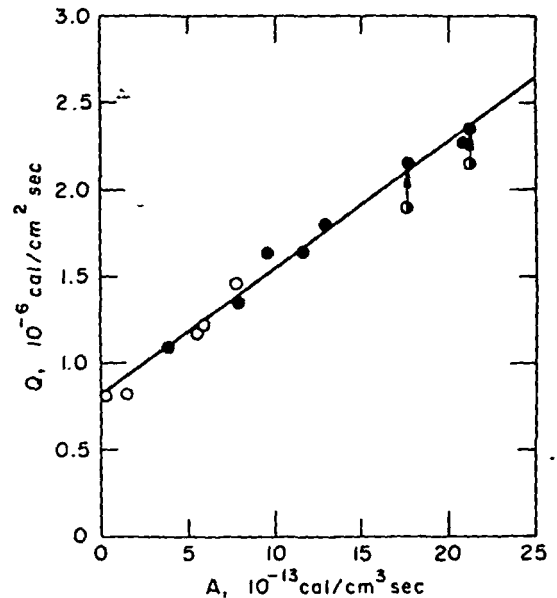


Fig. 2. Heat flow and heat productivity data for plutons in the New England area (solid circles) and the Central Stable Region (open circles). The line is fitted to both sets of data.

since Precambrian time, and is part of the area King [16] calls the Central Stable Region of North America. In the United States this area includes the Interior Lowlands and part of the Canadian Shield. Including the 4 determinations in the Adirondack Mountains discussed by Birch et al. [1], there are only 7 heat flow measurements in plutonic rocks of this large area for which we have radioactivity data. These points are plotted on fig. 2 as open circles. The line fitted to these points has a slope of 8.3 km and an intercept of 0.76 HFU. These parameters are not significantly different from those for the data in New England. Combining both sets of data the line has a slope of 7.5 km and an intercept of 0.79 HFU. This is considered the best average for the eastern United States. It is interesting to note that in a recent gravity study of a large area in the Canadian Shield, Gibb [3] found that density variations in the upper crust extend to a depth of about 8 km. One implication of the heat flow-heat production data is that heat flow variations measured in the sedimentary rocks of the Central Stable Region may be expected to reflect changes in basement values of heat generation.

Q, $10^{-6} \text{ cal/cm}^2 \text{ sec}$

Fig. 3. H
the Sierr
the two

5. SIEF

The
and pl
Valley
specifi
an east
Harvar
at abo
logical
and he
0.40 F
ness o
the ot
chang
Th
tral Si
Wolle
units
heat f
heat j
et al.

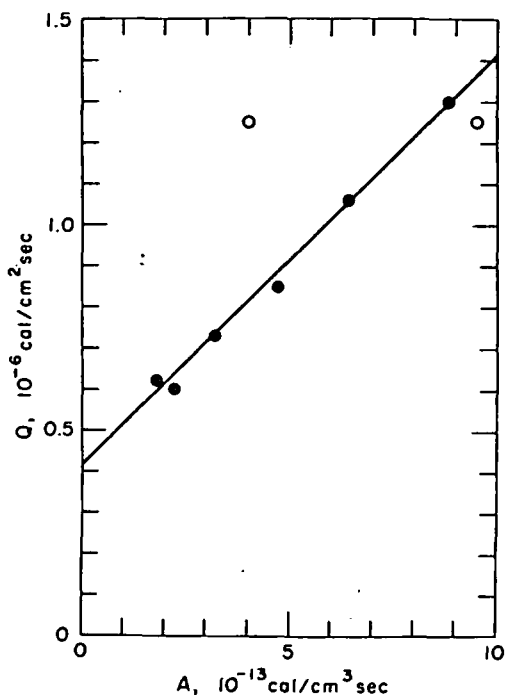


Fig. 3. Heat flow and heat productivity data for locations in the Sierra Nevada. The points shown as open circles represent the two values of heat generation measured near Loon Lake.

5. SIERRA NEVADA

The data in the Sierra Nevada are listed in table 2 and plotted in fig. 3. Excepting Loon Lake and Grass Valley, the determinations were made in holes drilled specifically for heat flow. Four of the holes are along an east-west profile at about 39° N drilled in 1965 by Harvard University and two holes are along a profile at about 37° N drilled in 1965-1967 by the U.S. Geological Survey. The slope of the line relating heat flow and heat production is 10.1 km and the intercept is 0.40 HFU. The gravity data are ambiguous but a thickness of the batholith of about 10 km is consistent with the observations [17]; seismic data indicate a velocity change at about 14 km [18].

The areal distribution of radioelements in the central Sierra Nevada (about 37° N) has been discussed by Wollenberg and Smith [12, 19]. They found several units of uniform heat production, and preliminary heat flow values in the units with highest and lowest heat production have been published by Lachenbruch et al. [11].

At 39° N two heat flow determinations were made in rocks with heat generation similar to that of Unit 2 (the 'Dinkey Creek' granodiorite) of Wollenberg and Smith, but the value at Loon Lake falls 0.4 HFU above the line relating heat flow and heat production and was not used in the slope calculation. However, several bodies of quartz monzonite outcrop within 5 km of the drill site [20]. Their average heat production is 9.6 HGU (see table 2). Thus the data suggest that a large body of the rock with higher heat production occurs beneath the drill hole.

Two models have been suggested for the vertical distribution of radioactive elements in the Sierra Nevada batholith: one, a layered batholith (Lachenbruch et al. [11]) with radioactive element concentration decreasing with depth, the older intrusions having lower heat production at the present surface because of deeper erosion; the other a uniform surface layer about 10 km thick (Hamilton and Myers [21]). The results shown in fig. 3 are consistent with either model. As examples, two general two-dimensional models are suggested which might explain the data (fig. 4). The models are not based on any specific section through the Sierra Nevada, but are idealized models composed of representatives of each of the major heat generation units present. Because the width of most of the units is only 30 to 40 km, the pluton thickness for the model with constant heat production (Model 1) must be slightly larger than is implied by the slope calculation (11 instead of 10 km). In model 2 a layered pluton with each layer having a uniform radioactivity typical of one of the major units present is assumed. The thickness of the layers was determined from the increment in heat flow between different units. A model with smaller increments in heat flow from each layer, and thus thinner layers, might be more satisfactory, but the most important point is the rapid decrease in heat production with depth. These models will be discussed in more detail in a paper in preparation. Although the two models appear quite different the important conclusions of extreme upward concentration of radioactive elements and slight variation of heat flow from below the radioactive layer are common to both, for if the bottom of the intrusive rocks in Model 2 were put at 10-11 km, the variation in heat flow at that depth would be only 0.4-0.6 instead of the variation in surface heat flow of 0.6-1.3 HFU.

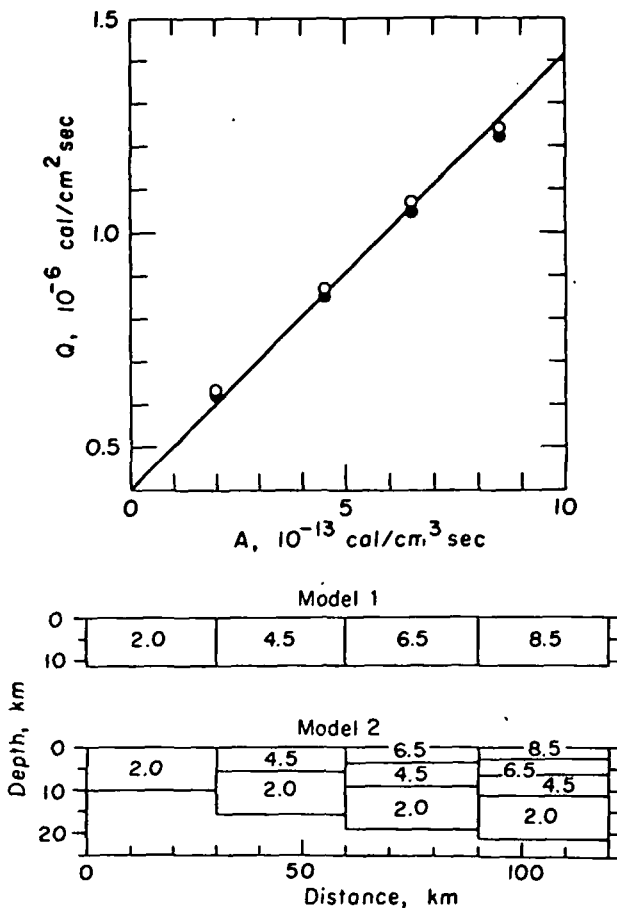


Fig. 4. Idealized models for the Sierra Nevada batholith which give a linear Q versus A relationship. For Model 1 an 11 km thick batholith and a constant value of heat production (values within blocks) versus depth is assumed. The calculated heat flow values for drill holes in the center of 30 km wide bodies with 0.40 HFU from below 11 km are shown as open circles. For Model 2 a discontinuously decreasing heat production versus depth and 0.40 HFU from below the batholith is assumed. The heat flow values at the centers of the 30 km wide blocks are shown as solid circles. The solid line is the observed relationship.

6. BASIN AND RANGE PROVINCE

All of the heat flow determinations in the Basin and Range province, with the exception of those made by Warren et al. [13] were made in holes drilled for economic purposes. Consequently, for this particular use most of the locations are less than satisfactory due to

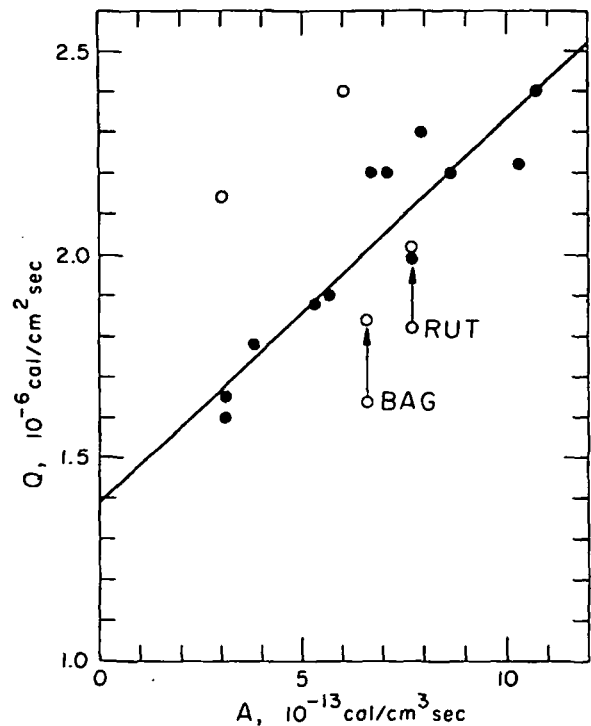


Fig. 5. Heat flow and heat productivity data for locations in the Basin and Range province. The points shown as open circles were not used in calculating the parameters of the straight line.

the possibility that the heat generation values were measured on samples from unrepresentative regions of the plutonic bodies. The data are shown in fig. 5. In general, the geology in the vicinity of the drill holes is not well known; however, at the two localities that fall well below the line, Bagdad, Arizona (BAG) and Ruth, Nevada (RUT), the quartz monzonite stocks are small and intrude less radioactive country rocks. Corrections for the finite size of these bodies increase the heat flow by 0.2 ± 0.1 HFU for reasonable assumptions about the geometry. The slope of the least squares straight line fitted to the solid dots is 9.4 km and the intercept is 1.4 HFU.

Blackwell [22] has presented evidence that the Basin and Range thermal anomaly may be extended to include most of the Northern Rocky Mountains. Data from the Boulder batholith in Montana fall on the line for the Basin and Range province.

In plutons with heat generation values as high as

some value
Basin
pre-
sured
that r
al. [9
locali
most
and of
that th
from t
crust c

7. DISCUSSION

7.1. Discussion

Only
appears
between h
bodies. I
product
ential c
Lachenb
depende
limiting
with dep
from cru
must be i
States.

The ac
elements,
ly of great
equivocal
in radioact
additional
regions of
probably h
the present
vertical dist
tory first ap

The data
facies meta
for an abrupt
large pluton
late heat flo
rocks becau

some of those measured in New England, heat flow values of up to 3.5 HFU might be expected in the Basin and Range province. The highest heat flow value presently available which can be explained by measured radioactivity is about 2.4 HFU. Thus it appears that most of the values over 2.5 reported by Roy et al. [9], approximately 15% of the Basin and Range localities, have an additional heat source term. The most reasonable general explanation for these points and others which plot well above the line in fig. 5 is that the heat flow at these sites has a large component from transient sources such as recent intrusions in the crust or nearby hot spring activity.

7. DISCUSSION

7.1. *Distribution of radioactive heat sources*

Only a limited class of radioelement distributions appears to be consistent with the linear relation between heat flow and heat production in plutonic bodies. The limiting cases are nearly constant heat production to the lower limit of plutons, or an exponential decrease in heat production with depth. A. H. Lachenbruch (personal communication, 1968) has independently arrived at a similar conclusion about the limiting case of exponential decrease of radioactivity with depth. In either case the heat flow variations from crust and mantle beneath the radioactive layer must be insignificant over large areas of the United States.

The actual vertical distribution of heat producing elements, whether constant or decreasing, is obviously of great importance. Presently available data are equivocal [4, 5, 12], but tend to favor little change in radioactivity with depths of 1–2 km. While many additional opportunities exist for surface sampling in regions of high relief, a solution to the problem will probably have to await the results of deep drilling. At the present time the assumption of nearly constant vertical distribution within a pluton seems a satisfactory first approximation.

The data of Lambert and Heier [23] on granulite facies metamorphic rocks furnish additional evidence for an abrupt diminution of heat production below large plutons. In this paper no attempt is made to relate heat flow and heat production in metamorphic rocks because of sampling uncertainties. Whether or

not a similar decrease in radioactivity occurs at some depth in metamorphic terranes must be based on geochemical arguments alone at the present time.

Clark and Ringwood [24] suggest that the normal heat flux from the mantle is 0.5–0.6 HFU. These values appear to be upper limits and together with the data on upper crustal radioactivity and layer thickness imply a heat production of < 2.0 HGU for rocks in the lower crust.

7.2. *Thickness of the radioactive layer*

Recently, based on the geochemical data of Lambert and Heier [23], Hyndman et al. [25] have suggested a crustal heat source distribution similar to that discussed here. In that paper different regional heat flow values are explained by assumed variations in the thickness of the heat producing layer with the mantle contribution considered to be almost constant everywhere. However, data from this study suggest that the thickness of the heat producing surface layer varies little (7–11 km in the areas discussed) while the different regional values arise from variations in heat flux from the lower crust and mantle. Heat flow and heat production values typical of two areas in the Australian shield [25], one area in eastern Australia [25], and the Rum Jungle complex [26, 27] in north-central Australia are plotted in fig. 6, which is a summary of the lines calculated for the three regions in the United States. The data from the Australian shield fall near the line characteristic of the eastern United States while the data point for the Snowy Mountains falls near the line characteristic of the Basin and Range province. Although isolated from other heat flow data, the Rum Jungle was included in the high heat flow zone of eastern Australia by Howard and Sass [26]. However, it appears equally likely that Rum Jungle is an area analogous to the White Mountains in New England, and the value is actually appropriate for the shield region. The data from Australia are thus consistent with the ideas presented above.

The possibility of large variations in the thickness of the radioactive layer is certainly not ruled out. The layer may indeed be thinner than the average found here for some parts of the shields. An area from the United States where a thicker radioactive layer may explain high heat flow values is the Southern Rocky Mountains [28].

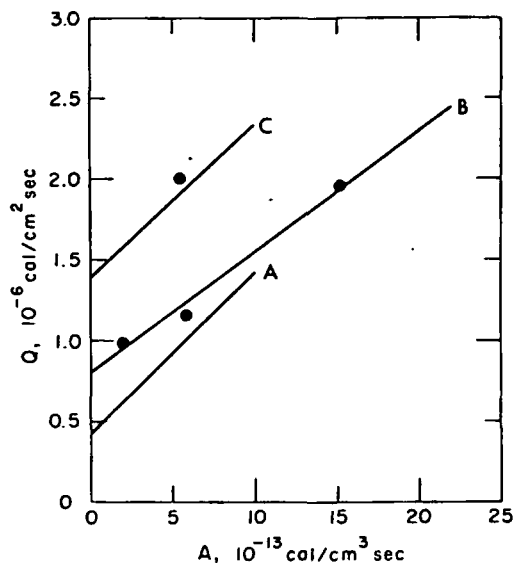


Fig. 6. Summary of relationship between heat flow and surface heat production in the Sierra Nevada (A), eastern United States (B), and Basin and Range province (C). The data points are from Australia (see text).

7.3. Temperatures

The more definite idea of the vertical distribution of heat sources which has resulted from this study allows more precise calculation of temperature in the crust. Three temperature-depth models are shown in fig. 7. The one-dimensional models were calculated using the parameters shown and assuming steady state conditions. For the Basin and Range in particular the assumption of steady state is probably invalid and the calculation gives a lower limit for the temperature distribution. The average thermal conductivity for approximately 100 sites in plutonic rocks in the United States reported by Roy et al. [9] is 7.0 millical/cm sec °C. The conductivity of the upper layer of the models was taken to be 6.5 millical/cm sec °C (the lower value because of the temperature dependence of thermal conductivity). The temperature-depth curves were calculated for heat flow values of 1.2, 0.95, and 1.9 HFU for the eastern United States, Sierra Nevada, and Basin and Range regions. The value of 1.2 HFU was chosen for the eastern United States because the mode for most continents is 1.1–1.2 HFU [29].

The extreme upward concentration of radioactivity

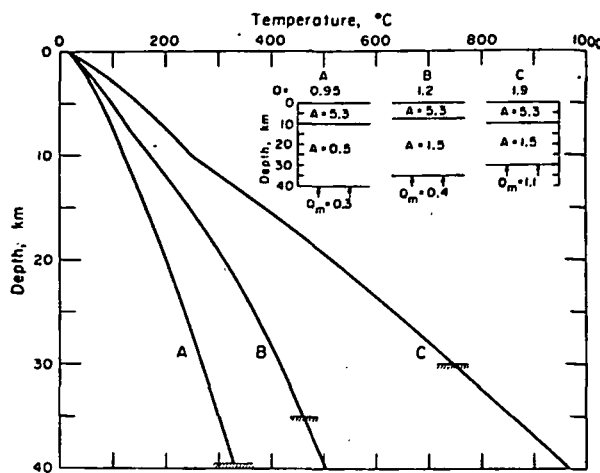


Fig. 7. Temperature-depth curves for the three heat flow provinces for the models shown (assumes steady state). The thermal conductivity is 6.5×10^{-3} cal/cm sec °C for the upper layer and 5.0×10^{-3} cal/cm sec °C for the lower layer of the crust.

implied by the relationship between heat flow and heat production results in small temperature differences within provinces while the lower crustal or upper mantle origin for regional differences results in large temperature variations between provinces. For example the maximum range of temperatures at the base of the crust in the eastern United States is less than 70°C for a heat flow variation of 0.8 to 2.0 HFU, whereas regional temperature differences for a similar range in heat flow may be 400°C or more (fig. 7).

The range of A corresponding to a range of 1.1–1.2 HFU for the curve characteristic of the eastern United States is 4.0–5.3 HGU. The heat production of the 'continental crust' is estimated to be 4.4 HGU by Heier and Rogers [30]. Nearly the same average value was found for all areas in the western United States underlain by Mesozoic batholiths, nearly 250 000 km², by Phair and Gottfried [4] and by Shaw [31] for rocks of the Canadian Shield. Thus 1.1–1.2 HFU would be the mean as well as the modal value for continents if anomalous regions such as the Basin and Range and Sierra Nevada were excluded from the averages. It is to be emphasized that the average heat production values apply only to a 7–11 km thick layer on the continents, *not* the whole thickness of the crust.

Table 3
Parameters of straight lines relating heat flow and heat production in the United States

Province	Number of data points	Slope (km)	Standard error (km)	Intercept	Standard error
				$\frac{10^{-6}\text{cal}}{\text{cm}^3 \text{ sec}}$	$\frac{10^{-6}\text{cal}}{\text{cm}^3 \text{ sec}}$
New England	8	7.2	0.4	0.84	0.05
Central Stable Region	7	8.3	0.6	0.76	0.03
Eastern United States	15	7.5	0.2	0.79	0.02
Sierra Nevada	6	10.1	0.1	0.40	0.03
Basin and Range Province	12	9.4	1.3	1.40	0.09

7.4. Heat flow provinces

Based on the results of this study we propose the identification and definition of continental heat flow provinces on the characteristic relationship between heat flow and heat production — the average thickness of the radioactive layer and the heat flow contributed by the lower crust and upper mantle. We can now define three such provinces in the United States (see fig. 6 and table 3): the eastern United States; the Basin and Range province; and the Sierra Nevada.

The heat flow - heat production relation characteristic of the eastern United States is based on data from New England and the Central Stable Region. The same line may apply to the Australian shield as well. The Northern Appalachians have been stable since early in the Mesozoic and the other areas for somewhat longer. The broad applicability of this line to stable regions suggests that it may be considered the reference curve for *normal* continental heat flow. This hypothesis is strengthened by the coincidence of modal heat flow values from different continents with the value predicted by this relationship for the average radioactivity of the upper part of the continental crust.

The heat flow - heat production relation for the Basin and Range province has an intercept of 1.4 HFU, 0.6 higher than the intercept for the eastern United States. If the mantle contribution to the heat flow is the same in the two regions the lower crust in the Basin and Range must have a heat productivity of 4–5 HGU. Such a value is incompatible with seismic and geochemical inferences on the composition of the lower crust [23, 32]. If the lower crust in this region has a heat productivity similar to that inferred for the Central Stable Region approximately 1.1 HFU is coming from the mantle in the Basin and Range province, and tem-

peratures are much higher than if most of the excess heat flow comes from radioactive sources in the crust. Because of the high temperatures the melting point is probably reached at shallow depths in the mantle. For example, the temperature depth curve for the Basin and Range province (fig. 7, curve C), if extended downward intersects the solidus for dry pyrolite [24] at 50 to 60 km. With a small amount of water partial melting would occur at still shallower depths. The presence of a partially molten zone at shallow depths in the upper mantle is consistent with the seismic, gravity, and electrical conductivity data in the Basin and Range province [33]. Because the melting point gradient is only 2 to 4°C/km [34] the top of the partially molten zone is essentially an isotherm, the depth of which determines the excess heat flow from the mantle. The continental crust is usually 30 to 40 km thick while the oceanic crust is only 5 to 10 km thick; if a partially molten upper mantle approaches the base of the crust in thermal anomaly regions, as the evidence suggests, then regional heat flow values might approach 2.5 HFU on continents and 5 to 10 HFU in oceanic regions. For example the region off the Oregon coast with an average heat flow of 4–5 HFU [35] occurs on the extension of a zone of 2⁺ HFU on the continent [36]. Once melting begins in the upper mantle or crust the conducted heat flow above the melt zone will soon reach quasi-equilibrium and continued addition of heat to the system from below will be released by local intrusive or extrusive activity. Thus it is reasonable that the average heat flow in the Basin and Range province is near the upper limit of conducted heat flow on a regional scale and that heat flow - radioactivity data from other analogous thermal anomaly regions may plot close to the Basin and Range curve.

The heat flow - heat production plot for the Sierra Nevada is remarkable for its linearity in a region where crustal thickness varies by a factor of two, and for its extremely low intercept. At present it is unclear whether the low intercept is due to transient or steady state causes and it should be emphasized that the temperatures shown in fig. 7 are based on the steady state assumption. The Sierra model (fig. 7, curve A) requires negligible radioactivity in the lower crust if the heat flow from the mantle is comparable to that inferred for the eastern United States (fig. 7, curve B). This implies some process in crustal evolution which efficiently impoverishes the lower crust of radiogenic heat sources in a large region. The depletion would be permanent and we might expect to find other regions which have undergone a similar process. The zone of low heat flow in western Lake Superior reported by Hart et al. [37] might be part of such a region. Alternatively a transient heat sink in the lower crust or upper mantle, for example a layer undergoing an endothermic reaction, might absorb a large component of the mantle heat flow for a limited time. In this event other areas in similar tectonic settings might have equally low values of heat flow. For example, in Japan [29, p. 104], Chile [38] and eastern Australia [39], there are measurements of heat flow with values as low or lower than the intercept for the eastern United States. As with the Sierra, these measurements are located between the Pacific and known or postulated zones of high heat flow.

7.5. Further implications

There are many implications of the remarkable relationship between heat flow and heat production. Among those we have mentioned but not elaborated on are the geochemistry of the continental crust and the nature of batholiths. Many questions are raised, for example the nature of the base of the radioactive layer - is it a change in bulk composition or an isograd representing a transition to rocks of the same composition but impoverished of radioactive elements? A related problem is the significance of the similar depth to which the radioactive layer extends in regions of deep erosion (the Adirondack Mountains) and regions of little erosion (the White Mountains). A stability level of some sort is implied.

One conclusion of this study is that the variability of continental heat flux over relatively large regions

is related to heat sources in the outermost few kilometers. On the other hand the three provinces, which bear a very close relationship with surface geologic provinces, differ primarily in the amount of heat coming from the mantle. Thus for continental drift to occur and yet different geological regions preserve their identity over geologic eras, the plane of slip must be well below the base of the crust.

The modal heat flow value for stable portions of continents (1.1 - 1.2 HFU) apparently represents the heat flow appropriate for a crust with average radioactivity overlying a normal mantle. The coincidence of the continental mode with the average heat flow in ocean basins is surprising if one is controlled by an essentially static distribution of heat sources and the other by a purely dynamic process related to sea floor spreading. This coincidence revives the argument for equality of radioactive sources beneath continents and oceans but with different vertical distributions.

ACKNOWLEDGMENTS

The radioactivity measurements at Blodgett, Wrights Lake and Loomis, California, and all the localities in New England were made by J. A. S. Adams and J. J. W. Rogers at Rice University. We are grateful to L. T. Silver and T. L. Henyey for their assistance with the design of the alpha counting equipment and to H. A. Wollenberg for measuring, by gamma ray spectrometry, the U, Th and K contents of 20 composite samples to check the alpha counting results. Additional checks were also made by R. I. Tilling (chemical), L. T. Silver (isotope dilution) and G. R. Tilton (gamma ray spectrometry). H. T. Baldwin did most of the sample preparation and measurements of alpha activity. E. Bingham did the K analyses by X-ray fluorescence. We would like to thank R. E. Warren, J. G. Sclater and V. Vacquier for permission to use four preliminary values of heat flow from their measurements in Arizona and New Mexico. We would also like to thank D. L. Anderson, C. B. Archambeau, J. N. Brune, E. R. Decker, J. H. Sass, L. T. Silver and H. A. Wollenberg for reading the manuscript and suggesting improvements. This work was supported by the National Science Foundation, Grant GA-715 at the California Institute of Technology and Grant No. GP-701 at Harvard University.

REFERENCES

- [1] F. Birch, R. F. Roy and E. R. Decker, Heat flow and thermal history in New York and New England, in: *Studies of Appalachian Geology: Northern and Maritime*, eds. E-an Zen, W. S. White, J. B. Haddley and J. B. Thompson, Jr. (John Wiley and Sons, Inc. - Interscience Publishers, New York, in press, 1968).
- [2] M. H. P. Bott and S. B. Smithson, Gravity investigations of subsurface shape and mass distributions of granitic batholiths, *Bull. Geol. Soc. Am.* 78 (1967) 859.
- [3] R. A. Gibb, A geological interpretation of the Bouguer anomalies adjacent to the Churchill-Superior boundary in northern Manitoba, *Can. J. Earth Sci.* 5 (1968) 439.
- [4] G. Phair and D. Gottfried, The Colorado Front Range, Colorado, USA, as a uranium and thorium province, in: *The Natural Radiation Environment*, eds. J. A. S. Adams and W. Lowder (University of Chicago Press, Chicago, Illinois, 1964) p.7.
- [5] K. A. Richardson, Thorium, uranium and potassium in the Conway granite, New Hampshire, USA, in: *The Natural Radiation Environment*, eds. J. A. S. Adams and W. Lowder (University of Chicago Press, Chicago, Illinois, 1964) p.39.
- [6] G. Simmons, Interpretation of heat flow anomalies, I, Contrasts in heat production, *Rev. Geophys.* 5 (1967) 43.
- [7] J. A. S. Adams, Laboratory γ -ray spectrometer for geochemical studies, in: *The Natural Radiation Environment*, eds. J. A. S. Adams and W. Lowder (University of Chicago Press, Chicago, Illinois, 1964) p. 485.
- [8] F. Birch, Heat from radioactivity, in: *Nuclear Geology*, ed. H. Faul (John Wiley and Sons, New York, 1954) p. 148.
- [9] R. F. Roy, E. R. Decker, D. D. Blackwell and F. Birch, Heat flow in the United States, *J. Geophys. Res.*, in press (1968).
- [10] S. P. Clark, Jr., Heat flow at Grass Valley, California, *Trans. Am. Geophys. Union* 38 (1957) 239.
- [11] A. H. Lachenbruch, H. A. Wollenberg, G. W. Green and A. R. Smith, Heat flow and heat production in the central Sierra Nevada, preliminary results, *Trans. Am. Geophys. Union* 47 (1966) 179.
- [12] H. A. Wollenberg and A. R. Smith, Radiogeologic studies in the central part of the Sierra Nevada batholith, California, *J. Geophys. Res.* 73 (1968) 1481.
- [13] R. E. Warren, J. G. Sclater, V. Vacquier and R. F. Roy, A comparison of terrestrial heat flow and transient geomagnetic fluctuations in the southwestern United States, in preparation (1968).
- [14] D. D. Blackwell and E. C. Robertson, Variation of heat flow with depth in the Boulder batholith near Butte, Montana, in preparation (1968).
- [15] T. L. Henyey, Heat flow near major strike slip faults in southern California, Ph. D. Thesis, California Institute of Technology (1968).
- [16] P. B. King, *The evolution of North America* (Princeton University Press, Princeton, New Jersey, 1959).
- [17] G. A. Thompson and M. Talwani, Crustal structure from Pacific Basin to central Nevada, *J. Geophys. Res.* 69 (1964) 4813.
- [18] J. P. Eaton, Crustal structure in northern and central California from seismic evidence, *Calif. Div. Mines and Geol. Bull.* 190 (1966) 419.
- [19] H. A. Wollenberg and A. R. Smith, Radioactivity and radiogenic heat in Sierra Nevada plutons, *J. Geophys. Res.* 69 (1964) 3471.
- [20] R. G. Strand and J. B. Koenig, Geological map of California, Sacramento sheet, *Calif. Div. of Mines and Geol.* (1966).
- [21] W. Hamilton and W. B. Meyers, The nature of batholiths, *U. S. Geol. Surv. Prof. Paper* 554-C (1967).
- [22] D. D. Blackwell, Heat flow determinations in the northwestern United States, *J. Geophys. Res.*, in press (1968).
- [23] I. B. Lambert and K. S. Heir, The vertical distribution of uranium, thorium, and potassium in the continental crust, *Geochim. Cosmochim. Acta* 31 (1967) 377.
- [24] S. P. Clark, Jr. and A. E. Ringwood, Density distribution and constitution of the mantle, *Rev. Geophys.* 2 (1964) 35.
- [25] R. D. Hyndman, I. B. Lambert, K. S. Heir, J. C. Jaeger and A. E. Ringwood, Heat flow and surface radioactivity measurements in the Precambrian Shield of western Australia, *Phys. Earth and Planet. Interiors* 1 (1968) 129.
- [26] L. E. Howard and J. H. Sass, Terrestrial heat flow in Australia, *J. Geophys. Res.* 69 (1964) 1617.
- [27] K. S. Heir and J. M. Rhodes, Thorium, uranium and potassium concentrations in granites and gneisses of the Rum Jungle complex, Northern Territory, Australia, *Econ. Geol.* 51 (1966) 563.
- [28] E. R. Decker, Terrestrial heat flow in Colorado and New Mexico, Ph.D. thesis, Harvard University (1966).
- [29] W. H. K. Lee and S. Uyeda, Review of heat flow data, in: *Terrestrial Heat Flow*, ed. W. H. K. Lee (Geophys. Monograph 8, Am. Geophys. Union, Washington, D.C., 1965) p. 87.
- [30] K. S. Heir and J. J. W. Rogers, Radiometric determinations of thorium, uranium and potassium in basalts and in two magmatic differentiation series, *Geochim. Cosmochim. Acta* 27 (1963) 137.
- [31] D. M. Shaw, U, Th, and K in the Canadian Precambrian shield and possible mantle compositions, *Geochim. Cosmochim. Acta* 31 (1967) 1111.
- [32] L. C. Pakiser and R. Robinson, Composition of the continental crust as estimated from seismic observations, in: *The Earth beneath the Continents*, eds. J. S. Steinhardt and T. J. Smith (Geophys. Monograph 10, Am. Geophys. Union, Washington, D.C., 1966) p. 620.
- [33] C. B. Archambeau, R. F. Roy, D. D. Blackwell, D. L. Anderson, L. Johnson and B. Julian, A geophysical study of continental structure, *Trans. Am. Geophys. Union* 49 (1968) 328.

- [34] K. Itô and G. C. Kennedy, Melting and phase relations in a natural peridotite, *Am. J. Sci.* 265 (1967) 519.
- [35] R. P. Von Herzen, Ocean floor heat flow measurements west of the United States and Baja California, *Marine Geology* 1 (1964) 225.
- [36] R. F. Roy, J. N. Brune and T. L. Henyey, A sharp transition in regional heat flow across the San Andreas fault near Hollister, California, in preparation (1968).
- [37] S. R. Hart, J. S. Steinhart and T. J. Smith, Heat flow, in: *Year Book 66* (Carnegie Institution of Washington, Washington, D.C., 1968) p.52.
- [38] W. H. Diment, F. O. Ortiz, L. R. Silva and C. F. Ruiz, Terrestrial heat flow at two localities near Vallenar, Chile, *Trans. Am. Geophys. Union* 46 (1965) 175.
- [39] R. D. Hyndman, Heat flow in Queensland and Northern Territory, Australia, *J. Geophys. Res.* 72 (1967) 527.

E

fou
nes
tin
tign
the
for
Ap
ver
thr
ize

a b
cro

tha
lar

the
phi
car

fro
po
ide

*T
e
n

SUBJ
GPHYS
HF
RHG

Vol. 5, No. 2, 1942, pp 41-47

UNIVERSITY OF UTAH
RESEARCH INSTITUTE
EARTH SCIENCE LAB.

RADIOACTIVE HEAT GENERATION IN ROCKS.

E. C. Bullard, F.R.S.

(Received 1942 February 28)

It has long been known that the amounts of Radium, Thorium and Potassium in a thickness of a few kilometres of the rocks occurring at the surface of the Earth are sufficient to produce the observed amount of heat flowing out of the Earth. For such calculations the amounts of heat produced in the disintegration of the Uranium and Thorium series and of Potassium are required. The values generally quoted are those given by Holmes and Lawson.* More recently Holmes † has given a value for Potassium that is six times less than the former one. A great amount of data on the energies of these disintegrations has since been accumulated, and it is now possible to derive values which are unlikely to be in error by an amount that is of any significance for geophysical problems. As the literature is scattered and specialised it seems worth while to publish a note indicating the best values available and the sources of the information. After this paper was finished a paper by Evans and Goodman ‡ appeared containing similar calculations. Their results are not very different from ours, but the methods by which they are obtained cannot be expected to yield the best values.

The first step is to calculate the energies evolved in the transformation of one atom of Uranium or Thorium into lead by adding the energies of the particles emitted. This is done in Tables I and II; most of the α particle energies have been determined relative to that of the RaC' α 's by magnetic focusing. The absolute value of the latter has been determined with an accuracy of about one in a thousand by Rosenblum and Dupouy§; the value they obtained has been confirmed by Briggs|| Only those of UI , UII , Io and Th depend on range measurements. The error in the sum is certainly considerably less than 1 per cent. Allowance has been made for the energies of the recoiling nuclei. The accuracy of the energies obtained in this way is confirmed by direct measurement of the heat generated in some of the transformations. Ra , $RaTh$ and ThC give α particles of more than one energy; if one of the lower energy α 's is emitted the balance of the energy appears as a γ ray, and if these are neglected and the maximum energy of the α particles is used the right total energy will be obtained. The branching of the Th series has been allowed for by taking 35 per cent. of the energy of the ThC α particles and ThC' β 's and 65 per cent. of the ThC' α 's and ThC β 's; the proportion of the atoms going into the RaC'' branch is so small that its effect on the energies is negligible.

The β and γ ray energies are much more uncertain than those of the α rays, but as they only contribute about 10 per cent. of the total energy the uncertainty has no great effect on the final result. In the decay of an atom in a state with energy E_1 above the ground state the first event is the emission of a β particle and a neutrino. The sum of their energies may in general have a number of discrete values E_1, E_2, \dots . The balance of the energy ($E_1 - E_2$), ($E_1 - E_3$) . . . is emitted as γ rays and as β particles belonging to the line spectrum. Let the probability of these modes of disintegration be p_1, p_2, \dots . The energy of the β particles corresponding to disintegration with energy E_r will be

* A. Holmes and R. W. Lawson, *Phil. Mag.*, 2, 1218-1233, 1926.
† A. Holmes, *J. Wash. Acad. Sci.*, 23, 169-195, 1933.
‡ R. D. Evans and C. Goodman, *Bull. Geol. Soc. Amer.*, 52, 459-490, 1941.
§ S. Rosenblum and G. Dupouy, *J. Phys. Radium* (7), 4, 262-268, 1933.
|| G. H. Briggs, *Proc. Roy. Soc., A*, 157, 183-194, 1936.

TABLE I

Atom	Energy MEV			References		
	α	β	γ	α	β	γ
UI	4.31			*		
UX ₁		0.06	0.00		†	‡‡
UX ₂		0.65	0.04		†	†
UII	4.89			*		
Io	4.84			*		
Ra	4.88			†		
Rn	5.59			†		
RaA	6.11			†		
RaB		0.14	1.72	*	*	§§
RaC		0.72			*	
RaC'	7.83			†		
RaD		0.01	0.05		§	
RaE		0.34	0.00		¶	
RaF	5.40			†		
Total	43.85	1.92	1.81			

TABLE II

Atom	Energy MEV			References		
	α	β	γ	α	β	γ
Th	4.16			*		
MsTh ₁		0.01	0.00	*	§	§
MsTh ₂		0.49	0.78		**	¶¶
RdTh	5.52					
ThX	5.79			†		
Tn	6.40			†		
ThA	6.90			†		
ThB		0.15			*	
ThC	(35%) 2.17	(65%) 0.32	1.43	†	††	§§
ThC'	(65%) 5.82			†		
ThC''		(35%) 0.19			*	
Total	36.76	1.16	2.21			

* N. Feather, *Nuclear Physics*, Cambridge, 1936.

† W. B. Lewis and B. V. Bowden, *Proc. Roy. Soc., A*, 145, 235-249, 1934.

‡ J. S. Marshall, *Proc. Roy. Soc., A*, 173, 391-410, 1939.

§ D. D. Lee and W. F. Libby, *Phys. Rev.*, 55, 252-258, 1939.

|| L. Meitner and W. Orthmann, *Z. Phys.*, 60, 143-155, 1930.

¶ G. J. Neary, *Proc. Roy. Soc., A*, 175, 71-87, 1940.

** N. Feather, *Proc. Camb. Phil. Soc.*, 34, 115-119, 1938.

†† W. J. Henderson, *Proc. Roy. Soc., A*, 147, 572-582, 1934.

‡‡ N. Feather, *Proc. Roy. Soc., A*, 165, 530-551, 1938.

§§ L. H. Gray, *Proc. Roy. Soc., A*, 159, 263-283, 1937.

¶¶ E. Rutherford and H. Richardson, *Phil. Mag.*, 26, 324-333, 1913.

||| E. Rutherford, J. Chadwick and C. D. Ellis, *Radiations from Radioactive Substances*, Cambridge, 1930.

distribute
is then Σ
energy is
The γ ra
knowledg
the form
and the n
of disinte
energy ha
to be 0.3
energy di
who foun
therefore

This 1
or no γ r
leaves Ra
obtain 0.2
RaE) will
must lead
contribute
systems a
arbitrary
times the
For RaB,
for RaC 0

The ei
Ellis ¶¶
and ThC'
ionise the
Tables I
energies 0

The γ
measur em
obtained b
small with
of the ioni

The h
but the pu

The to
and 40.1
Radium C
per second

* L. M

† A me

0.320 \pm 0.00

‡ L. H.

§ G. J.

|| R. W.

¶ C. D.

** C. D.

†† F. Op

‡‡ L. H.

§§ N. Fe

||| Flerov

distributed between zero and E_r ; let the mean be $K_r E_r$. The total energy in the β rays is then $\Sigma p_r K_r E_r$. The energy carried away by the neutrinos is $\Sigma p_r (1 - K_r) E_r$; this energy is lost, as the range of the neutrino is great compared with the radius of the Earth. The γ ray energy is $\Sigma (E_1 - E_r) p_r$. The estimation of the β particle energy requires a knowledge of the energies and probabilities of the various modes of disintegration and the form of the function giving the distribution of the energy between the β particle and the neutrino for each mode. RaE emits no γ rays and therefore has only one mode of disintegration. The maximum energy of the β particles is 1.18 MEV, whilst the mean energy has been found from calorimetric measurements by Meitner and Orthmann* to be 0.337 ± 0.020 MEV.† This result has been confirmed by measurements of the energy distribution in the β ray spectrum by Martin and Townsend‡ and by Neary§, who found 1.17 and 0.340 MEV. The ratio of the mean energy to the maximum is therefore 0.288.

This ratio may also be assumed for UX_1 , UX_2 , RaD and $MsTh_1$, which emit little or no γ rays, and for ThC'' , which always emits a 0.6 MEV γ ray and no others. This leaves RaB , RaC , $MsTh_2$, ThB and ThC . If the same method is used for these we shall obtain $0.288 E_1$ instead of $\Sigma K_r E_r p_r$. The assumption that K_r is 0.288 (the value for RaE) will probably not introduce serious error, but the substitution of E_1 for $\Sigma E_r p_r$ must lead to an overestimate as $E_1 > E_r$ and $p_r < 1$. On this assumption these elements contribute 1.09 MEV to the radium series and 1.11 MEV to the Th series. The level systems are so uncertain that an accurate calculation is not possible and a more or less arbitrary allowance must be made. The figures given in Tables I and II are 0.288 times the maximum β particle energy for all atoms except RaB , RaC , $MsTh_2$ and ThC . For RaB , $MsTh_2$ and ThC they are 0.288 times the maximum energy less 0.1 MEV and for RaC 0.288 times the maximum less 0.2 MEV.

The energies of the line β spectra may be calculated from data given by Gurney||, Ellis¶** and Oppenheimer.†† The results are RaB 0.055, RaC 0.011, ThB 0.047 and ThC'' 0.014 MEV. These are the total energies including the energy necessary to ionise the atom. They have been added to the continuous β spectrum energies in Tables I and II, that for ThC'' being first multiplied by the branching ratio. The energies of all other line β spectra are negligible.

The γ ray energies of $Ra(B+C)$ and $Th(B+C)$ may be determined from Gray's‡‡ measurements of the ionisation produced. The results are consistent with those obtained by adding the energies of the γ ray lines. The remaining γ ray energies are small with the exception of that of $MsTh_2$, which has been determined §§ by comparison of the ionisation produced with that produced by $Ra(B+C)$.

The heat generated by the spontaneous fission of Uranium is probably negligible, but the published information |||| is not sufficient to estimate it.

The total energies liberated in the disintegration of one atom of UI and Th are 47.6 and 40.1 MEV, with a maximum uncertainty of about 0.5 MEV. The International Radium Commission has adopted 3.70×10^{10} as the number of atoms of Ra disintegrating per second per gram. This value depends essentially on accepting the determinations

* L. Meitner and W. Orthmann, *Z. Phys.*, 60, 143-155, 1930.

† A more recent determination by I. Zlotowski (*Phys. Rev.*, 60, 483-488, 1941) gives 0.320 ± 0.005 MEV.

‡ L. H. Martin and A. A. Townsend, *Proc. Roy. Soc., A*, 170, 190-205, 1939.

§ G. J. Neary, *Proc. Roy. Soc., A*, 175, 71-87, 1940.

|| R. W. Gurney, *Proc. Roy. Soc., A*, 112, 380-390, 1926.

¶ C. D. Ellis, *Proc. Roy. Soc., A*, 138, 318-339, 1932.

** C. D. Ellis, *Proc. Roy. Soc., A*, 143, 350-357, 1934.

†† F. Oppenheimer, *Proc. Camb. Phil. Soc.*, 32, 328-335, 1936.

‡‡ L. H. Gray, *Proc. Roy. Soc., A*, 159, 263-283, 1937.

§§ N. Feather, *Nuclear Physics*, Cambridge, 1936.

|||| Flerov and Petrjak, *Phys. Rev.*, 58, 89, 1940.

of Braddick and Cave, Ward Wynn-Williams and Cave, and Watson and Henderson, and rejecting the low values of Jedrejowski, and Geiger and Werner.* The adopted value is probably correct to within 1 per cent. Taking the electronic charge as 4.80×10^{-10} e.s.u. the mechanical equivalent of heat as 4.19 joules/cal. and one e.s.u. as 299.8 volts, the heat generated by the substances in equilibrium with one gram of *Ra* is 0.0673 cal./gm. *Ra* sec.

The Actinium series is derived from *AcU*, an isotope of *UI*, the parent of the *UI-Ra* series. The two series will therefore be present in a fixed ratio, and it is convenient to add the heat generated by the Actinium series to that generated by the *UI* series. The most direct method of determining the ratio of the number of atoms of *AcU* disintegrating per second to the number of *UI* is to separate some member of the *Ac* series chemically and determine its activity. Mutually consistent measurements † on protoactinium have given 4.0 ± 0.1 per cent. for this ratio. A more indirect determination from the ratios *UI/AcU* and Pb^{206}/Pb^{207} in minerals of known age has given 4.6 ± 0.1 per cent. We adopt the former result (4.0 per cent.), as it is independent of the rock ages which are subject to some uncertainty. The total energy of the Actinium series determined by the same methods as those for the *UI* and *Th* series is 43.7 *MEV*. The energy associated with the series is therefore $4.0 \times 43.7/47.6 = 3.7$ per cent. of that from the *UI* series, and the energy from the amounts of the two series associated with one gram of *Ra* is

$$0.0698 \text{ cal./gm. } Ra \text{ sec.}$$

The number of *Th* atoms disintegrating per gm. per sec. has been determined by Kovarik and Adams ‡ as 4.11×10^9 with a limit of error of 2 per cent. From this and the value given above for the energy per atom the total amount of heat generated by the substances in equilibrium with one gram of *Th* is

$$6.30 \times 10^{-9} \text{ cal./gm. } Th \text{ sec.}$$

These figures are probably not more than 2 or 3 per cent. from the true values.

Holmes quotes the amount of heat per gram of Uranium per year. It seems preferable to give the results per gram of Radium since the measurements on the radioactivity of rocks are made relative to a standard Radium solution, and to get the results in terms of Uranium introduces the somewhat uncertain *Ra : U* ratio without any compensating advantage. To obtain a figure comparable with Holmes's we require the number of disintegrations from one gram of Uranium in a second. This has been determined by Kovarik and Adams §, who obtained 24,770 α particles per sec. from a gram of Uranium. As discussed above, 4 out of every 204 of these belong to the Actinium series. The remainder are equally divided between Uranium I and Uranium II. The numbers of *UI* and *AcU* disintegrations per second per gram of Uranium are therefore 12,140 and 490. Combining these with the energies of the two series (47.6 and 43.7 *MEV*) we get the total energy liberated per gram per year. The results for Uranium and Thorium are

$$\begin{array}{l} 0.723 \text{ cal./gm. } U \text{ year} \\ 0.200 \text{ " } Th \text{ " } \end{array}$$

compared with 0.790 and 0.230 obtained by Holmes and 0.741 and 0.203 by Evans and Goodman. The latter authors have underestimated the total α particle energy for the Uranium series by 0.51 *MEV*, and overestimated the β particle energy by 0.36 *MEV* and the γ ray energy by 1.45 *MEV*. The latter differences arise from their assumption that the ratio of the β and γ to the α particle energies is always the same as that given by Rutherford, Chadwick and Ellis* for *Ra(B+C)*. Further the decay constant of *UI*

* E. Rutherford, J. Chadwick and C. D. Ellis, *Radiations from Radioactive Substances*, Cambridge, 1930.

† M. Francis and T. Da-Chang, *Phil. Mag.*, 20, 623-632, 1935; E. Gleditsch and E. Foyt, *C.R.*, 199, 412, 1934; A. v. Grosse, *Phys. Rev.*, 42, 565-570, 1932.

‡ A. F. Kovarik and N. I. Adams, *Phys. Rev.*, 54, 413-421, 1938.

§ A. F. Kovarik and N. I. Adams, *Phys. Rev.*, 40, 718-726, 1932.

is taken fr
of the *Ac*
There is a
gm. *U*. T
for the rati
is that obta
gram of *U*
of *AcU* for

Potassi
shown that
mean energ
MEV. Ar
correspond
weight of H
that 27 ± 9
method get
difficult to
chamber, as
the chambe
a thick laye
particles co
 25 ± 10 as t
0.22 *MEV*
by the β ra
Kolhørs
ionisation a
same weigh
 1.3×10^{-10}

Muhlho
Ra(B+C),
this as pro
of the γ ray
times less in
by the β 's

This value
cal./gm. year
1933. Our
adopted for
 5×10^{-6} cal
practically t

The low
produced b

* A. O. I

† D. Boc

‡ C. D.

§ A. Brai

¶ W. Mu

‡ G. Ort

•• W. Ko

†† Běhou

‡‡ Gray a

§§ L. H. (

is taken from Kovarik and Adams without correction for the *Ac* series. As the energy of the *Ac* series is later added on, it has effectively been included one and a half times. There is also an arithmetical error without which their results would be 0.753 cal./yr. gm. *U*. These errors are largely compensated by the low value (2.84×10^8) recommended for the ratio of the weights of *U* and *Ra* in equilibrium. The best value of this quantity is that obtained from the numbers of *UI* and *Ra* atoms disintegrating in a second in one gram of *U* and *Ra* ($12,140$ and 3.70×10^{10}) corrected for the fact that there is * one atom of *AcU* for every 139 atoms of *UI*. The result is 3.06×10^8 .

Potassium disintegrates with the production of β and γ rays. Bocciairelli † has shown that the β 's are of two different energies, and estimates that 60 per cent. have a mean energy of 0.13 *MEV* and 40 per cent. of 0.35 *MEV*, giving a mean energy of 0.22 *MEV*. Anderson and Neddermeyer ‡ give over 0.7 *MEV* for the maximum energy corresponding to 0.20 for the mean energy. By counting the particles from a known weight of Potassium with a Geiger-Mühler counter, Bramley and Brewer § have found that 27 ± 9 particles are emitted from one gram in a second. Muhlhoff || by the same method gets 23, whilst Orbán ¶, by expansion chamber photographs, gets 78. It is difficult to get reliable absolute results for the number of particles with the expansion chamber, as both the volume in which tracks can be photographed and the time for which the chamber is active are somewhat indefinite. In all the experiments except Muhlhoff's a thick layer of salt was used, and the calculation of the thickness of salt from which particles could come causes great uncertainty. We reject Orbán's result and adopt 25 ± 10 as the number of particles emitted in one second by one gram of Potassium, and 0.22 *MEV* as the energy. This gives 2.1×10^{-13} cal./sec. gm. *K* for the heat generated by the β rays.

Kolhörster ** found that the γ rays from Potassium produced 5×10^{-11} times less ionisation at a given distance than those from the *Ra(B+C)* in equilibrium with the same weight of Radium; Muhlhoff found the ratio to be 3.3×10^{-11} ; Běhounek †† found 1.3×10^{-10} †† and Gray and Tarrant §§ found 1.6×10^{-11} .

Muhlhoff found the γ 's to have an absorption coefficient 1.1 times greater than the *Ra(B+C)* γ rays, whilst Kolhörster found them to be twice as penetrating but regarded this as probably an overestimate. Gray and Tarrant found 2.0 *MEV* for the energy of the γ rays. Assuming the rays to be similar to those from *Ra(B+C)* and 1.6×10^{-11} times less intense, the γ ray energy is 0.4×10^{-13} cal./sec. gm. *K*. The total heat generated by the β 's and γ 's is then

$$2.5 \times 10^{-13} \text{ cal./gm. } K \text{ sec.}$$

This value may be uncertain by as much as 50 per cent.; it corresponds to 7.9×10^{-6} cal./gm. year compared with Holmes's estimate of 120×10^{-6} in 1926 and 20×10^{-6} in 1933. Our value is lower than his 1933 result principally because of the lower value adopted for the number of β particles emitted per second. Evans and Goodman give 5×10^{-6} cal./gm. year, but it is not clear how they get so low a value as their data are practically the same as ours.

The low value of the heat generated by Potassium makes its contribution to the heat produced by rocks only about 5-10 per cent. of that from Uranium and Thorium.

* A. O. Nier, *Phys. Rev.*, 55, 150-153, 1939.

† D. Bocciairelli, *R.C. Accad. Lincei*, 17, 830-836, 1933.

‡ C. D. Anderson and S. H. Neddermeyer, *Phys. Rev.*, 45, 653-654, 1934.

§ A. Bramley and A. K. Brewer, *Phys. Rev.*, 53, 502-510, 1938.

|| W. Muhlhoff, *Ann. Phys. Lpz.* (5), 7, 205-224, 1930.

¶ G. Orbán, *S.B. Akad. Wiss. Wien* (2A), 140, 121-139, 1931.

** W. Kolhörster, *Z. Geophys.*, 6, 341-357, 1930.

†† Běhounek, *Z. Phys.*, 69, 654-663, 1931.

‡‡ Gray and Tarrant quote this as 1.3×10^{-11} .

§§ L. H. Gray and G. T. P. Tarrant, *Proc. Roy. Soc., A*, 143, 681-706, 1934.

Further investigations into the β and γ rays from Potassium to place this important result beyond doubt are very desirable.

Table III gives the rate of heat generation calculated from the mean amounts of Ra , Th and K given by Evans and Goodman* for a large number of rocks.† The results are between 8 and 22 per cent. greater than those given in Evans and Goodman, Table XIII. The main cause of these differences is that the values for Ra in Table III are calculated from the amounts of Ra given in Evans and Goodman's Table X, whereas their rates of heat generation have been calculated from the amounts of U , and for some reason that is not clear the amounts of U have only been calculated for 81 out of the 132 specimens.

TABLE III

Rock type	Proportion by Weight			Heat Generation 10^{-8} cal./gm. yr.			
	Ra $\times 10^{-12}$	Th $\times 10^{-8}$	K $\times 10^{-3}$	Ra	Th	K	Total
Acidic	1.37	13.0	2.8	3.0	2.6	0.2	5.8
Intermediate	0.51	4.4	2.0	1.1	0.9	0.2	2.2
Basic	0.38	3.9	1.4	0.8	0.8	0.1	1.7
Sedimentary	0.57	3.3	2.0	1.2	0.7	0.2	2.1

The radioactivity of Potassium † is due to the rare isotope ^{40}K , which constitutes $1/9000$ of the whole.§ Using this and the above number of disintegrations per second we get a half-life of 1.5×10^9 years. The U/Pb ratios give the ages for the oldest rocks as $1.5-2.2 \times 10^9$ years; the heat generation by Potassium in the rocks has therefore at no time been more than about twice what it is now. This is directly contrary to the conclusion of Brewer.|| He assumes that all the ^{40}Ca in the rocks has been formed from ^{40}K ; this requires the Earth to be 15×10^9 years old. There is little reason for the assumption, and the conclusion is contrary to everything that is known about the age of the Earth. He then proceeds to calculate the temperature of the surface of the Earth in the past by a method that tacitly assumes the present temperature to be controlled by radioactive heating. In fact the heat arriving at the surface from within is less than 10^{-4} of that received from the Sun.

In addition to the elements considered above, Rb , Nd , Sm and Lu are radioactive with periods comparable to the age of the Earth. They occur so sparsely that their heating effect is quite negligible. The large number of artificial radioactive isotopes of known elements that have been prepared in the laboratory all have lives much too short for them to be of any geological significance. It is possible, however, that there have in the past existed radioactive isotopes with lives of about 10^8 years. If these were present when the Earth was formed they would by now have decayed so far as to escape detection, and yet would have such long periods that they would not be detected if formed by artificial disintegration. The former existence of such isotopes would have important geological consequences and would help to explain the widespread intrusions of early Pre-Cambrian time. By eliminating isotopes that are known to be stable or to have short lives and those which would lead to products of extreme rarity, the possible isotopes with long periods may be much reduced, and it is probable that the progress of studies in artificial disintegration will in the near future so narrow the field

* R. D. Evans and C. Goodman, *Bull. Geol. Soc. Amer.*, 52, 459-490, 1941.

† It is doubtful if these results form a homogeneous series and therefore if the mean has any exact significance (see H. Jeffreys, *M.N.R.A.S.*, *Geophys. Suppl.*, 5, 37-40, 1942. The figures do, however, give an indication of the relative importance of Ra , Th and K).

‡ G. J. Neary, *Proc. Roy. Soc.*, A, 175, 71-87, 1940; A. O. Nier, *Phys. Rev.*, 48, 283-284, 1935.

§ A. K. Brewer, *Phys. Rev.*, 48, 640, 1935; A. O. Nier, *Phys. Rev.*, 48, 283-284, 1935.

|| W. R. Smythe and A. Hemmendinger, *Phys. Rev.*, 51, 178-182, 1937.

|| A. K. Brewer, *Indust. Engng. Chem.*, 30, 893-896, 1938.

that it will be bilities. The AcU . The h determined w per second d integrating pe years. If this about 1.6×10 disintegrating of the half-pe integrating an years for the that of v. G were correct, 60 per cent. c considerable period of AcU

I am indebted

The heat g values are:

7.0×10^{-2} c
 6.3×10^{-9} c
 2.5×10^{-18}

The results might be in error

The value only 5-10 per Potassium. It important geolo

that it will be worth while to make an intensive examination of the few remaining possibilities. The only known isotope which might have the right period and abundance is *AcU*. The half-period may be most directly determined by combining the ratio *UI/AcU* determined with the mass spectroscopie *, the ratio of the number of atoms disintegrating per second determined by chemical separation of *Pa*, and the number of *UI* atoms disintegrating per sec. per gm. determined by counting α particles. The result is 8.2×10^8 years. If this is correct, the number of atoms disintegrating when the Earth was formed about 1.6×10^9 years ago would be about 16 per cent. of the number of atoms of *UI* now disintegrating and no large effect would be produced. More indirect determinations of the half-period of *AcU* from the ratio of the number of atoms of *UI* and *AcU* disintegrating and the Pb^{207}/Pb^{206} ratios in lead from minerals of known age, give $2.7-7.0 \times 10^8$ years for the half-period (see Nier †), the best value by this method being perhaps that of v. Grosse ‡, who obtained 4.0×10^8 years. If this low value of the period were correct, the heat generated by the *Ac* series 1.6×10^9 years ago would have been 60 per cent. of that now generated by the *UI* series. So large an increase might have considerable geological effects, and it is very desirable that the uncertainty about the period of *AcU* should be cleared up.

I am indebted to Dr. N. Feather for advice on radioactive matters.

Summary

The heat generation by *Ra*, *Th* and *K* is considered. It is concluded that the best values are:

7.0×10^{-2} cal./sec. gm. *Ra* (0.72 cal./gm. *U* yr., 2.20×10^6 cal./gm. *Ra* yr.).

6.3×10^{-9} cal./sec. gm. *Th* (0.200 cal./gm. *Th* yr.).

2.5×10^{-13} cal./sec. gm. *K* (8×10^{-6} cal./gm. *K* yr.).

The results for *Ra* and *Th* should be correct within 2 or 3 per cent., but that for *K* might be in error by 50 per cent.

The value for Potassium is considerably less than those previously accepted, and only 5-10 per cent. of the heat generated by radioactivity in a rock is produced by Potassium. It seems unlikely therefore that the radioactivity of Potassium has any important geological consequences.

* A. O. Nier, *Phys. Rev.*, 55, 150-153, 1939.

† A. O. Nier, *Phys. Rev.*, 55, 153-163, 1939.

‡ A. v. Grosse, *Phys. Rev.*, 42, 565-570, 1932.